

Developing biomimetic scaffolds for osteocondral tissue engineering

by Xiaoqi LIN

Thesis submitted in fulfilment of the requirements for
the degree of

Master of Engineering (Research)

under the supervision of Dr. Jiao Jiao Li, Dr. Peter Su, Prof.
Ken Tye Yong, Dr. Haiyan Li

University of Technology Sydney
Faculty of Engineering and IT

Submitted in March 2025

Certificate of Original Authorship

I, *Xiaoqi LIN*, declare that this thesis is submitted in fulfilment of the requirements for the award of *Master of Engineering (Research)*, in the *School of Biomedical Engineering, Faculty of Engineering and IT* at the University of Technology Sydney.

This thesis is wholly my own work unless otherwise referenced or acknowledged. In addition, I certify that all information sources and literature used are indicated in the thesis.

This document has not been submitted for qualifications at any other academic institution.

This research is supported by the Australian Government Research Training Program.

Signature: Production Note:
Signature removed prior to publication.

Date: 14/03/2025

Acknowledgements

Have imagined more than 1000 scenes while piecing together a 1000-piece pure white puzzle.

Piece by piece, over the past two years, I have met more new people than I ever imagined, changing my ideas, reshaping my perspectives, and setting my mind on an endless evolution. I have come to realise that research is far more charming and romantic than I had ever thought.

I would like to express my deepest gratitude to my principal supervisor, Dr. Jiao Jiao Li, who has guided me through my Bachelor Honours and continued to support me throughout this Master by Research. Her supervision has been invaluable in shaping my academic journey and showing me what a supervisor can truly be like. She has inspired me to start thinking about the possibilities beyond research degrees. I feel incredibly fortunate to have met her and to have been under her supervision.

I am also profoundly thankful to my external supervisor, Prof. Ken Tye Yong, for providing me with access to the USYD lab, offering the space and resources necessary for hydrogel fabrication, which allowed me to find a sense of peace in the process of experimentation. I would also like to express my sincere gratitude to Joseph Yang for his assistance in managing lab logistics, purchasing consumables, and securing access to the lab, which made my work at USYD possible.

To my other external supervisor, Dr. Haiyan Li, I extend my heartfelt thanks for the RMIT trip and the opportunity to explore new possibilities in materials-based implantable scaffolds.

I am grateful to Dr. Ye Zhang, the postdoctoral fellow in our research team, who helped me immensely with cell culture-based experiments and showed patience during experiment guidance and collaboration in paper writing.

Throughout this Master's degree, I have imagined more than I could; not only because of the ideals inspired by my supervisors and other HDR students, as well as some lab managers and staff, but also because I gradually realised that each step can lead to the construction of a solid self.

I would also like to express my sincere gratitude to my psychological counsellor, Geoffrey Francis, who told me I am neurodivergent and patiently explained the neurodivergent brain, the limbic system, sensory avoidance, and more. Regardless of different perspectives or controversial points, understanding myself has been far more important than performing a superficial 'normality' just to maintain hypocritical 'relationships' in any unhealthy and less inclusive environment. In this

twisted world, encountering obscurity is inevitable, but knowing myself has allowed me to feel normal again. In realising my own existence as a living and breathing individual, this world began to deconstruct in my eyes.

Additionally, I would like to thank my ‘silkworm senpai’, the true masters of producing silk fibres and constructing silk cocoons. Their creations provided the natural biomaterials for my experiments and functioned as natural spinning machines. With intuition and curiosity, I look forward to more collaborations and experiments in future research, exploring the use of silk cocoons and fibres in biomedical applications. ♪(◡^◡^◡)♡

Because of these two years of research experience, I have come to see this narrow gate as a wide path and am looking forward to my future research degree.

Enigma

What is the university?

A place that nurtures independence of thought, the freedom of spirit?

Once, I regarded this as an idealistic slogan—hollow, distant. I thought I would merely pass through these halls, spend only a few years here — university was just a period of time, a stage for obtaining a degree, a place I would eventually leave.

I have always wondered: What does it truly mean to be educated? To be shaped, moulded, or tamed? Is the purpose of learning to make us obedient? To condition us to bow before authority, even when it demands belief without evidence, even when it cloaks itself in myth? When I read those tired justifications—*I was only following orders*—I shudder. Is a life of unexamined, unthinking compliance worth living?

There is a quiet defiance in the act of questioning. *Life and death are not bargaining chips; belief isn't a tool.* For years, this was an unsolvable riddle, a whisper in the dark. This world loves its labels, its neat categorisations—but beneath them, what remains of the human? Strip away the roles, the titles, the assigned meanings—what is left?

Perhaps nothing.

Perhaps everything.

How to interpret a living individual? Many frameworks claim to hold the answer, yet each risks reducing the human to a mere instrument—a hollowed-out vessel for

external meaning. In this narrative, everything is indifferent—and thus, everything is tedious. But why? The world forgives grown-ups easily; when they make such excuses, they are praised as thoughtful. But a child who speaks the same truth is deemed rebellious, childish. I told myself: “Do you understand what I mean? — Just grow up. Growing up obscures. It embellishes. It erases.”

Hence, I allow myself to retain a bit of absurdity — to cling to the insoluble questions, the ones that cannot be answered, only carried. This is my last reverence for life itself — until the day I learn to see the world on my own terms, to navigate its chaos with my own compass...

Enigma — a reflection of the questions that have haunted me, shaped me, and, in many ways, defined me. As I stand at its completion, I acknowledge the forces — seen and unseen — that have guided me here.

There is a place in my mind I will never reach, a shore my ship will never find.

Hope the journey is a long one, full of adventure, full of discovery...

The boulder rolls in eternal silence, up and down, Sisyphus’s lonesome hill.

To Plato's Allegory of the Cave and its chained shadows...

To Minerva's owl, spreading its wings only when dusk falls.

To the no-longer-poetic world,

To the freedom of being a nihilist, a cynic, a fool.

Soar or fall?

Flames igniting the silent waters.

Fate or chance?

Like Pandora opening the forbidden box,

Unveiling taboo desires — yet never repenting.

Like this fall — uncontrolled yet exhilarating, tearing out and spreading wings.

—To my Ithaka, that never arrives in a lifetime—

Thesis Format Statement

This thesis is submitted in conventional structure in fulfilment of the requirements for the degree of Master by Research at the University of Technology Sydney. It comprises eight chapters, structured as follows:

Chapter 1: Introduction

This chapter provides an overview of chondral and osteochondral defects, introduces the concept of biomimetic scaffolds, and outlines the research objectives of the project.

Chapter 2: Literature Review

This chapter reviews current treatments for osteochondral defects and the state-of-the-art development of biomimetic scaffolds, with detailed categorisation of fibre orientations, porous structures, and bioactive molecule incorporation. (*Published paper*).

Chapter 3: Materials and Methods

This chapter details the degumming process of silk cocoon fibres for scaffold preparation. It describes the extraction and separation of silk fibroin and silk sericin, which are further utilised in hydrogel design and fabrication in the subsequent chapter. The results confirmed the effectiveness of using sodium carbonate decahydrate ($\text{Na}_2\text{CO}_3 \cdot 10\text{H}_2\text{O}$) for degumming, yielding both purified silk fibroin fibres and silk sericin.

Chapter 4: Degumming of Silk Cocoon

This chapter details the degumming process of silk cocoon fibres for scaffold preparation. It describes the extraction and separation of silk fibroin and silk sericin, which are further utilised in hydrogel design and fabrication in the subsequent chapter. The results confirmed the effectiveness of using sodium carbonate decahydrate ($\text{Na}_2\text{CO}_3 \cdot 10\text{H}_2\text{O}$) for degumming, yielding both purified silk fibroin fibres and silk sericin.

Chapter 5: Multilayered Hydrogel Scaffold Formation

This chapter outlines the fabrication process of multilayered hydrogel scaffolds designed to mimic the native zonal architecture of cartilage. A layer-by-layer mould casting method is described to achieve seamless integration of the superficial, middle, and deep zones within a single scaffold. The fabricated tri-layered scaffold demonstrated the potential for zone-specific cartilage reconstruction with both functional and structural restoration.

Chapter 6: Physical Characterisation

SEM results confirmed a clear transition from fibrous to porous regions between the superficial and middle zones, and a gradient pore distribution from the middle to the deep zones, while maintaining overall scaffold integrity. Swelling and degradation tests demonstrated comparable properties across the layers. Mechanical testing further verified the structural integrity of the tri-layered scaffold, which remained intact under compression, indicating strong interfacial bonding between layers.

Chapter 7: In Vitro Studies

This chapter describes the biological evaluation of the scaffolds through *in vitro* studies. MTT assay results indicated the viability and growth of BMSCs from day 4 to day 7, suggesting that the scaffold materials are biocompatible and support BMSCs adhesion and proliferation. Histological analysis further demonstrated the seamless integration of the three layers in the hydrated state and confirmed cell attachment on the scaffold surface, highlighting the importance of the porous hydrogel design for effective cell interaction.

Chapter 8: Conclusion and Outlook

This chapter summarises the main findings of the project, highlighting the significance of the developed multilayered scaffold for osteochondral tissue engineering. It also discusses the limitations of the current study and proposes possible future research directions to optimise scaffold performance and clinical applicability.

List of Publications

This first author review paper forms Chapter 2 of this thesis:

- [1] **Lin, X.**, Zhang, Y., Li, J., Oliver, B. G., Wang, B., Li, H., Yong, K.-T., & Li, J. J. (2025). Biomimetic multizonal scaffolds for the reconstruction of zonal articular cartilage in chondral and osteochondral defects. *Bioactive Materials*, 43, 510-549. DOI: 10.1016/j.bioactmat.2024.10.001

I also contributed to the below publications during my degree, but these contributions did not form part of this thesis:

- [2] Fang, L.[^], **Lin, X.**[^], Xu, R., Liu, L., Zhang, Y., Tian, F.*^{*}, Li, J. J.*^{*}, & Xue, J.*^{*} (2025). Advances in the Development of Gradient Scaffolds Made of Nano-Micromaterials for Musculoskeletal Tissue Regeneration. *Nano-Micro Letters*, 17(1), 75. [^]Equal first authors; ^{*}Corresponding authors. DOI: 10.1007/s40820-024-01581-4
- [3] Yang, Z., Jaiswal, A., Yin, Q., **Lin, X.**, Liu, L., Li, J., Liu, X., Xu, Z., Li, J. J., & Yong, K.-T. (2024). Chiral nanomaterials in tissue engineering. *Nanoscale*, 16, 5014-5041. DOI: <https://doi.org/10.1039/d3nr05003c>
- [4] Carr, J. C., Pedagandham, S. P., Giugni, A., Shen, C., Kim, A. M., Cribbin, E. M., **Lin, X.**, Oomatia, A., Lu, W., Al Muderis, M., Xing, D., & Li, J. J. (2024). Bone mineral density in osseointegration implant surgery: A review of current studies (Review). *Biomed Rep*, 21(2), 122. DOI: <https://doi.org/10.3892/br.2024.1809>

Statement of contribution of authors

The published review paper titled ‘Biomimetic multizonal scaffolds for the reconstruction of zonal articular cartilage in chondral and osteochondral defects’ constitutes the Chapter 2 Literature Review of this thesis. I am the first author of this review article and was responsible for literature gathering, synthesis and critical analysis, as well as writing the initial draft of the paper and generating all figures and tables. Below are signatures of all co-authors of this review article to confirm these contributions.

Author name	Signature	Date
Ye Zhang	Production Note: Signature removed prior to publication.	2 June 2025
Jiarong Li	Production Note: Signature removed prior to publication.	2 June 2025
Brian G. Oliver	Production Note: Signature removed prior to publication.	02/06/25
Bin Wang	Production Note: Signature removed prior to publication.	02/06/25
Haiyan Li	Production Note: Signature removed prior to publication.	03/06/2025
Ken-Tye Yong	Production Note: Signature removed prior to publication.	24/06/2025
Jiao Jiao Li	Production Note: Signature removed prior to publication.	2 June 2025

Table of Contents

<i>Certificate of Original Authorship</i>	<i>i</i>
<i>Acknowledgements</i>	<i>ii</i>
<i>Thesis Format Statement</i>	<i>v</i>
<i>List of Publications</i>	<i>vii</i>
<i>Statement of contribution of authors</i>	<i>viii</i>
<i>Table of Contents</i>	<i>ix</i>
<i>List of Figures</i>	<i>xiii</i>
<i>List of Tables</i>	<i>xvii</i>
<i>List of Abbreviations</i>	<i>xviii</i>
<i>Abstract</i>	<i>xix</i>
Chapter 1 Background Introduction	1
1.1 Classification of Defects and Zonal Articular Cartilage	1
1.2 Concept of Biomimetic Scaffolds.....	5
1.3 Research Hypothesis & Aims	6
1.4 Research Questions & Objectives of this Thesis.....	7
1.4.1 Research questions	7
1.4.2 Objectives of this Thesis	9
1.5 Significance of the Study	10
Chapter 2 Literature Review	12
Acknowledgements (Chapter 2).....	12
2.1 Overview	13
Chapter 3 Research Methodology	15
3.1 Scaffold Description & Fabrication Approach	15
3.1.1 Design parameters	15
3.1.2 Materials selection & Fabrication techniques.....	15

3.2	Experimental Design Outline	16
3.2.1	Aim 1: Synthesis of hydrogel scaffold.....	17
3.2.2	Aim 2: To assess the physical and mechanical properties of the scaffolds	18
3.2.3	Aim 3: Assess biological properties of the zonal scaffold using MSCs	19
3.3	Ethical stance	19
Chapter 4	<i>Degumming of Silk: Silk Fibroin Fibres and Silk Sericin</i>	20
4.1	Silk	20
4.2	Silk Cocoons and Biomimetic Approach in Tissue Engineering.....	20
4.2.1	Natural silkworm spinning behaviour and bioinspired approaches	21
4.2.2	Silk fibroin fibres and Silk sericin	22
4.2.3	Degumming methods	24
4.3	Silk Cocoons Degumming Experiment: Methods and Procedures	25
4.3.1	Pre-test: degumming and alignment of fibres	26
4.3.2	Optimised degumming process of silk cocoons	27
4.4	Obtain Silk Fibre and Sericin Powder	28
4.4.1	Expand and collect the silkworm silk fibres.....	28
4.4.2	Sterilisation of silk and sericin before application.....	28
4.5	Sericin Hydrogel Preparation	30
4.5.1	Sericin-PVA hydrogel	31
4.5.2	Preliminary sericin/PVA hydrogel cell seeding	33
4.6	Summary, Optimisation & Outline of Scaffold Designs and Fabrication Procedures.....	37
Chapter 5	<i>Multilayered Hydrogel Scaffolds: Design and Optimisation</i>	38
5.1	Hydrogels in Tissue Engineering.....	38
5.1.1	Alginate hydrogels	39
5.1.2	PVA hydrogels	41
5.2	Materials and Hydrogel Samples Preparation.....	42
5.2.1	Materials	42
5.2.2	Alginate-based hydrogel preparations and pre-test	43
5.2.3	PVA hydrogel preparation and concentration range determination	47
5.2.4	PVA-sericin hydrogel fabrication	48

5.3	Step-by-Step Standardisation of Sequential Layering Procedures	51
5.3.1	Time intervals test sequential layering: Biphasic alginate-based hydrogel	51
5.3.2	Alginate-PVA composite double-network crosslinking hydrogels	53
5.3.3	Composite Alginate-PVA bi-layered scaffold	55
5.3.4	Tri-layered hydrogel mimicking zonal articular cartilage	56
5.4	Summary	60
Chapter 6	Physical Characterisations	62
6.1	Overview	62
6.2	Hydrogel Characterisation Procedures	62
6.2.1	Sample freeze drying & Morphology analysis	63
6.2.2	Hydrogel swelling test and liquid uptake	64
6.2.3	Degradation test	65
6.2.4	Mechanical properties	66
6.3	Results and Discussion	68
6.3.1	Morphology of hydrogel cross-section	68
6.3.2	Hydrogel swelling and water uptake	74
6.3.3	Degradation	77
6.3.4	Mechanical properties	80
6.4	Summary	91
Chapter 7	<i>In vitro Chondral Tissue Regeneration using Human Mesenchymal Stem Cells</i>	92
7.1	Overview	92
7.2	Biological Assessments and Methods	92
7.2.1	Sterilisation of hydrogels	92
7.2.2	Cell seeding and MTT assay	95
7.2.3	Chondrogenesis Histology	97
7.3	Results and Discussion	98
7.3.1	Cell seeding and MTT	98
7.3.2	Chondrogenesis Histology	102
7.4	Summary	108
Chapter 8	Conclusion and Outlook	109

8.1	Conclusion of this project	109
8.2	Future perspectives.....	111
	<i>Bibliography</i>.....	114
	<i>List of Appendices</i>.....	123

List of Figures

Figure 1-1 The cartilage defect grade system corresponds to the severity level. Reproduced from the ICRS Cartilage Injury Evaluation Package.[11]	4
Figure 1-2 Zonal chondral scaffold design replicating the superficial, middle, and deep zones.	10
Figure 2-1 The illustration depicts the distribution of collagen fibres, chondrocyte morphology and mineral components in the superficial, middle, and deep zones of articular cartilage.[10]	14
Figure 3-1 Schematic outline of the project, showing the experimental components corresponding to the thesis chapters.	17
Figure 4-1 A scheme of the buccal spinneret of the silkworm, image adapted from Ref.[19]; the silk gland structure, image adapted from Ref.[17]; and bioinspired process of spinning mechanism, image adapted from Ref.[16]	22
Figure 4-2 Silk structure silk fibroin coating with a layer of sericin, image adapted from Ref.[19]	23
Figure 4-3 Pre-test of silk cocoon pieces showing failure to obtain continuous fibres.....	26
Figure 4-4 Schematic illustration to demonstrate the degumming process of entire silk cocoons.	28
Figure 4-5 Processing steps for degummed silk fibroin fibres: network expansion, air-drying, and subsequent fibre collection.....	30
Figure 4-6 PVA-based hydrogel with the addition of 2% w/v sericin powder: (A) Hydrogel samples after one freeze-thaw cycle, frozen at -20°C and thawed at room temperature; (B) Photograph of hydrogel samples after three freeze-thaw cycles, with the last two cycles frozen at -80°C and thawed at room temperature.	33
Figure 4-7 Above: Representative image of cell viability in pre-test PVA-sericin hydrogel groups ; below: Quantitative cell viability analysis of cells cultured on PVA hydrogels with varying concentrations. Data presented as mean \pm SD (n = 3) (below).	36
Figure 5-1 Comparison of slow-gelling alginate hydrogels (first three from the left) produced using the CaCO ₃ -GDL method at different concentrations versus the instantaneously crosslinked macroblock formed by CaCl ₂ -alginate (right). Image adapted from Ref.[64]	41
Figure 5-2 Flowchart illustrating the preparation process of alginate hydrogel via CaCO ₃ -GDL internal ionotropic gelation.....	43
Figure 5-3 SEM imaging of pure alginate hydrogel samples fabricated via CaCO ₃ -GDL ionotropic gelation. Cross-sectional morphology of three concentration groups, highlighting CO ₂ -induced porous features (red circles).....	45
Figure 5-4 The photos and graphs illustrate the differences between the original pure alginate hydrogel and the freeze-thawed alginate hydrogel, with the same concentration and composition. Significant differences in stiffness and stretchability are revealed.	47
Figure 5-5 Pure PVA hydrogel in a thin layer (left) and a mould-casting thick hydrogel (right).	48

Figure 5-6 Flowchart illustrating the preparation process of PVA-sericin hydrogel synthesized using the freeze-thaw physical crosslinking method, along with photographs comparing freeze-thawed samples frozen at different temperatures.	50
Figure 5-7 Alginate-based bilayered scaffold. The pure alginate hydrogel forms the cartilage layer, while the bottom mineralised layer was prepared using hydrogel material mixed with hydroxyapatite (HAp) (left) or bioactive glass (right).	53
Figure 5-8 Alginate-PVA double-network crosslinking hydrogel fabricated with three freeze-thawing cycles.	55
Figure 5-9 Combined scaffold showing the pure PVA hydrogel layer at the top (simulating cartilage) and the PVA-alginate-HAp double-network crosslinking hydrogel at the bottom (simulating subchondral bone).	56
Figure 5-10 Tri-layered hydrogel examples and composition confirmation. From left to right: a freshly fabricated tri-layered scaffold, the scaffold under compressive force, and the scaffold in a swollen state after the swelling test.	57
Figure 5-11 Final design of the tri-layered chondral scaffold, including compositions and materials used for each layer.	60
Figure 6-1 Photograph of the swelling test setup, showing 3 groups of hydrogel samples (superficial, middle, and deep layers), each with 4 replicates ($n = 4$).	65
Figure 6-2 Photograph of the degradation test, 3 groups of hydrogel samples with 3 replicates ($n=3$) in each.	66
Figure 6-3 The cross-section SEM images (pre-test). Pure alginate-based hydrogel resembling the cartilage layer (left), and hydrogel with the addition of the hydroxyapatite for the subchondral bone layer (right).	68
Figure 6-4 The PVA-alginate hydrogel forms a double-crosslinked network through a combination of freeze-thaw-induced physical crosslinking and internal ionotropic chemical crosslinking.	69
Figure 6-5 SEM image of the cross-section morphology of the tri-layered scaffold exhibiting three distinct zones.	71
Figure 6-6 SEM images of the superficial-to-middle layer transition (left) and middle-to-deep layer transition (right).	72
Figure 6-7 Swelling behaviour of three hydrogel concentration sets, showing water uptake capacity reflected by the swelling ratio over time (hours) within a total duration of 60 h.	76
Figure 6-8 Comparison of the hydrogel in different states during the swelling test. From left to right: as-prepared hydrogel, fully dried state, and swollen state after PBS immersion.	77
Figure 6-9 Degradation rates of three hydrogel formulations (three separated layers) over 30 days.	79
Figure 6-10 Photos during the compression and tensile mechanical test, pre-test and post-test of the '15%PVA + 2%sericin + aligned silk fibres' superficial hydrogel.	81

Figure 6-11 Compression test results and graphs generated by the instrument of the superficial hydrogel layer.....	82
Figure 6-12 Tensile test results and graphs generated by the instrument for the superficial hydrogel layer.....	82
Figure 6-13 Photos during the compression and tensile mechanical test, pre-test and post-test of the '10% PVA + 1% Alginate' middle hydrogel.	83
Figure 6-14 Compression test results and graphs generated by the instrument of the middle hydrogel layer.....	84
Figure 6-15 Tensile test results and graphs generated by the instrument for the middle hydrogel layer.....	84
Figure 6-16 Photos during the compression and tensile mechanical test, pre-test and post-test of the '5% PVA + 2%Alginate + 5%HAp' deep hydrogel.	85
Figure 6-17 Compression test results and graphs generated by the instrument of the deep hydrogel layer.....	86
Figure 6-18 Tensile test results and graphs generated by the instrument for the deep hydrogel layer.	86
Figure 6-19 Photos during the compression mechanical test, pre-test and post-test of the tri-layered chondral hydrogel scaffold.	87
Figure 6-20 Compression test results and graphs generated by the instrument of the tri-layered chondral scaffold.	87
Figure 6-21 Graph illustrating the compression test results for three individual layers of similar thickness and the combined tri-layered scaffold fabricated through sequential layering.	89
Figure 6-22 Graph depicting the tensile test results for three separated layers of similar thickness.	90
Figure 7-1 Flowchart of the sterilisation protocol for hydrogel samples before biological assessment.	94
Figure 7-2 MTT assay photo shows hydrogel samples in each tested well, with a visible purple colouration after incubation, indicating cell viability.	97
Figure 7-3 Overview: Comparison of cell proliferation levels among different hydrogel formulations, including 15% PVA, 15% PVA + 2% sericin with and without silk incorporation, 10% PVA + 1% alginate composite hydrogel, and 5% PVA + 2% alginate + 5% HAp mineralised hydrogel, on day 4 and day 7.	99
Figure 7-4 Comparison: The impact of sericin incorporation on cell proliferation in 15% w/v PVA-based hydrogels, highlighting increased cell growth from day 4 to day 7.	100
Figure 7-5 Designed Hydrogel Layers: Comparison of cell viability across the three hydrogel layers, indicating a zonal proliferation trend consistent with native cartilage structure.	101

Figure 7-6 H&E-stained sections of the three separated hydrogel layers, indicating cell attachment, distribution, and ingrowth capacity across different layer concentration formulations.	103
Figure 7-7 Toluidine blue-stained sections of the three separate hydrogel layers, indicating the cell growth and ingrowth capacity of each concentration group.	104
Figure 7-8 H&E and toluidine blue-stained images of the cell-seeded tri-layered scaffold, compared with mouse joint cartilage and a blank tri-layered scaffold (without cells).	106
Figure 7-9 Staining and SEM image comparison reflecting tri-layered scaffold integration and structure.	107
Figure 8-1 Tendon-bone model which can further apply textile technique to modify the transitional fibrocartilage zones.	113
Figure 8-2 Future application of silk fibres in tissue engineering for musculoskeletal disease (intervertebral disc)	113

List of Tables

Table 4-1 Summary of main degumming methods for silk cocoons, highlighting their advantages and disadvantages.	25
Table 4-2 Concentration ratios between sericin and PVA (in weight concentration, % w/v).	32
Table 5-1 Mass concentrations of the three components (sodium alginate, calcium carbonate, and glucono- δ -lactone) used in the fabrication of alginate hydrogels.	45
Table 5-2 Concentration designs of Alginate/PVA composite scaffold test.	54
Table 6-1 Hydrogel concentration sets and the corresponding layers in the multizonal chondral scaffold design.....	63
Table 6-2 SEM images of the three layers: superficial, middle, and deep zones, along with their descriptions.	70
Table 6-3 Summary of numerical mechanical test results.	88

List of Abbreviations

3D	Three-dimensional
BMSCs	Bone marrow-derived mesenchymal stem cells
BTE	Bone tissue engineering
CaCl ₂	Calcium chloride
CaCO ₃	Calcium carbonate
CO ₂	Carbon dioxide
DMEM	Dulbecco's Modified Eagle Medium
ECM	Extracellular Matrix
GDL	Glucono- δ -lactone/Gluconolactone
H&E	Hematoxylin and eosin
Ir	Iridium
MTT	3-(4,5-Dimethylthiazol-2-yl)-2,5-Diphenyltetrazolium Bromide
OA	Osteoarthritis
PVA	Polyvinyl alcohol
SA	Sodium alginate
SEM	Scanning electron microscope
TB	Toluidine blue
UV	Ultraviolet

Abstract

Chondral and osteochondral tissues are essential for joint function, providing mechanical support and enabling smooth movement through lubrication. However, the limited self-healing capacity of articular cartilage makes repairing stratified chondral defects particularly challenging. Untreated articular cartilage damage can lead to irreversible joint degeneration and increase the risk of osteoarthritis progression. This project aimed to address these challenges by developing multizonal chondral scaffolds capable of restoring the zonal structure of cartilage tissue. The central hypothesis was that a biomimetic, multilayered scaffold could promote zonal cartilage regeneration. To achieve this, the study focused on designing scaffolds with distinct structural zones and compositional gradients, mimicking the superficial, middle, and deep layers of native cartilage.

A key aspect of the design was the integration of silk fibres, facilitating a transition from a fibrous superficial layer to a porous architecture that enhances cell attachment and growth. Experimental results demonstrated that the multizonal scaffold successfully combined three distinct layers while maintaining cell viability. This research advances cartilage tissue engineering by presenting a biomimetic scaffold design and offers valuable insights into bioactive, biodegradable materials for improved cartilage repair strategies in orthopaedic medicine.

Chapter 1 Background Introduction

Osteochondral and chondral defects and the risk of osteoarthritis: Zonal nature of articular cartilage and biomimetic scaffold experiment in this project

1.1 Classification of Defects and Zonal Articular Cartilage

Chondral and osteochondral injuries frequently lead to osteochondral defects (OCDs) within the joint tissue, typically originating in the articular cartilage region and probably extending into the underlying subchondral bone. OCDs predominantly occur in the knee and ankle joints but are also observed in other anatomical sites such as the hands and spine.[1] Symptomatic cases often present with severe pain, swelling, and impaired mobility, significantly impacting patients' quality of life. Possible aetiology of OCDs can be attributed to genetics, overeating, sedentary lifestyles, microtrauma, post-traumatic arthritis, acute and repetitive sports injuries, ligament instability, meniscus tears, and chronic stress caused by limb axis malalignment. Due to the inherent characteristics of the joint microenvironment, characterised by inadequate blood supply and limited presence of stem/progenitor cells, mature chondrocytes exhibit low metabolic activity and are avascular, resulting in a restricted ability to proliferate and migrate. This diminished capacity for self-repair leaves osteochondral defects vulnerable to altering the distribution of forces within the joint. After an injury or even reconstructive surgery, the critical-sized defect in cartilage has a poor capacity for long-term repair, resulting in tissue degeneration that can lead to the progression of osteoarthritis (OA) and eventually necessitate entire joint replacement.[2] Consequently, the loading forces can accelerate the deterioration of surrounding tissues, potentially culminating in the onset of osteoarthritis and other complex pathological conditions.[3] Articular cartilage thinning and degeneration, joint space narrowing, osteophyte formation, and subchondral bone remodelling all occur as OA progresses.[4]

OA is a leading global cause of chronic disability, frailty, and unhealthy ageing. Patients of all ages are affected, from young athletes with injured joints to elderly people (the most commonly found age range is 60-80 years). According to a 2018 report by the Australian Institute of Health and Welfare, OA is the most common musculoskeletal problem, accounting for 33% of hospital admissions for musculoskeletal conditions in Australia.

In the early stage of OA, prior to substantial tissue degeneration, tissue engineering approaches can be employed to repair cartilage defects and subchondral bone damage to achieve functional restoration and tissue maintenance within the joint. In biomaterials-based tissue engineering, the application of three-dimensional scaffolds (with or without the addition of cells and biological molecules) can support or induce tissue repair and regeneration.[4] Developing biomimetic scaffolds using novel combinations and designs of biomaterials is a promising approach for the restoration of osteochondral injuries to restore joint anatomy and function and prevent further joint degeneration or the development of OA. In addition, recent research has highlighted that the most significant challenge towards osteochondral bone tissue engineering is the reconstruction of zonal cartilage layers ('chondral tissue').

Anatomically, within a joint, the bone surface is covered with a thin layer of articular (hyaline) cartilage, which serves as lubrication during movement and supports the distribution of loading forces to the subchondral bone. Thus, without adequate treatment, or if treatment is suboptimal, there is a heightened risk of symptom exacerbation and progression to osteoarthritis, resulting in severe chronic pain and disability.

Cartilage lesion grade is a vital sign in determining the appropriate treatment, which is classified based on severity, with each defect grade having its own corresponding treatment plan and pain management. Following the standards of the International Cartilage Repair Society Classification (ICRSC), Cartilage defects can be classified into four levels. The ICRS Grades 1-3 are known as 'chondral tissue defect'. [5-7] In Grade 3, the cartilage lesion extends down to more than 50% of the thickness, but it does not reach the subchondral bone. Osteochondral defects (OCD) typically refer to the most severe form of cartilage and bone defect identified as Grade 4, characterised by the complete loss of cartilage, including articular and calcified cartilage, with the defect eventually tearing down to the subchondral bone.[8] Osteochondral defects can significantly aggravate joint symptoms, such as locking or catching the joint. These defects can considerably impact a person's quality of life and physical activity. In this review, both the Grade 3 full-thickness cartilage defects and the Grade 4 osteochondral defects models are considered, which are classified as 'Severely Abnormal', requiring full-layer reconstruction to relieve pain and prevent secondary arthritis.[9]

In accordance with the standards of the International Cartilage Repair Society Classification (ICRSC), cartilage defects can be classified into four levels. In this thesis, both the Grade 3 full-thickness cartilage defects and the Grade 4 osteochondral defects, which are classified as ‘Severely Abnormal’ (**Figure 1-1**) are taken into consideration. Cartilage lesion grade is a vital sign in determining the appropriate treatment, which is classified based on severity, each with its own corresponding treatment plan and pain management.

The ICRS Grades 1-3 are known as chondral tissue defects. In Grade 3, the cartilage lesion extends down to more than 50% of the thickness, but it does not reach the subchondral bone. Grade 3 defects signified the full-thickness damage of articular cartilage, indicating that the cartilage covering is completely damaged and can vary in size and shape with respect to the specific location and extent of the cartilage loss within the joint. Besides, Grade 3 chondral defects can progress in severity over time if left unrepaired, potentially leading to joint diseases, as patients can experience joint pain, swelling, and limited function.

Osteochondral defects (OCD) typically refer to the most severe form of cartilage and bone defect identified as Grade 4, which involves a tear and defect disruption across the depth of the entire chondral tissue and further exposure of the subchondral bone. Osteochondral defects can significantly aggravate joint symptoms such as locking or catching of the joint. These defects can have a considerable impact on the quality of life and physical activity of the patient.

The primary cause of the delayed cartilage extracellular matrix (ECM) turnover is the inadequate supply of blood and stem or progenitor cells. This happens because mature chondrocytes, with low metabolic activity, are avascular and have a restricted ability to proliferate and migrate. Without the capability to repair itself quickly, empty osteochondral defects can alter the distribution of forces on the joint, and the loading forces can accelerate the destruction of surrounding tissues, further progressing to osteoarthritis and other complicated diseases. With a potential risk of severe pathologies, regenerative medicine faces a significant challenge, indicating that cartilage damage will worsen and remain unfilled and impaired over time, in addition to the fact that regenerative capacity itself decreases with age.

Therefore, a major unmet need is the development of strategies to repair cartilage defects, restore ECM function, and recover joint mobility rapidly and effectively. This project addresses this challenge by considering the depth and zonal involvement of cartilage lesions. Articular cartilage is a complex, multilayered tissue with distinct structural and functional zones, each contributing to its load-bearing and low-friction properties. Its heterogeneous composition, varying in porosity, mechanical strength, and biochemistry, poses a key hurdle in tissue engineering, particularly for designing multizonal scaffolds that replicate its hierarchical organisation.[10]

To achieve functional regeneration, scaffold design is expected to account for zonal-specific properties, such as nanofibrous architecture, gradient pore distribution, and biomechanical cues. The following sections detail the zonal characteristics of cartilage and osteochondral tissue, the limitations of current repair strategies, and the potential of advanced biomaterials and scaffolding techniques, the central focus of this study.

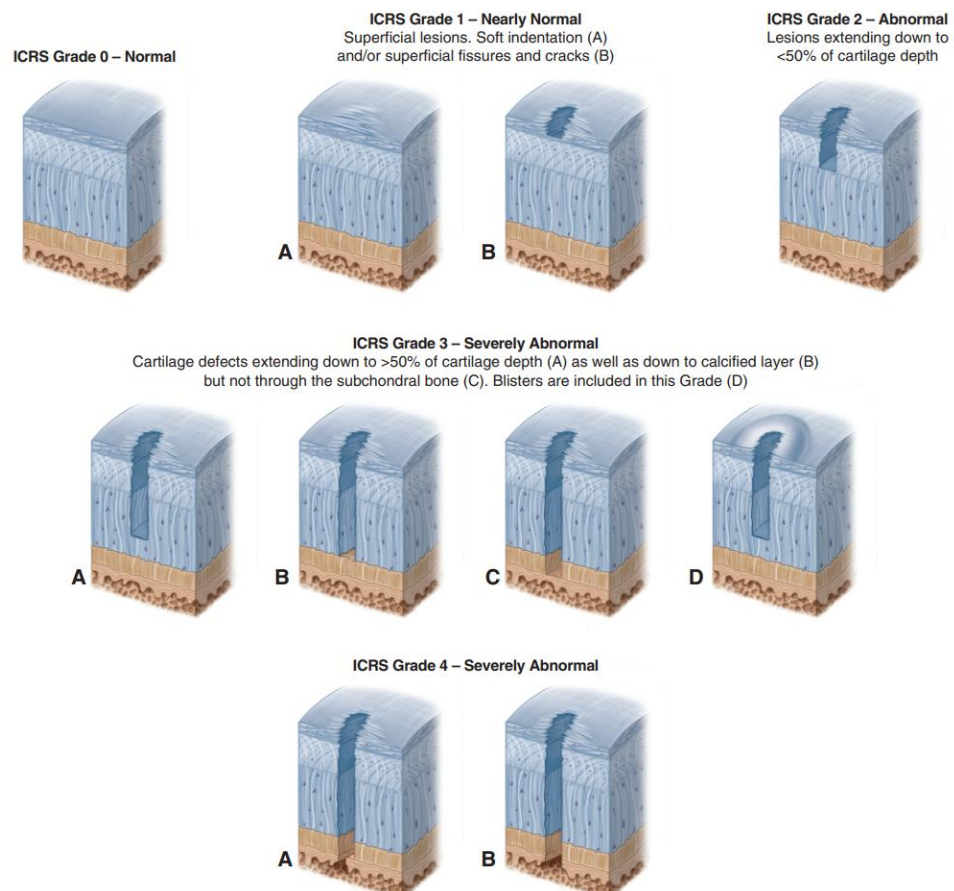


Figure 1-1 The cartilage defect grade system corresponds to the severity level. Reproduced from the ICRS Cartilage Injury Evaluation Package.[11]

1.2 Concept of Biomimetic Scaffolds

In recent years, tissue-engineering methods have garnered significant attention, employing a combination of biomaterials, scaffolds, and biomolecules to rejuvenate diseased or injured osteochondral tissues, notably in treating osteochondral defects (OCDs).[12; 13] At the forefront of this innovation is the development of biomimetic scaffolds, engineered materials designed to replicate the natural extracellular matrix (ECM) of zonal cartilage and bone. Biomimetic scaffolds are inspired by the intricate architecture and biochemical composition of native tissues. They are designed to resemble the structural and functional properties of the ECM, providing a conducive environment for cellular activities crucial for tissue repair. The ECM is a complex network of proteins, glycoproteins, and proteoglycans that provide mechanical support and regulate various cellular functions. For chondral tissue repair, an ideal scaffold is expected to possess a hierarchical structure that can guide the regeneration of both stratified cartilage and subchondral bone, often necessitating a biphasic or multiphasic design. These scaffolds aim to support cell adhesion, proliferation, and differentiation, facilitating the repair and regeneration of damaged tissues. Advancements in biomaterials and fabrication technologies have propelled the development of implantable constructs, offering promising avenues for improving clinical outcomes.[3] However, the regeneration and reconstruction of osteochondral defects remain formidable challenges in tissue engineering and orthopaedic surgery due to the intricate hierarchical structure of osteochondral tissue.[14] Key hurdles include the creation of bioactive scaffolds capable of accurately mimicking the natural structure and functionality of regional osteochondral tissue, including the zonal articular cartilage.

The designed scaffold should have biocompatible and matched mechanical properties, and the key characteristics of effective biomimetic scaffolds are:

- **Biocompatibility and biodegradability:** Scaffolds must be biocompatible to avoid adverse immune responses, and their degradation rate must match the rate of tissue regeneration to ensure that the scaffold provides temporary support during the formation of new tissue.

- Porosity and pore interconnectivity: High porosity and interconnected pores are essential for nutrient diffusion, waste removal, and vascularisation, which are crucial for tissue viability and integration.
- Mechanical properties: The mechanical properties of the scaffold are expected to match those of the target tissues. In osteochondral applications, this typically requires a stiffness gradient that transitions from softer, cartilage-like regions to stiffer, bone-like regions.
- Surface properties: The scaffold surface is supposed to promote cell adhesion and proliferation. In this project, this was achieved by incorporating aligned silk fibres to guide cell attachment and growth.

Previous studies often focused on homogeneous structures that simplified chondral tissue, failing to replicate the zonal and stratified properties of cartilage, including the superficial, middle, and deep zones. Many multizonal scaffolds also lack seamless integration between zones, leading to potential delamination under mechanical stress. Additionally, their compressive and tensile moduli often fall short of the values observed in native tissue. Furthermore, the degradation rates of multizonal scaffolds often vary between layers and fail to align with the timeline of tissue regeneration, resulting in either premature loss of mechanical support or delayed degradation.

Hence, the aim of current research is to design a multizonal scaffold using simple methods to produce a multizonal architecture comprising superficial, middle, and deep layers whilst maintaining a smooth transition between layers.

1.3 Research Hypothesis & Aims

The central hypothesis of this project is that the novel multizonal scaffolds designed to replicate the hierarchical zonal structure and biochemical composition of native articular cartilage extracellular matrix can effectively support the reconstruction and regeneration of chondral defects.

Aim 1: To design and fabricate multizonal scaffolds containing the cartilage zones

Design and fabricate gradient scaffolds with bioactive hydrogel layers to regenerate the zonal compartments of articular cartilage. This includes optimising material

combinations, gel solution concentrations, and scaffold architecture (e.g., pore size, geometry) to mimic the layered structure and composition of native articular cartilage.

Incorporate mineral content (e.g., hydroxyapatite) or other bioactive components to replicate the calcified cartilage zone and transition to subchondral bone, ensuring a smooth gradient and mechanical support at the weight-bearing site.

Aim 2: To assess the physical and mechanical properties of the scaffolds

Develop technology for constructing the zonal chondral scaffold by combining the cartilage hydrogel layer and bone scaffold compartments, ensuring that the scaffold mimics the structure and properties of native chondral and osteochondral tissue while having strong integration between the zonal cartilage compartments without risk of delamination.

Further assessment of the physical characterisations, including pore size measurement, degradation rate, and swelling ratio of scaffolds. Assess the mechanical and biological properties of the multizonal scaffold, and separately assess cartilage zonal compartments, along with the scaffold. The mechanical tests are expected to include compression testing to measure the stiffness of fabricated hydrogel scaffolds and tensile testing to evaluate the ability of the material to withstand stretching or pulling forces.

Aim 3: To assess the *in vitro* biological properties of the scaffolds, including cell viability and ability to support zonal cartilage regeneration

Biological testing will be conducted using human bone marrow-derived stem cells (BMSCs) to evaluate cell-material interactions, including cell adhesion, proliferation, and differentiation. Investigate the capacity of multizonal scaffolds to provide an adequate structure for supporting cell growth towards cartilage repair.

1.4 Research Questions & Objectives of this Thesis

1.4.1 Research questions

This thesis attempts to interpret the novel designs of multiphase scaffolds, the innovative use of biomaterials in scaffold fabrication, the details of the material compositions, and the role of fibrous materials in mimicking the orientation of natural collagen fibres across

zones within the articular cartilage region. Through the exploration of architecture design, materials used and manufacturing methods, this project aims to provide the design model for applicable scaffolds in osteochondral defect repair. Besides, to date, despite the fact that emerging designs have applied complex materials and devices to scaffold fabrication, there are still knowledge gaps regarding the feasibility of clinical applications and sizing for human use.

To achieve these goals, this project conducted two experiments exploring materials such as alginate and PVA-based hydrogels and the incorporation of cocoons and fibres into scaffold designs using a simple casting method. To guide the investigation and ensure a comprehensive understanding of the potential of biomimetic scaffolds in repairing osteochondral defects, the following research questions will be addressed in this thesis:

- Research Question 1: What are the optimal design parameters (e.g., Materials used, fabrication procedures) for a multiphasic biomimetic scaffold that can effectively replicate the hierarchical structure of chondral and osteochondral tissue?
- Research Question 2: Can the scaffold maintain its structural integrity under physiological load conditions during the tissue regeneration process? What are the mechanical properties of the biomimetic scaffold compared to those of native cartilage zones?
- Research Question 3: How do cells interact with the scaffold in terms of adhesion, proliferation, and differentiation?

A further assessment of the comparison with existing treatments is then made: How does the performance of the biomimetic scaffold compare with current standard treatments for cartilage and osteochondral defects, such as microfracture and osteochondral autograft transfer? And evaluate the potential advantages and limitations of using biomimetic scaffolds over traditional methods in terms of long-term outcomes and patient recovery. By addressing these questions, the research aims to validate the efficacy of biomimetic scaffolds in osteochondral repair and provide a foundation for their potential clinical application.

1.4.2 Objectives of this Thesis

The primary aim of this thesis is to explore the development, characterisation, and application of biomimetic scaffolds for repairing cartilage and osteochondral defects. To achieve this, the research will be guided by the following specific objectives:

- Review of current strategies: To review the existing strategies and their disadvantages in cartilage and osteochondral defect repair.
- Design and development of biomimetic scaffolds: To design a multiphasic scaffold that mimics the hierarchical structure of zonal articular cartilage and transitional osteochondral tissue and provides a similar microenvironment and properties. For instance, the scaffold is expected to achieve a layered structure as shown in **Figure 1-2** to mimic regional cartilage. To select and optimise the use of materials and fabrication techniques that ensure the scaffold possesses appropriate mechanical properties, porosity, and surface characteristics.
- Characterisation of scaffold properties: Assess the mechanical properties of the scaffolds, including compression, tension and shear, and compare these properties with those of native cartilage and bone. To assess the structural integrity and porosity of the scaffold using imaging techniques such as scanning electron microscopy (SEM).
- Biocompatibility and biodegradation studies: To investigate the biocompatibility of the scaffold through *in vitro* studies such as cell viability, adhesion, proliferation, and differentiation.
- Investigating the ability of the different scaffold layers to support cell activities relevant to cartilage repair by conducting *in vitro* experiments using human BMSCs.

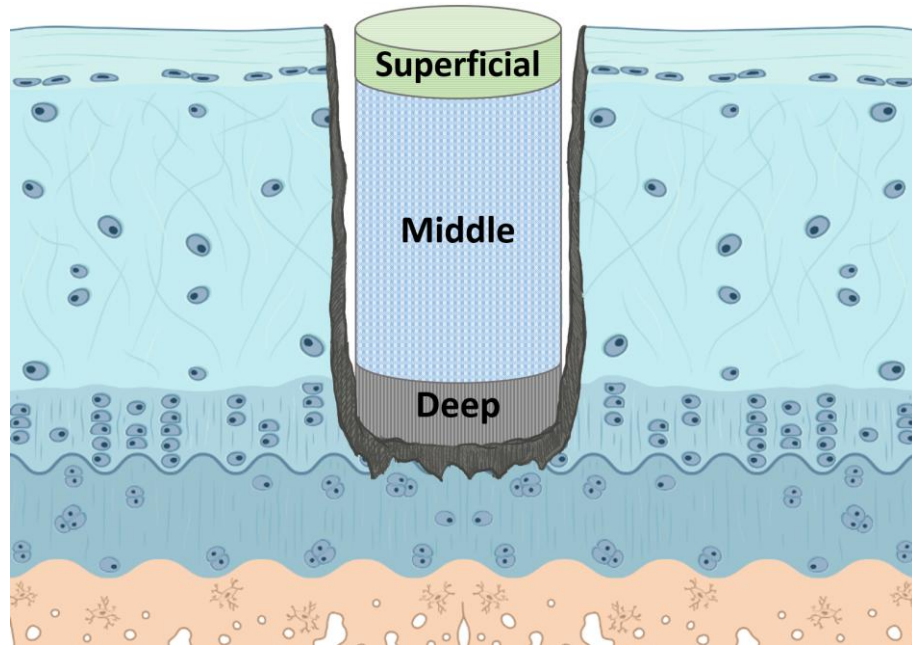


Figure 1-2 Zonal chondral scaffold design replicating the superficial, middle, and deep zones.

1.5 Significance of the Study

Zonal cartilage reconstruction remains a significant challenge, particularly in cases of Grade 3 full-thickness damage, which involves damage to multiple cartilage zones. This presents a major hurdle in the field of orthopaedic medicine. This project addresses this challenge by utilising non-complex, up-scalable fabrication technologies that do not require sophisticated equipment.

Given the critical roles of cartilage and bone in joint function and mobility, untreated cartilage defects can lead to chronic pain, impaired movement, and a diminished quality of life. Current treatment strategies, such as microfracture, autologous chondrocyte implantation, and osteochondral autograft transfer, often yield suboptimal results, particularly in the long-term regeneration of hyaline cartilage. In the field of scaffold therapy, the regeneration and repair of osteochondral defects remain major challenges in tissue engineering and orthopaedic surgery due to the complex structure of cartilage tissue.[14]

This project aims to provide insights to advance the field of biomaterials and tissue engineering. For instance, by creating hydrogel scaffolds with zonal structures, this project will enhance knowledge in cartilage tissue engineering. By producing bioactive

and biodegradable gradient or multilayered scaffolds, it will push the frontiers of load-bearing applications. Moreover, the knowledge and technological advances developed through this project are not limited to the reconstruction of zonal cartilage tissue but can also benefit the tissue engineering of other tissues with interfacial or hierarchical properties, such as intervertebral discs, tendons, and skeletal muscle.

Chapter 2 Literature Review

This Chapter reviews the challenges and limitations of current treatment strategies, emphasising the distinct, naturally layered structure of articular cartilage and the entire osteochondral tissue. Additionally, it reviews scaffold-based approaches for osteochondral defect repair, highlighting critical aspects of scaffold design, including fibre orientation, porous architecture, incorporation of cells and growth factors, and notable innovative features. Furthermore, a concise overview of the regulatory framework is presented owing to the prospective clinical and biomedical applications of biomimetic scaffolds.

Published Literature:

Lin, X., Zhang, Y., Li, J., Oliver, B. G., Wang, B., Li, H., Yong, K.-T., & Li, J. J. (2025). Biomimetic multizonal scaffolds for the reconstruction of zonal articular cartilage in chondral and osteochondral defects. *Bioactive Materials*, 43, 510-549. <https://doi.org/10.1016/j.bioactmat.2024.10.001>

Acknowledgements (Chapter 2)

The review paper titled 'Biomimetic multizonal scaffolds for the reconstruction of zonal articular cartilage in chondral and osteochondral defects' is included in this Chapter, authored by Xiaohu Lin as the first author under the supervision of Dr. Jiao Jiao Li. I would like to acknowledge the contributions of the following co-authors who assisted in drafting and constructing this review article:

- Ye Zhang: Writing – review & editing, Writing – original draft, Investigation, Formal analysis.
- Jiarong Li: Writing – review & editing, Writing – original draft, Investigation, Formal analysis.
- Brian G. Oliver: Writing – review & editing, Formal analysis.
- Bin Wang: Writing – review & editing, Formal analysis.
- Haiyan Li: Writing – review & editing, Supervision, Formal analysis.

- Ken-Tye Yong: Writing – review & editing, Supervision, Formal analysis.
- Jiao Jiao Li: Writing – review & editing, Writing – original draft, Supervision, Methodology, Investigation, Formal analysis, Conceptualization.

2.1 Overview

As shown in **Figure 2-1**, the ‘zonal structure’ of articular cartilage highlights factors including collagen fibre orientation, chondrocytes morphology and densities, and the distribution of mineral content. This ‘zonal’ definition forms the basis of this thesis and guides the experimental chapters, which aim to reconstruct and mimic these distinct zonal properties to replicate the native tissue architecture and microenvironment. Ultimately, this approach supports the effective repair of chondral and osteochondral defects.

This review outlines and highlights the relationship between zone-specific functions and structural differences. These include the orientation of collagen fibres and the distribution of mineral content, both of which play critical roles in providing mechanical support and maintaining the gradient stiffness required at the defect site. The selected studies reviewed span from hydrogels designed for articular cartilage regeneration to multiphasic scaffolds that include the calcified cartilage zone and its interface with the subchondral bone. These studies contribute to a field focused on mimicking the native zonal organisation of articular cartilage, with increasing efforts directed toward integrating multiple layers into a single scaffold for comprehensive osteochondral repair.

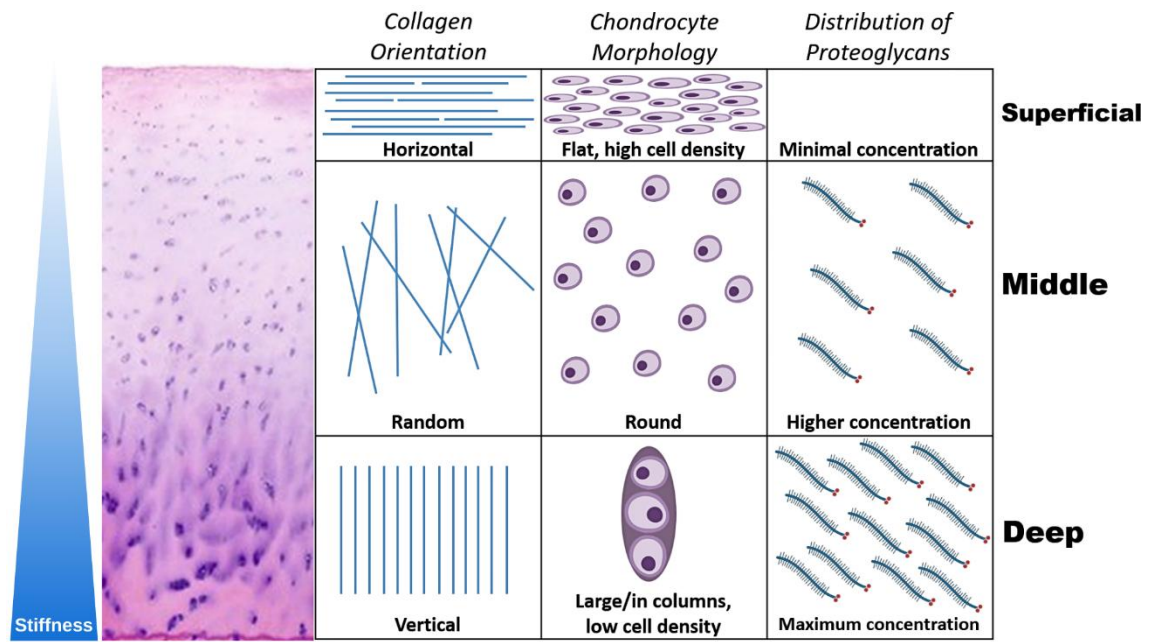


Figure 2-1 The illustration depicts the distribution of collagen fibres, chondrocyte morphology and mineral components in the superficial, middle, and deep zones of articular cartilage.[10]



Review article

Biomimetic multizonal scaffolds for the reconstruction of zonal articular cartilage in chondral and osteochondral defects

Xiaoqi Lin^a, Ye Zhang^b, Jiarong Li^a, Brian G. Oliver^{b,c}, Bin Wang^d, Haiyan Li^e, Ken-Tye Yong^f, Jiao Jiao Li^{a,c,*}

^a School of Biomedical Engineering, Faculty of Engineering and IT, University of Technology Sydney, NSW, 2007, Australia

^b School of Life Sciences, Faculty of Science, University of Technology Sydney, NSW, 2007, Australia

^c Woolcock Institute of Medical Research, Macquarie University, Macquarie Park, NSW, 2113, Australia

^d Department of Orthopaedic Surgery, The First Affiliated Hospital, Zhejiang University School of Medicine, Hangzhou, 310006, China

^e Chemical and Environmental Engineering Department, School of Engineering, STEM College, RMIT University, Melbourne, VIC, 3000, Australia

^f School of Biomedical Engineering, Faculty of Engineering, The University of Sydney, Sydney, NSW, 2006, Australia

ARTICLE INFO

Keywords:

Cartilage tissue engineering

Zonal cartilage

Osteochondral scaffolds

Multizonal scaffolds

Biomimetic scaffolds

ABSTRACT

Chondral and osteochondral injuries are frequently encountered in clinical practice. However, articular cartilage has limited self-healing capacity due to its sophisticated zonal structure and avascular nature, introducing significant challenges to the restoration of chondral and osteochondral tissues after injury. Improperly repaired articular cartilage can lead to irreversible joint damage and increase the risk of osteoarthritis progression. Cartilage tissue engineering using stratified scaffolds with multizonal design to match the zonal structure of articular cartilage may help to meet the complex regeneration requirements of chondral and osteochondral tissues, and address the drawbacks experienced with single-phase scaffolds. Navigating the heterogeneity in matrix organisation and cellular composition across cartilage zones is a central consideration in multizonal scaffold design. With emphasis on recent advances in scaffold design and fabrication strategies, this review captures emerging approaches on biomimetic multizonal scaffolds for the reconstruction of zonal articular cartilage, including strategies on replicating native tissue structure through variations in fibre orientation, porous structure, and cell types. Exciting progress in this dynamic field has highlighted the tremendous potential of multizonal scaffolding strategies for regenerative medicine in the recreation of functional tissues.

1. Introduction

Chondral and osteochondral injuries frequently lead to osteochondral defects (OCDs) within the joint tissue, typically originating in the articular cartilage and may extend into the underlying subchondral bone. OCDs predominantly occur in the knee and ankle joints, but are also observed in other anatomical sites such as the hands and spine [1]. Symptomatic cases often present with severe pain, swelling, and impaired mobility, significantly impacting patients' quality of life. Possible aetiology of OCDs includes genetics, overeating, sedentary lifestyle, microtrauma, post-traumatic arthritis, acute and repetitive sports injuries, ligament instability, meniscus tears, and chronic stress caused by limb axis malalignment. Studies have shown a higher incidence of knee OCDs among athletes compared to the general population,

with more than half of asymptomatic athletes showing full-thickness defects [2]. Meanwhile, osteochondritis dissecans is more prevalent in individuals aged 10 to 20, with higher occurrence in males [3]. Anatomically, within a joint, the bone surface is covered with a thin layer of articular (hyaline) cartilage, which serves as lubrication during movement and supports the distribution of loading forces to the subchondral bone [4]. Due to the inherent characteristics of the joint microenvironment, characterised by limited blood supply and availability of stem/progenitor cells, mature chondrocytes exhibit low metabolic activity and restricted ability to proliferate and migrate [5]. After cartilage injury and even with reconstructive surgery, critical-sized chondral or osteochondral defects have poor capacity for long-term repair. This diminished self-repair capacity leaves OCDs vulnerable to weight bearing, leading to altered force distribution within the joint that

Peer review under responsibility of KeAi Communications Co., Ltd.

* Corresponding author. School of Biomedical Engineering, Faculty of Engineering and IT, University of Technology Sydney, NSW, 2007, Australia.

E-mail address: jiaojiao.li@uts.edu.au (J.J. Li).

<https://doi.org/10.1016/j.bioactmat.2024.10.001>

Received 30 May 2024; Received in revised form 2 September 2024; Accepted 1 October 2024

Available online 11 October 2024

2452-199X/© 2024 The Authors. Publishing services by Elsevier B.V. on behalf of KeAi Communications Co. Ltd. This is an open access article under the CC BY-NC-ND license (<http://creativecommons.org/licenses/by-nc-nd/4.0/>).

can accelerate the deterioration of tissues surrounding the defect, potentially culminating in the onset of joint pathology [6]. The combination of tissue damage and biomechanical instability often results in irreversible tissue degeneration and the progression of osteoarthritis (OA) [7]. Without curative treatment, OA causes severe chronic pain and disability due to structural joint damage characterised by articular cartilage thinning and degeneration, joint space narrowing, osteophyte formation, and subchondral bone remodelling, eventually necessitating total joint replacement although this surgery is associated with many complications [8].

Cartilage lesion grade is critical in determining the appropriate treatment and pain management plan. According to the International Cartilage Repair Society Classification (ICRSC), cartilage defects are classified into four grades based on severity. ICRS Grades 1–3 are known as ‘chondral tissue defect’ [9–11]. In Grade 3, the lesion extends to more than 50 % of the cartilage thickness, but it does not reach the subchondral bone. OCDs belong to the most severe form of defect identified as Grade 4, characterised by the complete loss of articular and calcified cartilage accompanied by extension of the defect down to the subchondral bone [12]. In this review, both the Grade 3 full-thickness cartilage defects and the Grade 4 osteochondral defects are considered, which are classified as ‘Severely Abnormal’ requiring full-layer reconstruction to relieve pain and prevent secondary arthritis [13].

Current clinical methods of chondral and osteochondral repair present numerous drawbacks, often resulting in limited applicability or suboptimal long-term outcomes, necessitating the development of emerging tissue engineering strategies based on multiphasic scaffolds to improve repair outcomes [14,15]. Advances in biomaterials and fabrication technologies have propelled the development of implantable biomimetic scaffold constructs, offering promising avenues for improving clinical outcomes in osteochondral repair [6]. However, the intricate hierarchical structure of osteochondral tissue, incorporating stratified layers with variations in cell type and morphology, matrix composition and arrangement, and biomechanical properties pose significant challenges to regeneration using scaffold-based approaches [16]. Key hurdles include the creation of bioactive scaffolds capable of accurately mimicking the natural structure and functionality of different osteochondral tissue regions, particularly the zonal architecture of articular cartilage.

The development of biomimetic scaffolds utilising novel combinations and designs of biomaterials has emerged as a promising approach for the treatment of osteochondral injuries [17–19]. Biomimetic scaffolding strategies aim to restore joint anatomy and function by mimicking the natural composition and structure of osteochondral tissue, thereby preventing further joint degeneration or the development of OA. A number of recent studies have highlighted the advantages of regenerating full-thickness cartilage or osteochondral defects using multizonal scaffolds in animal models. By providing a more biomimetic structure with zonal variations in scaffold properties that better matched native tissues, multizonal scaffolds tested in rabbit osteochondral defects were found to achieve improved defect filling and integration with host tissues [20], more faithful reconstruction of hyaline-like cartilage with zone-specific variations in cells and ECM [21], and simultaneous regeneration of cartilage and subchondral bone accompanied by a more wear-resistant articulating surface [22], compared to single-layer scaffolds without a multizonal design. Biomimetic multizonal scaffolds, particularly those that specifically replicate the zonal variations seen in native articular cartilage, are an emerging direction for the effective treatment of chondral and osteochondral injuries.

Although other reviews have captured biomimetic scaffolding strategies for the repair of osteochondral tissues, such as multiphasic and gradient scaffolds [14–16,23], they focused on studies that attempted to replicate the whole osteochondral unit. Despite heterogeneous naming conventions including ‘multiphasic’, ‘multilayered’, ‘multizonal’, and ‘gradient’, these reviews tended to focus on scaffolds that treated the articular cartilage as a bulk tissue rather than differentiating among the

superficial, middle, and deep cartilage zones. The zonal architecture of articular cartilage introduces significant vertical heterogeneity in biophysical, biochemical, and cellular properties along the cartilage compartment of osteochondral tissue, which is a critical consideration for successful osteochondral reconstruction. In light of this, our review will provide a comprehensive evaluation of the current studies on constructing biomimetic chondral and osteochondral scaffolds, which specifically focused on faithfully replicating the zonal structure of articular cartilage. Our definition of ‘multizonal’ scaffolds in the rest of this review refers to scaffolds that attempted to mimic zonal cartilage architecture by incorporating different scaffold regions to match the superficial, middle, and deep cartilage zones. Diverging from the prevalent use of homogeneous hydrogels in existing research on cartilage tissue engineering, our review captures the latest research on a diverse range of scaffolding approaches to recreate the hierarchical structure of zonal articular cartilage.

This review will first briefly introduce the zonal organisation of articular cartilage and conventional treatment approaches, followed by an examination of biomimetic approaches for designing chondral and osteochondral scaffolds. It will then delve into the current scaffolding strategies that have specifically tried to recreate the zonal structure of articular cartilage, focusing on multizonal cartilage scaffolds incorporating design features such as fibre orientation, gradient composition and porous architecture, and the possible inclusion of cells and growth factors. This comprehensive review provides fresh insights into designing biomimetic zonal scaffolds for cartilage tissue engineering, and how these can be optimised to address a critical need in the realm of osteochondral tissue repair.

2. Characteristics of articular cartilage and current treatment approaches

2.1. Zonal articular cartilage and regional osteochondral hierarchy

Osteochondral tissue consists of articular cartilage (‘chondral region’) and underlying subchondral bone (‘osseous region’) [24]. As illustrated in Fig. 1A, native osteochondral tissue can be divided into three distinct but integrated layers: articular cartilage, calcified cartilage (interface or transition region between cartilage and bone), and subchondral bone (mainly trabecular bone) [25]. Within the chondral region, articular cartilage exhibits a transitional composition characterised by superficial, middle, and deep zones. Osteochondral tissue in different zones and regions exhibits different cellular and matrix compositions as well as unique structural and mechanical characteristics.

Articular cartilage, covering articular joint surfaces and comprising hyaline cartilage tissue, exhibits elastic properties and remarkable resistance to compression. Its smooth surface provides optimal lubrication, making it a crucial covering for the epiphyseal surface of joints that plays a vital role in supporting and cushioning the human body during movement. The thickness of articular cartilage varies depending on its location within the joint and the age of the individual. On average, it has a pore size of 6 nm, with normal thickness ranging 2.41 ± 0.53 mm [25]. Structurally, articular cartilage is a horizontally stratified tissue characterised by heterogeneity and anisotropy. This multilayered composition consists of superficial, middle, and deep zones, distinguished by variations in glycosaminoglycan (GAG) and collagen content and differences in collagen fibril orientation and cell density [26], as depicted in Fig. 1B. The superficial zone comprises 10–20 % of the total thickness, with densely packed, thin, aligned collagen fibres parallel to the cartilage surface. This zone has the lowest GAG concentration and highest permeability, with chondrocytes that are flat and tightly packed. The middle zone represents 40–60 % of the thickness, characterised by thick collagen fibres, arcades linked by smaller diameter fibres, and a higher concentration of GAGs. Chondrocytes are rounded and randomly distributed in this zone. The deep zone, accounting for 30–40 % of

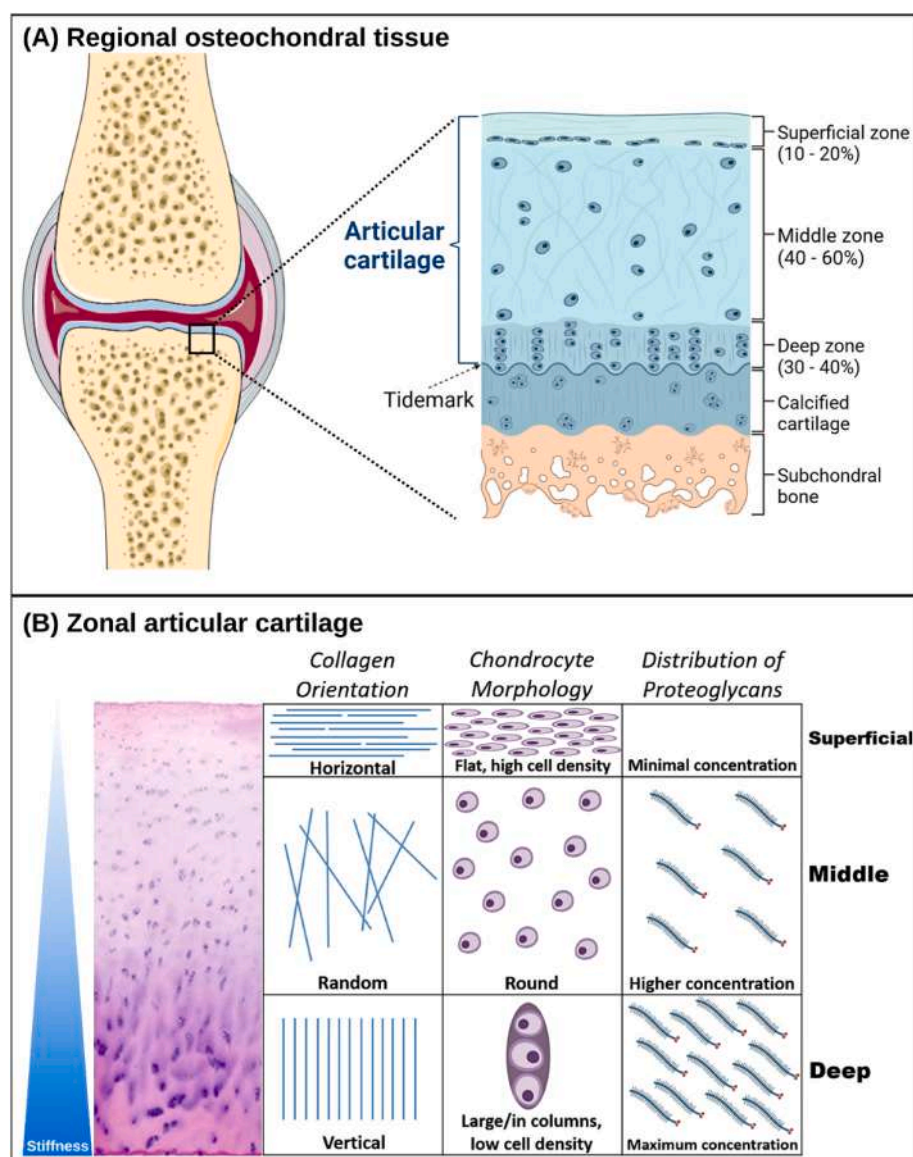


Fig. 1. Natural hierarchical structure of osteochondral tissue. **(A)** Organisation of osteochondral tissue regions. **(B)** Zonal structure of articular cartilage with variations in collagen fibril distribution, chondrocyte morphology, and mineral composition in the superficial, middle, and deep zones. Figure created using Microsoft PowerPoint.

cartilage thickness, features arranged collagen fibres and elongated chondrocytes perpendicular to the tidemark. It holds the highest GAG concentration but the lowest cell density, with low permeability and no fluid flow. The natural composition gradient, including collagen type and mineral content variations, imparts gradient biomechanical properties to the articular cartilage. Consequently, an increase in tissue depth from the superficial to deep layers is accompanied by a corresponding progressive increase in mechanical stiffness.

Between the hyaline articular cartilage and the subchondral bone, the calcified cartilage region is a transitional intermediate layer delimited by the upper tidemark and the lower cement line. Calcified cartilage contains dispersed, hypertrophic chondrocytes within lacunae in the calcified matrix, comprising collagen type I, sodium hyaluronate, and nanohydroxyapatite in varying proportions. Compared to adjacent regions, calcified cartilage exhibits transitional properties, with a lower content of collagen type II than articular cartilage and lower concentration of hydroxyapatite inorganic mineral than subchondral bone [27]. It hence endows osteochondral tissue with transitional mechanical properties characterised by a continuous increase in stiffness from top to

bottom that minimises shear stress ('stiffness gradient'). In addition, calcified cartilage acts as a barrier that limits diffusion and inhibits vascular invasion from the subchondral bone, thereby helping to preserve the structure and function of articular cartilage, while also allowing the transport of small solutes from the subchondral circulation to nourish the deeper cartilage regions. Articular cartilage hence derives its nutrients from both the superficial synovial fluid and the underlying subchondral bone.

The subchondral bone is the region with the highest mechanical strength, allowing the joint to withstand stress and absorb shock, and facilitating nutrient delivery through its rich vascular network. Subchondral bone comprises a diverse array of cells, with osteocytes being the predominant type (constituting 90–95 %), and plays a pivotal role in regulating bone formation (by osteoblasts) and bone resorption (by osteoclasts) as well as maintaining bone homeostasis. Structurally, the subchondral bone is akin to cancellous or trabecular bone, characterised by a spongy architecture with interconnected large pores. Its porosity typically ranges from 75 to 90 %, with pore sizes varying between 50 and 300 μm [28].

2.2. Existing clinical treatments for cartilage restoration

Clinical treatments for full-thickness chondral and osteochondral defects are limited, generally involving microfracture drills and tissue transplantation using osteochondral autografts or allografts. However, these treatments are only applicable for small-to mid-sized lesions [29]. A critical-sized cartilage/osteochondral defect in humans is usually defined as ≥ 3.0 cm in diameter [30]. Clinical cases of osteochondral injuries vary widely in defect area, but have been estimated to have an average size of 4.1 cm^2 [25], and may exceed the repairable size range using tissue transplantation. Moreover, tissue grafts usually only help to relieve symptoms such as pain, but do not actually promote osteochondral tissue regeneration. The lack of long-term effectiveness of existing therapies, particularly for extensive osteochondral injuries, drives research towards exploring more innovative strategies. Unlike conventional treatments, scaffold-based cartilage tissue engineering can provide a temporary 3D structure to reconstitute the structure and function of the native cartilage extracellular matrix (ECM), substituting the anatomy, mechanical properties, and biochemical composition of the damaged tissue and creating an environment that is conducive to cellular repair processes.

2.2.1. Non-surgical strategies

Non-surgical strategies for cartilage and osteochondral repair include non-pharmacological management, pharmacological management, and orthobiologics. Non-pharmacological interventions often involve exercises, weight management, physical therapy, and resistance training [31,32]. Braces and other orthoses may be used to provide structural support, aiming to alleviate pain and enhance joint function [32]. However, these approaches are aimed at palliative care, where the patient has little or no prospect of a cure and only derives symptomatic relief.

Pharmacological management options may include oral supplements, steroid injections, injectable viscosupplements, and other drug therapies with the central aim of providing pain relief [32]. However, these have potential to induce severe side effects, including renal, cardiovascular, and gastrointestinal injuries [33], particularly in older patients who are often affected by multiple chronic conditions and polypharmacy becomes an issue. Oral supplements often comprise the commonly applied non-steroidal anti-inflammatory drugs (NSAIDs), which inhibit cyclo-oxygenase activity and stimulate anti-inflammatory, anti-depressant and analgesic effects [34]. However, in addition to the risk of causing acute kidney injury and stroke, the clinical efficacy of oral supplements such as NSAIDs has been variable, with mixed results reported in studies evaluating their effectiveness [35]. Steroid injections have been used in joint injuries to reduce pain and improve function due to their local anti-inflammatory effects. However, they typically provide short-term benefits and are best suited for acute pain onset in cartilage injuries or early OA [32]. Side effects are commonly experienced after injection such as injection site pain, elevated blood glucose, and skin atrophy [36]. Meanwhile, injectable viscosupplements such as high molecular weight hyaluronic acid (HA) base on the rationale that they may help to enhance joint lubrication by improving viscoelasticity, as well as provide anti-inflammatory effects [37]. However, they have shown variable therapeutic benefits and also do not prevent long-term progression of joint degeneration [38].

Orthobiologics treatment involves using biological substances, such as platelet-rich plasma (PRP) [39], stromal vascular fraction (SVF) [40], and stem cells [41] to promote osteochondral tissue repair after injury. PRP is derived from centrifuged autologous blood and contains a concentrated mixture of platelets, growth factors, and other bioactive molecules. It has been shown to inhibit catabolic cytokines such as IL-1 β and TNF- α , which have integral roles in driving OA progression after joint injury, while promoting cellular secretion of anabolic factors such as fibroblast growth factor (FGF) and transforming growth factor- β (TGF- β) [42]. PRP injections have shown beneficial effects when used in

conjunction with surgical approaches to manage knee and hip OA [43]. SVF is a concentrated mixture of heterogeneous cell populations, including adipose-derived stem cells (ADSCs), pre-adipocytes, endothelial progenitor cells, and various immune cells, along with platelets, growth factors, and ECM materials. Intra-articular injection of SVF has shown some beneficial effects as a treatment for knee OA [40]. Stem cells, particularly mesenchymal stem cells (MSCs), hold promise as a therapy for cartilage repair or OA, mainly due to their paracrine function or ability to exert anti-inflammatory and trophic effects on surrounding tissues [44]. For instance, autologous MSCs have been reported to induce functional improvement in knee OA patients over a 12-month period [45]. However, despite some promising results obtained with orthobiologics in the treatment of joint pathologies [46], the majority of studies have applied these to patients at an advanced stage of OA, and often reporting inconsistent long-term benefits [47,48]. Their therapeutic effects in clinical cases of chondral and osteochondral injuries are less well characterised, and possibly limited by the need for injections at high doses and/or frequency as well as injection-related side effects [49].

2.2.2. Surgical strategies

Surgical strategies for cartilage and osteochondral repair include microfracture, autologous chondrocyte implantation (ACI), and osteochondral grafts. Microfracture (bone marrow stimulation) creates micro-size or nano-size drills into the subchondral bone beneath the damaged cartilage. This induces rapid infiltration of stem cells from the bone marrow through microscopic injuries in the subchondral bone surface, and the subsequent formation of a fibrin clot. Being performed through arthroscopy, it has the advantages of being minimally invasive, resulting in shorter surgical time and reduced postoperative pain. However, microfracture stimulates unnatural cartilage healing through scarring, promoting the formation of fibrocartilage to fill the defect [50]. This repair tissue is substantially different from hyaline cartilage, being vulnerable to mechanical forces and is only helpful in the short-term for delaying cartilage degeneration, with degenerative changes typically expected beyond five years following microfracture surgery irrespective of the lesion size [51].

ACI involves treating cartilage injuries through transplantation of the patient's cultured chondrocytes into the damaged area, which may be aided by a biomaterial (matrix-induced ACI or MACI) [52]. ACI is capable of inducing hyaline-like cartilage formation that closely resembles the properties of native articular cartilage, hence providing better long-term outcomes compared to fibrocartilaginous repair in microfracture [53]. However, although using cultured chondrocytes in ACI provides a personalised approach for repairing larger-sized defects, there are limitations associated with the surgical process and possible need for large amounts of chondrocytes [54]. For instance, the harvesting of healthy cartilage from a non-weight-bearing site in the patient and subsequent culturing of extracted chondrocytes inevitably prolong the treatment timeline, while the need to perform a complex surgery for implantation reduces the accessibility of this technique in some regions. Moreover, ACI is limited to the repair of cartilage damage, while a bone grafting procedure must also be performed for defects penetrating deeper than 6–8 mm into the subchondral bone [26]. For this reason, full-thickness osteochondral defects currently have limited and suboptimal surgical options for repair.

Osteochondral grafting can provide an option for restoring full-thickness osteochondral lesions. Conventional strategies are widely known as autograft and allograft cartilage implantation [55]. Autografting involves cartilage transplantation from another non-load-bearing joint in the same person, but is often limited by the amount of healthy cartilage available particularly in extensive injuries. Harvesting autologous tissue can also cause additional damage at the donor site. Allografting involves transplanting a cartilage tissue graft from another individual, often a deceased donor. However, this carries a risk of immune rejection and subsequent graft failure, as well as possible

tissue mismatch with the defect and lack of bioactivity in the transplanted graft.

Conventional treatment approaches for chondral and osteochondral injuries are largely ineffective at restoring original cartilage structure and properties to achieve adequate long-term repair and prevent further degenerative changes. Consequently, there is a pressing need for new therapeutic interventions that can effectively repair critical-sized cartilage defects. The design and application of biomimetic stratified scaffolds through tissue engineering approaches offer new hope for addressing current challenges.

3. Design considerations for biomimetic chondral and osteochondral scaffolds

Biomimetic chondral and osteochondral scaffolds are designed to closely mimic the spatial organisation, tissue composition, and functional properties of native tissues. Earlier approaches using homogeneous monolayer scaffolds were mostly shown to be suboptimal for regenerating zone-specific osteochondral tissues, as they were unable to satisfy variations in the conditions required for different types of tissue regeneration along the depth of the defect [14,15]. The design of a biomimetic, stratified zonal scaffold depends on several key factors (Fig. 2), including layered architecture, materials selection, corresponding fabrication methods, and optional incorporation of cells and growth factors [23]. The desired outcomes include a hierarchical structure and zonal properties within the regenerated cartilage region to match native tissue characteristics, which may include zone-specific variations in matrix composition, collagen fibre orientation, mechanical properties, cellular phenotypes, and bioactive growth factors. Fig. 3A illustrates a representative multizonal hydrogel model based on a ‘full-thickness cartilage defect (grade 3)’, replicating the zonal structure of the natural articular cartilage in the superficial, middle, and deep

zones. Multizonal osteochondral scaffolds aim to restore the physical and biochemical properties of the stratified structure of articular cartilage zones, with additional considerations for calcified cartilage and subchondral bone to reconstruct the entire osteochondral unit, as depicted in Fig. 3B.

Current designs for chondral and osteochondral scaffolds still face some important challenges. Firstly, it is difficult to produce truly biomimetic scaffold designs that faithfully replicate the hierarchical structure and composition of zonal cartilage tissue and regional osteochondral tissue, particularly without involving complex fabrication processes that might pose hurdles in scale-up manufacturing. Secondly, there is a significant challenge in fabricating multiphasic scaffolds with integrated layers that respectively accommodate the regeneration requirements of superficial, middle, and deep zone cartilage as well as calcified cartilage and subchondral bone, while maintaining seamless integration between the different layers. Thirdly, chondral and osteochondral defects often occur at weight-bearing sites within the joint. However, much of the current biomimetic scaffold designs for treating these defects are created using hydrogels, which may not possess adequate mechanical properties for physiological load-bearing. These challenges form the basis of the design requirements for multizonal cartilage scaffolds discussed in detail later in this review, including biomimetic zone-specific architecture, seamless transition or integration between zones, and mechanical stability or biomimicry in mechanical properties. Current scaffold designs have attempted to meet these design needs through zone-specific modulation of fibre orientation, composition or pore structure, and cell types or growth factors.

3.1. Architecture comparison between multilayered and gradient scaffolds

Biomimetic multilayered scaffolds mimic natural osteochondral tissue structure and function, comprising both cartilage and subchondral

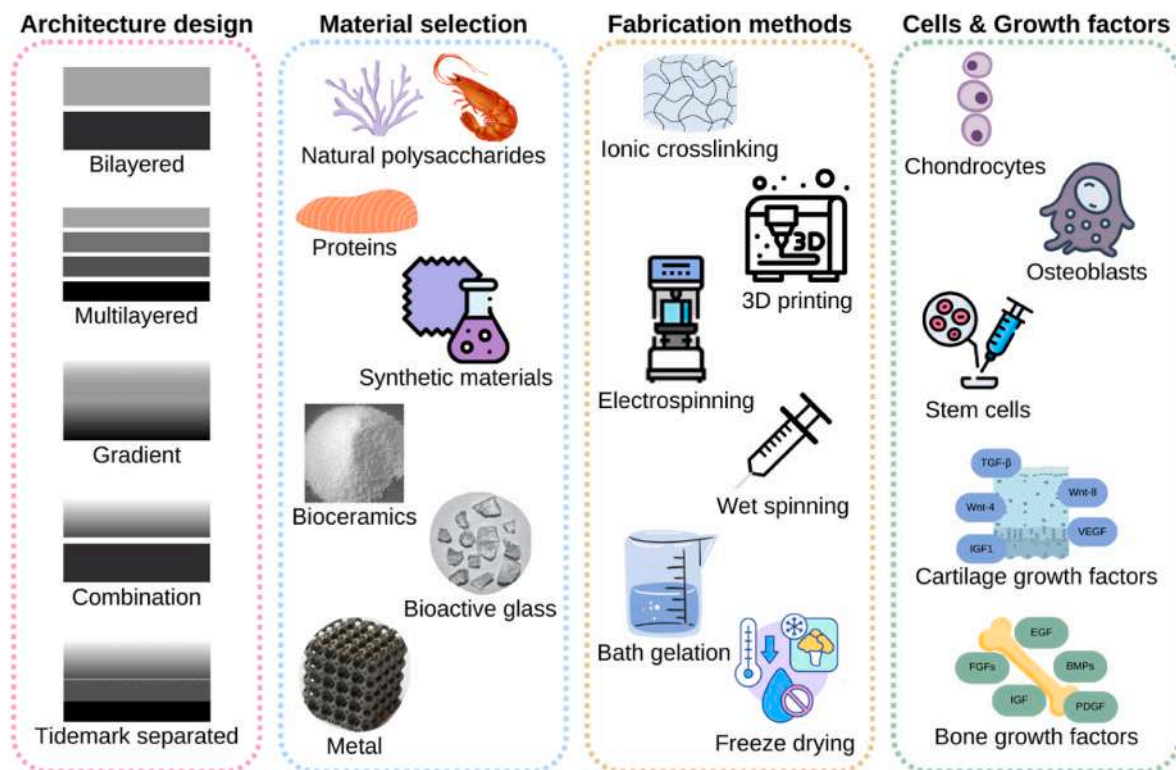


Fig. 2. Critical factors in the design of biomimetic zonal chondral/osteochondral scaffolds, such as architecture design and material selection, may define the success of reconstructing zonal properties and mechanical performance of native tissues. Fabrication methods need to be selected and adapted according to the materials used to increase the degree of control over structural and compositional parameters. Loading cells and/or growth factors is an additional strategy to promote chondrogenesis and osteogenesis in the corresponding regions by providing microenvironmental cues. Figure created using Microsoft PowerPoint.

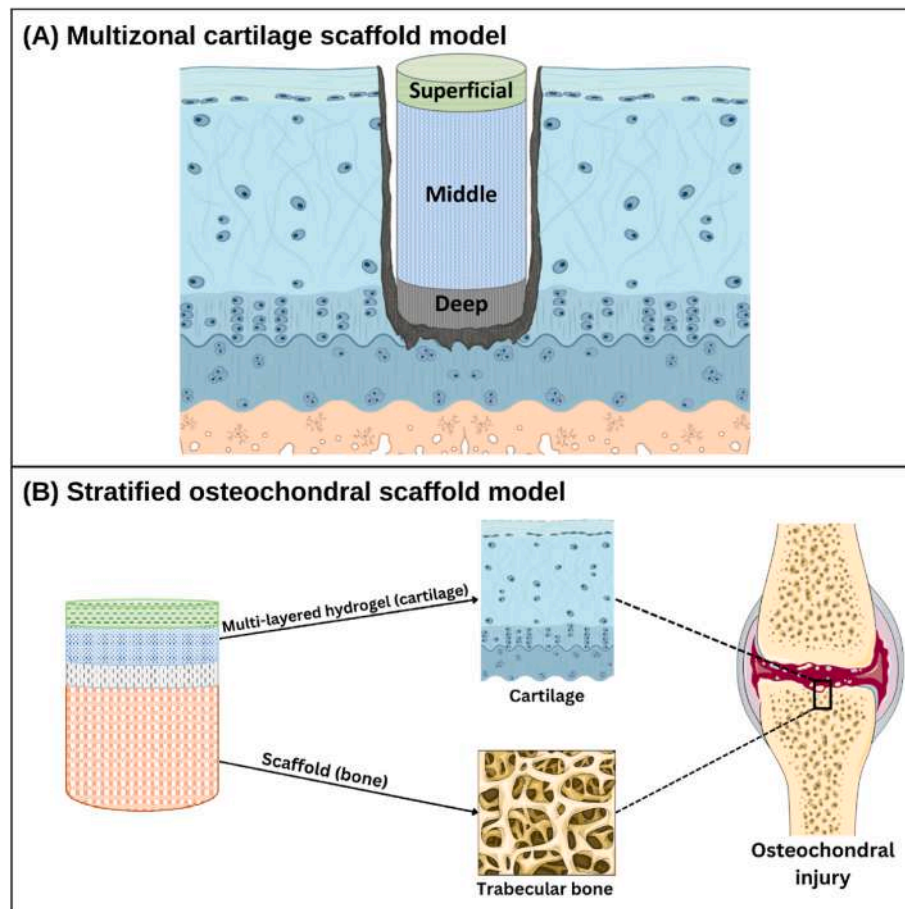


Fig. 3. Multizonal and stratified scaffold models. **(A)** A multizonal hydrogel model based on a ‘full-thickness cartilage defect (grade 3)’, replicating natural hierarchical structure of cartilage tissue. **(B)** A stratified osteochondral scaffold model combines a soft multilayered cartilaginous scaffold and a rigid subchondral bone scaffold. Figure created using Microsoft PowerPoint.

bone components. Because these are intended for repairing damaged or degenerated joints, particularly in weight-bearing joints such as the knee, scaffolds need to be designed to provide improved load distribution and seamless integration between cartilage and bone, and facilitate joint function under complex biomechanics. Multilayered and gradient architectures are the two most commonly considered scaffold designs, each with unique advantages and disadvantages.

3.1.1. Multilayered scaffolds with discrete structure

Multilayered scaffolds can contain three or more compartments with dissimilar architectures comprising different biomaterials to reconstruct the anatomical microstructure of articular cartilage, often with a concurrent transition layer facilitating integration with the subchondral bone. This design provides a relatively simple approach to recreating zonal variations in articular cartilage, as the different scaffold layers can be constructed separately and later integrated through various means. The scaffold hence provides greater tissue specificity in its different regions for matching native tissue characteristics. Particularly in osteochondral scaffolds where weight-bearing becomes increasingly important, the multilayered design can achieve higher mechanical properties by allowing wider materials selection that is not limited to hydrogels. Moreover, it is easier to create separation in the cartilage and bone regions of the scaffold through distinct layers, helping to prevent cell migration between the two tissue types and therefore enabling better maintenance of region-specific tissue phenotype. However, issues may arise due to inherent discontinuities in the multilayered structure, leading to mismatch of mechanical properties and biodegradation rates between adjacent layers. Resulting mechanical instability may result in

poor tissue integration or even collapse of newly formed tissues [15]. In addition, weak interfacial mechanical properties and the risk of inter-layer delamination may reduce long-term implant performance [23].

3.1.2. Gradient scaffolds with continuous layers

Gradient scaffolds exhibit a transition in material properties that varies gradually from one end to the other, creating a continuous gradient structure rather than having discrete layers. Gradient variation in scaffold architecture and/or properties allows seamless transition from one tissue region to another, which can effectively improve interfacial integration and minimise the risk of delamination [56]. The gradient design may also enable simpler and more reproducible fabrication, since often the same raw materials are used to create a continuous change in pore structure, biomaterial ratio, or the composition of biological agents [23]. Nevertheless, some common challenges are encountered in accurately modelling tissue specificity or precisely replicating the variation in properties seen in native zonal cartilage. Because a majority of gradient scaffolds is constructed by sequential layering and crosslinking of hydrogels, they often fail to provide the mechanical support necessary for cartilage and bone regeneration in weight-bearing regions or in a highly stressed joint environment.

3.2. Zonal variations in mechanical properties and porous design

Critical design factors that should be considered for zonal chondral and osteochondral scaffolds include the gradient variations in pore structure and mechanical characteristics of native cartilage and bone tissue, as shown in Table 1.

Table 1

Depth-dependent variation in pore structure, mechanical properties, and functional behaviour of human osteochondral tissue.

Tissue zone	Pore size/porosity	Mechanical properties	Functional behaviour
Superficial cartilage zone	Depth-dependent variations across zones [57,58] Pore sizes: 2–6 nm Porosity: 60–85 %	Tensile modulus: 10.1 MPa [10] Compressive modulus: 0.2 MPa [10] to 0.3 MPa [62]	Lubrication and load distribution. Responsible for the behaviour of cartilage under pressure at the weight-bearing site. Resistance against shear forces, reducing the risk of damage during joint movement.
Middle cartilage zone	Diameter of collagen fibrils: from thinnest 30–35 nm (superficial zone) to thickest 40–80 nm (deep zone)	Tensile modulus: 5.4 MPa [10]	Resistance against compressive forces.
Deep cartilage zone		Compressive modulus: 6.4 MPa [10] to 9.8 MPa [62]	Perpendicular collagen fibres and the resulting arcadic structure support the overlying load. Greatest resistance to compressive forces.
Calcified cartilage	Pore size: 10.71 ± 6.45 nm [63]	Indentation modulus: ~ 19 GPa [64]	Shock absorption. Interlocked tightly with the upper articular cartilage and the lower subchondral bone plate, resisting shear forces and preventing detachment from the underlying bone.
Cortical bone	Pore size: 30–50 μ m Porosity: 3–5% [65], 5–10 % [59,60]	Average values from literature [65]: Tension strength: longitudinal 135 ± 15.6 MPa, transverse 53 ± 10.7 MPa; Compression strength: longitudinal 205 ± 17.3 MPa, transverse 131 ± 20.7 MPa Compressive modulus: 18–22 GPa [16]	Protective bone covering with a high degree of bending and twisting resistance, supporting the weight of the body.
Trabecular bone	Non-homogeneous anisotropic properties Pore size: 300–500 μ m [61] Porosity: 50–90 % [59,60]	Average values from literature [65]: Vertebra 2.4 ± 1.6 MPa; Tibia 5.3 ± 2.9 MPa; Femur 6.8 ± 2.9 MPa Subchondral bone ultimate strength: 10–40 MPa (varies with medial/lateral region and depth below surface) [66] Compressive modulus: 0.1–0.9 GPa [16]	Sponge-like geometric arrangement can withstand localised forces transmitted through the bone while porous structure provides light weighted-ness.

Adult articular cartilage responds in a depth-dependent manner to compressive weight bearing, due to its zonal variations in collagen and GAG distribution. In the cartilage region of osteochondral tissue, mesopores range in sizes of 2–6 nm with porosity of 60–85 %, with gradual increase in pore size from the superficial to deep zone [57,58]. Calcified cartilage is present in the transition region between hyaline cartilage and subchondral bone, where collagen fibres are immobilised in the subchondral bone to anchor the cartilage layer [27], and hydroxyapatite becomes more abundant with increasing depth down to the bone. The subchondral bone serves as the bottom support platform with the highest load-bearing resistance. Morphologically, the porosity of cortical bone is usually between 5 and 10 %, while the porosity of cancellous bone ranges from 50 to 90 % [59,60]. Pore sizes in cortical bone are smaller compared to cancellous bone, with diameters of 30–50 μ m (typically lower than 100 μ m). The interconnected pores in the trabeculae form a network of varying pore sizes, typically 300–500 μ m in diameter [61].

Mechanical properties of the designed scaffold are expected to match the load-bearing nature of the cartilage and restore its function to support joint movement, which includes replicating the mechanical variation seen in distinct cartilage zones. It is worth noting that the compressive modulus of the cartilage compartment is depth-dependent, increasing from the superficial to the deep zone from 0.2 to 6.44 MPa [16]. In the superficial zone, the tensile modulus is higher than in other zones, at 10.1 MPa, while this decreases to 5.4 MPa in the intermediate zone [10]. This mechanical gradient is created by depth-dependent variation in the ratio of collagen to GAG in the articular cartilage. Meanwhile, the subchondral bone is covered by a layer of cortical bone, characterised by Young's modulus of 15–20 GPa, with more porous cancellous bone underneath that has Young's modulus ranging between 0.1 and 2 GPa, contributing to its lighter and more flexible nature [67]. The mechanical variations along the osteochondral unit provide a combination of strength, resilience, flexibility, and adaptability to skeletal loads, creating a unique functional gradient that constitutes an important goal of biomimetic scaffold design.

Porosity and pore size are primary factors influencing the mechanical stiffness and biological properties of osteochondral scaffolds, while other secondary factors such as pore geometry are also of interest [61, 68]. In biomaterial-based osteochondral tissue engineering, the biological properties of the scaffold are often correlated with how closely the scaffold matches the mechanical properties of surrounding tissues [69].

While high porosity is useful for avoiding stress shielding and stimulating cartilage and bone ingrowth [61], a balance needs to be maintained as this also reduces mechanical strength and may impact the scaffold's load-bearing capacity. Particularly in full-thickness osteochondral defects, adequate mechanical stability of the subchondral bone region is important for anchoring the scaffold within host tissue and protecting the regenerating cartilage from damage due to overloading. In the cartilage region, scaffold layers are often not designed to replicate the mesopore structure of surrounding chondral tissue, as tiny, tightly interconnected pores are not conducive to chondrocyte survival and growth. Instead, larger pore sizes of 100–200 μ m [70] are employed to allow adequate space for cell adhesion, migration, and nutrient exchange. In deeper layers, the scaffold design often mimics highly porous cancellous bone with a large specific surface area to facilitate tissue integration. For instance, the optimal pore size for achieving osteogenesis and bone ingrowth ranges from 300 to 800 μ m with approximately 60 % porosity [71–73], closely matching the cancellous bone and resulting in improved bone ingrowth and osseointegration [74].

Pore geometry [75,76] is an emerging factor being increasingly considered in biomimetic scaffold design due to its role in providing extracellular cues, and precise control over this parameter can now be realised through computer-aided design coupled with additive manufacturing methods. Recent evidence suggests that cells respond to physical cues in the microenvironment through alterations in cell shape and movement, which can lead to changes in cell activity and fate, and further direct the morphogenesis, pathology, and repair of many tissues [77]. Variations in pore geometry can influence both surface topography and mechanical characteristics of the scaffold, thereby impacting cell behaviour and regenerative processes. For instance, irregular pore structure in bioceramic scaffolds can improve biocompatibility by resembling the irregular order of bone trabeculae [78]. With advances in fabrication technologies, unique topological designs with high geometrical complexity and small dimensions can now be created, such as 3D printed cellular metals [68], ceramic cellular materials [79], and polymeric cellular materials [80] with deliberately integrated voids, as well as lattice structures [81,82] including strut-based lattice structures [83] and lattice sandwich structures [84]. Modulating pore geometry can augment regional variations in biomimetic osteochondral scaffolds by introducing changes in mass, surface area-to-volume ratio, porosity, mechanical properties, and surface curvature, all of which influence the spatiotemporal arrangement of cells and hence the outcomes of tissue

regeneration.

In the design of multizonal cartilage scaffolds, it is essential to not only consider the pore structure and mechanical properties, but also the functional behaviour of articular cartilage. The most important function of cartilage in providing wear resistance and constant lubrication in articulating joints should be a design consideration in biomimetic cartilage scaffolds [85]. Recent advances in biomedical research have shed light on the frictional behaviour and lubrication mechanisms underlying cartilage wear and degradation, inspiring new therapeutic strategies for cartilage repair and regeneration [86]. The significance of wear resistance and friction reduction is beginning to emerge in some current designs of cartilage scaffolds [87,88]. For instance, the integration of a top lubrication layer may help to augment the functional properties of the cartilage scaffold, where hydrogels or natural polymeric materials stand out due to their ability to provide low surface friction and exceptional lubrication, as well as remarkable biocompatibility [89,90].

It is notable that the regeneration rate of articular cartilage varies across its different zones, forming a gradient of healing speed [57]. This variation is attributed to the distinct structural, compositional, and cellular characteristics of each zone. The superficial zone has the highest regeneration capacity due to its higher cell density and proximity to the synovial fluid, which provides easier access to nutrients and bioactive factors. The regeneration rate becomes slower transitioning from the middle to deep zone, due to reduced cell density and limited nutrient supply. Besides a depth-dependent gradient in regenerative capacity, articular cartilage exhibits very limited healing potential overall, compared to the highly metabolically active subchondral bone that demonstrates fast and efficient regeneration after injury [16]. Meanwhile, the regeneration of calcified cartilage that anchors the articular cartilage to subchondral bone is also very limited due to the dense, calcified nature of the matrix, which impedes healing due to the lack of vascularisation and cellular presence [63]. Moreover, cartilage regeneration can be influenced by several factors, including age, mechanical loading, anatomical location, and injuries or disease conditions that can impair cartilage regrowth [57]. Although complex and highly variable, the regeneration rate of cartilage is an important design consideration for scaffolding strategies, as the biomaterials used are expected to achieve a degradation rate synchronised with the rate of new tissue formation. This is crucial for restoring cartilage function and supporting physiological weight-bearing without re-injury at the regeneration site.

3.3. Biomaterials selection

Biomaterials selection is the first step and a key factor in composing an osteochondral scaffold [23]. Other than meeting the essential criteria for a tissue engineering scaffold, including bioactivity, biodegradability, processability, and mechanical stability, biomaterials used for osteochondral repair also need to be conducive to cartilage and bone formation, and be amenable to providing region-specific properties. Natural and synthetic polymers, alone or in blends are mainly used to formulate the cartilage region and help induce zonal cartilage regeneration, which may be supported by hard materials such as bioceramics and metals used to recreate the subchondral bone region.

Each class of material has its advantages and drawbacks as candidates for osteochondral scaffolds, and combining different types of materials increases the likelihood of producing better region-specific biomimetic properties, although this also raises the complexity of fabrication and may reduce reproducibility. The biodegradability of different material components in a scaffold should be considered, as a scaffold that degrades too quickly may not provide sufficient support for the migrating cells and newly formed tissue, while one that degrades too slowly may impede tissue remodelling and integration [91]. Polymeric materials including natural and synthetic polymers, and decellularised matrix are usually chosen for creating multizonal cartilage scaffolds (Fig. 4). Polymers offer good biocompatibility and biodegradability,

high water content, and good control over physicochemical characteristics, although they may have low stiffness and weak mechanical properties [92]. Bioceramics have poor elasticity but high stiffness, providing bioactivity and osteoconductive properties, and are usually used for creating the porous bone region. Metallic materials are widely used in orthopaedic implants because of their excellent mechanical support, which makes them possible candidates for replacing the subchondral bone. However, despite some applications as the bone part of osteochondral scaffolds, they are not considered tissue engineering materials due to biological inertness and non-biodegradability [9]. Newer developments in bioactive and biodegradable metal scaffolds sit at the interface of orthopaedic implants and tissue engineering [93–96]. Currently, multilayered osteochondral scaffolds usually comprise a bioactive polymer scaffold or hydrogel as the cartilage region, joined to a mechanically robust polymer/ceramic scaffold as the bone region, while gradient scaffolds are largely hydrogel constructs with regional variations in composition and/or properties. This section will briefly describe the classes of materials used for osteochondral scaffolds, as they have been extensively covered in other reviews [15,16]. Example studies on natural and synthetic polymers, and decellularised matrix illustrate the potential of these materials in promoting zonal cartilage regeneration. Bioceramics and metals are discussed in their capacity to be used as part of a ready-made subchondral support for zonal cartilage scaffolds.

3.3.1. Natural polymers

Natural polymers share structural similarities with ECM and typically have minimal risk of inducing immunological or inflammatory reactions within the body [100]. Biocompatible naturally derived polymers such as alginate, chitosan, gelatin, collagen, cellulose, and silk fibroin are widely used in tissue engineering of articular cartilage [96]. Due to their natural biomimetic properties, natural polymers can be layered to generate a bioactive environment for osteochondral repair, while also providing reasonable mechanical support for regenerating tissues. Natural polymers have been particularly useful in constructing bioinspired gradient scaffolds to mimic the stratified layers in osteochondral tissue, such as through gradient variations in pore structure, composition, and factors that induce osteochondrogenesis [101].

Alginate, derived from brown seaweed, is a natural polysaccharide frequently used to fabricate cartilage layers in the form of hydrogels, which can also facilitate the delivery of cells and therapeutic drugs [102]. They can be easily manufactured through cationic crosslinking such as by using divalent cations (e.g., Ca^{2+} , Cu^{2+} , Ba^{2+} , Sr^{2+} , Zn^{2+} , Co^{2+}) [102–107], trivalent cations (e.g., Fe^{3+} , Nd^{3+} , Tb^{3+}), and the combination of multiple cations [108–110]. Alginate hydrogels can provide a 3D environment for zonal cartilage regeneration and enable zone-specific chondrocyte density and growth [111]. Versatile processing options allow alginate hydrogels to be printed as a bioink, and used to construct multilayered zonal cartilage scaffolds embedding a gradient of cell densities to mimic the superficial, middle, and deep cartilage zones [112]. Alginate methacrylate hydrogels have also been used as cell encapsulation vehicles for infiltrating 3D printed synthetic polymer scaffolds with gradient pore structure designed for zonal cartilage repair [113].

Chitosan, derived from chitin in crustacean shells, is a polysaccharide that exhibits excellent biodegradability and structural similarity to GAGs [114]. The bioactivity of chitosan, reflected in its antimicrobial, antitumour, and antioxidant activities, contributes to reducing inflammation when chitosan scaffolds are used for cartilage defect repair [115]. Admittedly, chitosan itself has weak mechanical strength, and is often modified or enhanced by incorporating other materials to improve mechanical properties for cartilage regeneration, such as by short fibre segments [116] or blending with other materials [117]. Hyaluronic acid is another polysaccharide, and being a natural component of synovial fluid and cartilage, is often used in chondral hydrogel formulations because of its lubricating and viscoelastic

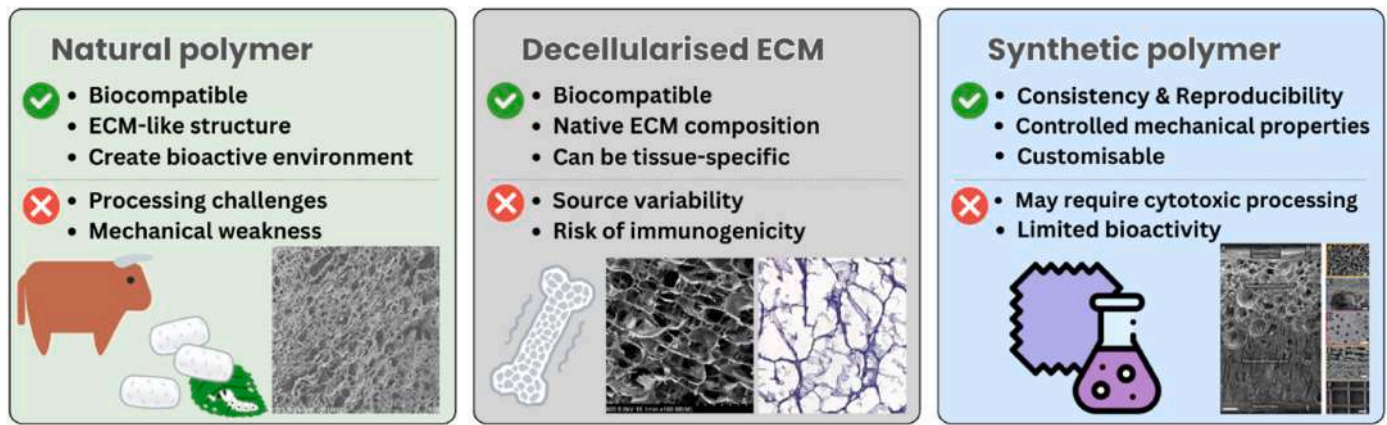


Fig. 4. For zonal cartilage regeneration, scaffolds are often constructed using polymeric materials, including naturally-derived (left), decellularised ECM (middle), and synthetic (right). Examples: Natural polymer scaffold (left) made from collagen/silk fibroin composites for chondrogenic differentiation, image adapted with permission from Ref. [97]. Decellularised ECM scaffold derived from human articular cartilage (middle) used in conjunction with microfracture for cartilage regeneration, image adapted with permission from Ref. [98]. Synthetic polymer scaffold (right) produced from PCL using multiple fabrication methods, with zonal microstructure for stratified cartilage repair, image adapted with permission from Ref. [99]. Figure created using Canva.

properties [118,119]. An emerging design approach for biomimetic cartilage scaffolds is to blend different types of natural polymers to achieve combinational properties. For example, one study used combinations of chitosan, collagen, hyaluronic acid, and silk fibroin to construct a bilayered chondral scaffold by freeze-drying, with different material composition and porous structure in the surface and transitional layers [20].

Other natural polymers commonly chosen to fabricate cartilaginous scaffolds include naturally derived proteins such as collagen and silk fibroin, partly due to their natural ability to enhance cell adhesion. Collagen, including the frequently used types I and II, is an abundant protein in mammals that can be derived from bovine, porcine, or even human tissues. Collagen is applied extensively in cartilage and bone tissue engineering, where one method to modulate region-specific properties is by varying the content of different types of collagens [120–122]. Silk fibroin, most commonly extracted from *Bombyx mori* cocoons, is a potent and newer type of natural polymer used for regenerating cartilage and bone tissues [123]. Silk scaffolds often possess superior mechanical strength, accompanied by a tailorable chemical structure and good bioactivity, elasticity, and degradability [124]. For scaffold fabrication, silk fibroin is usually dissolved in water-based solvents and can be easily reconstructed into a variety of formats, including films, mats, hydrogels, and sponges, through a range of techniques such as self-assembly, ultrasonication, pH adjustment, freeze-drying, and physical or chemical crosslinking [125]. Interestingly, one study reported that a nanoengineered silk surface with nanopillar arrays could regulate stem cell morphology, leading to a flattened ellipsoidal shape consistent with the appearance of chondrocytes in the superficial zone of articular cartilage [124]. A combination of collagen and silk fibroin could produce scaffolds with improved biological and mechanical properties compared to individual materials, for example, a hybrid scaffold with optimised ratio of 7:3 collagen/silk fibroin was shown to achieve efficient repair in a rabbit model of full-thickness cartilage defects [97].

3.3.2. Decellularised extracellular matrix

Decellularised extracellular matrix (dECM) has recently gained increasing interest as a new type of scaffolding material that is naturally derived from the ECM produced by cells and subsequently have the cells removed. dECM retains the intrinsic biochemical and biophysical cues of native ECM, providing structural and chemical signals that regulate cellular behaviour, such as adhesion, migration, proliferation, and differentiation [126–128]. Biochemical cues may include structural proteins, peptides, cytokines, and growth factors, while biophysical

properties are conveyed by 3D structure, porosity, and mechanical properties akin to native tissue [126,129].

Several studies have demonstrated the potential of dECM materials in cartilage tissue engineering, although they have not yet been utilised for constructing cartilage scaffolds with zone-specific structure. Peng et al. [98] fabricated a human articular cartilage-derived ECM scaffold, validating its capacity to support the survival, proliferation, migration, and maintenance of the human chondrocyte phenotype *in vitro*. *In vivo* experiments showcased the ability of the scaffold to independently repair articular cartilage in a large animal (sheep) model when combined with microfracture technique. When combined with injection of IL-4 to induce M2 macrophage polarisation, Tian et al. [130] showed that a decellularised cartilage matrix scaffold could induce cartilage regeneration as well as provide immunomodulatory effects in a rat osteochondral defect model. Browe et al. [131] developed decellularised cartilage ECM-derived scaffolds crosslinked using glyoxal and dehydrothermal treatment. These scaffolds supported cartilage ECM synthesis when seeded with fat pad-derived stromal cells and displayed high elastic properties in compression tests. Another group [132] also showed that the mechanical properties of dECM scaffolds could be significantly enhanced through the integration of electrospun nanofibers. Li et al. [133] developed an injectable hydrogel composed of cartilage dECM and hyaluronic acid methacrylate (HAMA). This hydrogel demonstrated robust adhesion strength to cartilage and significantly enhanced mechanical performance compared to cartilage dECM or HAMA alone. *In vitro* cultures showed that the hybrid hydrogel promoted chondrogenic differentiation of encapsulated porcine bone marrow MSCs after 21 days. *In vivo* subcutaneous implantation in a mouse model further illustrated improved biocompatibility of the hybrid hydrogel compared to HAMA alone. Li et al. [134] developed a bioinspired hydrogel scaffold produced by 3D printing with cartilage and bone dECM. When constructed as a bilayer hydrogel with tissue-specific dECM in the respective layers and supplemented with human MSC-derived exosomes, these hydrogel scaffolds accelerated the simultaneous regeneration of cartilage and subchondral bone tissues in rat osteochondral defects.

3.3.3. Synthetic polymers

A wide range of synthetic polymers can be used for osteochondral tissue engineering, sometimes with highly customised composition, but mostly involve polyethylene glycol (PEG), polyvinyl alcohol (PVA), polycaprolactone (PCL), and polylactic acid and its co-polymers (PLA, PLLA, PLGA) [100,135]. In particular, PCL has been a popular choice for fabricating the scaffold frame to realise various zonal cartilage designs, mainly due to its mechanical integrity and compatibility with 3D

printing fabrication techniques for producing customisable structures [99,136,137]. In general, due to their reproducible and tailorable chemical structure, synthetic polymers offer more precise control over scaffold characteristics compared to naturally derived materials, including mechanical stiffness, porosity, and degradation rate. However, their drawbacks include poor cell adhesion, potential immune response or adverse reactions upon implantation, and lack of inherent bioactive cues that facilitate cell signalling, ECM production, and tissue integration. Due to the substantially different properties required of materials for constructing chondral and osteochondral scaffolds, polymeric blends or co-polymers, as well as composites or hybrid materials formed through combination with other biomaterial classes, are commonly employed to fabricate biomimetic scaffold layers [96,138]. In combination with advanced manufacturing techniques such as digital light processing (DLP), scaffolds with specially designed mechanical property gradients can be constructed using synthetic polymers. For example, a photopolymerisable PEG diacrylate (PEGDA) hydrogel printed into a micro-truss structure and infiltrated with PEG-norbornene hydrogel to form composite trusses could exhibit regional stiffness variations within the scaffold ranging from 0.3 to 1.1 MPa, which is potentially useful for mimicking the differing mechanical properties between cartilage and bone in osteochondral tissue [139].

3.3.4. Bioceramics

Bioceramics are renowned for their excellent wear resistance, high stiffness, resistance to oxidation, and low friction coefficient, making them particularly suitable for bone tissue engineering [140]. Various modifications and fabrication processes can be applied to enhance the properties of bioceramics for use as the bone component of an osteochondral scaffold, for example, a biomimetic bone scaffold with stress transfer capability can be constructed by creating a biopolymer-bioceramic composite, using a coupling agent that serves as a ‘molecular bridge’ to establish interfacial reinforcement between materials [141]. With recent advances in additive manufacturing, 3D-printed bioceramic scaffolds can be constructed with diverse compositions and hierarchical structures, allowing precise control over their mechanical, degradation, permeability, and biological properties [142]. Through composite processing to modulate their elastic and other mechanical properties, bioceramics can also be applied in cartilage tissue regeneration, such as through the construction of a collagen/nano- β -tricalcium phosphate scaffold [143]. Although the majority of bioceramics used in osteochondral scaffolds are artificially made, emerging approaches have also considered naturally-derived bioceramics derived from marine organisms such as sponges, corals, or seashells [144].

Hydroxyapatite, $\text{Ca}_{10}(\text{PO}_4)_6(\text{OH})_2$, which has the same composition as the mineral component of bone, is a popular bioceramic used as bone grafts or coatings on orthopaedic implants due to its excellent biocompatibility and osteoconductivity [145]. Recent research has explored new methods to enhance the mechanical properties of this material towards load-bearing bone regeneration, for example, an interesting study generated 3D-printed hydroxyapatite scaffolds with greatly improved compressive strength through a triply periodic minimum surfaces (TPMS) design, characterised by unique non-self-intersecting, 3D periodic surface structures [146].

Bioactive glasses, composed mainly of silicon oxide, sodium oxide, calcium oxide, and phosphate, offer both osteoconductivity and osteoinductivity due to their ability to bond with both hard and soft tissues. A recent study has highlighted the applicability of bioactive glass-ceramic particles in long-term cartilage repair and promoting progressive bone growth, providing durable mechanical support to prevent late-stage cartilage collapse [147]. Other formulations of silicate-based bioceramics also exhibit excellent bioactivity and possible applications in subchondral bone and osteochondral tissue engineering [148,149].

3.3.5. Metallic scaffolds

Metal materials and their alloys are widely used in bone implants, with a long history of clinical application due to their biocompatibility, excellent corrosion resistance, and exceptional mechanical strength. In osteochondral tissue engineering, adopting a metallic subchondral bone scaffold can easily provide the essential mechanical support for articular cartilage repair to proceed under load-bearing conditions [61,150]. Titanium scaffolds were among the first metallic scaffolds considered for repairing osteochondral tissues, which can be made to match the properties of trabecular bone and provide sufficient space for bone ingrowth by altering their geometric structures [74] and porosities [151]. One interesting study designed a functionally graded porous lattice structure for a titanium bone scaffold with varying stiffness and density, providing spatial control of scaffold properties, which was fabricated using selective laser sintering (SLS) [152], as shown in Fig. 5A. The flexible chondral phase was a homogenous thin layer sponge fabricated through a sugar-leaching process, using a PDMS matrix and sugar as porogen, which was interlocked to the titanium scaffold during PDMS polymerisation. Although the assembled construct was able to support MSC growth and cellular communication, the distinct cartilage and bone layers were not well integrated. Addressing this problem, another study designed a tri-layered integrated osteochondral scaffold containing a titanium mesh cage as the bone scaffold [153]. Using 3D printing, PLGA hydrogel was directed printed on the titanium mesh to form a 30 μm dense layer, followed by porous PLGA layers with 100 μm pore size to form the cartilage region, as shown in Fig. 5B. Chondrocytes were then seeded into the cartilage scaffold, while autologous cancellous bone was filled into the titanium mesh to form the bone scaffold. This created an integrated scaffold structure, where the interfacial dense layer between cartilage and bone regions could inhibit the growth of new cartilage into the subchondral bone, and also shield the cartilage from excessive compression-related damage. *In vivo* study in a goat cartilage defect demonstrated the scaffold’s ability to reconstruct a homogeneous and smooth articular surface. Additionally, the tidemark area between native cartilage and subchondral bone was observed to coincide with the location of the intermediate dense layer in the scaffold. Other approaches have been used to create bionic osteochondral scaffolds featuring a dense interfacial layer and a titanium base scaffold [72,154], as presented in Fig. 5C. The dense layer was shown in sheep osteochondral models to prevent bone marrow from flowing into the cartilage region or synovial components from flowing into the bone region, ensuring separate osteogenesis and chondrogenesis.

Recent studies have demonstrated heightened interest in metallic materials as tissue engineering scaffolds by shifting from non-biodegradable to biodegradable metals, which include three main types: magnesium (Mg), iron (Fe), and zinc (Zn) [73]. Magnesium-based materials are susceptible to excessively high degradation rates, and hydrogen emissions from the degradation process can alter the peri-implant pH, potentially interfering with osteoblast survival and bone formation [93]. Iron-based materials have a longer degradation time than natural tissues, potentially hindering complete tissue repair [155]. Zinc-based materials exhibit a reasonable degradation rate, potential to provide essential trace elements, and minimal effect on changing environmental pH during degradation [94]. A recent study designed a biodegradable bilayered scaffold comprising a porous zinc scaffold and chondroitin sulphate hydrogel for full-thickness osteochondral tissue reconstruction [156], as presented in Fig. 5D. The zinc scaffold provided a favourable degradation rate, offering long-lasting mechanical support as well as eventual complete degradation. In a porcine osteochondral defect model, the bilayered scaffold achieved reconstruction of a smooth hyaline-like cartilage surface and superior integration with surrounding host tissues.

3.4. Fabrication strategy

Fabrication strategies to create biomimetic osteochondral scaffolds

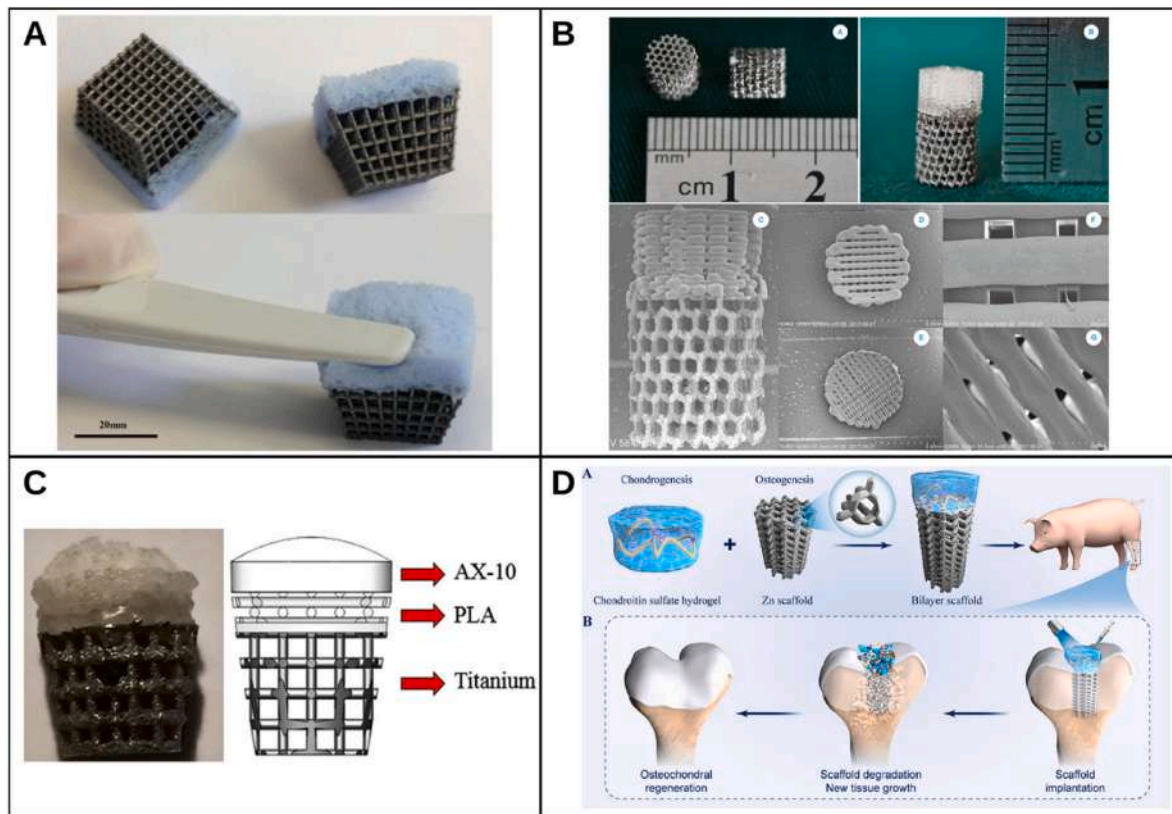


Fig. 5. Composite osteochondral scaffolds with a metallic bone component. (A) Bilayer osteochondral scaffold combining gradient titanium lattice scaffold and PDMS sponge, adapted with permission from Ref. [152]. (B) Tri-layered scaffold comprising a base titanium mesh cage and PLGA hydrogel, adapted with permission from Ref. [153]. (C) Multi-layer gradient osteochondral scaffold with titanium base, PLA intermediate layer and PLGA top layer, adapted with permission from Ref. [154]. (D) Biodegradable bilayered scaffold comprising porous zinc scaffold and chondroitin sulphate hydrogel, adapted with permission from Ref. [156].

have mainly involved the generation of fibrous or hydrogel structures for the articular cartilage compartment, which may or may not be reinforced with a subchondral bone compartment that provides higher stiffness and mechanical support. A variety of techniques may be used alone or in combination to realise scaffold designs that faithfully mimic the different components of osteochondral tissue, including the articular cartilage with zonal structure, interfacial calcified cartilage, and subchondral bone with high mechanical strength. Particularly for the cartilage component, fabrication methods have focused on precisely controlling fibre orientation in fibrous scaffolds or constructing compositional gradients in hydrogel scaffolds to produce zonal architecture and properties.

Traditionally, osteochondral and other types of tissue engineering scaffolds were fabricated using methods such as sol-gel [157,158], gas foaming [159,160], and emulsion freeze drying [161]. However, these methods were typically complex and time-consuming, providing low efficiency of tissue regeneration as well as inconsistent repair outcomes in osteochondral injuries. This was due to the lack of precise and spatial control over scaffold geometry, including porosity, pore size, and pore shape/distribution, leading to the inability to faithfully mimic original tissue structure, such as the depth-dependent zonal layers within articular cartilage, and the highly porous and interconnected but mechanically robust structure of subchondral bone.

Mould casting is a simple and versatile method compared to other approaches, which involves pouring a mixture of materials into a mould followed by gelling to create a wholesome scaffold. This method can create multi-layered scaffolds by sequentially casting the layers and adjusting the material composition of each layer [56,162]. Mould casting allows a high degree of control over the scaffold's final shape and dimensions. However, drawbacks include limited precision in the control of gradients, porosities, material properties, and manufacturing

details.

Electrospinning involves charging a polymer solution and directly writing the scaffold by depositing micro- or nano-scale fibres [163,164]. A fibrous mesh can hence be created that mimics the topography of native ECM, with adjustable porosity, pore interconnectivity, mechanical characteristics, and surface area. The fibrous sheets can also be layered to form multi-layered scaffolds with spatial variation in structure or material composition.

3D printing, a form of additive manufacturing, is commonly employed in current osteochondral scaffolds due to its high precision, enabling biomimetic and patient-specific designs through layer-by-layer printing [165]. Integrated with computer-aided design, it enables the fabrication of complex and customisable structures with potential to closely mimic the multizonal and hierarchical nature of osteochondral tissue [166–169]. However, several limitations remain including equipment cost, printing speed, and frequent need for post-processing to enhance mechanical or biological characteristics. Moreover, material selection may be limited, particularly in extrusion-based approaches due to problems with nozzle clogging, as well as in 3D bioprinting that involves the simultaneous incorporation of cells or biomolecules, essentially limiting choices to hydrogel materials [170,171].

Other fabrication strategies are defined by the unique properties of certain materials, such as freeze-thaw physical crosslinking [172–175] and freeze-casting [176] for PVA hydrogels. To create region-specific properties, fabrication techniques may also be combined with approaches involving self-assembly and response to external stimuli such as magnetism, light, pH, and temperature [177]. While attempting to create a biomimetic, stratified structure, the selection of manufacturing method for osteochondral scaffolds should also consider processing complexity and reproducibility in sight of scale-up applications.

3.5. Biomimetic bilayered osteochondral scaffolds and the push towards biomimetic multizonal cartilage scaffolds

Conventional scaffolds with single-layer structure and homogeneous properties are generally insufficient in meeting the functional requirements for restoring the osteochondral tissue unit. Bilayered scaffolds first evolved to address varying requirements of regeneration for interfacial tissues, comprising two distinct but integrated layers that can respectively support different types of tissue formation such as cartilage and bone [178]. From earlier designs largely involving the integration of two separately fabricated homogeneous layers, biomimetic bilayered scaffolds have evolved to incorporate sophisticated designs that more closely mimic the stratified structure of native osteochondral tissue. For example, Zhu et al. [179] developed an injectable bilayer osteochondral scaffold with stratified biomimetic structure, comprising a thermosensitive sodium alginate/agarose composite hydrogel as the cartilage layer and a sodium alginate/bioglass composite hydrogel as the bone layer, which encapsulated different cell types. This was found to induce region-specific cartilage and bone formation in a rat osteochondral model while maintaining integration between layers and benefitting from a minimally invasive approach for scaffold implantation. Similarly addressing interlayer integration challenges, Gan et al. [180] produced a mussel-inspired osteochondral scaffold comprising a bilayered gelatine methacryloyl-polydopamine hydrogel. The cartilage and bone layers were seamlessly integrated through simultaneous polymerisation, respectively containing immobilised TGF- β 3 and bone morphogenetic protein 2 (BMP-2), together with mineralised hydroxyapatite reinforcement in the bone layer. This biomimetic design was seen to promote osteochondral repair in a rabbit full-thickness cartilage defect. Also tested in rabbits, Zhou et al. [181] developed a biphasic scaffold using fish collagen to enable simultaneous cartilage and bone repair, where the cartilage layer comprised chondroitin sulphate-incorporated fish collagen with 128 μ m pores and the bone layer was a fish collagen-hydroxyapatite scaffold with 326 μ m pores.

Newer bilayered scaffolds have built on hydrogel-based strategies to address specific challenges in osteochondral tissue repair. For instance, one notable challenge is the integration of newly formed cartilage within the scaffold with surrounding native cartilage. In this space, Wu et al. [182] developed a methacrylated silk fibroin (Sil-MA) sealant containing TGF- β 3, with adhesive properties and the ability to chondrocyte migration and differentiation. This was used to provide ‘marginal sealing’ around a bilayer silk scaffold in rabbit osteochondral defects, which together achieved regeneration with superior lateral tissue integration. Jiang et al. [183] also used Sil-MA in their bilayered scaffold design, creating two integrated Sil-MA hydrogel layers through stratified photocuring, which served as a base matrix for the incorporation of silk fibroin microspheres. By loading the microspheres with kartogenin and berberine and anchoring them within the respective cartilage and bone layers, this all-silk bilayered scaffold achieved osteochondral repair in a rat model after 8 weeks of implantation. Another notable challenge lies in the generally insufficient mechanical properties of osteochondral scaffolds for promoting tissue regeneration in load-bearing regions. To achieve better mechanical reinforcement, Liu et al. [184] employed a 3D-printed porous hydroxyapatite ceramic platform that releases alendronate for promoting bone regeneration. This was integrated with a mechanically enhanced hyaluronic acid methacryloyl hydrogel that releases kartogenin as the cartilage layer, through a semi-immersion approach. This scaffold was found to encourage region-specific cartilage and bone formation during rat subcutaneous implantation, although tissue regeneration under load-bearing conditions remains to be tested. Also using 3D printing, Gao et al. [185] fabricated a high-strength supramolecular polymer hydrogel as the basis for a bilayered osteochondral scaffold. The hydrogel mechanical properties were significantly enhanced by photo-initiated polymerisation to combine poly (N-acryloyl 2-glycine) (PACG) with gelatin methacrylate (GelMA), greatly superceding the

ranges achievable with conventional GelMA hydrogels. A bilayered gradient structure was created by doping the cartilage layer with Mn²⁺ ions and the bone layer with bioactive glass, which was found to enhance osteochondral repair after 12 weeks of implantation in a rat model.

Biomimetic bilayered osteochondral scaffolds have generally demonstrated the ability to facilitate differential chondrogenesis and osteogenesis in the respective layers, and have provided important insights into the significance of scaffold microenvironment on lineage-specific tissue differentiation during osteochondral regeneration. However, the bilayered design encounters key challenges in recreating physiologically meaningful biomimetic structure, particularly in the articular cartilage compartment. Firstly, there is a lack of biomimetic transition between the hyaline cartilage and subchondral bone regions due to the absence of a calcified cartilage layer, leading to an increased risk of fracture between discrete scaffold regions [186]. Secondly, bilayered scaffolds have a homogeneous cartilage region that does not mimic zonal variations in the chondral matrix, including its depth-dependent gradient in collagen fibre organisation, GAG composition, pore size, and mechanical strength, as well as differences in chondrocyte morphology and arrangement. Recently, a variety of innovative approaches have emerged for creating biomimetic multizonal cartilage scaffolds to address these challenges.

4. Biomimetic multizonal cartilage scaffolds with zone-specific variation in scaffold properties

Biomimetic multizonal scaffolds are designed to reflect the anatomical microstructure of articular cartilage and its stratified regions, ideally comprising three or more distinguishable but continuous layers. These scaffold designs may fulfil the unique zonal property requirements for faithful articular cartilage regeneration, through depth-dependent modifications in collagen fibril orientations, matrix architectures, biomechanical properties, cell properties and phenotypes, and zone-specific growth factors. Current studies reporting biomimetic zonal cartilage scaffolds have mainly adopted three types of stratification approaches: fibre orientation, composition or porous architecture, and cell types and growth factors, as summarised in Table 2.

4.1. Creating zonal cartilage structure by varying fibre orientation

A central feature of zonal variation in native articular cartilage is collagen fibril orientation. The alignment of collagen fibres is the primary determinant to the region-specific mechanical properties and functionality of hyaline cartilage, providing a smooth and wear-resistant surface in the superficial layer and changing to more randomly aligned and interwoven fibres in the transition zone to provide better load-bearing properties, as well as to vertical fibre orientation in the deep zone for anchoring the cartilage in underlying mineralised tissues. Because of its capability to easily produce nanofibrous sheets mimicking the structure of native ECM, electrospinning has been commonly explored as a fabrication technique for creating biomimetic osteochondral scaffolds, initially as bilayered structures replicating the cartilage-bone interface [187,188]. However, a typical electrospun fibre mat has randomly distributed and oriented polymer fibres that may resemble the transition zone of articular cartilage but do not include characteristics of the superficial or deep zones, and also do not provide good adherence to the bone component scaffold. To create a more functionally graded scaffold resembling osteochondral tissue layers, including zonal variations in articular cartilage, Hejazi et al. [189] used electrospinning to fabricate a nanofibrous scaffold with five layers comprising different ratios of raw materials: PCL/gelatin and chitosan/PVA for the chondral layers, and PCL/gelatin with incorporated nanohydroxyapatite for the bony layers. The scaffold showed variation in fibre composition and porosity accompanied by smooth transition between layers, mimicking to some extent the change in matrix composition along the

Table 2

Summary of studies on multizonal cartilage scaffolds, broadly categorised by variations in fibre orientation, composition or pore architecture, and cell types or growth factors.

Type	Scaffold name	Fabrication method	Zonal structure		Main findings		Reference
			Cartilage scaffold features	Other features (e.g., bone)	Structural & mechanical characterisations	<i>In vitro</i> and <i>in vivo</i> study	
Fibre orientation	Bi-layered micro-fibre reinforced hydrogels	Melt electrospinning writing (MEW)	Materials: Soft gelatine-methacrylamide (GelMA) hydrogel embedded, melt electrospun written polycaprolactone (PCL) fibre scaffold Bi-layered structure: •Superficial tangential zone (STZ): Densely distributed crossed fibre mat, with tightly packed and tangentially oriented fibres (alternating angles: 0–45–90–135°) •Middle and deep zone (MDZ): A uniform box structure fibre organisation (cross-shaped 0–90° lay-down pattern)	N/A	Pore size (fibre spacing): •STZ: ~50 mm •MDZ: ~800 mm •Fibre diameter ~20 mm Mechanical properties: •Composite constructs with a thin STZ layer exhibited significantly higher peak modulus under incongruent and congruent loading conditions than hydrogels reinforced solely with a uniform MDZ structure. •The bi-layered composite constructs demonstrated a stress relaxation response similar to that of native cartilage tissue. •The STZ layer notably influenced the mechanical behaviour of the composite constructs under incongruent loading. •Capable of simulating native cartilage and supporting neo-cartilage formation upon physiologically relevant mechanical stimulation. •The STZ layer might play a more critical role under dynamic compression.	<i>In vitro</i> study Cells: Chondrocytes from cartilage of equine metacarpophalangeal joints Time period of <i>in vitro</i> culture: 28 days Findings: •STMDZ-reinforced hydrogels can support cartilaginous tissue formation upon physiologically relevant mechanical stimulation. •Hydrogel mechanical failure under dynamic loading indicates limited dynamic mechanical properties.	(Castilho et al., 2018; Castilho et al., 2019) [192,193]
	3D anisotropic tri-layered fibrous scaffolds	Electrospinning Layer-by-layer assembly	Materials: PCL-GO-collagen scaffold •Electrospun layers: Polycaprolactone (PCL) •Framework: Graphene oxide-collagen (GO-collagen) Tri-layered structure: •Superficial Layer: Fibres aligned parallel to the top surface of the scaffold. •Middle Layer: Random orientation of collagen fibres, the transition zone between the superficial and deep zones. •Deep Layer: Spiral-shaped, electrospun mesh rectangles, cut and rolled into cylinders, formed a vertically oriented fibrous network akin to natural cartilage tissue.	N/A	Morphology: •Superficial layer: fibre diameter of $1.20 \pm 0.51 \mu\text{m}$, 68 % of pores with diameters between 5 and $10 \mu\text{m}$ and 16 % of pores with sizes superior to $10 \mu\text{m}$; •Middle layer: larger fibre diameter ($2.00 \pm 0.63 \mu\text{m}$) and bigger pores as 53 % of pores between 5 and $10 \mu\text{m}$ and 31 % of pores with a diameter superior to $10 \mu\text{m}$ •Deep layer: larger pores to facilitate nutrient and oxygen transport, waste removal, and cell attachment. Mechanical properties: •The compression modulus varied with the direction of	N/A	(Girão et al., 2018) [194]

(continued on next page)

Table 2 (continued)

Type	Scaffold name	Fabrication method	Zonal structure		Main findings		Reference
			Cartilage scaffold features	Other features (e.g., bone)	Structural & mechanical characterisations	<i>In vitro</i> and <i>in vivo</i> study	
	Multizone scaffold	Electrospinning and Cryo-printing	Materials: Polycaprolactone (PCL) as base scaffold. Tri-layered structure: •Top layer (aligned fibres): Highly aligned fibres resembling cartilage's superficial zone. •Middle layer (randomly oriented fibres): Randomly deposited fibres on cryo-printed helix scaffolds. •Bottom layer (helix structure): PCL, providing interconnected architecture and compressive support, mimicking cartilage's deep zone.	N/A	fibre arrangement, decreasing from vertical to random to horizontal. •When the direction of the force was perpendicular to the direction of the fibres/ pores, the resistance to deformation was low. Fibre diameter & pore size: •Top zone aligned fibre diameter: $1.57 \pm 0.50 \mu\text{m}$ •Middle zone random fibre diameter: $1.94 \pm 0.51 \mu\text{m}$ •Bottom zone helix scaffold pore size: $3.62 \pm 2.46 \mu\text{m}$ Mechanical Properties: •The multizone scaffolds showed slightly higher compressive properties than the electrospun control scaffolds. •Compressive properties remained consistent over the 4-week culture period and were similar to acellular controls across all tested strains.	<i>In vitro</i> study Cells: Primary human adult chondrocytes Time period of <i>in vitro</i> culture: 5 weeks Time frame for culture: 24 h, 1 week, 3 weeks, 5 weeks Findings: Multizone scaffolds maintained chondrocyte phenotype and function and demonstrated their potential in cartilage tissue engineering applications.	(Munir et al., 2020) [195]
	Microribbon (μRB) scaffold	Hydrogel: mould casting μRBs : wet-spinning	Materials: •Hydrogel: Gelatine (GEL) methacrylate, chondroitin sulphate (CS) methacrylate • μRBs : gelatine (GEL) μRBs Spatially-patterned tri-layered scaffold: •Superficial zone: 100 % gelatin, aligned μRB •Middle zone: 90GEL:10CS Deep zone: 75GEL: 25CS	N/A	Mechanical properties: •Trilayer μRB scaffolds showed a significant increase in compressive modulus from superficial to deep zones, mirroring native cartilage. •Deep zones of μRB scaffolds exhibited a remarkable over 34-fold increase in compressive modulus, approaching values of native articular cartilage (464 kPa and 452 kPa for μRB and $\mu\text{RB} +$ aligned cultures, respectively). •Trilayer hydrogel (HG) scaffolds displayed only a marginal increase in compressive modulus in deep zones after 21 days, remaining significantly lower than native cartilage. •Interfacial shear strength of trilayer μRB scaffolds significantly surpassed that of trilayer HG scaffolds.	<i>In vitro</i> study Cell/scaffold type: MSC-seeded trilayer microribbon (μRB) Cells: Human MSCs Time period of <i>in vitro</i> culture: 21 days Findings: Trilayer μRB scaffolds maintained high cell viability throughout the culture. •Trilayer μRB scaffolds promoted significant cartilaginous ECM deposition by MSCs, with increasing sGAG production from superficial to deep zones. •Aligned μRB scaffolds enhanced ECM deposition, with a notable increase in sGAG content and collagen production, particularly in the superficial zone. •Varying the ratio of gelatin to chondroitin sulphate μRBs within the scaffold could impact MSC chondrogenesis, guiding zonal-specific differentiation. Trilayer μRB scaffolds enabled MSCs to produce zonal-specific	(Gegg & Yang, 2020) [190]

(continued on next page)

Table 2 (continued)

Type	Scaffold name	Fabrication method	Zonal structure		Main findings		Reference
			Cartilage scaffold features	Other features (e.g., bone)	Structural & mechanical characterisations	<i>In vitro</i> and <i>in vivo</i> study	
	Mesenchymal stem cells loaded 3D-printed gradient PCL/ALMA composite scaffold.	3D printing	Materials: <ul style="list-style-type: none"> •Poly (ε-caprolactone) (PCL) impregnated with methacrylate alginate (ALMA) •Embedded rat bone marrow mesenchymal stem cells (BMSCs), Cell density: 3×10^5 cells/ml Tri-layered PCL/ALMA scaffolds: Depth-dependent gradient, with 0°/90°, 0°/60°, and 0°/30° lay-down pattern respectively, mimicking chondral zonal layers	N/A	Both μRB groups (with and without aligned μRB layer) were able to withstand shear stress greater than 100 kPa before failure, whereas the HG groups fractured with just 7.5 kPa of shear stress applied. Pores: <ul style="list-style-type: none"> •Superficial layer: filament gap of 300 μm, 0°/90° lay-down pattern •Middle layer: filament gap of 500 μm, 0°/60° lay-down pattern •Deep layer: filament gap of 700 μm, 0°/30° lay-down pattern Mechanical properties gradient: <ul style="list-style-type: none"> •SL: tensile modulus 61.57 ± 2.05 MPa and compressive modulus 20.44 ± 1.32 MPa •Compressive modulus were SL-PMA > PCL/ALMA-gradient > ML-PMA > DL-PMA •The compressive modulus of the entire PCL/ALMA gradient scaffold was 9.52 ± 1.79 MPa Pores: <ul style="list-style-type: none"> •No numerical values for pore size in the superficial and middle zones •Deep zone has distinct microstructures depending on whether they are cut from hardwood or softwood: <ul style="list-style-type: none"> -Softwood: Square interlaced hollow channels, with widths 10–40 μm and average lengths 3–5 mm -Hardwood: Aligned hollow cellulose channels with gradient circular apertures, from a few to several tens of microns Mechanical properties: Zone-dependent complex mechanical adaptability <ul style="list-style-type: none"> •Superficial zone: Resists shear forces. Compressive modulus ~298 kPa. Modulus 	cartilage with biochemical and morphological properties closely resembling native tissue. Observed in native cartilage. <i>In vitro</i> study Cells: BMSCs from bone marrow extracted from the femora and tibiae of 6-week-old male Sprague-Dawley rats Time period of <i>in vitro</i> culture: Day 1, 3, 7 for cell proliferation assessment, 3 weeks of chondrogenic culture for gene expression analysis Findings: <ul style="list-style-type: none"> •PCL/ALMA hybrid scaffolds exhibited excellent compatibility with rat BMSCs. ALMA furnished an appropriate cartilage-growth microenvironment, with evidence of some larger cell masses and homogeneous distribution. 	(Cao et al., 2021) [113]
	Bio-inspired cellulose-reinforced anisotropic composite hydrogel	Mould casting, sequential hydrogel layering	Materials: <ul style="list-style-type: none"> •Polyethylene glycol diacrylate (PEGDA): Primary polymer matrix for hydrogel •Cellulose fibres: Structural reinforcement Three-zone structure: <ul style="list-style-type: none"> •Superficial zone: Cellulose fabric fibres, oriented parallel to the surface •Middle zone: Cellulose nanofibres, randomly distributed •Deep Zone: Wood cellulose fibres, oriented perpendicular to the surface 	N/A	Pores: <ul style="list-style-type: none"> •No numerical values for pore size in the superficial and middle zones •Deep zone has distinct microstructures depending on whether they are cut from hardwood or softwood: <ul style="list-style-type: none"> -Softwood: Square interlaced hollow channels, with widths 10–40 μm and average lengths 3–5 mm -Hardwood: Aligned hollow cellulose channels with gradient circular apertures, from a few to several tens of microns Mechanical properties: Zone-dependent complex mechanical adaptability <ul style="list-style-type: none"> •Superficial zone: Resists shear forces. Compressive modulus ~298 kPa. Modulus 	<i>In vitro</i> study Cells: BMSCs Time period of <i>in vitro</i> culture: 3 days (cell morphology), 7 days (cell proliferation assessment), 14 days (chondrogenic differentiation evaluation) Findings: <ul style="list-style-type: none"> •BMSCs showed alignment along the cellulose channels, indicating that anisotropic hydrogel structure could guide cell orientation. BMSCs showed good adhesion and growth on hydrogel surfaces. •Hydrogel could promote chondrogenic differentiation of BMSCs, where cells in the superficial zone produced significantly higher levels of collagen II compared to the deep zone. 	(Wang et al., 2020) [62]

(continued on next page)

Table 2 (continued)

Type	Scaffold name	Fabrication method	Zonal structure		Main findings		Reference
			Cartilage scaffold features	Other features (e.g., bone)	Structural & mechanical characterisations	<i>In vitro</i> and <i>in vivo</i> study	
					and stress increase with adding more layers of cellulose fabric. •Middle zone: Cushion to absorb forces from superficial zone. Compressive modulus ~182 kPa. Exhibits clear nonlinear compression behaviour, with modulus increasing slowly at low strain and rapidly at high strain. •Deep zone: Transfers force to subchondral bone. Compressive modulus significantly higher at ~9.8 MPa due to reinforcement by cellulose network. Anisotropic mechanical properties with higher compressive modulus and stress in longitudinal compared to radial direction.		
	Hypotrochoidal scaffolds	Fused Deposition Modelling (FDM) technology through a bioprinter.	Material: Poly (ϵ -caprolactone) (PCL) Arch-like Structure: •Hypotrochoidal Design: Mimicked collagen fibres in cartilage using curved patterns generated by smaller circles rolling inside larger ones. •Zone Division: Divided the scaffold into superficial, middle, and deep zones, replicating cartilage composition and cell density variations. •Pore Structure: Created gradient pores, with the smallest in the superficial zone and the largest in the deep zone, mimicking cartilage heterogeneity for nutrient transport.	N/A	Mechanical Properties •Scaffold with $r = 0.17$ showed Young's modulus similar to native cartilage, making it less stiff than the 0–90 woodpile design (14.1 MPa). •Yield strain and strength of $r = 0.17$ scaffold ranged from $7.9 \pm 0.0\%$ to $11.0 \pm 2.6\%$, indicating its ability to withstand deformation. • $r = 0.17$ design exhibited significantly higher toughness ($0.035 \pm 0.001 \text{ N mm}^2$) than other designs, crucial for load-bearing tissues like cartilage.	<i>In vitro</i> study Cells: ATDC5, a teratocarcinoma-derived chondrogenic cell line Time period of <i>in vitro</i> culture: 28 days Findings: • $r = 0.17$ scaffold in dynamic culture showed increased collagen type II deposition, promoting cartilage-specific protein synthesis. •Reduced expression of collagen type X suggests that the design may prevent hypertrophic changes detrimental to cartilage regeneration. •Higher stress areas in the scaffold exhibited increased glycosaminoglycan (GAG) synthesis, essential for cartilage function. •Enhanced cell proliferation and potential tissue regeneration indicated by increased DNA content per pore volume in $r = 0.17$ samples under dynamic stimulation.	(van Kampen et al., 2023) [137]
	Biomimetic arch-like 3D bioprinted construct	3D bioprinting, directed printing, photo-crosslinking	Materials: Gelatine Methacryloyl (GelMA) and Silk Fibroin-Gelatine (SF-G) bioinks Arch-like structures:	N/A	No information about pore size Mechanical properties: (no details about mechanical	<i>In vitro</i> study Cells: Human bone marrow MSCs Time period of <i>in vitro</i> culture: 21 days	(Chakraborty et al., 2023) [208]

(continued on next page)

Table 2 (continued)

Type	Scaffold name	Fabrication method	Zonal structure		Main findings		Reference
			Cartilage scaffold features	Other features (e.g., bone)	Structural & mechanical characterisations	<i>In vitro</i> and <i>in vivo</i> study	
526			<ul style="list-style-type: none"> •Arch-like Structure: Mimicked collagen II arrangement in native cartilage, replicating its layered characteristics: superficial, middle, and deep zones. •Layered Design: Varying porosities and fibre orientations in each layer simulate cartilage's natural structure and function. •Biomimetic Approach: Imitating cartilage's microstructure and biochemistry created a natural environment for chondrocytes, enhancing proliferation and differentiation. 		properties values): <ul style="list-style-type: none"> •The selection of bioinks (GelMA and SF-G) and the arch-like scaffold design, aimed to mimic the mechanical properties of native cartilage. •The arch-like architecture likely enhanced organised and anisotropic mechanical behaviour, resembling natural cartilage. 	Time frame for culture: 1, 7, and 21 days (gene expression analysis); 7 and 21 days (immunofluorescence, histological analysis) Findings: <ul style="list-style-type: none"> •SF-G constructs exhibited higher encapsulation efficiency and proliferation rates, along with a more uniform distribution of human bone marrow-derived mesenchymal stem cells (BM-MSCs) compared to GelMA constructs. •SF-G demonstrated superiority in forming a fibrous collagen network, promoting chondrogenesis, and facilitating the production of cartilage-specific extracellular matrix. •SF-G enabled the creation of 3D bioprinted arch-like structures for cartilage regeneration and regulation of the Wnt/β-catenin and TGF-β signaling pathways. 	
	Composition or porous architecture	Mould-casting, freeze-drying	Materials: A combination of chitosan (Cs), sodium β -glycerophosphate (GP), and gelatin (Gel) Zonal porous design: Gradient porous scaffolds were designed with varying pore sizes along the longitudinal dimension, smaller in the superficial zone and larger in the deep zone.	N/A	Porosity: Optimal cartilage defect repair was observed with a Cs:GP:Gel ratio of 9:1:5 with porosity at 95.2 %. No information about mechanical properties	<i>In vitro</i> study Cells: BMSCs from Tibia and femur of Sprague-Dawley (SD) rats Time period of <i>in vitro</i> culture: 14 days Findings: <ul style="list-style-type: none"> •Gradient scaffolds with a Cs/GP/Gel ratio of 9:1:5 exhibited good biocompatibility, supporting BMSCs survival, distribution, and extension. •This suggested that the scaffold's physical properties, including its gradient structure, were conducive to cell attachment. •The pore size gradient did not significantly influence cell proliferation. •The BMSCs showed potential for differentiation into osteoblasts and chondrocytes when cultured in specific induction media. 	(Hu et al., 2019) [201]
	Dual-layer scaffold with orientated porous structure	Surface layer: freeze-drying method Transitional layer: unidirectional freeze-drying technique	Materials: A combination of collagen, chitosan, hyaluronic acid, and silk fibroin Bi-layered structure: <ul style="list-style-type: none"> •The surface layer comprised collagen (COL), chitosan (CS), and hyaluronic acid sodium (HAS), with polylactic 	N/A	Morphology: The double structure resembled natural cartilage, featuring larger pores in the surface layer and a microtubule array structure in the transitional layer. This	<i>In vitro</i> study Cells: BMSCs from bone marrow of a 4-week-old male SD rat Time frame for culture: 1, 3, 5, 7 days (cell proliferation assessment); 3, 5, and 7 days of incubation (cell viability)	(Wang et al., 2019) [20]

(continued on next page)

Table 2 (continued)

Type	Scaffold name	Fabrication method	Zonal structure		Main findings		Reference
			Cartilage scaffold features	Other features (e.g., bone)	Structural & mechanical characterisations	<i>In vitro</i> and <i>in vivo</i> study	
			acid-glycolic acid (PLGA) microspheres (MPs) containing Kartogenin (KGN) embedded within. •The transitional layer incorporated collagen (COL), chitosan (CS), silk fibroin (SF), and polylysine-heparin sodium nanoparticles loaded with transforming growth factor- β 1 (TGF- β 1).		design aimed to guide bone marrow stromal cells (BMSCs) along the microtubule walls to the surface layer, promoting their differentiation into chondrocytes. Porosity: The ideal ratio of 1:1:0.1 (COL/CS/HAS) yielded favourable porosity at 50 %, promoting cell proliferation and tissue regeneration. COL/CS/0.5SF exhibited a porosity of up to 92 % Mechanical Properties: Wet biomimetic cartilage scaffolds demonstrated a compressive strength of 0.051 MPa, surpassing dry scaffolds (0.033 MPa), with an elastic modulus of 1.2 KPa.	assessment) Findings: The biomimetic cartilage scaffold promoted cell proliferation, maintained cell viability, and had the potential to regenerate damaged cartilage tissue. <i>In vivo</i> study Animal model: Male New Zealand white rabbits aged 16 weeks Time period/time frame of <i>in vivo</i> test: 4, 8, 12, 16 weeks post-operation Findings: The biomimetic cartilage scaffold effectively guided cartilage tissue regeneration in a knee osteoarthritis model. Its bi-layered structure with specific orientations and materials supported BMSCs' proliferation, migration, and differentiation, resulting in the formation of new cartilage tissue closely resembling normal cartilage.	
	Porous zonal microstructured scaffold	Multiple fabrication strategies: Electrospinning (aligned and random fibres), spherical porogen leaching (intermediate zone), directional freezing (deep zone), melt electrowetting (osteochondral interface).	Materials: Poly (ϵ -caprolactone) (PCL) Zonal design: •Superficial Zone: Features aligned electrospun fibres, mirroring the collagen alignment on the cartilage surface. •Intermediate Zone: Utilised a porogen-leached structure to provide an isotropic framework, facilitating the transition between superficial and deep zones. •Deep Zone: Exhibited a directionally frozen structure, imparting greater stiffness and vertical pore morphology akin to deeper cartilage layers. •Osteochondral Interface: Comprised of a fibrous layer facilitating the transition to the subchondral bone, fostering seamless integration.	Osteo component consisted of 20 μ m diameter fibres stacked at 200 μ m intervals in a 90-degree lay-down pattern	Pore Sizes: •The fibrous zone presented a median major axis pore size of 2.1 μ m and 123.3 μ m, fostering optimal cell attachment and proliferation. •The porogen-leached zone (PLZ) showcased a median major axis pore size of 44.4 μ m, emulating the intermediate cartilage zone with a more isotropic structure. •The directional frozen zone (DFZ) featured larger pores to enhance compressive stiffness, mimicking deeper cartilage regions. Pore geometries in the DFZ and fibrous zones were anisotropic, with smaller pores in the orthogonal direction. Porosity: •The microstructured scaffolds possessed an overall porosity of 97 ± 1 %, critical for enabling cell	<i>In vitro</i> study Cells: Bovine chondrocytes from stifle joints of approximately 1-year-old calves Time period of <i>in vitro</i> culture: 4 weeks Findings: The designed zonal microstructured scaffold can mimic the regional characteristics of articular cartilage and support the growth of chondrocytes and accumulation of ECM <i>in vitro</i> <i>In vivo</i> study Animal model: Female skeletally mature pigs (60–97 kg, mean 78 kg) with osteochondral defects Time period/time frame of <i>in vivo</i> test: 6 months Findings: •New bone formation was observed in the subchondral repair site, with evidence of osteointegration. •Microstructured scaffolds did not demonstrate superior repair quality based on histological scoring at six months. •The study suggested that at	(Steele et al., 2022) [99]

(continued on next page)

Table 2 (continued)

Type	Scaffold name	Fabrication method	Zonal structure		Main findings		Reference
			Cartilage scaffold features	Other features (e.g., bone)	Structural & mechanical characterisations	<i>In vitro</i> and <i>in vivo</i> study	
					infiltration, nutrient and oxygen diffusion, as well as waste removal. Mechanical properties •Compressive Modulus: DFZ: 1974 kPa PLZ: 38 kPa Combined DFZ and PLZ: 64 kPa •Mechanical Anisotropy: Exhibited different mechanical responses in different directions, resembling natural cartilage. •Strain Stiffening and Frequency Dependence: The modulus increased with strain during compression and varied with the frequency of loading. •Cyclic Loading Stability: Underwent a 28 kPa stress at 1 Hz for 12 h, demonstrating long-term stability under physiological loading conditions. Pore sizes: Bottom layer: interconnected macroporous structures, approximately 33.6 ± 13.2 μm and 27.4 ± 11.1 μm Middle layer: column pore architecture, pore sizes approximately 132.6 ± 24.2 μm , and the minor axis pore sizes being around 37.5 ± 8.6 μm . No information about the mechanical study	longer time points, further scaffold biodegradation may lead to increased matrix deposition and improved repair outcomes.	
	Functionally graded multilayer scaffolds	Top layer: Photopolymerisation under UV light (hydrogel encapsulating the hMSC) Bottom and middle layers: created as a single bilayer system using a cryogelation process	Materials: Poly (ethylene glycol)-diacrylate (PEGDA) and N-acryloyl 6-aminocaproic acid (A6ACA) Trilayer scaffold: •Top layer: chondrocytes encapsulated hydrogel to facilitate cartilage tissue formation (PEGDA). •Middle layer: cryogel with an anisotropic, columnar pore architecture to support cartilage tissue formation (PEGDA), hMSCs and chondrocyte-laden layer	Biom mineralisation of the bottom layer to mimic the calcium phosphate (CaP)-rich bone micro-environment, designed to support bone formation.		<i>In vitro</i> study Cell/scaffold type: Human mesenchymal stem cells (hMSCs) & bovine chondrocytes laden scaffold (middle layer) Medium: Chondrogenic-inducing medium Cells: Primary human adult MSCs, chondrocytes from articular cartilage of 8-week-old bovine legs Time period of <i>in vitro</i> culture: 9 weeks Time frame for culture: 3 days, 1 week, 5 weeks, and 9 weeks Findings: The designed trilayer scaffold was capable of supporting the formation of stratified cartilage-like tissue <i>in vitro</i> . <i>In vivo</i> study Animal model: Immunodeficient mice (3-month-old) Time period/time frame of <i>in vivo</i> test: 0, 4, and 8 weeks post-implantation Findings: The scaffold's design, integrating biomaterials with spatially	(Kang et al., 2018) [162]

(continued on next page)

Table 2 (continued)

Type	Scaffold name	Fabrication method	Zonal structure		Main findings		Reference
			Cartilage scaffold features	Other features (e.g., bone)	Structural & mechanical characterisations	<i>In vitro</i> and <i>in vivo</i> study	
						controlled cell differentiation and tissue formation, effectively supported osteochondral tissue regeneration. It integrated with host tissues, promoting the formation of both bone and cartilage components.	
	Biomimetic soft network composites (SNC)	Melt electrospinning writing (MEW), Numerical model-based approach	<p>Materials: The multiphasic SNC was combined with a mPCL and nHA architecture to mimic the cartilage calcified zone.</p> <p>Multiphasic structure: Structurally graded medical grade poly (ϵ-caprolactone) (mPCL) fibers</p> <ul style="list-style-type: none"> •Superficial zone: 800 μm pore •Transitional zone: 400 μm pore •Deep zone: 200 μm •Calcified: 10 layers of mPCL/nHA composite fibers <p>The biomimetic SNC comprised a water-swollen hydrogel matrix and a reinforced fibrous network optimised using an <i>in silico</i> design library-based numerical model.</p>	N/A	<p>Pore size (fibre spacing):</p> <ul style="list-style-type: none"> •Superficial zone: 800 μm •Transitional zone: 400 μm •Deep zone: 200 μm <p>Fibre diameter</p> <ul style="list-style-type: none"> •Superficial zone: 25 μm •Transitional zone: 25 μm •Deep zone: 20 μm <p>Mechanical Properties (E_{SNC})</p> <ul style="list-style-type: none"> •Superficial zone: 491.7 \pm 103.0 kPa •Transitional zone: 1340.4 \pm 143.7 kPa •Deep zone: 2425.8 \pm 574.6 kPa <p>•The printed fibrous networks were used to reinforce the GelMA hydrogel with E_{Matrix} = 39.8 \pm 3.8 kPa</p> <p>The zonal mechanical differences in articular cartilage were highly associated with the variations in the organisation and density of the fibre network</p>	N/A	(Bas et al., 2018) [199]
	3D printing multiphasic osteochondral tissue constructs Novelty: Nano hydroxyapatite	Fused deposition modelling (FDM) 3D printing, computer-aided design (CAD) and fused	<p>Materials: Primary component: Polycaprolactone (PCL)-based shape memory material, polycaprolactone-triol, castor oil, and poly (hexamethylene diisocyanate)</p> <p>Multiphasic constructs (articular cartilage):</p> <ul style="list-style-type: none"> •Superficial region: horizontal pattern •Intermediate region: randomly oriented hexagonal pore structure •Deep region: orthogonal pattern •The upper half of the constructs: without nHA, was soaked in a dopamine hydrochloride solution to polymerise polydopamine (PDA) on the strcuts surface and in bovine serum protein (BSA) to protect the activity of growth factor TGF-β1 	Polycaprolactone (PCL)-based orthogonal pattern scaffold layer: Nanocrystalline hydroxyapatite (nHA) was synthesised and printed into the subchondral bone layers	<p>No information about the Pore sizes</p> <p>Mechanical Properties: The addition of nHA and polymerised polydopamine (PDA) coating was shown to improve the compressive strength and Young's modulus of the scaffold, making it suitable for load-bearing applications.</p>	<p><i>In vitro</i> study</p> <p>Cells: human bone marrow MSCs</p> <p>Chondrogenic factors: including TGF-β1</p> <p>Time frame of <i>in vitro</i> culture: 1, 2, and 3 weeks (differentiation/ chondrogenic studies)</p> <p>Findings:</p> <ul style="list-style-type: none"> •Enhanced hMSC differentiation in cartilage constructs and osteochondral constructs •constructs with nHA and those with nHA, PDA, and TGF-β1 significantly outperformed all other constructs in terms of total collagen production in the upper portion •3D printed constructs containing nHA and bioactive cues had better 	(Nowicki et al., 2020) [200]

(continued on next page)

Table 2 (continued)

Type	Scaffold name	Fabrication method	Zonal structure		Main findings		Reference
			Cartilage scaffold features	Other features (e.g., bone)	Structural & mechanical characterisations	<i>In vitro</i> and <i>in vivo</i> study	
	Bone marrow stromal cell (BMSC)-laden anisotropic hydrogels	3D-bioprinting	Materials: Poly (ϵ -caprolactone) (PCL) Structure (micropattern): Gradient scaffolds (Gradient group: 150, 350, 550, 750 μm pore layers)	N/A	Pore sizes: •Non-gradient scaffolds Small pore size (SPZ): 150 μm Transitional pore sizes: 350 μm , 550 μm Large pore size (LPS): 750 μm No information about mechanical properties	mechanical properties and enhanced hMSC adhesion, growth, and differentiation <i>In vitro</i> study Cells: BMSCs from rabbit bone marrow aspirates Time period of <i>in vitro</i> culture: 6 weeks Findings: Pore size-dependent chondrogenesis of BMSCs in the SPZ scaffold was modulated by the HIF1 α -regulated cell adhesion signalling pathway. <i>In vivo</i> study Animal model: Adult male New Zealand white rabbits weighing 3.0–3.5 kg, knee full-thickness cartilage defect model Time period of <i>in vivo</i> test: 24 weeks post-implantation period Findings: The gradient anisotropic scaffolds had a better cartilage-repairing effect and joint protection function after transplantation compared to Non-gradient scaffolds N/A	(Sun et al., 2021) [21]
	Biomimetic multidirectional scaffolds	Freeze-casting, Lyophilization bonding	Materials: Superficial zone (SZ) scaffold: collagen-hyaluronic acid Transitional zone: collagen-hyaluronic acid suspension Structure (zone-specific fibre orientation): Matrices contained a thin, highly aligned superficial zone that interfaced with a cellular transition zone (TZ) vertically oriented calcified cartilage (OCZ) and osseous zones (OZ).	Lamellar Osseous Zone (OZ) scaffold: collagen-hydroxyapatite-containing suspensions	Zone pore size: SZ: $48 \pm 5 \mu\text{m}$ TZ: $105 \pm 16 \mu\text{m}$ OCZ: $88 \pm 16 \mu\text{m}$ OZ: $98 \pm 15 \mu\text{m}$ Porosity (%): SZ: 75 TZ: 89 OCZ: 92 OZ: 92 Mechanical properties: Compressive testing of hydrated scaffold zones confirmed an increase in stiffness with scaffold depth, where compressive moduli of chondral and osseous zones fell within or near ranges conducive for chondrogenesis or osteogenesis of mesenchymal stem cells. No information about pore size Mechanical properties: •CollGTA first network exhibited a very low Young's		(Clearfield et al., 2018) [205]
	Collagen–Hyaluronic Acid Cryogels	Directional freezing and cryogelation (CollGTA first network), UV light crosslinking (MeHA second network)	Material: Collagen glutaraldehyde–hyaluronic acid methacryloyl (CollGTA–MeHA) Arcade-like structure: •Arcade-like structure: the growth of	N/A		<i>In vitro</i> study Cells: Human chondrocytes from femoral head of an osteoarthritic patient Time period of <i>in vitro</i> culture:	(Yamamoto et al., 2022) [210]

(continued on next page)

Table 2 (continued)

Type	Scaffold name	Fabrication method	Zonal structure		Main findings		Reference
			Cartilage scaffold features	Other features (e.g., bone)	Structural & mechanical characterisations	<i>In vitro</i> and <i>in vivo</i> study	
			ice crystals from copper pins at cryogenic temperatures •The directional cryogel formation enabled the organised growth of ice crystals over a large distance (>4 mm).		modulus (1.6 Pa). MeHA alone exhibited a higher elastic modulus (233 kPa) and stress at break (260 kPa). •MeHA-CollGTA DNs network •exhibited a high early elastic modulus (~200 kPa) and a stress at break of ~184 kPa.	24 h Finding: •No evident toxicity effect on human chondrocytes in contact with CollGTA-MeHA DN was found.	
Cell types & growth factors	Zonal-Specific Cell Density Scaffold	3D bioprint	Material: Alginate-based bioink containing human articular chondrocytes. Structure (three cell densities): 3D print a PCL-reinforced alginate-based scaffold containing human chondrocytes with clinically relevant thicknesses and zone-specific cell densities: •Superficial zone: 20×10^6 cells/mL. •Middle zone: 10×10^6 cells/mL •Deep zone: 5×10^6 cells/mL	N/A	No information about pore size Mechanical properties: PCL frame design significantly increased the bulk mechanical properties compared to the bioink alone.	<i>In vitro</i> study Cell/scaffold type: Human articular chondrocytes from hyaline cartilage in the knee Time period of <i>in vitro</i> culture: 25 days Findings: •Generated a zonal cell density with high viability. •A smooth transition between the zones in terms of cell distribution and a higher sulphated glycosaminoglycan deposition in the highest cell density zone.	(Dimaraki et al., 2021) [112]
	Bilayered fibrin hydrogel Scaffold integrated with dynamic microcarrier expanded zonal chondrocytes	N/A	Material: •Autologous chondrocytes extracted from articular cartilage in the non-weight bearing (NWB) cartilage region of the knee. Large/DZ chondrocytes (S3) 40 %; Medium size/MZ (S2) 40 %; Small/SZ chondrocytes (S1) 20 % •Fibrin hydrogel Structure (zonal chondrocytes): •Bilayered fibrin hydrogel construct	N/A	No information about pore size Mechanical properties: S2S3 chondrocytes from both weight bearing (WB) and NWB regions generated tissue constructs with comparable Young's Modulus, with significantly higher strength than their respective S1 constructs.	Cell source for scaffold: Chondrocytes from femoral condyle and trochlea of articular cartilage in 11–13 months old micropigs <i>In vivo</i> study Animal model: Porcine knee chondral defect mode Time period of <i>in vivo</i> test: 6 months post-implantation Findings: •Zonal phenotype of regenerated tissues •Bilayered implantation of dynamic microcarrier-expanded zonal chondrocytes resulted in substantial recapitulation of zonal architecture, including chondrocyte arrangement, specific Proteoglycan 4 distribution, and collagen alignment, that was accompanied by healthier underlying subchondral bone.	(Tee et al., 2022; Tee et al., 2023) [202, 203]
	Tri-layered PCEC scaffolds, fibre-reinforced GelMA Hydrogels with the incorporation of growth factor-loaded PLGA microspheres	Melt electrowetting (MEW) for microfibre fabrication. UV cross-linking casting method, infiltration and crosslinking procedures for the injection of	Materials: •Poly (ϵ -caprolactone)-poly (ethylene glycol) (PCEC) fibres with depth-dependent fibre organisation •Gelatin methacrylamide (GelMA) hydrogel incorporating rabbit bone-derived MSCs (BMSCs)	Subchondral Bone layer (B): 10 mg BMP-2@PLGA microspheres/ml	Pores size: •S layer: 100 μ m •D layer: 200 μ m •B layer: 600 μ m Lay-down patterns: •S layer: 0°–30° •D and B layer: 0°–90°	<i>In vitro</i> study Cells: Bone marrow MSCs from male New Zealand white rabbits (4 weeks old) Medium: Cell-incorporating constructs were incubated in the chondrogenic and osteogenic	(Qiao et al., 2021) [22]

(continued on next page)

Table 2 (continued)

Type	Scaffold name	Fabrication method	Zonal structure		Main findings		Reference
			Cartilage scaffold features	Other features (e.g., bone)	Structural & mechanical characterisations	<i>In vitro</i> and <i>in vivo</i> study	
		hydrogels into fibre networks	<ul style="list-style-type: none"> •Zone-specific growth factor (GF)-loaded poly (lactic-co-glycolic acid) (PLGA) microspheres •Scaffold: Spatially varying PCEC microfibre configuration (diameters, spacings, and interweaving angle) and biomaterial composition (PCEC-HA fibre for bone layer): PCEC microfibre and PCEC-HA fibre scaffolds •Hydrogel: spatial distribution of the bioactive factors of the transforming growth factor-β (TGF-β) and bone morphological protein (BMP) <p>Zone-specific growth factors:</p> <ul style="list-style-type: none"> •Superficial cartilage (S) layer: 6 mg BMP-7@PLGA microspheres/ml + 2 mg TGF-β1@PLGA microspheres/ml (growth factors: TGF-β1 + BMP-7) •Deep cartilage (D) layer: 8 mg TGF-β1@PLGA microspheres/ml (growth factor: TGF-β1) 		<p>Scaffold porosities:</p> <ul style="list-style-type: none"> •S layer 86.89 %, •D layer 92.27 % •B layer 60.46 %. <p>Thickness of <i>in vivo</i> implanted scaffold:</p> <ul style="list-style-type: none"> •S layer 150 μm, •D layer 450 μm •B layer 2.5 mm <p>Spherical PLGA microspheres average diameter: 3.12 \pm 0.87 μm.</p> <p>Compressive mechanical properties (E):</p> <ul style="list-style-type: none"> •GelMA hydrogel: 28.4 \pm 2.3 kPa •Fibrous networks: •S layer alone: 46.1 \pm 3.8 kPa, •D layer alone: 34.8 \pm 2.7 kPa •SD layer alone: 165.8 \pm 27.6 kPa (significantly low compared with that of human articular cartilage, which is \approx 1 MPa) •S layer-reinforced construct: 283.6 \pm 22.3 kPa •D layer-reinforced construct: 256.6 \pm 24.9 kPa •SD layer reinforcement: 964.2 \pm 56.8 kPa. •B layer (scaffold alone): 46.1 \pm 4.2 MPa •B layer (PCEC/hydrogel composite): 55.8 \pm 5.4 MPa 	<p>induction medium.</p> <p>Time frame of <i>in vitro</i> culture: 7, 14, and 21 days (chondrogenic induction and osteogenesis test); 14 days (cell viability); 21 days (protein expression analysis & immunofluorescence)</p> <p>Findings:</p> <ul style="list-style-type: none"> •The infilled hydrogels and PLGA microspheres did not negatively affect the cell viability. •Differential mRNA expression of osteochondral-related zonal markers in three layers (S, D, and B constructs) confirmed chondrogenesis and osteogenesis. •S layer constructs were more aligned along the fibrous networks; cytoskeletons were elongated and mainly oriented parallel to the fibres in the S layer, while in the deeper zones, the cytoskeletons were oriented more randomly. •Stratified osteochondral tissue function in guiding native-like cell orientation and zonal marker protein deposition. <p><i>In vivo</i> study</p> <p>Animal model: New Zealand white rabbits, three-month-old, weighting 2.5–3.0 kg</p> <p>Time period of <i>in vivo</i> test: 24 weeks post-surgery</p> <p>Findings:</p> <ul style="list-style-type: none"> •The S layer in the defect region enabled lubrication (lower roughness), which endowed the regenerated cartilage with a smoother surface. (compared between B + D and B + D + S groups) •Tri-layered B + D + S group acquired a more lubricating and wear-resistant repair surface. •The stratified structure enabled the entire osteochondral tissue repair 	
	Cytokine-containing microsphere-loaded scaffold	Melt electro-writing (MEW) and Inkjet printing technology (microsphere)	<p>Scaffold materials:</p> <p>Polycaprolactone (PCL) or PCL/hydroxyapatite (HA) scaffolds</p> <p>Multilayer scaffolds (zone-specific growth factors):</p> <ul style="list-style-type: none"> •Surface layer (SL): PCL scaffold 	N/A	<p>Microsphere particle size</p> <ul style="list-style-type: none"> •83.6 % of 1–5 μm diameter •30.2 % of 3–4 μm diameter <p>Pore structures</p> <ul style="list-style-type: none"> •SL: 100 μm; ML & DL: 200 μm 	<p><i>In vitro</i> study</p> <p>Cells: Bone marrow MSCs from New Zealand rabbits (male, 2–4 weeks)</p> <p>Time period of <i>in vitro</i> culture: 21 days</p>	(Han et al., 2020) [136]

(continued on next page)

Table 2 (continued)

Type	Scaffold name	Fabrication method	Zonal structure		Main findings		Reference
			Cartilage scaffold features	Other features (e.g., bone)	Structural & mechanical characterisations	<i>In vitro</i> and <i>in vivo</i> study	
			containing PLGA microsphere encapsulating transforming growth factor- β 1 and bone morphogenetic protein-7 (TGF β 1+BMP-7) •Middle layer (ML): PCL scaffold containing PLGA microsphere encapsulating transforming growth factor- β 1 and insulin-like growth factor-1 (TGF β 1+IGF-1) •Deep layer: PCL/10 % hydroxyapatite (HA) scaffold with PLGA microsphere incorporating transforming growth factor- β 1 (TGF β 1+HA)		•Even fibre shape and smooth surface. Mechanical properties: Mixing HA with PCL improves the scaffold's compressive strength, which is suitable for the performance of the cartilage calcification layer while reducing the tensile strength.	Time frame for culture: 7, 14, 21 days (gene expression analysis) Findings: •The composite biological scaffold was conducive to adhesion, proliferation, and differentiation of mesenchymal stem cells. •The environmental differences between the scaffold's layers contributed to the regional heterogeneity of chondrocytes and secreted proteins to promote functional cartilage regeneration. <i>In vivo</i> study Animal model: Six-month-old male New Zealand rabbits weighing about 3–4 kg Time frame of <i>in vivo</i> test: 3 weeks, 6 weeks, 12 weeks, and 24 weeks Findings: •The composite cartilage group formed smooth cartilage on the surface at 12 w, and the cross-section showed that the scaffold was well integrated with the surrounding tissue. •Adding cytokine-loaded microspheres significantly enhanced the scaffold's biological activity.	

osteocondral unit. However, the scaffold is constructed by iterative layering of numerous electrospun fibre mats, which is relatively tedious and the random fibre orientations within each layer also do not reflect the natural arrangement of collagen fibres in articular cartilage, progressing from parallel to random and then perpendicular. Another approach might be to simply incorporate directionally oriented polymer fibres, such as in the form of microribbons [190], into a hydrogel matrix to create zonal variation within the scaffold, but hydrogels typically exhibit insufficient mechanical properties for applications in load-bearing osteochondral regions. Continued advances in electrospinning technology will enable the construction of nanofibres with specialised designs, and their assembly into sophisticated 3D morphologies that may have versatile applications in the fabrication of multizonal cartilage scaffolds [191].

To create more biomimetic cartilage zones while ensuring load-bearing capability, Castilho et al. [192,193] employed the melt electrospinning (MEW) technique, where the PCL is melted and extruded through a spinneret connected to a high-voltage source to fabricate a bilayered microfibre-reinforced chondral scaffold, comprising a superficial tangential zone (STZ) and a middle and deep zone (MDZ) with varying fibre orientations, as shown in Fig. 6A. The STZ contains densely distributed cross-fibres along the tangential direction, with the fibres laid at alternating angles (0–45–90–135°). This fibre orientation is designed to resist shear forces and provide a smooth, low-friction surface for joint movement. The MDZ contains cross-fibres with a cross-shaped laying pattern of 0–90°, creating a uniform box structure with more randomly oriented fibres, designed to withstand compressive loads, maintain tissue integrity, and provide structural support. The fibrous scaffold is then created by integrating the fibres into a GelMA solution and setting the mixture by UV crosslinking to form a stable hydrogel matrix that encapsulates the fibres. When cultured with chondrocytes, the scaffold showed ability to support the maintenance of chondrogenic phenotype and the continued synthesis of cartilage-specific ECM components such as collagen type II and GAG. However, the different layers did not necessarily produce region-specific mechanical properties, in fact, the hydrogel showed signs of mechanical failure under dynamic loading. This highlights the need for further improvements in the hydrogel system to enhance its fracture toughness and durability under cyclic loading conditions.

Also through electrospinning, Girão et al. [194] developed a tri-layered chondral scaffold using PCL as the bulk material combined with a graphene-oxide (GO)-collagen microporous network, with depth-dependent control over fibre orientation through the generation of horizontally, randomly, and vertically aligned fibres in the corresponding layers, as shown in Fig. 6B. Fibres were first electrospun onto a rotating drum to form a mesh. Cylindrical sheets were then cut from this mesh to serve as the superficial zone. For the deep zone, a small rectangular piece of the electrospun mesh was rolled and embedded within a GO-collagen hydrogel. The middle zone was created by electrospinning fibres into an ethanol-water bath, resulting in a distribution of randomly loosened fibres. This multilayered scaffold showed variation in fibre diameter and pore size among layers, which was considered beneficial for offering topographical cues that could improve cellular organisation and zonal ECM production, although this was not tested in the study. Mechanical testing results suggested that the compressive modulus varied with the direction of fibre arrangement, increasing from the superficial to deep scaffold layers. Moreover, the scaffold exhibited a linear stress-strain curve at low strains, suggesting that the fibres remained straight during compression and the scaffold could maintain its structural integrity.

Another tri-layered scaffold was produced by Munir et al. [195] using a novel combination of cryo-printing and electrospinning, as presented in Fig. 6C. The scaffold design aimed to mimic the zonal structure of articular cartilage through variations in fibre orientation and mechanical properties. PCL was used as the base material throughout the scaffold, first to fabricate a printed helix structure

through cryo-printing that represents the deep zone of cartilage. Electrospinning was then used to deposit PCL on the helix as randomly oriented fibres mimicking the middle zone, followed by highly aligned fibres on the top mimicking the superficial zone. *In vitro* tests confirmed that the multizone scaffold facilitated chondrocyte attachment, survival, and chondrogenic differentiation, as well as promoted the production of cartilage-specific ECM components while maintaining structural and mechanical integrity over the 4-week culture period, providing a potentially effective platform for cartilage tissue engineering.

Using 3D printing, Cao et al. [113] fabricated a tri-layer zonal cartilage scaffold with each layer characterised by unique pore structure and filament gaps. All layers were constructed using PCL impregnated with methacrylate alginate (ALMA). The superficial layer had an orthogonal architecture with a 0°/90° lay-down pattern and filament gap of 300 µm, the middle layer comprised a 0°/60° diagonal pattern with filament gap of 500 µm, and the deep layer had a denser diagonal pattern exhibiting smaller pores and a 0°/30° lay-down pattern with filament gap of 700 µm. These design elements were used to provide structural integrity and mechanical stability for the scaffold when used in areas subjected to high pressures. PCL was used to create the primary scaffold framework, while the ALMA hydrogel was used for encapsulating MSCs and integrated into the scaffold through photo-crosslinking. Subsequent *in vitro* culture showed the ability of the scaffold to promote MSC survival, proliferation, and chondrogenic differentiation over 3 weeks, although differential cell activity within the three layers in the integrated scaffold was not separately assessed.

Using unique naturally-derived materials, Wang et al. [62] constructed a bioinspired three-zone hydrogel scaffold with anisotropic pores and zone-dependent, non-linear viscoelastic mechanical properties, as presented in Fig. 6D. The hydrogel layers comprised a PEGDA polymer matrix combined with cellulose fabric, cellulose nanofibres, and wood cellulose fibres respectively to form the superficial, middle, and deep zones, mimicking the native structure of articular cartilage. Moreover, fibre orientations were made to exhibit zonal variations, with parallel alignment in the superficial zone to resist shear forces, transitioning to random distribution in the middle zone, and perpendicular alignment in the deep zone to enable force transfer to the subchondral bone. This also led to regional variation in mechanical properties, where the compressive modulus of layers changed from 298 kPa to 182 kPa respectively in the superficial and middle zones, to 9.8 MPa in the deep zone. A very interesting observation arising from the study was that the wood cellulose fibres used to construct the deep zone had capillary channel-like structure, which could aid the transport of nutrients and cells. Moreover, cellulose fibres from softwood and hardwood showed distinct structural differences that could be utilised to enhance cartilage regeneration. The softwood fibres exhibited uniformly oriented square channels in the longitudinal direction and interlaced hollow channels in the radial direction, compared to hardwood fibres which showed aligned hollow channels with gradient circular openings longitudinally and orthogonally arranged fibres radially. These aligned anisotropic properties were thought to enhance liquid transport and mechanical performance in the deep zone, and be beneficial for cartilage regeneration. The scaffold showed ability to support the proliferation, migration, and chondrogenic differentiation of MSCs during *in vitro* experiments. Although its performance in aiding *in vivo* cartilage repair remains to be verified, this scaffold provides interesting design ideas for biomimetic multizonal scaffolds, deriving inspirations from nature to recreate the zone-specific structural and mechanical features of articular cartilage.

4.2. Creating zonal cartilage structure by gradient composition or porous architecture

Incorporating gradient composition or depth-dependent porous architecture in multizonal scaffolds is a widely applied strategy for recreating the unique structural features of articular cartilage. A gradient

composition can be achieved through several strategies such as by blending different materials, adjusting mineral concentration, and creating continuous transitions using techniques such as 3D printing. Levingstone et al. [196] provided one of the earlier examples of combining compositional and structural gradients for osteochondral repair by fabricating a tri-layer scaffold through an ‘iterative layering’ freeze-drying method. Each layer contained a different material composition, with collagen types I and II in the cartilage layer, collagen types I and II together with hydroxyapatite in the intermediate layer, and collagen I and hydroxyapatite in the bone layer. The layers were integrated seamlessly by sequentially depositing subsequent layers and iterative freeze-drying, leading to a three-layer gradient structure with high porosity and pore interconnectivity as well as some variation in pore structure between layers. Employing a similar compositional gradient, Cao et al. [197] designed a tri-layered biomimetic scaffold containing collagen type II and chondroitin sulphate in the cartilage layer, collagen type II and hydroxyapatite in the calcified cartilage layer, and collagen type I and hydroxyapatite in the bone layer. This scaffold was seen to promote region-specific tissue repair in rabbit osteochondral defects after 4 months of implantation. Camarero-Espinosa et al. [198] instead focused on changing pore orientation in different scaffold layers to mimic articular cartilage zones. The tri-layered scaffold contained polylactic acid (PLA) in the superficial layer with tubular pores parallel to the surface, an isotropic porous middle layer comprising PLA and sulphated cellulose nanocrystals (CNCs), and a deep layer composed of PLA and phosphate CNCs with tubular pores oriented perpendicular to the subchondral bone. To reduce the risk of mismatch between layers, Parisi et al. [56] created a multilayered scaffold comprising a collagen matrix throughout with depth-dependent distribution of hydroxyapatite particles, ensuring a smooth transitional gradient from the superficial cartilage layer to the bone layer.

In an attempt to satisfy the differing structural, compositional, and biochemical requirements for regeneration of zonal articular cartilage, Wang et al. [20] designed a dual-layer biomimetic scaffold with orientated porous structure resembling the superficial and transitional cartilage zones, as shown in Fig. 7A. The surface layer contained larger pores, while the transitional layer contained a microtubular array structure, which were fabricated through freeze-drying. To match the varying ECM composition of cartilage, the scaffold contained collagen and chitosan in both layers, together with hyaluronic acid in the surface layer or silk fibroin in the transitional layer. Moreover, to provide adequate biochemical cues in different layers, PLGA microspheres loaded with kartogenin and TGF- β 1 were respectively incorporated into the surface and transitional layers. *In vitro* experiments showed that the scaffold structure enhanced the adhesion and proliferation of bone marrow MSCs, while *in vivo* testing in a rabbit knee osteoarthritis model demonstrated the scaffold’s ability to achieve defect filling and cartilage repair, with the repair tissue exhibiting cell morphologies almost matching the normal cartilage after 16 weeks.

Bas et al. [199] introduced a systematic, modelling-based approach to designing biomimetic soft network composites (SNC) as cartilage scaffolds, as presented in Fig. 7B. This approach combined MEW, numerical modelling, injection moulding, and photo-crosslinking to enable precise control over the structure and properties of the engineered constructs. The scaffold design process involved using an *in silico* design library and numerical modelling to simulate the mechanical properties of SNCs, based on hydrogel matrix properties and fibre network structure, under various conditions to mimic the responses of articular cartilage. This allowed selection of the most promising designs for proceeding to fabrication. The scaffold structure was fabricated by MEW using medical grade PCL to create a reinforced fibrous network containing the desired porous structure, with depth-dependent variations in fibre diameter and pore size. Subsequently, injection moulding was combined with photo-crosslinking to infiltrate the GelMA hydrogel matrix into the pores of the printed fibrous network. The resulting scaffold constructs exhibited a zonal architecture with distinct

differences in compressive modulus values between zones, which were highly associated with variations in the organisation and density of the fibre network. The impact of this design on chondrogenic behaviour remains to be confirmed.

Nowicki et al. [200] integrated fused deposition modelling (FDM) as a form of 3D printing with a casting technique to produce a gradient osteochondral scaffold using a novel bioink, as shown in Fig. 7C. The scaffold structure was printed using a PCL-based shape memory material, incorporated with nanohydroxyapatite in the bone part and chondrogenic growth factors in the cartilage part. The gradient structure featured depth-dependent variation in pore distribution and geometry, transitioning from a horizontally aligned superficial zone to a randomly oriented middle zone with a hexagonal pattern, and finally to a stacked orthogonal pattern in the bottom region including the deep zone, calcified zone, and subchondral bone area. The scaffold was found to enhance the adhesion, growth, and chondrogenic differentiation of human MSCs.

Kang et al. [162] created a tri-layer scaffold with depth-varying pore architecture using a poly (ethylene glycol)-diacrylate (PEGDA)-based polymer hydrogel for osteochondral tissue engineering, as shown in Fig. 7D. Initially, the porous bottom and middle layers were fabricated as a single bilayer system using cryogelation. The bottom layer featured an interconnected macroporous structure with pore sizes along the major and minor axes measuring approximately $33.6 \pm 13.2 \mu\text{m}$ and $27.4 \pm 11.1 \mu\text{m}$, respectively. These pore sizes were designed to facilitate cell infiltration and provide a supportive environment for bone formation. The middle layer had a columnar pore architecture with much larger pore sizes of approximately $132.6 \pm 24.2 \mu\text{m}$ along the major axis and $37.5 \pm 8.6 \mu\text{m}$ along the minor axis. The anisotropic pore structure in this layer was designed to guide cell alignment and nutrient transport for cartilage repair. Prior to fabricating the top layer, the bilayer scaffold was subjected to biomineralisation in the bottom layer to provide an environment rich in calcium phosphate that is conducive to bone regeneration. The top layer consisted of a hydrogel without interconnected pores formed by photopolymerisation. For *in vitro* testing, the scaffold was cultured in chondrogenic medium with human MSCs and bovine chondrocytes in the middle layer, together with human MSC aggregates in the top layer and an acellular bottom layer. The cells were capable of chondrogenic differentiation without concurrent osteogenic differentiation, evidenced by minimal collagen type I and osteocalcin staining in the top and middle layers. The scaffold also supported tissue formation resembling osteochondral tissue structure when implanted subcutaneously in mice.

Through mould casting and freeze-drying, Hu et al. [201] fabricated a gradient scaffold comprising chitosan/ β -glycerophosphate/gelatin with gradual variation in pore size, as shown in Fig. 7E. Preliminary experiments identified an optimal mass ratio of materials at 9:1:5 for use in scaffold fabrication, which provided the highest porosity and water absorption rate. Through a gravity-aided mixing and casting process followed by freeze-drying, the resulting scaffolds exhibited a gradient of pore sizes along the longitudinal dimension, with smaller pores in the superficial zone and larger pores in the deep zone. *In vitro* tests using bone marrow MSCs showed the scaffold’s ability to support cell survival and distribution, as well as chondrogenic and osteogenic differentiation when cultured in specific induction media, although the pore size gradient was not observed to significantly influence cell proliferation compared to non-gradient scaffolds.

Using a 3D bioprinting technique, Sun et al. [21] constructed a four-layered cartilage scaffold with an anisotropic gradient in pore structure, comprising a PCL framework with varying fibre spacing and a natural polymer composite hydrogel encapsulating bone marrow MSCs that was printed into the microchannels between PCL fibres, as shown in Fig. 7F. The spacing between PCL fibres varied from $150 \mu\text{m}$ in the top layer to 350 , 550 , and $750 \mu\text{m}$ in the subsequent layers to create the gradient structure. This resulted in smaller pore size in the top layer, designed to mimic the superficial cartilage zone, which would restrict

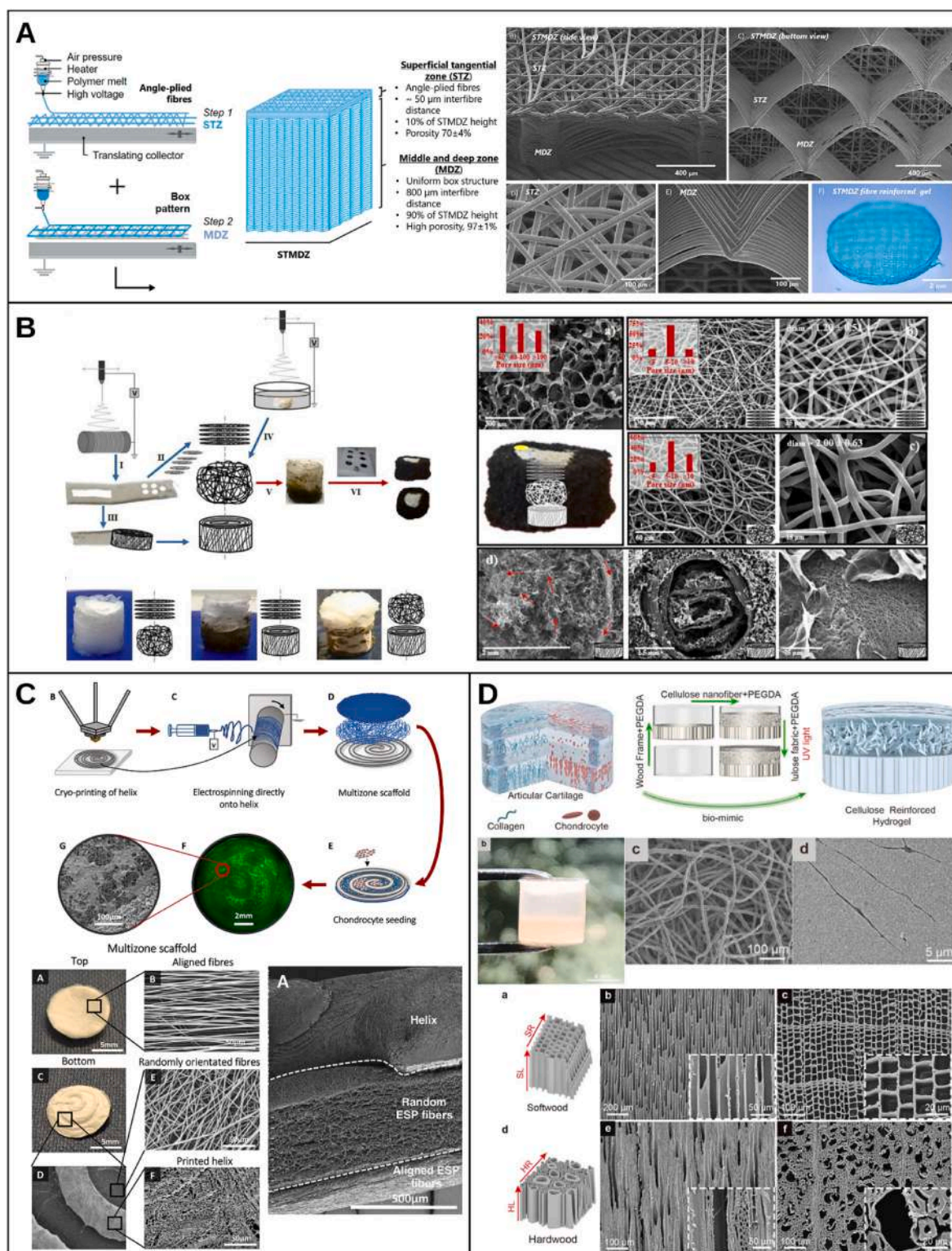


Fig. 6. Examples of zonal cartilage scaffolds based on varying fibre orientation. (A) Bilayered microfibre-reinforced chondral scaffold obtained by melt-electrospinning (MEW) with superficial tangential zone (STZ) and middle-deep zone (MDZ) simulated the structure of articular cartilage, adapted with permission from Ref. [193]. (B) Tri-layered anisotropic fibrous scaffold fabricated by electrospinning and modifying the electrospun mesh to mimic the three distinct cartilage zones, adapted with permission from Ref. [194]. (C) Tri-layered scaffold fabricated by integrating cryo-printing and electrospinning to precisely mimic the superficial cartilage zone with aligned fibres, the middle zone with random fibres, and the deep zone with a printed porous structure, adapted with permission from Ref. [195]. (D) Scaffold with zone-dependent variation in fibre diameter and orientation, and mechanical properties to closely replicate the stratified structure of articular cartilage, composed with cellulose nanofibres and a wood cellulose frame reinforced by polyethylene glycol-based anisotropic composite hydrogel, adapted with permission from Ref. [62].

vascularisation and provide a conducive microenvironment for chondrogenic differentiation while also enhancing scaffold strength. In the bottom layer, the large pore size was designed for maximising the penetration of nutrients and oxygen to promote angiogenesis, which would support cartilage maturation, tissue calcification, and scaffold integration with surrounding tissues. When tested separately, the scaffold layers with different pore sizes were seen to influence chondrogenic differentiation and cartilage ECM formation by MSCs. Specifically, scaffold layers with smaller pores upregulated genes associated with superficial hyaline chondrocytes, such as HIF1 α , ACAN, and COL2A1, while layers with larger pores upregulated genes associated with deep hypertrophic chondrocytes, such as COL10A1 and RUNX2. Interestingly, the study revealed that the pore size-dependent chondrogenic behaviour of MSCs was modulated by the HIF1 α /FAK signalling axis. When tested in full-thickness cartilage defects in the rabbit knee, the gradient scaffold was shown to achieve better cartilage repair and joint protection compared to single-layer scaffolds with small or large pore sizes, with faithful reconstruction of hyaline-like cartilage that exhibited zone-specific cell morphology and ECM formation approximating the structure of native tissue.

Steele et al. [99] employed multiple fabrication strategies to produce a porous zonal microstructured scaffold closely mimicking the variation in architecture, ECM composition, and mechanical properties within the osteochondral tissue unit, as shown in Fig. 7G. Uniquely, the scaffold was fabricated from PCL as the only material constituent, with various gradients created through different processing techniques. Electrospinning was used to fabricate the uppermost layer with aligned fibres for the superficial zone, as well as the bottommost layer with random fibres for the osteochondral interface. The intermediate zone was formed using thermoset gelatin microspheres as porogens, which were subsequently removed by lyophilisation. The deep zone was constructed by directional freezing, involving phase separation of the polymer solution to form longitudinal pore orientations with large pore diameters. MEW was used to print the bone component with a grid-like structure, comprising 20 μ m fibres spaced at 200 μ m intervals. This study possibly represented the most biomimetic scaffold design for osteochondral tissue, providing not only architectural and pore size gradients but also transition in mechanical properties between layers that faithfully replicated many of the zonal features of articular cartilage as well as the region-specific properties of cartilage and bone. Notably, the scaffold exhibited dynamic loading response, where the modulus increased with strain during compression and varied with the frequency of loading. Long-term mechanical stability was also observed with cyclic loading under physiologically relevant conditions. This was one of the few studies where detailed mechanical characterisation was performed and showed that the scaffold replicated many of the mechanical features of native osteochondral tissue. When tested *in vitro*, the scaffold supported chondrocyte growth and ECM deposition that mimicked the zonal characteristics of articular cartilage. Uniquely, the scaffold was then tested *in vivo* using a clinically relevant large animal model, and assessed for its capacity to induce osteochondral repair in skeletally mature pigs over 6 months. The zonal scaffold showed mechanical stability and reproducible repair quality within the defect, with clear osseointegration and restoration of a flush articular surface. However, the repair quality did not exceed the control based on histological scoring. The thorough investigations in this study have also underlined the difficulty of relating outcomes obtained in smaller animals to larger animals and clinical application due to inherent differences in physiology and tissue repair capacity between species.

4.3. Creating zonal cartilage structure by incorporating cells or growth factors

In addition to providing architectural or compositional gradients, biomimetic scaffolds may be augmented in their capacity to induce zonal cartilage formation through the incorporation of zone-specific cell

populations and/or growth factors, which can help to create stratified variations in the regenerative microenvironment. Variation in cell population alone within the same base scaffold material has been shown to help with recapitulating the zonal architecture of articular cartilage. For instance, Tee et al. [202,203] isolated chondrocytes from the non-weight-bearing femoral condyle and trochlea regions of porcine articular cartilage and sorted them by size-based strategies. The superficial zone (SZ) chondrocytes were smaller and more elongated compared to cells in other zones, and produced high amounts of PRG4 crucial for lubrication. Middle zone (MZ) chondrocytes had intermediate size, and were primarily responsible for producing cartilage ECM components such as collagen type II and aggrecan. Deep zone (DZ) chondrocytes were larger and responsible for producing a robust ECM that could withstand high compressive forces. Autologous zonal chondrocytes were isolated and expanded, then sorted by size and incorporated into fibrin hydrogels for implantation into porcine knee cartilage defects. When evaluated at 6 months after implantation, bilayered fibrin hydrogels containing SZ and MZ/DZ chondrocytes respectively in the top and bottom layers outperformed the same hydrogels containing a homogeneous chondrocyte population with mixed zonal phenotypes. The bilayered constructs formed cartilage tissues with zone-specific biochemical and biomechanical properties, including variations in chondrocyte arrangement, PRG4 distribution, and collagen alignment between the two layers accompanied by elevated subchondral bone health.

To mimic the zone-specific variations in cell density observed in articular cartilage, Dimaraki et al. [112] constructed a zonal scaffold comprising a PCL outer skeleton and 3D bioprinted cellular layers built using an alginate-based bioink, as shown in Fig. 8A. Human articular chondrocytes were embedded in the scaffold layers at different densities, with the cell distribution controlled to reflect a natural zonal gradient: 20×10^6 cells/mL in the superficial zone, 10×10^6 cells/mL in the middle zone, and 5×10^6 cells/mL in the deep zone. The scaffold was structured as a cube with dimensions of 7.2 mm \times 7.2 mm \times 3 mm, and divided into 15 layers distributed among the three zones. *In vitro* culture in chondrogenic medium for 25 days showed that the bioprinted zonal scaffold with gradient variation in cell densities could maintain its structure and promote the formation of cartilage-like tissue. A smooth transition in cell distribution was noted between zones, and increased GAG deposition was found in the zone with the highest cell density.

Other studies have augmented biomimetic zonal scaffold designs with zone-specific variation in growth factors. For example, a study by Wang et al. [20] discussed earlier produced a dual-layer scaffold with orientated porous structure, which was supplemented by the incorporation of PLGA microspheres encapsulating kartogenin and TGF- β 1 in the surface and transitional scaffold layers, respectively. Through a somewhat similar approach that combined gradients in scaffold architecture and distribution of growth factors, Qiao et al. [22] developed a bioinspired tri-layered scaffold based on a MEW poly (ϵ -caprolactone) and poly (ethylene glycol) (PCEC) network that provided depth-dependent variation in fibre structure according to diameter, spacing, and interweaving angle, as shown in Fig. 8B. In addition to this architectural gradient, a biochemical gradient was created by polymerising GelMA hydrogels loaded with MSCs and zone-varying growth factors. The selection of growth factors was based on their abilities for guiding MSC differentiation in different zones to induce specific tissue formation corresponding to the stratified morphology of articular cartilage. Specifically, the superficial cartilage layer contained TGF- β 1 and BMP-7 for inducing chondrogenic differentiation and enhancing the expression of superficial zone protein (SZP) to improve the lubricating and wear-resistant properties of the cartilage surface. Meanwhile, the deep cartilage layer contained TGF- β 1 to promote the formation of a proteoglycan-rich, interconnected cartilaginous matrix, and the subchondral bone layer was loaded with BMP-2 to stimulate osteogenic differentiation and the formation of a mineralised bone-like matrix. Through targeted delivery of growth factors, the scaffold enabled

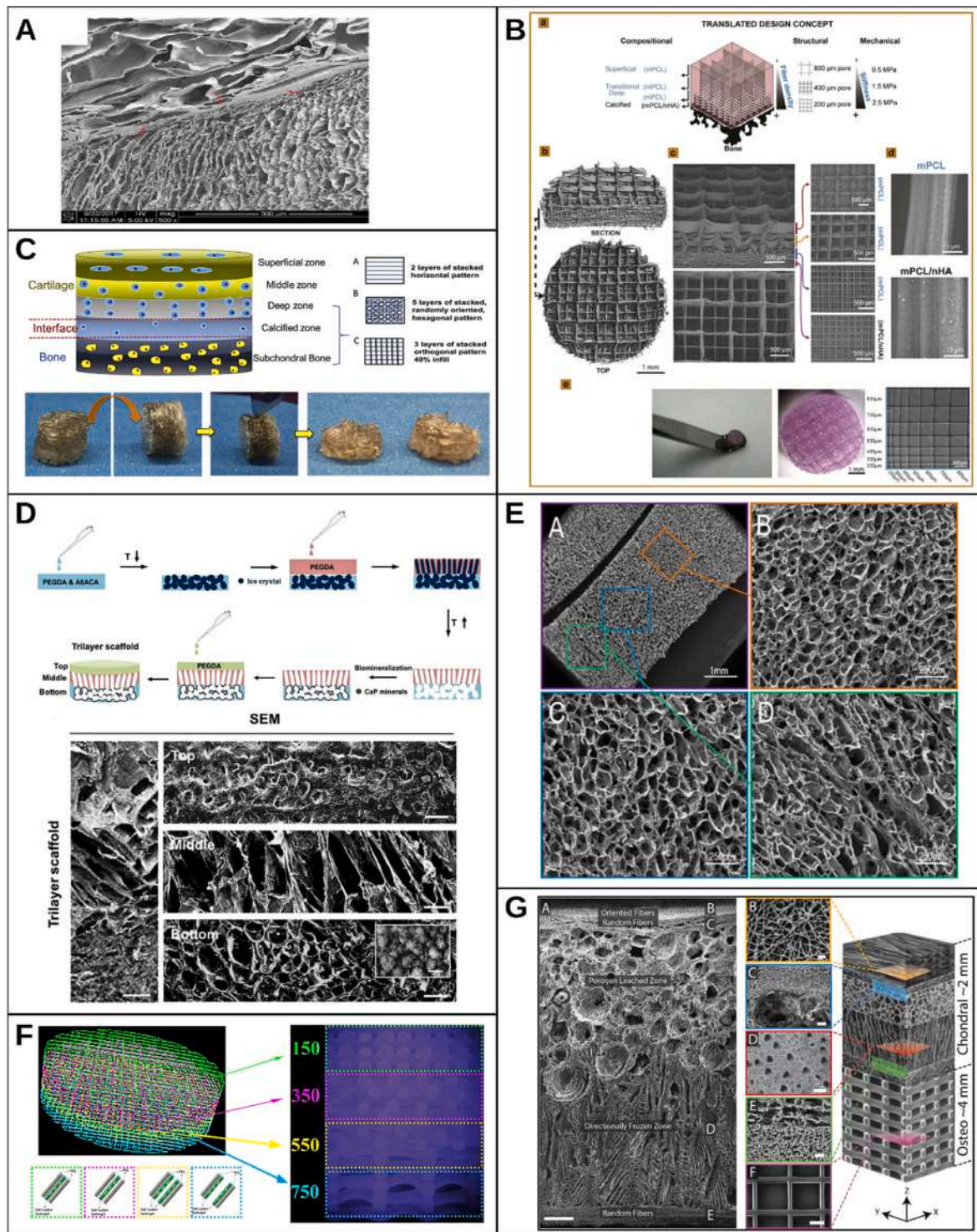


Fig. 7. Examples of zonal cartilage scaffolds based on gradient composition and porous architecture. (A) Dual-layer biomimetic cartilage scaffold resembling the surface and transition layers of articular cartilage (SEM image indicates the distinct microstructure between layers), adapted with permission from Ref. [20]. (B) Multilayered soft network composites with spatial stratification of structural fibre spaces, compositional differences, and gradient mechanical stiffness, adapted with permission from Ref. [199]. (C) Gradient osteochondral scaffold produced by FDM with change in pore distribution and geometry, adapted with permission from Ref. [200]. (D) Tri-layer scaffold with depth-varying porous design and biomimetic environment, adapted with permission from Ref. [162]. (E) Gradient scaffold with gradual variation in pore size, adapted with permission from Ref. [201]. (F) 3D-bioprinted four-layered scaffold with a pore structure gradient, adapted with permission from Ref. [21]. (G) Porous zonal microstructured scaffold with gradient variation in architecture, composition, and mechanical properties, adapted with permission from Ref. [99].

zone-specific deposition of protein markers related to chondrogenesis and osteogenesis by MSCs after *in vitro* culture for 28 days, including SZP in the superficial layer, aggrecan in the deep layer, collagen type II in both superficial and deep layers, and collagen type I in the bone layer. When implanted into rabbit osteochondral defects for 24 weeks, the tri-layer scaffold achieved osteochondral tissue repair throughout the defect region, particularly noting a lubricating and wear-resistant repair surface. It should be mentioned that the *in vivo* study compared the tri-layer scaffold to other scaffold variations with fewer layers, rather than between scaffolds loaded with or without growth factors.

Through a different selection of growth factor distribution, Han et al. [136] produced a multilayer scaffold through MEW, comprising a network of PCL fibres and PCL + hydroxyapatite fibres in the respective cartilage and bone regions, as shown in Fig. 8C. PLGA microspheres containing different types of growth factors were inkjet printed onto the scaffold layers during fabrication to create a zone-specific distribution, characterised by TGF- β 1 throughout the surface, middle, and deep scaffold layers, BMP-7 only in the surface layer, and IGF-1 only in the middle layer. The deep layer comprising the bone region hence contained TGF- β 1 and hydroxyapatite in addition to PCL. After culturing with bone marrow MSCs for 21 days, the scaffold induced zone-specific expression of mRNA and proteins associated with chondrogenesis, including higher levels of PRG4 in the surface layer and CILP in the middle layer, as well as COLII and SOX9 in all three layers. When implanted in a rabbit osteochondral defect for 12 weeks, the scaffold loaded with growth factors achieved significantly better repair compared to a scaffold control group not containing growth factors, demonstrated by the formation of a smooth cartilage surface, strong integration with surrounding tissue, and greatly increased deposition of collagen type II and compressive modulus of the repair tissue towards functional cartilage regeneration. Multizonal cartilage scaffolds based on spatial variation in growth factors may also benefit from having ‘dynamically adaptive’ properties, for instance, scaffolds can be designed to dynamically release different types of growth factors in response to physiological or mechanical changes in the environment during the healing process [204].

4.4. Other special zonal scaffold designs

Other interesting designs of zonal cartilage scaffolds have been generated by specific modulation of oriented pore structures through freezing and controlling the direction of heat transfer [169,205–207]. It is also possible to generate biomimetic arcade-like structures within the scaffold through various methods including 3D printing [137,208,209] and directional freezing [210]. By modifying freeze-drying kinetics with the aid of a mould, scaffolds can be made into either an isotropic porous structure containing random pores or an anisotropically aligned porous structure, depending on the direction of heat transfer. For example, Clearfield et al. [205] developed an osteochondral scaffold with multi-directional layers through directional freezing, as shown in Fig. 9A. The superficial cartilage layer and subchondral bone layer were respectively created by unidirectional freeze casting of collagen-hyaluronic acid and collagen-hydroxyapatite solutions, utilising a temperature gradient to allow for directional solidification. The two layers were then joined through a lyophilisation bonding process involving a collagen-hyaluronic acid suspension to mimic the transition zone. This led to the formation of an integrated scaffold with pores aligned in different directions within the superficial, transition, and osseous zones. Cellular responses to this biomimetic scaffold remain to be verified.

The arcade-like structure is a new type of scaffold architecture design that directly resembles the collagen fibre orientation within the articular cartilage region. In an example study, Yamamoto et al. [210] fabricated such structures through a relatively simple method of directional cryogel formation from collagen and hyaluronic acid derivatives, by inducing the growth of ice crystals from copper pins, as shown in Fig. 9B. The scaffolds exhibited an anisotropic structure with pores and polymer

fibres aligned in specific directions, guided by the growth direction of ice crystals, forming distinct zones with different fibre orientations and packing densities mimicking the zonal architecture of articular cartilage.

An interesting concept of ‘hypotrochoidal scaffolds’ was recently demonstrated by van Kampen et al. [137] who used FDM to build up a PCL construct layer by layer, as shown in Fig. 9C. This scaffold featured a unique architecture comprising a hypotrochoidal pore network mimicking the arch-like organisation of collagen type II fibres in articular cartilage. The hypotrochoidal curve was generated by tracing a point linked to a smaller circle rolling inside a larger circle. This hypotrochoidal scaffold design exhibited a gradient in pore size, with the smallest pores in the superficial zone and the most prominent pores in the deep zone, replicating the heterogeneous structure of articular cartilage. A specific design with radius (r) of the smaller circle $r = 0.17$ was found to result in optimal scaffold mechanical properties approaching native cartilage in Young’s modulus, as well as provide high toughness and ability to withstand deformation. The same design also enhanced chondrogenic behaviour by a commonly used cell line, evidenced by increased collagen type II and GAG deposition accompanied by reduced expression of collagen type X.

5. Outlook and perspectives

Satisfactory treatment of osteochondral defects has been a long-standing clinical challenge due to the intricate structure of the chondral region and its limited self-healing capacity. The last few years have seen growing research interest in scaffold-based approaches for engineering stratified cartilage and osteochondral tissues [15,211]. Scaffold designs have attempted to address the distinct, region-specific regenerative requirements of osteochondral tissue by introducing various architectures, material compositions, and fabrication methods [9,212]. Multizonal or zone-specific scaffolds are now emerging as an innovative concept for osteochondral repair, with the aim of specifically replicating the unique spatial organisation of articular cartilage to achieve functional tissue restoration. The recapitulation of native tissue characteristics may be considered from several aspects to achieve a biomimetic microenvironment, including zone-specific matrix composition, collagen fibre orientation, mechanical properties, cellular phenotypes, and bioactive factors [213,214].

As seen through the example studies discussed in this review, biomimetic multizonal cartilage scaffolds hold great promise in restoring the physical and biochemical properties necessary for recreating the stratified structure seen in native articular cartilage. However, a few factors need to be considered for translating the outcomes of current studies towards clinical applications. For instance, many of the studies discussed in the review have focused on recreating the zonal architecture or composition of articular cartilage, but did not actually verify the ability of the scaffold design to induce zone-specific cellular behaviour *in vitro* or better cartilage repair outcomes *in vivo*. Moreover, it is relatively easier to create separate scaffold layers for satisfying the disparate requirements of zonal cartilage and subchondral bone regeneration, imposing challenges for seamless integration at the layer interfaces. In particular, the transition in properties from one layer to the next can introduce a mismatch in mechanical properties and degradation rates, leading to increased shear stress between layers and a risk of non-integration or scaffold failure when used in load-bearing regions. This risk increases with the number of distinct layers within a single scaffold, which may also hinder the rate of integration with host tissues [10]. The greater processing complexity of zonal compared to homogeneous chondral scaffolds may pose another issue, as this reduces the reproducibility of fabrication and scale-up potential. This issue may be exacerbated by the popular selection of naturally-derived materials for constructing chondral scaffolds, which often present batch-to-batch variability in composition or properties [215]. Hence, despite the apparent advantages of biomimetic multizonal scaffold designs for cartilage regeneration, current limitations in materials selection and

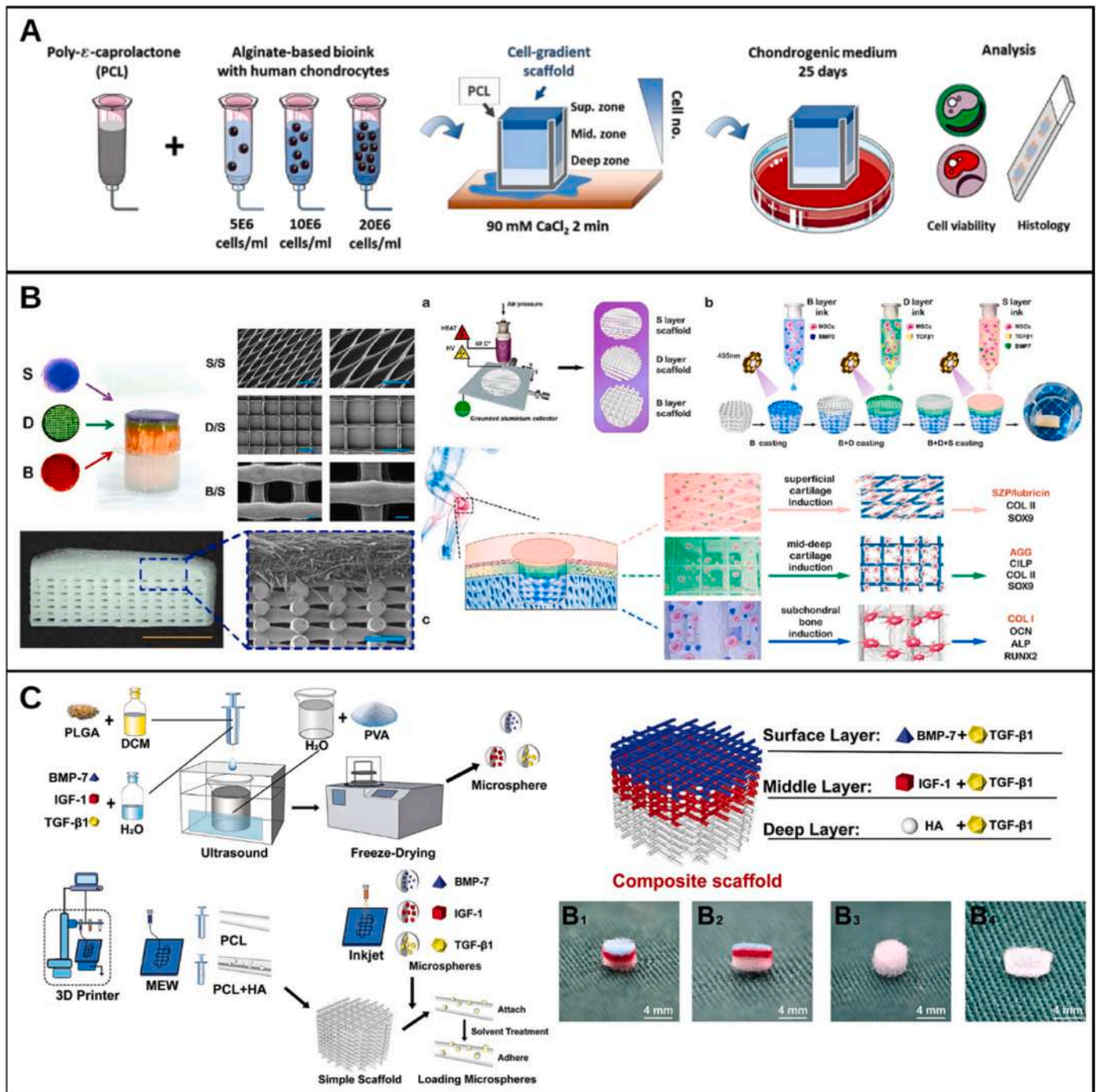


Fig. 8. Examples of zonal cartilage scaffolds based on variations in cell type or growth factors. **(A)** Zonal-specific cell density scaffold mimicking the natural cell concentrations across superficial, middle and deep cartilage zones, adapted with permission from Ref. [112]. **(B)** Bioinspired stratified electrospun fibre-reinforced hydrogel constructs with zone-specific variation in the growth factors BMP-2, TGF-β1 and BMP-7 across the subchondral bone, middle-deep cartilage zone, and superficial cartilage zone, adapted with permission from Ref. [22]. **(C)** High-precision multilayer scaffolds with zone-specific variation in the growth factors BMP-7 and IGF-1 to resemble the depth-dependent microenvironment of articular cartilage, adapted with permission from Ref. [136].

manufacturing techniques may pose some practical hurdles for generating complex scaffolds that are suitable for real-world applications. While these limitations are beginning to be addressed by continuous advances in biomaterials and biomanufacturing technologies, further research on cartilage scaffolds should aim to strike a balance between the benefits and limitations of employing a biomimetic multizonal design.

5.1. Future directions in designing multizonal cartilage scaffolds

Some of the abovementioned issues for creating practically-relevant, biomimetic multizonal scaffolds may be addressed through advances in biomanufacturing to achieve greater precision and control over scaffold characteristics, including fabrication techniques such as 3D bioprinting [168,216] and direct writing electrospinning [163], and imaging techniques such as MRI to guide the design of patient-specific biometric scaffolds that incorporate details about the morphology and

composition of native tissue [217]. Through the integration of new fabrication technologies and biomaterial selections, scaffold designs can be generated with tailored geometries and material properties that closely mimic the native tissue environment [218]. Moreover, multi-modal approaches incorporating stem cells, growth factors, and other bioactive molecules hold promise for improving patient-specific tissue regeneration and scaffold-tissue integration [219]. Ongoing research into biomimetic materials with tunable mechanical properties and degradation rates may help to address the challenges of mismatched

mechanical properties and variability in biodegradation rates between scaffold layers [22,192,220]. Meanwhile, advanced computational modelling will further aid in scaffold design optimisation, enabling the prediction of scaffold-tissue interactions based on scaffold architecture and mechanical behaviour [221,222]. Artificial intelligence (AI) can be leveraged to optimise cell populations and deliver zone-specific growth factors, thereby streamlining the research process and reducing costs and time associated with experimentation [223]. The advancement of biomimetic scaffolds into bionic scaffolds that simultaneously deliver

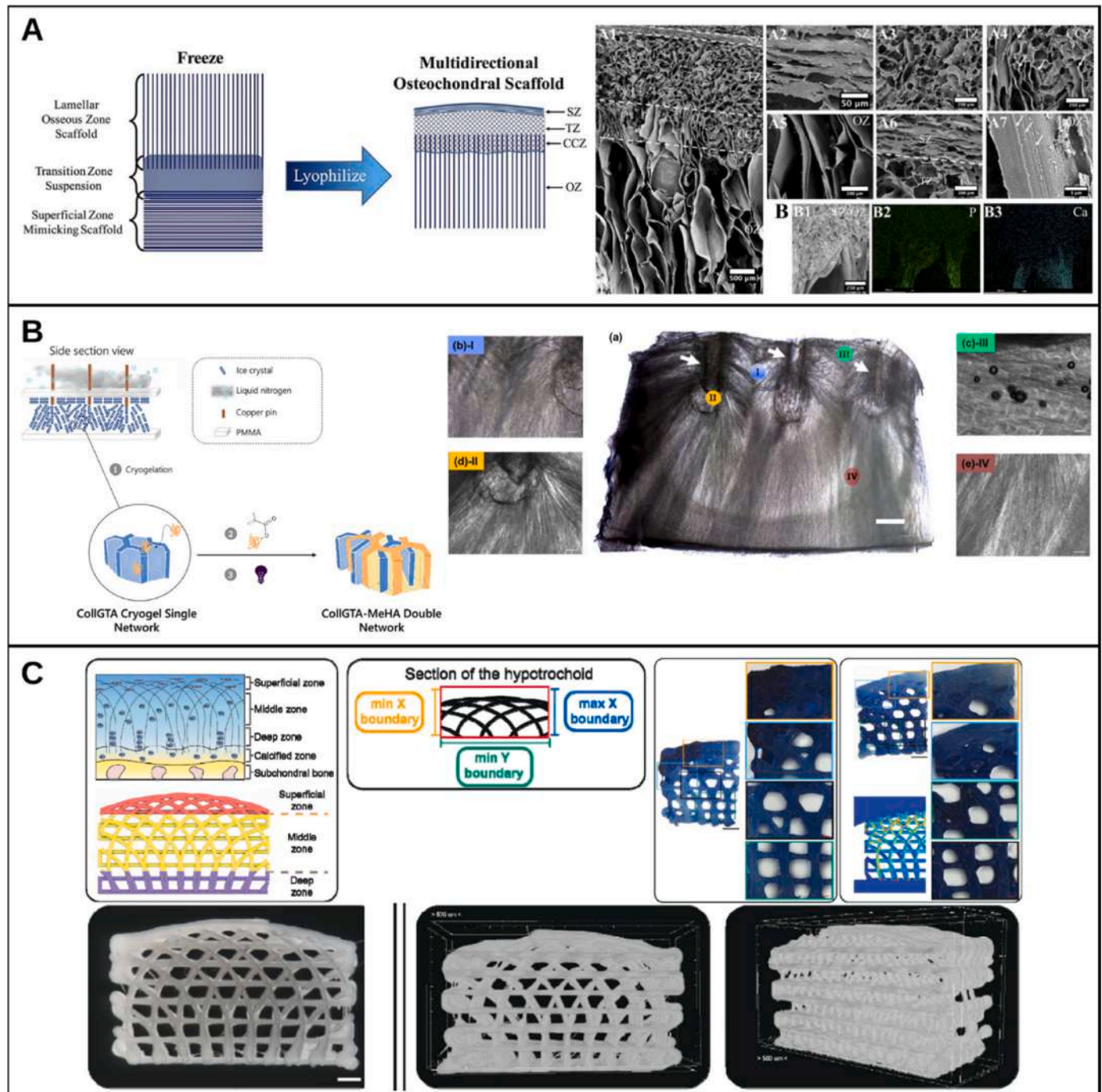


Fig. 9. Other types of special designs for zonal cartilage scaffolds. (A) Multidirectional osteochondral scaffolds generated by directional freezing formed three different pore orientations simulating the collagen fibre spacing of articular cartilage zones, adapted with permission from Ref. [205]. (B) Collagen-hyaluronic acid cryogels with arcade-like structure mimicking continuous variations in articular cartilage collagen fibre orientation and force distribution, adapted with permission from Ref. [210]. (C) Hypotrochoidal scaffolds resembling the arch-like organisation of collagen type II along the entire depth of articular cartilage, adapted with permission from Ref. [137].

therapeutic effects while enabling in-situ real-time monitoring of tissue repair may lead to a new era of multizonal cartilage scaffolds. For instance, utilising electroactive nature of living organisms, smart nanoengineered electronic scaffolds may be developed to stimulate cartilage repair while also providing timely assessment of disease progression and treatment effects [224].

As an alternative to creating distinct scaffold layers for representing the zone-specific properties of articular cartilage, emerging one-pot strategies based on innovative fabrication techniques may provide new food for thought. For example, a new light-based biofabrication method known as Filamented Light (FLight) can be applied to photo-sensitive bioresins to efficiently create macroporous anisotropic scaffolds, composed of hydrogels containing microchannels of $14 \pm 5 \mu\text{m}$ and microfilaments of $8 \pm 2 \mu\text{m}$ [225]. This scaffold was found to be effective in instructing anisotropic cell growth and directional deposition of collagen, resulting in improved maturation of cartilage-like tissues that mimicked the ECM architecture and mechanical properties of native deep zone cartilage. Another study utilised laser micro-patterning technology (LMPT) to directly modify the surface of native porcine osteochondral grafts [226]. By optimising LMPT parameters to create the most suitable density and morphology of pores on the graft surface, the osteochondral grafts demonstrated improved permeability while maintaining mechanical stability, enabling more efficient decellularisation and subsequent recellularisation for use as osteochondral transplants. *In vivo* implantation in a goat model showed significant regeneration of both cartilage and subchondral bone at 6 and 12 months. While these examples did not specifically attempt to recreate the zonal cartilage structure, they provided a simple approach for generating biomimetic osteochondral tissue that could potentially include zonal variations in the chondral region.

Other exciting advances in scaffold biomanufacturing for tissue engineering include 4D bioprinting, which has evolved from 3D bioprinting but with the addition of a fourth dimension – time [227]. This allows the construction of smart or stimuli-responsive dynamic scaffolds that exhibit programmable variation in structure, properties, and functionality over time or when exposed to specific external stimuli, such as pH, light, temperature, water, and electric or magnetic fields. The programmable dynamic structures of 4D printed scaffolds can be achieved by using smart bioinks, comprising specialised materials capable of altering their shape or characteristics when exposed to external cues. Current biomaterials employed as smart bioinks include shape memory polymers (SMPs), shape-morphing hydrogels (SMHs), and their composite materials. Based on some limited evidence of applying 4D bioprinting in cartilage tissue engineering [228], SMHs may be more favourable than SMPs for this purpose, due to their ability to undergo reversible shape deformation in response to external stimuli [229]. SMHs may therefore mimic the dynamic and functional properties of native cartilage, by adapting their structure over time to better integrate with the surrounding tissue or respond to physiological changes. Some examples of SMHs used as bioinks in 4D bioprinting to generate cartilage-like tissue constructs include silk fibroin [230], oxidized methacrylate alginate (OMA) without [231] or with GelMA [232], and tyramine-functionalised hyaluronan (HAT) without or with alginate [233].

Future strategies in using bioprinting to construct multizonal cartilage scaffolds may also benefit from the integration of nanoparticles, to create nanocomposite scaffolds with enhanced control over their structural, physicochemical, mechanical, and biological properties, stemming from the shape, size, surface chemistry, concentration, and/or source material of the nanoparticles [234]. A diverse array of nanomaterials have been integrated into bioinks for scaffold bioprinting, including carbon-based nanoparticles such as graphene and graphene oxide, carbon nanotubes, and carbon nanofibers; ceramic nanoparticles such as silica-based bioceramics, calcium phosphates, various oxides, and bioactive glasses; natural and synthetic biopolymeric nanoparticles; and a variety of metallic nanoparticles. Excitingly, the incorporation of

nanomaterials may help with 4D bioprinting of cartilage scaffolds. In addition to conferring improved mechanical strength to the polymeric matrix, nanoparticles may be stimuli-responsive, thereby allowing the bioprinted nanocomposite scaffold to respond with changes in properties under exogenous cues. For example, Ricotti's group used 4D printing to create a nanocomposite bioactive hydrogel that incorporated piezoelectric barium titanate nanoparticles and graphene oxide nanoflakes [235]. This was the first study to explore the synergistic use of piezoelectric nanomaterials with ultrasound stimulation for enhancing cartilage regeneration. Adipose-derived MSCs embedded within the hydrogel were stimulated with dose-controlled ultrasound waves at a range of frequencies and intensities. The optimal stimulation regimen at 1 MHz frequency and 250 mW/cm^2 intensity once every two days over ten days resulted in significantly increased expression of chondrogenic genes such as COL2A1, ACAN, and SOX9 with simultaneous reduction of fibrotic and catabolic markers such as COL1A1 and MMP13. The improved anti-inflammatory and chondrogenic responses of MSCs were thought to be enabled by stimulus-responsive changes in the nanocomposite hydrogel, leading to an electric field that modulated mechanotransduction pathways in cells and consequent alterations in gene and protein expression. It should be noted that the type of approach and technology used in this study is still in the very early stages of development, and further *in vivo* studies are needed to demonstrate proof-of-concept. Nevertheless, the emergence of 4D bioprinting and continued innovations in nanocomposite materials may be partnered to help with the design of a new generation of multizonal cartilage scaffolds.

5.2. Preclinical evaluation of multizonal cartilage scaffolds

To evaluate the potential efficacy of new multizonal cartilage scaffolds, their biological performance needs to be rigorously assessed *in vitro* and *in vivo* using physiologically relevant preclinical models. The evaluation of tissue repair outcomes should be conducted through comprehensive and comparable analytical methods. However, there is significant heterogeneity among studies reporting new chondral and osteochondral scaffolds in their use of *in vitro* and *in vivo* evaluation methods [236], which is also reflected in the example studies listed in Table 2. This makes it extremely difficult to meaningfully compare outcomes among studies, or identify 'optimal' scaffold designs.

The majority of studies in Table 2 conducted *in vitro* evaluation of the reported scaffolds, mainly using chondrocytes and/or MSCs derived from humans or other species such as murine, leporine, and bovine. To assess biocompatibility, cell viability or proliferation was usually measured over 1–7 days after seeding onto scaffolds, while chondrogenic differentiation was measured at 3–5 weeks usually by gene expression or immunofluorescence staining of cartilage markers. A few studies also conducted long-term *in vitro* cultures to assess cartilage-like tissue maturation within the scaffolds, such as over 6 weeks [21] or 9 weeks [162]. For multizonal cartilage scaffolds, their ability to generate or maintain zone-specific cellular or ECM properties from the superficial to deep layers should be an essential part of the *in vitro* evaluation, although this was only performed in some of the studies [21,22,62,99,112,136]. Considering the possible influences of a chronic injury or osteoarthritic joint environment on resident cells [7], it would also be relevant to test the cartilage regeneration capacity of scaffolds using cells derived from diseased joint tissues, although this was only attempted in one of the discussed studies [210].

Only ~30 % of studies in Table 2 performed *in vivo* evaluation using a preclinical animal model, the majority of which employed chondral or osteochondral defects in small animals such as rats or rabbits. Only two studies evaluated the scaffold in larger animals, one in micropigs [203] and another in skeletally mature pigs [99], both over a 6 month period. Steele et al.'s study in mature pigs with average weight of 78 kg was one of the very few in the broader field of osteochondral scaffolds to have used a physiologically and clinically relevant animal model with weight,

skeletal structure and maturity, and injury type mimicking those of humans. Interestingly, they found that the multizonal scaffold could support *in vitro* chondrogenesis with zone-specific properties, but the same scaffold did not produce better cartilage repair quality compared to the commercially available MaioRegen® control scaffold (without zonal architecture in the chondral layer). This comprehensive study highlighted the translational challenges associated with heterogeneous regeneration outcomes for scaffold-based approaches when scaling up from *in vitro* and small animal models. In the broader field of osteochondral scaffolds without zonal cartilage architecture, limited studies have investigated various types of single- or bi-layered scaffolds in large animals, using caprine and ovine [72,237–242] or equine [243] models. While the scientific community concurs that large animal models are more clinically relevant due to their skeletal similarities to humans, including anatomical size, cartilage thickness, and tissue regeneration potential, the use of these models remains restricted by complex logistical, financial, and ethical challenges [244]. In light of this, there is a need for better standardisation of *in vivo* evaluation methods to enable more meaningful comparisons among studies which used different types and sizes of animal models for scaffold testing.

To evaluate whether multizonal cartilage scaffolds can induce physiologically relevant tissue regeneration and functional recovery of the cartilage injury in animal models, rather than simply filling the defect with an anatomically similar but functionally futile implant, preclinical assessments should involve detailed analysis of the macroscopic, microscopic, and functional characteristics of the regenerated tissue. Macroscopic evaluation is conducted in the majority of *in vivo* studies testing osteochondral scaffolds, where gross morphological inspection of the implantation site can serve as a first-line screening tool to rule out ineffective designs, and allow straightforward comparison between studies. For example, it gives direct visual information on scaffold integration with the surrounding tissue, and the level or quality of cartilage repair, noting that a yellow or brownish tissue may be an indication of undesirable fibrocartilage formation. There is some consensus in the macroscopic scoring systems used in the literature for scaffold-based osteochondral repair, with >50 % of studies published since 2015 using the International Cartilage Repair Society (ICRS) scoring system [236] that evaluates the degree of defect repair, integration of the border zone, and macroscopic cartilage appearance. Other studies have used alternative scoring systems such as the Wayne score [245], which is based on tissue coverage, colour, surface, and defect margins.

For microscopic evaluation of repair tissue quality, studies on osteochondral scaffolds have used heterogeneous analysis methods such as histological staining using general and cartilage-specific stains, as well as immunofluorescence or immunohistochemical staining for cartilage matrix components [246]. A comprehensive evaluation of microscopic cartilage repair quality can be derived by combining the observations of different stains, including: i) haematoxylin and eosin (H&E) for overall cellular organisation and morphology, tissue integration, ECM formation, surface smoothness, any inflammatory infiltration and scaffold degradation; ii) Masson's trichrome or picosirius red for collagen expression and fibre orientation; iii) safranin O/fast green or toluidine blue for cartilage matrix components such as glycosaminoglycans (GAGs), mineralisation of subchondral bone, and tidemark formation. A variety of histological scoring systems have been used, each considering different aspects of the repair tissue quality, including ICRS [247], OARSI [248], Wakitani [249], O'Driscoll [250], and the newer modified O'Driscoll [251] scoring systems. To confirm whether the repair tissue is hyaline cartilage or fibrocartilage, histological findings can be coupled with immunohistochemistry to identify the presence of different collagens. The vast majority of studies that conducted immunohistochemical analysis examined collagen type II as an essential ECM component of hyaline cartilage, followed by collagen type I as an indication of fibrocartilage. The examination of other relevant markers is more limited, such as aggrecan and Sox9 for cartilage, collagen type X

for calcified cartilage, and osteocalcin for subchondral bone [236,246].

As a final point, functional evaluation of implanted osteochondral scaffolds should be an essential component of scaffold testing in pre-clinical studies, to ensure that the scaffold can help sustain physiological loads. This is often a challenge in translating new scaffold designs, as they may achieve favourable macroscopic and histological repair outcomes but fall short of the requirements for restoring normal joint biomechanics. However, mechanical testing has only been conducted in <20 % of preclinical studies on osteochondral scaffolds [236]. Among the analytical techniques used, indentation test was the most common followed by compression loading, while push-out test was rarely performed. Considering the patterns of physiological loading in native osteochondral tissues, a combination of nanoindentation, compression, and push-out or shear testing would give the best indication of the functional biomechanical properties of the osteochondral scaffold or repair tissues, by providing information on tissue stiffness, compressive strength, stress relaxation, strain at failure, and interfacial strength [252,253]. As new designs of multizonal cartilage scaffolds evolve, the use of comprehensive and standardised *in vitro* and *in vivo* evaluation methods for their biological performance would accelerate the journey of translation into clinical applications.

5.3. Towards clinical applications of multizonal cartilage scaffolds

Currently, there are no multizonal cartilage scaffolds with zonal cartilage design that have become commercially available or been tested in clinical studies. All current scaffolds have only been tested *in vitro* or in preclinical *in vivo* models. Nevertheless, a few multiphasic osteochondral scaffolds containing a bulk cartilage compartment are commercially available and have been tested in early-stage clinical studies, such as MaioRegen® (Fincera, Italy), Agili-C™ (CartiHeal, Israel), and Chondrotissue® (BioTissue, Switzerland) [15]. While the early results are promising, their longer-term performance in achieving physiologically relevant osteochondral repair and preventing injury-related progression of degenerative joint diseases require continuous monitoring. The successful progression of osteochondral scaffolds from preclinical testing to clinical studies demonstrates the future potential to apply multizonal cartilage scaffolds in the clinical repair of chondral and osteochondral injuries. However, as noted with commercially available osteochondral scaffolds [15], the scaffold design as well as incorporation of cellular or biologically active components may be critical influences to long-term repair outcomes using multizonal cartilage scaffolds.

The transformation of multizonal osteochondral scaffolds from experimental research into clinical applications presents a myriad of regulatory challenges. A primary hurdle is the stringent approval process required for innovative biomedical devices and tissue-engineered products. Regulatory bodies such as the U.S. Food and Drug Administration (FDA) and the European Medicines Agency (EMA) have established rigorous frameworks to ensure the safety, efficacy, and quality of complex medical products. These frameworks require comprehensive preclinical studies demonstrating biocompatibility, mechanical integrity, and biological functionality, followed by phased clinical trials to assess therapeutic outcomes in humans. The pathway of scaffold-based tissue engineering therapy from experimental design to clinical application can take three routes: a traditional pathway of clinical trials designed to collect research evidence; the non-research innovative therapy pathway of improving patient accessibility such as off-label use, compassionate use, and hospital exemption; and unproven commercial interventions that are ready to be marketed prior to completion of proof of efficacy and safety [254]. The first key challenge in this process is the demonstration of consistent manufacturing practices for multizonal scaffolds, which often involve intricate biomaterial compositions and multi-step fabrication processes [255]. The reproducibility and scalability of scaffold production must meet Good Manufacturing Practice (GMP) standards to ensure product reliability and safety [256]. This

requirement poses challenges for many types of complex scaffold designs in scaling from small-batch laboratory production to large-scale clinical manufacturing.

The second key challenge is the diverse regulatory classification schemes applied to novel multilayered scaffold products, each with distinct regulatory pathways and requirements, impacting the time and resources required for market approval [257]. Depending on the product composition, regulatory agencies such as the FDA and EMA may categorise the same product differently. Currently, there is no dedicated regulatory framework for tissue engineering products, resulting in the combined use of regulations for both medical devices and biological products. Cell-based products are typically classified as biological products or drugs, while cell-free strategies are often categorised as medical devices. In clinical practice, tissue engineered scaffolds with a cellular component may be assessed as combination products, with the primary focus on the drug or biological component and the device considered secondary. This dual classification often results in extended and costly regulatory approval processes. The stringent requirements for biological or combination products, which entail more rigorous testing and longer timelines, have led to increased interest in developing cell-free materials for cartilage repair [257,258]. Moreover, the same tissue engineered product may be categorised differently depending on the jurisdiction responsible for its oversight. For example, in the European Union, it may be classified as a Tissue Engineered Product or Combined Advanced Therapy Medicinal Product (TEP/CATMP); in the United States, as human cells, tissues, and cellular and tissue-based products (HCT/PS); in Canada, as a biologic drug; in Australia, biologics; in Japan, as a regenerative medicine product; and in South Korea, as a biological cell therapy product. Each country has its own specific authorisation process, with varying requirements and timelines, leading to significant differences in regulatory compliance, which may favour the market translation of one particular type of product to some countries [257,259].

Another regulatory challenge is the definition and standardisation of clinical endpoints in trials involving multizonal scaffolds [258]. Stratified chondral and osteochondral defects encompass a wide range of severity and patient-specific factors, complicating the establishment of universally accepted outcome measures. Regulatory bodies require clear demonstration of clinical benefit, which necessitates rigorous and often lengthy clinical trials with appropriate control groups and long-term follow-up. To boost bench to bedside translation, a global initiative aimed at standardising the international classification and regulatory evaluation pathways of multizonal osteochondral scaffold products is in progress [257,259].

Despite the significant need to develop biomimetic osteochondral scaffolds in orthopaedic medicine, very few scaffolds have proceeded to evaluation in clinical studies. Currently, the commercially available osteochondral scaffolds such as MaioRegen® and Agili-C™ contain a homogenous cartilage layer which does not account for zone-specific variations in native articular cartilage [14,15]. Global research effort into biomimetic multizonal scaffolds will hopefully bring us closer to a clinical solution for chondral and osteochondral defects, through innovations in materials science, fabrication technologies, design methods, and collaborations across disciplines to enable the creation of bioactive, functionally mimetic, personalisable, and smart scaffolds.

CRedit authorship contribution statement

Xiaoqi Lin: Writing – review & editing, Writing – original draft, Methodology, Investigation, Formal analysis, Conceptualization. **Ye Zhang:** Writing – review & editing, Writing – original draft, Investigation, Formal analysis. **Jiarong Li:** Writing – review & editing, Writing – original draft, Investigation, Formal analysis. **Brian G. Oliver:** Writing – review & editing, Formal analysis. **Bin Wang:** Writing – review & editing, Formal analysis. **Haiyan Li:** Writing – review & editing, Supervision, Formal analysis. **Ken-Tye Yong:** Writing – review & editing,

Supervision, Formal analysis. **Jiao Jiao Li:** Writing – review & editing, Writing – original draft, Supervision, Methodology, Investigation, Formal analysis, Conceptualization.

Declaration of competing interest

There are no conflicts of interest to declare.

Acknowledgements

We acknowledge funding support from the National Stem Cell Foundation of Australia.

References

- [1] L. Zhou, V.O. Gjvm, J. Malda, M.J. Stoddart, Y. Lai, R.G. Richards, K. Ki-Wai Ho, L. Qin, Innovative tissue-engineered strategies for osteochondral defect repair and regeneration: current progress and challenges, *Adv. Healthcare Mater.* 9 (2020) 2001008.
- [2] D.C. Flanagan, J.D. Harris, T.Q. Trinh, R.A. Siston, R.H. Brophy, Prevalence of chondral defects in athletes' knees: a systematic review, *Med. Sci. Sports Exerc.* 42 (2010) 1795–1801.
- [3] F. Accadbled, J. Vial, J. Sales de Gauzy, Osteochondritis dissecans of the knee, *Orthop. Traumatol. Surg. Res.* 104 (2018) S97–S105.
- [4] A.J. Sophia Fox, A. Bedi, S.A. Rodeo, The basic science of articular cartilage: structure, composition, and function, *Sport Health* 1 (2009) 461–468.
- [5] D. Dehghan-Baniani, B. Mehrjou, P.K. Chu, W.Y.W. Lee, H. Wu, Recent advances in "functional engineering of articular cartilage zones by polymeric biomaterials mediated with physical, mechanical, and biological/chemical cues", *Adv. Healthcare Mater.* 12 (2023) e2202581.
- [6] L.P. Yan, J.M. Oliveira, A.L. Oliveira, R.L. Reis, Current concepts and challenges in osteochondral tissue engineering and regenerative medicine, *ACS Biomater. Sci. Eng.* 1 (2015) 183–200.
- [7] V. Shang, J. Li, C.B. Little, J.J. Li, Understanding the effects of mesenchymal stromal cell therapy for treating osteoarthritis using an in vitro co-culture model, *Eur. cells mater* 45 (2023) 143–157.
- [8] M.T. Frassica, M.A. Grunlan, Perspectives on synthetic materials to guide tissue regeneration for osteochondral defect repair, *ACS Biomater. Sci. Eng.* 6 (2020) 4324–4336.
- [9] W. Wei, H. Dai, Articular cartilage and osteochondral tissue engineering techniques: recent advances and challenges, *Bioact. Mater.* 6 (2021) 4830–4855.
- [10] O. Urbaneck, D. Kolbuk, M. Wróbel, Articular cartilage: new directions and barriers of scaffolds development – review, *Int. J. Polym. Mater.* 68 (2018) 396–410.
- [11] T. Paatela, A. Vasara, H. Nurmi, H. Kautiainen, I. Kiviranta, Assessment of cartilage repair quality with the international cartilage repair society score and the Oswestry arthroscopy score, *J. Orthop. Res.* 38 (2020) 555–562.
- [12] M. Wasyleczko, W. Sikorska, A. Chwojnowski, Review of synthetic and hybrid scaffolds in cartilage tissue engineering, *Membranes* 10 (2020) 348.
- [13] Z. Wang, H. Le, Y. Wang, H. Liu, Z. Li, X. Yang, C. Wang, J. Ding, X. Chen, Instructive cartilage regeneration modalities with advanced therapeutic implantations under abnormal conditions, *Bioact. Mater.* 11 (2022) 317–338.
- [14] C. Ai, Y.H.D. Lee, X.H. Tan, S.H.S. Tan, J.H.P. Hui, J.C. Goh, Osteochondral tissue engineering: perspectives for clinical application and preclinical development, *J. Orthop. Translat.* 30 (2021) 93–102.
- [15] R. Chen, J.S. Pye, J. Li, C.B. Little, J.J. Li, Multiphasic scaffolds for the repair of osteochondral defects: outcomes of preclinical studies, *Bioact. Mater.* 27 (2023) 505–545.
- [16] B. Zhang, J. Huang, R.J. Narayan, Gradient scaffolds for osteochondral tissue engineering and regeneration, *J. Mater. Chem. B* 8 (2020) 8149–8170.
- [17] J.J. Chung, H. Im, S.H. Kim, J.W. Park, Y. Jung, Toward biomimetic scaffolds for tissue engineering: 3D printing techniques in regenerative medicine, *Front. Bioeng. Biotechnol.* 8 (2020) 586406.
- [18] S. Jiang, M. Wang, J. He, A review of biomimetic scaffolds for bone regeneration: toward a cell-free strategy, *Bioeng. Transl. Med.* 6 (2021) e10206.
- [19] S. Wu, X. Liu, K.W.K. Yeung, C. Liu, X. Yang, Biomimetic porous scaffolds for bone tissue engineering, *Mater. Sci. Eng., R* 80 (2014) 1–36.
- [20] J. Wang, Y. Wang, X. Sun, D. Liu, C. Huang, J. Wu, C. Yang, Q. Zhang, Biomimetic cartilage scaffold with orientated porous structure of two factors for cartilage repair of knee osteoarthritis, *Artif. Cells, Nanomed. Biotechnol.* 47 (2019) 1710–1721.
- [21] Y. Sun, Q. Wu, Y. Zhang, K. Dai, Y. Wei, 3D-bioprinted gradient-structured scaffold generates anisotropic cartilage with vascularization by pore-size-dependent activation of HIF1 α /FAK signaling axis, *Nanomedicine.* 37 (2021) 102426.
- [22] Z. Qiao, M. Lian, Y. Han, B. Sun, X. Zhang, W. Jiang, H. Li, Y. Hao, K. Dai, Bioinspired stratified electrospun fiber-reinforced hydrogel constructs with layer-specific induction capacity for functional osteochondral regeneration, *Biomaterials* 266 (2021) 120385.
- [23] L. Yu, S. Cavellier, B. Hannon, M. Wei, Recent development in multizonal scaffolds for osteochondral regeneration, *Bioact. Mater.* 25 (2023) 122–159.

- [24] L. Fu, Z. Yang, C. Gao, H. Li, Z. Yuan, F. Wang, X. Sui, S. Liu, Q. Guo, Advances and prospects in biomimetic multilayered scaffolds for articular cartilage regeneration, *Regen. Biomater.* 7 (2020) 527–542.
- [25] S.E. Doyle, F. Snow, S. Duchi, C.D. O'Connell, C. Onofrillo, C. Di Bella, E. Pirogova, 3D printed multiphasic scaffolds for osteochondral repair: challenges and opportunities, *Int. J. Mol. Sci.* 22 (2021) 12420.
- [26] J. Antons, M.G.M. Marascio, J. Nohava, R. Martin, L.A. Applegate, P.E. Bourban, D.P. Pioletti, Zone-dependent mechanical properties of human articular cartilage obtained by indentation measurements, *J. Mater. Sci. Mater. Med.* 29 (2018) 57.
- [27] W. Wang, R. Ye, W. Xie, Y. Zhang, S. An, Y. Li, Y. Zhou, Roles of the calcified cartilage layer and its tissue engineering reconstruction in osteoarthritis treatment, *Front. Bioeng. Biotechnol.* 10 (2022) 911281.
- [28] X. Wang, Z. Zhu, H. Xiao, C. Luo, X. Luo, F. Lv, J. Liao, W. Huang, Three-Dimensional, MultiScale, and interconnected trabecular bone mimic porous tantalum scaffold for bone tissue engineering, *ACS Omega* 5 (2020) 22520–22528.
- [29] M. Tamaddon, L. Wang, Z. Liu, C. Liu, Osteochondral tissue repair in osteoarthritic joints: clinical challenges and opportunities in tissue engineering, *Bio-Des, Man (Lond.)* 1 (2018) 101–114.
- [30] J.J. Li, D.L. Kaplan, H. Zreiqat, Scaffold-based regeneration of skeletal tissues to meet clinical challenges, *J. Mater. Chem. B* 2 (2014) 7272–7306.
- [31] F. Buttgerit, G.R. Burmester, J.Y. Bijlsma, Non-surgical management of knee osteoarthritis: where are we now and where do we need to go? *RMD Open* 1 (2015) e000027.
- [32] K. Solanki, S. Shanmugasundaram, N. Shetty, S.J. Kim, Articular cartilage repair & joint preservation: a review of the current status of biological approach, *J. Clin. Orthop. Trauma* 22 (2021) 101602.
- [33] S.H. Edwards, Intra-articular drug delivery: the challenge to extend drug residence time within the joint, *Vet. J.* 190 (2011) 15–21.
- [34] C. Cooper, R. Chapurlat, N. Al-Daghri, G. Herrero-Beaumont, O. Bruyere, F. Rannou, R. Roth, D. Uebelhart, J.Y. Reginster, Safety of oral non-selective non-steroidal anti-inflammatory drugs in osteoarthritis: what does the literature say? *Drugs Aging* 36 (2019) 15–24.
- [35] B. Gallagher, F.P. Tjoumakaris, M.I. Harwood, R.P. Good, M.G. Ciccotti, K. B. Freedman, Chondroprotection and the prevention of osteoarthritis progression of the knee: a systematic review of treatment agents, *Am. J. Sports Med.* 43 (2015) 734–744.
- [36] N. Garg, L. Perry, A. Deodhar, Intra-articular and soft tissue injections, a systematic review of relative efficacy of various corticosteroids, *Clin. Rheumatol.* 33 (2014) 1695–1706.
- [37] M. Telikicherla, S.U. Kamath, Accuracy of needle placement into the intra-articular space of the knee in osteoarthritis patients for viscosupplementation, *J. Clin. Diagn. Res.* 10 (2016) RC15–R17.
- [38] M.M. Richards, J.S. Maxwell, L. Weng, M.G. Angelos, J. Golzarian, Intra-articular treatment of knee osteoarthritis: from anti-inflammatories to products of regenerative medicine, *Phys. Sportsmed.* 44 (2016) 101–108.
- [39] G.D. Abrams, R.M. Frank, L.A. Fortier, B.J. Cole, Platelet-rich plasma for articular cartilage repair, *Sports Med. Arthrosc. Rev.* 21 (2013) 213–219.
- [40] S. Shanmugasundaram, A. Vaish, V. Chavada, W.D. Murrell, R. Vaishya, Assessment of safety and efficacy of intra-articular injection of stromal vascular fraction for the treatment of knee osteoarthritis—a systematic review, *Int. Orthop.* 45 (2021) 615–625.
- [41] Y.H. Chang, H.W. Liu, K.C. Wu, D.C. Ding, Mesenchymal stem cells and their clinical applications in osteoarthritis, *Cell Transplant.* 25 (2016) 937–950.
- [42] J.G. Kim, Y.A. Rim, J.H. Ju, The role of transforming growth factor beta in joint homeostasis and cartilage regeneration, *Tissue Eng. C Methods* 28 (2022) 570–587.
- [43] D. Dallari, C. Stagni, N. Rani, G. Sabbioni, P. Pelotti, P. Torricelli, M. Tschon, G. Giavaresi, Ultrasound-guided injection of platelet-rich plasma and hyaluronic acid, separately and in combination, for hip osteoarthritis: a randomized controlled study, *Am. J. Sports Med.* 44 (2016) 664–671.
- [44] G. Wang, D. Xing, W. Liu, Y. Zhu, H. Liu, L. Yan, K. Fan, P. Liu, B. Yu, J.J. Li, B. Wang, Preclinical studies and clinical trials on mesenchymal stem cell therapy for knee osteoarthritis: a systematic review on models and cell doses, *Int. J. Rheum. Dis.* 25 (2022) 532–562.
- [45] R. Soler, L. Orozco, A. Munar, M. Huguet, R. Lopez, J. Vives, R. Coll, M. Codinach, J. Garcia-Lopez, Final results of a phase I-II trial using ex vivo expanded autologous Mesenchymal Stromal Cells for the treatment of osteoarthritis of the knee confirming safety and suggesting cartilage regeneration, *Knee* 23 (2016) 647–654.
- [46] E. Estrada, J.L. Decima, M. Rodriguez, M. Di Tomaso, J. Roberti, Patient-reported outcomes after platelet-rich plasma, bone marrow aspirate, and adipose-derived mesenchymal stem cell injections for symptomatic knee osteoarthritis, *Clin. Med. Insights Arthritis Musculoskelet. Disord.* 13 (2020) 1–4.
- [47] B.J. Sherman, J. Chahla, J. Glowney, R.M. Frank, The role of orthobiologics in the management of osteoarthritis and focal cartilage defects, *Orthopedics* 42 (2019) 66–73.
- [48] K. Huebner, R.M. Frank, A. Getgood, Ortho-biologics for osteoarthritis, *clin, Sports Med.* 38 (2019) 123–141.
- [49] Z. Shang, P. Wanyan, B. Zhang, M. Wang, X. Wang, A systematic review, umbrella review, and quality assessment on clinical translation of stem cell therapy for knee osteoarthritis: are we there yet? *Stem Cell Res. Ther.* 14 (2023) 91.
- [50] J.M. Case, J.M. Scopp, Treatment of articular cartilage defects of the knee with microfracture and enhanced microfracture techniques, *sports med, Arthrosc. Rev.* 24 (2016) 63–68.
- [51] D. Goyal, S. Keyhani, E.H. Lee, J.H. Hui, Evidence-based status of microfracture technique: a systematic review of level I and II studies, *Arthroscopy* 29 (2013) 1579–1588.
- [52] R.L. Davies, N.J. Kuiper, Regenerative medicine: a review of the evolution of autologous chondrocyte implantation (ACI) therapy, *Bioengineering* 6 (2019) 22.
- [53] G.H. Gou, F.J. Tseng, S.H. Wang, P.J. Chen, J.F. Shyu, C.F. Weng, R.Y. Pan, Autologous chondrocyte implantation versus microfracture in the knee: a meta-analysis and systematic review, *Arthroscopy* 36 (2020) 289–303.
- [54] E.V. Medvedeva, E.A. Grebenik, S.N. Gornostaeva, V.I. Telpuhov, A.V. Lychagin, P.S. Timashev, A.S. Chagin, Repair of damaged articular cartilage: current approaches and future directions, *Int. J. Mol. Sci.* 19 (2018) 2366.
- [55] K.R. Sochacki, K. Varshneya, J.G. Calcei, M.R. Safran, G.D. Abrams, J. Donahue, C. Chu, S.L. Sherman, Comparison of autologous chondrocyte implantation and osteochondral allograft transplantation of the knee in a large insurance database: reoperation rate, complications, and cost analysis, *Cartilage* 13 (2021) 1187S, 94S.
- [56] C. Parisi, L. Salvatore, L. Veschini, M.P. Serra, C. Hobbs, M. Madaghiele, A. Sannino, L. Di Silvio, Biomimetic gradient scaffold of collagen-hydroxyapatite for osteochondral regeneration, *J. Tissue Eng.* 11 (2020) 1–13.
- [57] S. Ansari, S. Khorshidi, A. Karkhaneh, Engineering of gradient osteochondral tissue: from nature to lab, *Acta Biomater.* 87 (2019) 41–54.
- [58] D. Majda, A. Bhattarai, J. Riikonen, B.D. Napruszewska, M. Zimowska, A. Michalik-Zym, J. Töyräs, V.P. Lehto, New approach for determining cartilage pore size distribution: NaCl-thermoporometry, *Microporous Mesoporous Mater.* 241 (2017) 238–245.
- [59] A. Di Luca, A. Longoni, G. Criscenti, C. Mota, C. van Blitterswijk, L. Moroni, Toward mimicking the bone structure: design of novel hierarchical scaffolds with a tailored radial porosity gradient, *Biofabrication* 8 (2016) 045007.
- [60] I. Sahafnejad-Mohammadi, S. Rahmati, N. Najmoodin, M. Bodaghi, Biomimetic polycaprolactone-graphene oxide composites for 3D printing bone scaffolds, *Macromol. Mater. Eng.* 308 (2023) 2200558.
- [61] J. Jiao, Q. Hong, D. Zhang, M. Wang, H. Tang, J. Yang, X. Qu, B. Yue, Influence of porosity on osteogenesis, bone growth and osteointegration in trabecular tantalum scaffolds fabricated by additive manufacturing, *Front. Bioeng. Biotechnol.* 11 (2023) 1117954.
- [62] D. Wang, H. Xu, J. Liu, Z. Chen, Y. Li, B. Hu, D. Zhang, J. Li, H. Chu, Bio-inspired cellulose reinforced anisotropic composite hydrogel with zone-dependent complex mechanical adaptability and cell recruitment characteristics, *Compos. B Eng.* (2020) 202.
- [63] B. Pouran, A. Raoof, D.A.M. de Winter, V. Arbabi, R. Bley, F.J. Beekman, A. A. Zadpoor, J. Malda, H. Weinans, Topographic features of nano-pores within the osteochondral interface and their effects on transport properties - a 3D imaging and modeling study, *J. Biomech.* 123 (2021) 110504.
- [64] V.L. Ferguson, A.J. Bushby, A. Boyde, Nanomechanical properties and mineral concentration in articular calcified cartilage and subchondral bone, *J. Anat.* 203 (2003) 191–202.
- [65] X. Wang, S. Xu, S. Zhou, W. Xu, M. Leary, P. Choong, M. Qian, M. Brandt, Y. M. Xie, Topological design and additive manufacturing of porous metals for bone scaffolds and orthopaedic implants: a review, *Biomaterials* 83 (2016) 127–141.
- [66] Y. Harada, H.W. Wevers, T.D.V. Cooke, Distribution of bone strength in the proximal tibia, *J. Arthroplasty* 3 (1988) 167–175.
- [67] J. Scheinpflug, M. Pfeiffenberger, A. Damerau, F. Schwarz, M. Textor, A. Lang, F. Schulze, Journey into bone models: a review, *Genes* 9 (2018) 247.
- [68] O. Al-Ketan, R. Rowshan, R.K. Abu Al-Rub, Topology-mechanical property relationship of 3D printed strut, skeletal, and sheet based periodic metallic cellular materials, *Addit. Manuf.* 19 (2018) 167–183.
- [69] J. Zhou, H. Huang, L.-J. Wang, M. Tamaddon, C.-Z. Liu, Z.-Y. Liu, T.-B. Yu, Y.-Z. Zhang, Stable mechanical fixation in a bionic osteochondral scaffold considering bone growth, *Rare Met.* 41 (2022) 2711–2718.
- [70] Y. Han, M. Lian, Q. Wu, Z. Qiao, B. Sun, K. Dai, Effect of pore size on cell behavior using melt electrowritten scaffolds, *Front. Bioeng. Biotechnol.* 9 (2021) 629270.
- [71] N. Abbasi, S. Hamlet, R.M. Love, N.-T. Nguyen, Porous scaffolds for bone regeneration, *JS: amd* 5 (2020) 1–9.
- [72] M. Tamaddon, G. Blunn, R. Tan, P. Yang, X. Sun, S.M. Chen, J. Luo, Z. Liu, L. Wang, D. Li, R. Donate, M. Monzon, C. Liu, In vivo evaluation of additively manufactured multi-layered scaffold for the repair of large osteochondral defects, *Bio-Des. Manuf.* 5 (2022) 481–496.
- [73] Y. Qin, P. Wen, H. Guo, D. Xia, Y. Zheng, L. Jauer, R. Poprawe, M. Voshage, J. H. Schleifenbaum, Additive manufacturing of biodegradable metals: current research status and future perspectives, *Acta Biomater.* 98 (2019) 3–22.
- [74] F. Deng, L. Liu, Z. Li, J. Liu, 3D printed Ti6Al4V bone scaffolds with different pore structure effects on bone ingrowth, *J. Biol. Eng.* 15 (2021) 4.
- [75] S. Van Bael, Y.C. Chai, S. Truscetto, M. Moesen, G. Kerckhofs, H. Van Oosterwyck, J.P. Kruth, J. Schrooten, The effect of pore geometry on the in vitro biological behavior of human periosteum-derived cells seeded on selective laser-melted Ti6Al4V bone scaffolds, *Acta Biomater.* 8 (2012) 2824–2834.
- [76] P.F. Egan, Integrated design approaches for 3D printed tissue scaffolds: review and outlook, *Materials* 12 (2019) 2355.
- [77] S.J.P. Callens, R.J.C. Uytendaele, L.E. Fratila-Apachitei, A.A. Zadpoor, Substrate curvature as a cue to guide spatiotemporal cell and tissue organization, *Biomaterials* 232 (2020) 119739.
- [78] C. Jiao, D. Xie, Z. He, H. Liang, L. Shen, Y. Yang, Z. Tian, G. Wu, C. Wang, Additive manufacturing of Bio-inspired ceramic bone Scaffolds: structural Design, mechanical properties and biocompatibility, *Mater. Des.* 217 (2022) 110610.

- [79] M. Shen, W. Qin, B. Xing, W. Zhao, S. Gao, Y. Sun, T. Jiao, Z. Zhao, Mechanical properties of 3D printed ceramic cellular materials with triply periodic minimal surface architectures, *J. Eur. Ceram. Soc.* 41 (2021) 1481–1489.
- [80] D.W. Abueidda, M. Bakir, R.K. Abu Al-Rub, J.S. Bergström, N.A. Sobh, I. Jasiuk, Mechanical properties of 3D printed polymeric cellular materials with triply periodic minimal surface architectures, *Mater. Des.* 122 (2017) 255–267.
- [81] F. Teng, Y. Sun, S. Guo, B. Gao, G. Yu, Topological and mechanical properties of different lattice structures based on additive manufacturing, *Micromachines* 13 (2022) 1017.
- [82] P. Bogusz, A. Poplawski, M. Stankiewicz, B. Kowalski, Experimental research of selected lattice structures developed with 3D printing technology, *Materials* 15 (2022) 378.
- [83] H.M.A. Ali, M. Abdi, Y. Sun, Insight into the mechanical properties of 3D printed strut-based lattice structures, *Prog. Addit. Manuf.* 8 (2022) 919–931.
- [84] N. Kladovasilakis, P. Charalampous, K. Tsongas, I. Kostavelis, D. Tzetzis, D. Tzovaras, Experimental and computational investigation of lattice sandwich structures constructed by additive manufacturing technologies, *J. Manuf. Mater. Process.* 5 (2021) 95.
- [85] M. Parkes, F. Tallia, G.R. Young, P. Cann, J.R. Jones, J.R.T. Jeffers, Tribological evaluation of a novel hybrid for repair of articular cartilage defects, *Mater. Sci. Eng., C* 119 (2021) 111495.
- [86] W. Lin, J. Klein, Recent progress in cartilage lubrication, *Adv. Mater.* 33 (2021) e2005513.
- [87] W. Zhao, Y. Zhang, X. Zhao, Z. Ji, Z. Ma, X. Gao, S. Ma, X. Wang, F. Zhou, Bioinspired design of a cartilage-like lubricated composite with mechanical robustness, *ACS Appl. Mater. Interfaces* 14 (2022) 9899–9908.
- [88] S. Affatato, D. Trucco, P. Taddei, L. Vannozzi, L. Ricotti, G.D. Nessim, G. Lisignoli, Wear behavior characterization of hydrogels constructs for cartilage tissue replacement, *Materials* 14 (2021).
- [89] Y. Wu, X. Li, Y. Wang, Y. Shi, F. Wang, G. Lin, Research progress on mechanical properties and wear resistance of cartilage repair hydrogel, *Mater. Des.* 216 (2022) 110575.
- [90] V. Adibnia, M. Mirbagheri, J. Faivre, J. Robert, J. Lee, K. Matyjaszewski, D. W. Lee, X. Banquy, Bioinspired polymers for lubrication and wear resistance, *Prog. Polym. Sci.* 110 (2020) 101298.
- [91] A. Trengove, C. Di Bella, A.J. O'Connor, The challenge of cartilage integration: understanding a major barrier to chondral repair, *Tissue Eng., Part B* 28 (2022) 114–128.
- [92] X. Yang, S. Li, Y. Ren, L. Qiang, Y. Liu, J. Wang, K. Dai, 3D printed hydrogel for articular cartilage regeneration, *Compos. B Eng.* 237 (2022) 109863.
- [93] V. Manescu, I. Antoniac, A. Antoniac, D. Laptoiu, G. Paltanea, R. Ciocoiu, I. V. Nemoianu, L.G. Gruionu, H. Dura, Bone regeneration induced by patient-adapted Mg alloy-based scaffolds for bone defects: present and future perspectives, *Biomimetics* 8 (2023) 618.
- [94] I. Cockerill, Y. Su, S. Sinha, Y.X. Qin, Y. Zheng, M.L. Young, D. Zhu, Porous zinc scaffolds for bone tissue engineering applications: a novel additive manufacturing and casting approach, *Mater. Sci. Eng., C* 110 (2020) 110738.
- [95] L. Li, F. Yu, L. Zheng, R. Wang, W. Yan, Z. Wang, J. Xu, J. Wu, D. Shi, L. Zhu, X. Wang, Q. Jiang, Natural hydrogels for cartilage regeneration: modification, preparation and application, *J. Orthop. Translat.* 17 (2019) 26–41.
- [96] X. Zhao, D.A. Hu, D. Wu, F. He, H. Wang, L. Huang, D. Shi, Q. Liu, N. Ni, M. Pakvasa, Y. Zhang, K. Fu, K.H. Qin, A.J. Li, O. Hagag, E.J. Wang, M. Sabharwal, W. Wagstaff, R.R. Reid, M.J. Lee, J.M. Wolf, M. El Dafrawy, K. Hynes, J. Strelzow, S.H. Ho, T.C. He, A. Athiviraham, Applications of biocompatible scaffold materials in stem cell-based cartilage tissue engineering, *Front. Bioeng. Biotechnol.* 9 (2021) 603444.
- [97] S. Yu, X. Shu, L. Chen, C. Wang, X. Wang, J. Jing, G. Yan, Y. Zhang, C. Wu, Construction of ultrasonically treated collagen/silk fibroin composite scaffolds to induce cartilage regeneration, *Sci. Rep.* 13 (2023) 20168.
- [98] L. Peng, H. Li, H. Deng, T. Gao, R. Li, Z. Xu, Q. Tian, T. Zhao, J. Li, Y. Yang, C. Wang, S. Liu, Q. Guo, Combination of a human articular cartilage-derived extracellular matrix scaffold and microfracture techniques for cartilage regeneration: a proof of concept in a sheep model, *J. Orthop. Translat.* 44 (2024) 72–87.
- [99] J.A.M. Steele, A.C. Moore, J.P. St-Pierre, S.D. McCullen, A.J. Gormley, C. C. Horgan, C.R. Black, C. Meinert, T. Klein, S. Saifzadeh, R. Steck, J. Ren, M. A. Woodruff, M.M. Stevens, In vitro and in vivo investigation of a zonal microstructured scaffold for osteochondral defect repair, *Biomaterials* 286 (2022) 121548.
- [100] X. Bai, M. Gao, S. Syed, J. Zhuang, X. Xu, X.Q. Zhang, Bioactive hydrogels for bone regeneration, *Bioact. Mater.* 3 (2018) 401–417.
- [101] Y. Peng, Y. Zhuang, Y. Liu, H. Le, D. Li, M. Zhang, K. Liu, Y. Zhang, J. Zuo, J. Ding, Bioinspired gradient scaffolds for osteochondral tissue engineering, *Explorations* 3 (2023) 20210043.
- [102] H. Zhang, Y. Lu, L. Huang, P. Liu, J. Ni, T. Yang, Y. Li, Y. Zhong, X. He, X. Xia, J. Zhou, Scalable and versatile metal ion solidified alginate hydrogel for skin wound infection therapy, *Adv. Healthcare Mater.* 12 (2024) 2303688.
- [103] A. Sergeeva, A.S. Vikulina, D. Volodkin, Porous alginate scaffolds assembled using vaterite CaCO₃ crystals, *Micromachines* 10 (2019) 357.
- [104] K. Mikula, D. Skrzypczak, B. Ligas, A. Witek-Krowiak, Preparation of hydrogel composites using Ca²⁺ and Cu²⁺ ions as crosslinking agents, *SN Appl. Sci.* 1 (2019) 643.
- [105] Y. Chen, J. Feng, M. Fang, X. Wang, Y. Liu, S. Li, L. Wen, Y. Zhu, L. Jiang, Large-scale, ultrastrong Cu²⁺ cross-linked sodium alginate membrane for effective salinity gradient power conversion, *ACS Appl. Polym. Mater.* 3 (2021) 3902–3910.
- [106] Z. Cai, Y. Li, W. Song, Y. He, H. Li, X. Liu, Anti-inflammatory and prochondrogenic in situ-formed injectable hydrogel crosslinked by strontium-doped bioglass for cartilage regeneration, *ACS Appl. Mater. Interfaces* 13 (2021) 59772–59786.
- [107] M. Sarker, M. Izadifar, D. Schreyer, X. Chen, Influence of ionic crosslinkers (Ca²⁺+/Ba²⁺/Zn²⁺) on the mechanical and biological properties of 3D Bioprinted Hydrogel Scaffolds, *J. Biomater. Sci. Polym. Ed.* 29 (2018) 1126–1154.
- [108] H. Malektaj, A.D. Drozdov, J. deClaville Christiansen, Mechanical properties of alginate hydrogels cross-linked with multivalent cations, *Polymers* 15 (2023) 3012.
- [109] W. Liu, H. Madry, M. Cucchiari, Application of alginate hydrogels for next-generation articular cartilage regeneration, *Int. J. Mol. Sci.* 23 (2022) 1147.
- [110] P. Yu, Y. Li, H. Sun, X. Ke, J. Xing, Y. Zhao, X. Xu, M. Qin, J. Xie, J. Li, Cartilage-inspired hydrogel with mechanical adaptability, controllable lubrication, and inflammation regulation abilities, *ACS Appl. Mater. Interfaces* 14 (2022) 27360–27370.
- [111] A.A. Golebiowska, S.P. Nukavarapu, Bio-inspired zonal-structured matrices for bone-cartilage interface engineering, *Biofabrication* 14 (2022) 025016.
- [112] A. Dimaraki, P.J. Diaz-Payno, M. Minneboo, M. Nouri-Goushki, M. Hosseini, N. Kops, R. Narcisi, M.J. Mirzaali, G.J.V.M. van Osch, L.E. Fratila-Apachitei, A. A. Zadpoor, Bioprinting of a zonal-specific cell density scaffold: a biomimetic approach for cartilage tissue engineering, *Appl. Sci.* 11 (2021) 7821.
- [113] Y. Cao, P. Cheng, S. Sang, C. Xiang, Y. An, X. Wei, Z. Shen, Y. Zhang, P. Li, Mesenchymal stem cells loaded on 3D-printed gradient poly(ϵ -caprolactone)/methacrylated alginate composite scaffolds for cartilage tissue engineering, *Regen. Biomater.* 8 (2021) rba019.
- [114] B. Sultankulov, D. Berillo, K. Sultankulova, T. Tokay, A. Saparov, Progress in the development of chitosan-based biomaterials for tissue engineering and regenerative medicine, *Biomolecules* 9 (2019) 470.
- [115] H. Li, C. Hu, H. Yu, C. Chen, Chitosan composite scaffolds for articular cartilage defect repair: a review, *RSC Adv.* 8 (2018) 3736–3749.
- [116] Y. Shen, Y. Xu, B. Yi, X. Wang, H. Tang, C. Chen, Y. Zhang, Engineering a highly biomimetic chitosan-based cartilage scaffold by using short fibers and a cartilage-decellularized matrix, *Biomacromolecules* 22 (2021) 2284–2297.
- [117] P. Haghighi, A. Shamloo, Fabrication of a novel 3D scaffold for cartilage tissue repair: in-vitro and in-vivo study, *Mater. Sci. Eng., C* 128 (2021) 112285.
- [118] C. Antich, J. de Vicente, G. Jimenez, C. Chocarro, E. Carrillo, E. Montanez, P. Galvez-Martin, J.A. Marchal, Bio-inspired hydrogel composed of hyaluronic acid and alginate as a potential bioink for 3D bioprinting of articular cartilage engineering constructs, *Acta Biomater.* 106 (2020) 114–123.
- [119] T. He, B. Li, T. Colombani, K. Joshi-Navare, S. Mehta, J. Kisiday, S.A. Bencherif, A.G. Bajpayee, Hyaluronic acid-based shape-memory cryogel scaffolds for focal cartilage defect repair, *Tissue Eng.* 27 (2021) 748–760.
- [120] Q. Zhang, H. Lu, N. Kawazoe, G. Chen, Pore size effect of collagen scaffolds on cartilage regeneration, *Acta Biomater.* 10 (2014) 2005–2013.
- [121] V. Irawan, T.C. Sung, A. Higuchi, T. Ikoma, Collagen scaffolds in cartilage tissue engineering and relevant approaches for future development, *Tissue Eng. Regen. Med.* 15 (2018) 673–697.
- [122] C. Intini, M. Lemoine, T. Hodgkinson, S. Casey, J.P. Gleeson, F.J. O'Brien, A highly porous type II collagen containing scaffold for the treatment of cartilage defects enhances MSC chondrogenesis and early cartilaginous matrix deposition, *Biomater. Sci.* 10 (2022) 970–983.
- [123] C. Belda Marin, V. Fitzpatrick, D.L. Kaplan, J. Landoulsi, E. Guenin, C. Egles, Silk polymers and nanoparticles: a powerful combination for the design of versatile biomaterials, *Front. Chem.* 8 (2020) 604398.
- [124] D. Dehghan-Baniani, B. Mehrjou, P.K. Chu, H. Wu, A biomimetic nano-engineered platform for functional tissue engineering of cartilage superficial zone, *Adv. Healthcare Mater.* 10 (2021) 2001018.
- [125] H. Zheng, B. Zuo, Functional silk fibroin hydrogels: preparation, properties and applications, *J. Mater. Chem. B* 9 (2021) 1238–1258.
- [126] A.A. Golebiowska, J.T. Intravaia, V.M. Sathe, S.G. Kumbar, S.P. Nukavarapu, Decellularized extracellular matrix biomaterials for regenerative therapies: advances, challenges and clinical prospects, *Bioact. Mater.* 32 (2024) 98–123.
- [127] P. Xu, R.K. Kankala, S. Wang, A. Chen, Decellularized extracellular matrix-based composite scaffolds for tissue engineering and regenerative medicine, *Regen. Biomater.* 11 (2023) rba0107.
- [128] X. Zhang, X. Chen, H. Hong, R. Hu, J. Liu, C. Liu, Decellularized extracellular matrix scaffolds: recent trends and emerging strategies in tissue engineering, *Bioact. Mater.* 10 (2022) 15–31.
- [129] S. Yelawarapu, S. Chameettachal, A.K. Bera, F. Pati, Smooth muscle matrix bioink promotes myogenic differentiation of encapsulated adipose-derived stem cells, *J. Biomed. Mater. Res. A* 110 (2022) 1761–1773.
- [130] G. Tian, S. Jiang, J. Li, F. Wei, X. Li, Y. Ding, Z. Yang, Z. Sun, K. Zha, F. Wang, B. Huang, L. Peng, Q. Wang, Z. Tian, X. Yang, Z. Wang, Q. Guo, W. Guo, S. Liu, Cell-free decellularized cartilage extracellular matrix scaffolds combined with interleukin 4 promote osteochondral repair through immunomodulatory macrophages: in vitro and in vivo preclinical study, *Acta Biomater.* 127 (2021) 131–145.
- [131] D.C. Browe, O.R. Mahon, P.J. Diaz-Payno, N. Cassidy, I. Dudurych, A. Dunne, C. T. Buckley, D.J. Kelly, Glyoxal cross-linking of solubilized extracellular matrix to produce highly porous, elastic, and chondro-permissive scaffolds for orthopedic tissue engineering, *J. Biomed. Mater. Res. A* 107 (2019) 2222–2234.
- [132] Y. Li, Y. Liu, X. Xun, W. Zhang, Y. Xu, D. Gu, Three-Dimensional porous scaffolds with biomimetic microarchitecture and bioactivity for cartilage tissue engineering, *ACS Appl. Mater. Interfaces* 11 (2019) 36359–36370.

- [133] J. Li, B. Jiang, P. Zhang, J. Wu, N. Fan, Z. Chen, Y. Yang, E. Zhang, F. Wang, L. Yang, Cartilage decellularized extracellular matrix-based hydrogel with enhanced tissue adhesion and promoted chondrogenesis for cartilage tissue engineering, *ACS Appl. Polym. Mater.* 6 (2024) 4394–4408.
- [134] Q. Li, H. Yu, F. Zhao, C. Cao, T. Wu, Y. Fan, Y. Ao, X. Hu, 3D printing of microenvironment-specific bioinspired and exosome-reinforced hydrogel scaffolds for efficient cartilage and subchondral bone regeneration, *Adv. Sci.* 10 (2023) 2303650.
- [135] K.D. Ngadimin, A. Stokes, P. Gentile, A.M. Ferreira, Biomimetic hydrogels designed for cartilage tissue engineering, *Biomater. Sci.* 9 (2021) 4246–4259.
- [136] Y. Han, M. Lian, B. Sun, B. Jia, Q. Wu, Z. Qiao, K. Dai, Preparation of high precision multilayer scaffolds based on Melt Electro-Writing to repair cartilage injury, *Theranostics* 10 (2020) 10214–10230.
- [137] K.A. van Kampen, E. Olaret, I.C. Stancu, D.F. Duarte Campos, H. Fischer, C. Mota, L. Moroni, Hypotrochoidal scaffolds for cartilage regeneration, *Mater. Today Bio.* 23 (2023) 100830.
- [138] D. Yari, M.H. Ebrahimzadeh, J. Movaffagh, A. Shahroodi, M. Shirzad, D. Qujeq, A. Moradi, Biochemical aspects of scaffolds for cartilage tissue engineering: from basic science to regenerative medicine, *Arch. Bone Jt. Surg.* 10 (2022) 229–244.
- [139] K.N. Eckstein, J.E. Hergert, A.C. Uzcategui, S.A. Schoonraad, S.J. Bryant, R. R. McLeod, V.L. Ferguson, Controlled mechanical property gradients within a digital light processing printed hydrogel-composite osteochondral scaffold, *Ann. Biomed. Eng.* 52 (2024) 2162–2177.
- [140] J.J. Li, M. Ebied, J. Xu, H. Zreiqat, Current approaches to bone tissue engineering: the interface between biology and engineering, *Adv. Healthcare Mater.* 7 (2018) e1701061.
- [141] C. Shuai, L. Yu, P. Peng, C. Gao, S. Peng, Interfacial reinforcement in bioceramic/biopolymer composite bone scaffold: the role of coupling agent, *Colloids Surf. B Biointerfaces* 193 (2020) 111083.
- [142] H. Ma, C. Peng, J. Chang, C. Wu, 3D-printed bioceramic scaffolds: from bone tissue engineering to tumor therapy, *Acta Biomater.* 79 (2018) 37–59.
- [143] Y.M. Lv, Q.S. Yu, Repair of articular osteochondral defects of the knee joint using a composite lamellar scaffold, *Bone Joint Res* 4 (2015) 56–64.
- [144] A. Tampieri, E. Kon, M. Sandri, E. Campodoni, M. Dapporto, S. Sprio, Marine-inspired approaches as a smart tool to face osteochondral regeneration, *Mar. Drugs* 21 (2023) 212.
- [145] H. Shi, Z. Zhou, W. Li, Y. Fan, Z. Li, J. Wei, Hydroxyapatite based materials for bone tissue engineering: a brief and comprehensive introduction, *Crystals* 11 (2021) 149.
- [146] Q. Zhang, L. Ma, X. Ji, Y. He, Y. Cui, X. Liu, C. Xuan, Z. Wang, W. Yang, M. Chai, X. Shi, High-strength hydroxyapatite scaffolds with minimal surface macrostructures for load-bearing bone regeneration, *Adv. Funct. Mater.* 32 (2022) 2204182.
- [147] B. Liu, Y. Zhao, T. Zhu, S. Gao, K. Ye, F. Zhou, D. Qiu, X. Wang, Y. Tian, X. Qu, Biphasic double-network hydrogel with compartmentalized loading of bioactive glass for osteochondral defect repair, *Front. Bioeng. Biotechnol.* 8 (2020) 752.
- [148] V. Bupetch, X. Zhang, T. Li, J. Lin, E.P. Maswikiti, Y. Wu, D. Cai, J. Li, S. Zhang, C. Wu, H. Ouyang, Silicate-based bioceramic scaffolds for dual-lineage regeneration of osteochondral defect, *Biomaterials* 192 (2019) 323–333.
- [149] Q. Yu, J. Chang, C. Wu, Silicate bioceramics: from soft tissue regeneration to tumor therapy, *J. Mater. Chem. B* 7 (2019) 5449–5460.
- [150] Y. Wu, J. Liu, L. Kang, J. Tian, X. Zhang, J. Hu, Y. Huang, F. Liu, H. Wang, Z. Wu, An overview of 3D printed metal implants in orthopedic applications: present and future perspectives, *Heliyon* 9 (2023) e17718.
- [151] S. Wang, L. Liu, K. Li, L. Zhu, J. Chen, Y. Hao, Pore functionally graded Ti6Al4V scaffolds for bone tissue engineering application, *Mater. Des.* 168 (2019) 107643.
- [152] A. Diaz Lantada, H. Alarcon Iniesta, J.P. Garcia-Ruiz, Composite scaffolds for osteochondral repair obtained by combination of additive manufacturing, leaching processes and hMSC-CM functionalization, *Mater. Sci. Eng., C* 59 (2016) 218–227.
- [153] C. Zhai, Q. Zuo, K. Shen, J. Zhou, J. Chen, X. Zhang, C. Luo, H. Fei, W. Fan, Utilizing an integrated tri-layered scaffold with Titanium-Mesh-Cage base to repair cartilage defects of knee in goat model, *Mater. Des.* 193 (2020) 108766.
- [154] Z. Liu, M. Tamaddon, S.M. Chen, H. Wang, V. San Cheong, F. Gang, X. Sun, C. Liu, Determination of an initial stage of the bone tissue ingrowth into titanium matrix by cell adhesion model, *Front. Bioeng. Biotechnol.* 9 (2021) 736063.
- [155] Y. Li, P. Pavanram, J. Zhou, K. Lietaert, P. Taheri, W. Li, H. San, M.A. Leeftang, J. M.C. Mol, H. Jahr, A.A. Zadpoor, Additively manufactured biodegradable porous zinc, *Acta Biomater.* 101 (2020) 609–623.
- [156] F. Yang, Y. Li, L. Wang, H. Che, X. Zhang, H. Jahr, L. Wang, D. Jiang, H. Huang, J. Wang, Full-thickness osteochondral defect repair using a biodegradable bilayered scaffold of porous zinc and chondroitin sulfate hydrogel, *Bioact. Mater.* 32 (2024) 400–414.
- [157] A. Farazin, A.H. Ghasemi, Design, synthesis, and fabrication of chitosan/hydroxyapatite composite scaffold for use as bone replacement tissue by sol–gel method, *J. Inorg. Organomet. Polym. Mater.* 32 (2022) 3067–3082.
- [158] B.A.E. Ben-Arfa, R.C. Pullar, A comparison of bioactive glass scaffolds fabricated by robocasting from powders made by sol–gel and melt-quenching methods, *Processes* 8 (2020) 615.
- [159] M. Costantini, C. Colosi, P. Mozetic, J. Jaroszewicz, A. Tosato, A. Rainer, M. Trombetta, W. Swieszkowski, M. Dentini, A. Barbeta, Correlation between porous texture and cell seeding efficiency of gas foaming and microfluidic foaming scaffolds, *Mater. Sci. Eng., C* 62 (2016) 668–677.
- [160] Y. Li, S. Sun, P. Gao, M. Zhang, C. Fan, Q. Lu, C. Li, C. Chen, B. Lin, Y. Jiang, A tough chitosan-alginate porous hydrogel prepared by simple foaming method, *J. Solid State Chem.* 294 (2021) 121797.
- [161] C.Y. Chen, C.J. Ke, K.C. Yen, H.C. Hsieh, J.S. Sun, F.H. Lin, 3D porous calcium-alginate scaffolds cell culture system improved human osteoblast cell clusters for cell therapy, *Theranostics* 5 (2015) 643–655.
- [162] H. Kang, Y. Zeng, S. Varghese, Functionally graded multilayer scaffolds for in vivo osteochondral tissue engineering, *Acta Biomater.* 78 (2018) 365–377.
- [163] H. Chen, A. Malheiro, C. van Blitterswijk, C. Mota, P.A. Wieringa, L. Moroni, Direct writing electrospinning of scaffolds with multidimensional fiber architecture for hierarchical tissue engineering, *ACS Appl. Mater. Interfaces* 9 (2017) 38187–38200.
- [164] W.E. King 3rd, G.L. Bowlin, Near-field electrospinning and melt electrowriting of biomedical polymers-progress and limitations, *Polymers* 13 (2021) 1097.
- [165] M. Bahraminasab, Challenges on optimization of 3D-printed bone scaffolds, *Biomed. Eng. Online* 19 (2020) 69.
- [166] X. Zhou, T. Esworthy, S.J. Lee, S. Miao, H. Cui, M. Plesiniak, H. Fenniri, T. Webster, R.D. Rao, L.G. Zhang, 3D Printed scaffolds with hierarchical biomimetic structure for osteochondral regeneration, *Nanomedicine* 19 (2019) 58–70.
- [167] J. Liu, L. Li, H. Suo, M. Yan, J. Yin, J. Fu, 3D printing of biomimetic multi-layered GelMA/nHA scaffold for osteochondral defect repair, *Mater. Des.* 171 (2019) 107708.
- [168] C. Qin, J. Ma, L. Chen, H. Ma, H. Zhuang, M. Zhang, Z. Huan, J. Chang, N. Ma, C. Wu, 3D bioprinting of multicellular scaffolds for osteochondral regeneration, *Mater. Today Off.* 49 (2021) 68–84.
- [169] A. Dewle, N. Pathak, P. Raksham, A. Srivastava, Multifarious fabrication approaches of producing aligned collagen scaffolds for tissue engineering applications, *ACS Biomater. Sci. Eng.* 6 (2020) 779–797.
- [170] G. Liu, X. Wei, Y. Zhai, J. Zhang, J. Li, Z. Zhao, T. Guan, D. Zhao, 3D printed osteochondral scaffolds: design strategies, present applications and future perspectives, *Front. Bioeng. Biotechnol.* 12 (2024) 1339916.
- [171] S. Agarwal, S. Saha, V.K. Balla, A. Pal, A. Barui, S. Bodhak, Current developments in 3D bioprinting for tissue and organ regeneration—A review, *Front. Mech. Eng.* 6 (2020) 589171.
- [172] Y. Wang, Y. Xue, J. Wang, Y. Zhu, Y. Zhu, X. Zhang, J. Liao, X. Li, X. Wu, Y.X. Qin, W. Chen, A composite hydrogel with high mechanical strength, fluorescence, and degradable behavior for bone tissue engineering, *Polymers* 11 (2019) 1112.
- [173] S. Todros, S. Spadoni, S. Barbon, E. Stocco, M. Confalonieri, A. Porzionato, P. G. Pavan, Compressive mechanical behavior of partially oxidized polyvinyl alcohol hydrogels for cartilage tissue repair, *Bioengineering* 9 (2022) 789.
- [174] W. Lan, M. Xu, X. Zhang, L. Zhao, D. Huang, X. Wei, W. Chen, Biomimetic polyvinyl alcohol/type II collagen hydrogels for cartilage tissue engineering, *J. Biomater. Sci. Polym. Ed.* 31 (2020) 1179–1198.
- [175] Y. Liu, W. Wang, K. Gu, J. Yao, Z. Shao, X. Chen, Poly(vinyl alcohol) hydrogels with integrated toughness, conductivity, and freezing tolerance based on ionic liquid/water binary solvent systems, *ACS Appl. Mater. Interfaces* 13 (2021) 29008–29020.
- [176] M. Hua, S. Wu, Y. Ma, Y. Zhao, Z. Chen, I. Frenkel, J. Strzalka, H. Zhou, X. Zhu, X. He, Strong tough hydrogels via the synergy of freeze-casting and salting out, *Nature* 590 (2021) 594–599.
- [177] S. Liu, J.M. Yu, Y.C. Gan, X.Z. Qiu, Z.C. Gao, H. Wang, S.X. Chen, Y. Xiong, G. H. Liu, S.E. Lin, A. McCarthy, J.V. John, D.X. Wei, H.H. Hou, Biomimetic natural biomaterials for tissue engineering and regenerative medicine: new biosynthesis methods, recent advances, and emerging applications, *Mil. Med. Res.* 10 (2023) 16.
- [178] J.J. Li, D.L. Kaplan, H. Zreiqat, Scaffold-based regeneration of skeletal tissues to meet clinical challenges, *J. Mater. Chem. B* 2 (2014) 7272–7306.
- [179] Y. Zhu, L. Kong, F. Farhadi, W. Xia, J. Chang, Y. He, H. Li, An injectable continuous stratified structurally and functionally biomimetic construct for enhancing osteochondral regeneration, *Biomaterials* 192 (2019) 149–158.
- [180] D. Gan, Z. Wang, C. Xie, X. Wang, W. Xing, X. Ge, H. Yuan, K. Wang, H. Tan, X. Lu, Mussel-inspired tough hydrogel with in situ nanohydroxyapatite mineralization for osteochondral defect repair, *Adv. Healthcare Mater.* 8 (2019) 1901103.
- [181] H. Zhou, R. Chen, J. Wang, J. Lu, T. Yu, X. Wu, S. Xu, Z. Li, C. Jie, R. Cao, Y. Yang, Y. Li, D. Meng, Biphasic fish collagen scaffold for osteochondral regeneration, *Mater. Des.* 195 (2020) 108947.
- [182] X. Wu, M. Zhou, F. Jiang, S. Yin, S. Lin, G. Yang, Y. Lu, W. Zhang, X. Jiang, Marginal sealing around integral bilayer scaffolds for repairing osteochondral defects based on photocurable silk hydrogels, *Bioact. Mater.* 6 (2021) 3976–3986.
- [183] W. Jiang, X. Xiang, M. Song, J. Shen, Z. Shi, W. Huang, H. Liu, An all-silk-derived bilayer hydrogel for osteochondral tissue engineering, *Mater. Today Bio.* 17 (2022) 100485.
- [184] X. Liu, Y. Wei, C. Xuan, L. Liu, C. Lai, M. Chai, Z. Zhang, L. Wang, X. Shi, A biomimetic biphasic osteochondral scaffold with layer-specific release of stem cell differentiation inducers for the reconstruction of osteochondral defects, *Adv. Healthcare Mater.* 9 (2020) 2000076.
- [185] F. Gao, Z. Xu, Q. Liang, H. Li, L. Peng, M. Wu, X. Zhao, X. Cui, C. Ruan, W. Liu, Osteochondral regeneration with 3D-printed biodegradable high-strength supramolecular polymer reinforced-gelatin hydrogel scaffolds, *Adv. Sci.* 6 (2019) 1900867.
- [186] L. Chen, L. Wei, X. Su, L. Qin, Z. Xu, X. Huang, H. Chen, N. Hu, Preparation and characterization of biomimetic functional scaffold with gradient structure for osteochondral defect repair, *Bioengineering* 10 (2023) 213.
- [187] J. Liu, Q. Zou, C. Wang, M. Lin, Y. Li, R. Zhang, Y. Li, Electrospinning and 3D printed hybrid bi-layer scaffold for guided bone regeneration, *Mater. Des.* 210 (2021) 110047.

- [188] S. Tamburaci, B. Cecen, O. Ustun, B.U. Ergur, H. Havticioglu, F. Tihminlioglu, Production and characterization of a novel bilayer nanocomposite scaffold composed of chitosan/Si-nHap and zein/POSS structures for osteochondral tissue regeneration, *ACS Appl. Mater. Interfaces* 2 (2019) 1440–1455.
- [189] F. Hejazi, S. Bagheri-Khouloujani, N. Olov, D. Zeini, A. Solouk, H. Mirzadeh, Fabrication of nanocomposite/nanofibrous functionally graded biomimetic scaffolds for osteochondral tissue regeneration, *J. Biomed. Mater. Res. A* 109 (2021) 1657–1669.
- [190] C. Gegg, F. Yang, Spatially patterned microribbon-based hydrogels induce zonally-organized cartilage regeneration by stem cells in 3D, *Acta Biomater.* 101 (2020) 196–205.
- [191] X. Wan, Y. Zhao, Z. Li, L. Li, Emerging polymeric electrospun fibers: from structural diversity to application in flexible bioelectronics and tissue engineering, *Explorations* 2 (2022) 20210029.
- [192] M. Castilho, G. Hochleitner, W. Wilson, B. van Rietbergen, P.D. Dalton, J. Groll, J. Malda, K. Ito, Mechanical behavior of a soft hydrogel reinforced with three-dimensional printed microfibre scaffolds, *Sci. Rep.* 8 (2018) 1245.
- [193] M. Castilho, V. Mouser, M. Chen, J. Malda, K. Ito, Bi-layered micro-fibre reinforced hydrogels for articular cartilage regeneration, *Acta Biomater.* 95 (2019) 297–306.
- [194] A.F. Girão, A. Semitel, G. Ramalho, A. Completo, P.A.A.P. Marques, Mimicking nature: fabrication of 3D anisotropic electrospun polycaprolactone scaffolds for cartilage tissue engineering applications, *Compos. B Eng.* 154 (2018) 99–107.
- [195] N. Munir, A. McDonald, A. Callanan, Integrational technologies for the development of three-dimensional scaffolds as platforms in cartilage tissue engineering, *ACS Omega* 5 (2020) 12623–12636.
- [196] T.J. Levingstone, A. Matsiko, G.R. Dickson, F.J. O'Brien, J.P. Gleeson, A biomimetic multi-layered collagen-based scaffold for osteochondral repair, *Acta Biomater.* 10 (2014) 1996–2004.
- [197] R. Cao, Y. Xu, Y. Xu, D.D. Brand, G. Zhou, K. Xiao, H. Xia, J.T. Czernuszka, Development of tri-layered biomimetic atelocollagen scaffolds with interfaces for osteochondral tissue engineering, *Adv. Healthcare Mater.* 11 (2022) 2101643.
- [198] S. Camarero-Espinosa, B. Rothen-Rutishauser, C. Weder, E.J. Foster, Directed cell growth in multi-zonal scaffolds for cartilage tissue engineering, *Biomaterials* 74 (2016) 42–52.
- [199] O. Bas, S. Lucarotti, D.D. Angella, N.J. Castro, C. Meinert, F.M. Wunner, E. Rank, G. Vozzi, T.J. Klein, I. Catelas, E.M. De-Juan-Pardo, D.W. Hutmacher, Rational design and fabrication of multiphasic soft network composites for tissue engineering articular cartilage: a numerical model-based approach, *Chem. Eng. J.* 340 (2018) 15–23.
- [200] M. Nowicki, W. Zhu, K. Sarkar, R. Rao, L.G. Zhang, 3D printing multiphasic osteochondral tissue constructs with nano to micro features via PCL based bioink, *Bioprinting* 17 (2020) e00066.
- [201] X. Hu, W. Li, L. Li, Y. Lu, Y. Wang, R. Parungao, S. Zheng, T. Liu, Y. Nie, H. Wang, K. Song, A biomimetic cartilage gradient hybrid scaffold for functional tissue engineering of cartilage, *Tissue Cell* 58 (2019) 84–92.
- [202] C.A. Tee, J. Han, J.H.P. Hui, E.H. Lee, Z. Yang, Perspective in achieving stratified articular cartilage repair using zonal chondrocytes, *Tissue Eng., Part B* 29 (2023) 310–330.
- [203] C.A. Tee, Z. Yang, Y. Wu, X. Ren, M. Baranski, D.J. Lin, A. Hassan, J. Han, E. H. Lee, A pre-clinical animal study for zonal articular cartilage regeneration using stratified implantation of microcarrier expanded zonal chondrocytes, *Cartilage* 13 (2022) 1–16.
- [204] Y. Peng, Y. Zhuang, Y. Zhang, J. Zuo, J. Ding, Dynamically adaptive scaffolds for cartilage tissue engineering, *MedComm – Biomaterials and Applications* 2 (2023) e49.
- [205] D. Clearfield, A. Nguyen, M. Wei, Biomimetic multidirectional scaffolds for zonal osteochondral tissue engineering via a lyophilization bonding approach, *J. Biomed. Mater. Res. A* 106 (2018) 948–958.
- [206] D.C. Browe, P.J. Diaz-Payno, F.E. Freeman, R. Schipani, R. Burdis, D.P. Ahern, J. M. Nulty, S. Guler, L.D. Randall, C.T. Buckley, P.A.J. Brama, D.J. Kelly, Bilayered extracellular matrix derived scaffolds with anisotropic pore architecture guide tissue organization during osteochondral defect repair, *Acta Biomater.* 143 (2022) 266–281.
- [207] S. Zadehan, B. Vahidi, J. Nourmohammadi, A. Shojaei, N. Haghighipour, Evaluation of rabbit adipose derived stem cells fate in perfused multilayered silk fibroin composite scaffold for Osteochondral repair, *J. Biomed. Mater. Res. B Appl. Biomater.* 112 (2024) e35396.
- [208] J. Chakraborty, J. Fernández-Pérez, K.A. van Kampen, S. Roy, T. Ten Brink, C. Mota, S. Ghosh, L. Moroni, Development of a biomimetic arch-like 3D bioprinted construct for cartilage regeneration using gelatin methacryloyl and silk fibroin-gelatin bioinks, *Biofabrication* 15 (2023) 035009.
- [209] M. Younesi, V.M. Goldberg, O. Akkus, A micro-architecturally biomimetic collagen template for mesenchymal condensation based cartilage regeneration, *Acta Biomater.* 30 (2016) 212–221.
- [210] T. Yamamoto, R. Randriantsilefisoa, C.M. Sprecher, M. D'Este, Fabrication of collagen-hyaluronic acid cryogels by directional freezing mimicking cartilage arcade-like structure, *Biomolecules* 12 (2022) 1809.
- [211] J.N. Fu, X. Wang, M. Yang, Y.R. Chen, J.Y. Zhang, R.H. Deng, Z.N. Zhang, J.K. Yu, F.Z. Yuan, Scaffold-based tissue engineering strategies for osteochondral repair, *Front. Bioeng. Biotechnol.* 9 (2021) 812383.
- [212] J. Liang, P. Liu, X. Yang, L. Liu, Y. Zhang, Q. Wang, H. Zhao, Biomaterial-based scaffolds in promotion of cartilage regeneration: recent advances and emerging applications, *J. Orthop. Translat.* 41 (2023) 54–62.
- [213] Y. Yu, J. Wang, Y. Li, Y. Chen, W. Cui, Cartilaginous organoids: advances, applications, and perspectives, *Adv. Nanobiomed Res.* 3 (2022) 2200114.
- [214] Y. Wang, Y. Guo, Q. Wei, X. Li, K. Ji, K. Zhang, Current researches on design and manufacture of biopolymer-based osteochondral biomimetic scaffolds, *Bio-Des, Man (Lond.)* 4 (2021) 541–567.
- [215] Š. Ryglová, M. Braun, T. Suchý, M. Hříbal, M. Žaloudková, L.J.F.R.I. Vištějnová, The investigation of batch-to-batch variabilities in the composition of isolates from fish and mammalian species using different protocols, *Food Res. Int.* 169 (2023) 112798.
- [216] J. Du, Z. Zhu, J. Liu, X. Bao, Q. Wang, C. Shi, C. Zhao, G. Xu, D. Li, 3D-printed gradient scaffolds for osteochondral defects: current status and perspectives, *Int. J. Bioprinting.* 9 (2023) 724.
- [217] D. Kilian, P. Sembdner, H. Bretschneider, T. Ahlfeld, L. Mika, J. Lütznier, S. Holtzhausen, A. Lode, R. Stelzer, M. Gelinsky, 3D printing of patient-specific implants for osteochondral defects: workflow for an MRI-guided zonal design, *Bio-Des, Man (Lond.)* 4 (2021) 818–832.
- [218] T. Ahlfeld, N. Cubo-Mateo, S. Cometta, V. Guduric, C. Vater, A. Bernhardt, A. R. Akkineeni, A. Lode, M. Gelinsky, A novel plasma-based bioink stimulates cell proliferation and differentiation in bioprinted, mineralized constructs, *ACS Appl. Mater. Interfaces* 12 (2020) 12557–12572.
- [219] P. Gonzalez-Fernandez, C. Rodriguez-Nogales, O. Jordan, E. Allemann, Combination of mesenchymal stem cells and bioactive molecules in hydrogels for osteoarthritis treatment, *Eur. J. Pharm. Biopharm.* 172 (2022) 41–52.
- [220] S. Critchley, E.J. Sheehy, G. Cuniffe, P. Diaz-Payno, S.F. Carroll, O. Jeon, E. Alsberg, P.A.J. Brama, D.J. Kelly, 3D printing of fibre-reinforced cartilaginous templates for the regeneration of osteochondral defects, *Acta Biomater.* 113 (2020) 130–143.
- [221] D. Pearce, S. Fischer, F. Huda, A. Vahdati, Applications of computer modeling and simulation in cartilage tissue engineering, *Tissue Eng. Regen. Med.* 17 (2020) 1–13.
- [222] B.L. Devlin, M.C. Allenby, J. Ren, E. Pickering, T.J. Klein, N.C. Paxton, M. A. Woodruff, Materials design innovations in optimizing cellular behavior on melt electrowritten (MEW) scaffolds, *Adv. Funct. Mater.* 16 (2024) 2313092.
- [223] H. Nosrati, M. Nosrati, Artificial intelligence in regenerative medicine: applications and implications, *Biomimetics* 8 (2023) 442.
- [224] O. Yue, X. Wang, M. Hou, M. Zheng, D. Hao, Z. Bai, X. Zou, B. Cui, C. Liu, X. Liu, Smart nanoengineered electronic-scaffolds based on triboelectric nanogenerators as tissue batteries for integrated cartilage therapy, *Nano Energy* 107 (2023) 108158.
- [225] A. Puigalfi-Jou, R. Rizzo, A. Bonato, P. Fisch, S. Ponta, D.M. Weber, M. Zenobi-Wong, FLIGHT biofabrication supports maturation of articular cartilage with anisotropic properties, *Adv. Healthcare Mater.* 13 (2024) 2302179.
- [226] H. Meng, X. Liu, R. Liu, Y. Zheng, A. Hou, S. Liu, W. He, Y. Wang, A. Wang, Q. Guo, J. Peng, Decellularized laser micro-patterned osteochondral implants exhibit zonal recellularization and self-fixing for osteochondral regeneration in a goat model, *J. Orthop. Translat.* 46 (2024) 18–32.
- [227] J. Lai, Y. Liu, G. Lu, P. Yung, X. Wang, R.S. Tuan, Z.A. Li, 4D bioprinting of programmed dynamic tissues, *Bioact. Mater.* 37 (2024) 348–377.
- [228] A.N. Aufa, Z. Ismail, M. Zaki Hassan, Emerging trends in 4d printing of hydrogels in the biomedical field: a review, in: *Materials Today: Proceedings, 2023*, <https://doi.org/10.1016/j.matpr.2023.01.101>.
- [229] S. Naficy, R. Gately, R. Gorkin, H. Xin, G.M. Spinks, 4D printing of reversible shape morphing hydrogel structures, *Macromol. Mater. Eng.* 302 (2017) 1600212–n/a.
- [230] S.H. Kim, Y.B. Seo, Y.K. Yeon, Y.J. Lee, H.S. Park, M.T. Sultan, J.M. Lee, J.S. Lee, O.J. Lee, H. Hong, H. Lee, O. Ajitser, Y.J. Suh, S.-H. Song, K.-H. Lee, C.H. Park, 4D-bioprinted silk hydrogels for tissue engineering, *Biomaterials* 260 (2020) 120281.
- [231] A. Ding, O. Jeon, D. Cleveland, K.L. Gasvoda, D. Wells, S.J. Lee, E. Alsberg, Jammed micro-flake hydrogel for four-dimensional living cell bioprinting, *Adv. Mater.* 34 (2022).
- [232] A. Ding, S.J. Lee, R. Tang, K.L. Gasvoda, F. He, E. Alsberg, 4D cell-condensate bioprinting, *Small* 18 (2022).
- [233] P.J. Diaz-Payno, M. Kalogeropoulou, I. Muntz, E. Kingma, N. Kops, M. D'Este, G. H. Koenderink, L.E. Fratila-Apachitei, G.J.V.M. van Osch, A.A. Zadpoor, Swelling-dependent shape-based transformation of a human mesenchymal stromal cells-laden 4D bioprinted construct for cartilage tissue engineering, *Adv. Healthcare Mater.* 12 (2023).
- [234] K. Loukelis, Z.A. Helal, A.G. Mikos, M. Chatzinikolaïdou, Nanocomposite bioprinting for tissue engineering applications, *Gels* 9 (2023).
- [235] L. Ricotti, A. Cafarelli, C. Manferdini, D. Trucco, L. Vannozzi, E. Gabusi, F. Fontana, P. Dolzani, Y. Saleh, E. Lenzi, M. Columbaro, M. Piazzi, J. Bertacchini, A. Aliperta, M. Cain, M. Gemmi, P. Parlanti, C. Jost, Y. Fedutik, G.D. Nessim, M. Telkhozhaeva, E. Teblum, E. Dumont, C. Delbaldo, G. Codispoti, L. Martini, M. Tschon, M. Fini, G. Lisignoli, Ultrasound stimulation of piezoelectric nanocomposite hydrogels boosts chondrogenic differentiation in vitro, in both a normal and inflammatory milieu, *ACS Nano* 18 (2024) 2047–2065.
- [236] C. Lesage, M. Lafont, P. Guihard, P. Weiss, J. Guicheux, V. Delplace, Material-assisted strategies for osteochondral defect repair, *Adv. Sci.* 9 (2022).
- [237] P.P.W. van Hughten, R.M. Jeuken, E.E. Asik, H. Overing, T.J.M. Welting, C.C. van Donkelaar, J.C. Thies, P.J. Emans, A.K. Roth, In vitro and in vivo evaluation of the osseointegration capacity of a polycarbonate-urethane zirconium-oxide composite material for application in a focal knee resurfacing implant, *J. Biomed. Mater. Res., Part A* 112 (2024) 1424–1435.
- [238] H. Meng, X. Liu, R. Liu, Y. Zheng, A. Hou, S. Liu, W. He, Y. Wang, A. Wang, Q. Guo, J. Peng, Decellularized laser micro-patterned osteochondral implants exhibit zonal recellularization and self-fixing for osteochondral regeneration in a goat model, *J. Orthop. Translat.* 46 (2024) 18–32.

- [239] Y. Huo, B. Bai, R. Zheng, Y. Sun, Y. Yu, X. Wang, H. Chen, Y. Hua, Y. Zhang, G. Zhou, X. Wang, In vivo stable allogenic cartilage regeneration in a goat model based on immunoisolation strategy using electrospun semipermeable membranes, *Adv. Healthcare Mater.* 12 (2023).
- [240] T.J. Levingstone, E.J. Sheehy, C.J. Moran, G.M. Cuniffe, P.J. Diaz Payno, R. T. Brady, H.V. Almeida, S.F. Carroll, J.M. O'Byrne, D.J. Kelly, P.A. Brama, F.J. O'Brien, Evaluation of a co-culture of rapidly isolated chondrocytes and stem cells seeded on tri-layered collagen-based scaffolds in a caprine osteochondral defect model, *Biomater. Biosyst.* 8 (2022).
- [241] D.C. Browe, P.J. Díaz-Payno, F.E. Freeman, R. Schipani, R. Burdis, D.P. Ahern, J. M. Nulty, S. Guler, L.D. Randall, C.T. Buckley, P.A.J. Brama, D.J. Kelly, Bilayered extracellular matrix derived scaffolds with anisotropic pore architecture guide tissue organization during osteochondral defect repair, *Acta Biomater.* 143 (2022) 266–281.
- [242] D.C. Browe, R. Burdis, P.J. Díaz-Payno, F.E. Freeman, J.M. Nulty, C.T. Buckley, P. A.J. Brama, D.J. Kelly, Promoting endogenous articular cartilage regeneration using extracellular matrix scaffolds, *Mater. Today Bio.* 16 (2022).
- [243] M. de Ruijter, P. Diloksumpan, I. Dokter, H. Brommer, I.H. Smit, R. Levato, P. R. van Weeren, M. Castilho, J. Malda, Orthotopic equine study confirms the pivotal importance of structural reinforcement over the pre-culture of cartilage implants, *Bioeng. Trans. Med.* 9 (2024).
- [244] R. Chen, J.S. Pye, J. Li, C.B. Little, J.J.J.B.M. Li, Multiphasic Scaffolds for the Repair of Osteochondral Defects: Outcomes of Preclinical Studies, vol. 27, 2023, pp. 505–545.
- [245] J.S. Wayne, C.L. McDowell, K.J. Shields, R.S. Tuan, In vivo response of polylactic acid–alginate scaffolds and bone marrow-derived cells for cartilage tissue engineering, *Tissue Eng.* 11 (2005) 953–963.
- [246] M. Maglio, S. Brogini, S. Pagani, G. Giavaresi, M. Tschon, Current trends in the evaluation of osteochondral lesion treatments: histology, histomorphometry, and biomechanics in preclinical models, *BioMed Res. Int.* 2019 (2019) 4040236, 27.
- [247] P. Mainil-Varlet, T. Aigner, M. Brittberg, P. Bullough, A. Hollander, E. Hunziker, R. Kandel, S. Nehrer, K. Pritzker, S. Roberts, E. Stauffer, Histological assessment of cartilage repair : a report by the histology endpoint committee of the international cartilage repair society (ICRS), *JBJS* 85 (2003) 45–57.
- [248] S.S. Glasson, M.G. Chambers, W.B. Van Den Berg, C.B. Little, The OARSI histopathology initiative – recommendations for histological assessments of osteoarthritis in the mouse, *Osteoarthritis Cartilage* 18 (2010) S17–S23.
- [249] S. Wakitani, T. Goto, S.J. Pineda, R.G. Young, J.M. Mansour, A.I. Caplan, V. M. Goldberg, Mesenchymal cell-based repair of large, full-thickness defects of articular cartilage, *JBJS* 76 (1994) 579–592.
- [250] S.W. O'Driscoll, R.G. Marx, D.E. Beaton, Y. Miura, S.H. Galloway, J.S. Fitzsimmons, Validation of a simple histological-histochemical cartilage scoring system, *Tissue Eng.* 7 (2001) 313–320.
- [251] B. Hiemer, B. Genz, J. Ostwald, A. Jonitz-Heincke, A. Wree, T. Lindner, T. Tischer, S. Dommerich, R. Bader, Repair of cartilage defects with devitalized osteochondral tissue: a pilot animal study, *J. Biomed. Mater. Res., Part B* 107 (2019) 2354–2364.
- [252] B.A. Lakin, B.D. Snyder, M.W. Grinstaff, Assessing cartilage biomechanical properties: techniques for evaluating the functional performance of cartilage in health and disease, *Annu. Rev. Biomed. Eng.* 19 (2017) 27–55.
- [253] F. Gullotta, D. Izzo, F. Scalera, B. Palazzo, I. Martin, A. Sannino, F. Gervaso, Biomechanical evaluation of hMSCs-based engineered cartilage for chondral tissue regeneration, *J. Mech. Behav. Biomed. Mater.* 86 (2018) 294–304.
- [254] A.J. de Kanter, K.R. Jongsma, M.C. Verhaar, A.L. Bredenoord, The ethical implications of tissue engineering for regenerative purposes: a systematic review, *Tissue Eng., Part B* 29 (2023) 167–187.
- [255] A.M. Gonçalves, A. Moreira, A. Weber, G.R. Williams, P.F. Costa, Osteochondral tissue engineering: the potential of electrospinning and additive manufacturing, *Pharmaceutics* 13 (2021) 983.
- [256] D. Bicho, S. Pina, R.L. Reis, J.M. Oliveira, Commercial products for osteochondral tissue repair and regeneration, *Adv. Exp. Med. Biol.* 1058 (2018) 415–428.
- [257] X. Guo, Y. Ma, Y. Min, J. Sun, X. Shi, G. Gao, L. Sun, J. Wang, Progress and prospect of technical and regulatory challenges on tissue-engineered cartilage as therapeutic combination product, *Bioact. Mater.* 20 (2023) 501–518.
- [258] K.B. McGowan, G. Stigman, Regulatory challenges for cartilage repair technologies, *Cartilage* 4 (2013) 4–11.
- [259] C.V. Oberweis, J.A. Marchal, E. López-Ruiz, P. Gálvez-Martín, A worldwide overview of regulatory frameworks for tissue-based products, *Tissue Eng., Part B* 26 (2020) 181–196.

Chapter 3 Research Methodology

Experimental setup outline and design of critical-sized stratified chondral scaffolds.

3.1 Scaffold Description & Fabrication Approach

3.1.1 Design parameters

The multizonal biomimetic scaffold designed for this study consists of three distinct layers, forming a tri-layered cartilage scaffold. The zonal cartilage layers are engineered with a gradient mechanical transition, providing increased flexibility to mimic the properties of the superficial cartilage zone. In contrast, the lower deep layer is designed to be more rigid to withstand mechanical loading. The transition between these layers is intended to be seamless, ensuring proper integration and functionality within the tissue environment.

- **Layer composition/ Material selection:** The cartilage zonal layers will be designed to mimic cartilage, and materials such as alginate, collagen, and chitosan will be used due to their biocompatibility and similarity to native cartilage extracellular matrix (ECM). Synthetic materials such as PVA can be applied to fabricate composite scaffolds for enhancing mechanical stretchability. While in the deep transitional zone or bone layer, the incorporation of mineral content hydroxyapatite (HAp) for enhanced osteoconductivity, will be utilised.
- **Porosity and Pore Size:** The scaffold will have a gradient in porosity, with smaller pores in the cartilage layer and larger, interconnected pores in the bone layer to facilitate vascularisation and nutrient diffusion.

3.1.2 Materials selection & Fabrication techniques

To achieve the aim and novelty of fabricating a fibrous structure that mimics the collagen fibre orientation across different zones of chondral tissue, the fibres are expected to provide sufficient mechanical properties in both compression and tension and be easily aligned.

In initial tests and experiments on fibrous hydrogel fabrication, alginate-based fibres generated by wet spinning failed to meet the expected mechanical strength and were too thick to effectively mimic the target structure. Additionally, alginate fibres exhibited inadequate mechanical strength to support the required structural integrity and functionality. Even when incorporated into bulk hydrogel, these fibre sheets were ineffective in the superficial or middle zones and enhanced complexity to maintaining consistency across replicated samples.

Inspired by natural fibres and their potential for biomedical applications due to biocompatibility and tissue-like structure and composition, natural silk fibres derived from *Bombyx mori* silkworm cocoons have attracted significant attention. These silk fibres exhibit consistent thickness with minimal variation between individual cocoons. By investigating and optimising degumming and sterilisation standards for silk cocoons, this process can further advance research and contribute to scaffold development.

For fabrication methods aimed at achieving a consistent, controllable structure, this project employed a simple mould-casting technique, chosen for its ease of handling. In the initial design, mould-casting was deemed more conducive to the biological evaluation of the new material. A layer-by-layer sequential layering method was then employed to achieve continuous or layer-specific chondral scaffolds, ensuring seamless transitions and strong interfacial bonding between layers.

3.2 Experimental Design Outline

The experimental sections of this thesis are presented in Chapters 4 to Chapter 7, as outlined in **Figure 3-1**. Chapter 4 provides an overview of the use of silk cocoons in biomedical applications, covering the degumming process, the collection of silk fibroin fibres, and the potential biomedical applications of silk sericin. Chapter 5 builds on the silk extraction and preparation process, utilising the silk fibres as reinforcement for hydrogel fabrication to achieve a zonal architecture and create a seamless transition across the superficial, middle, and deep zones. Chapter 6 and Chapter 7 focus on the physical characterisations and subsequent biological assessments, respectively.

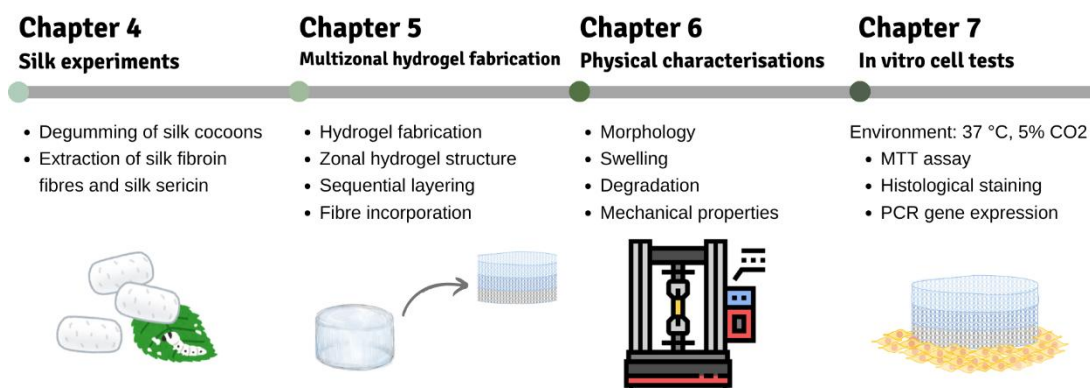


Figure 3-1 Schematic outline of the project, showing the experimental components corresponding to the thesis chapters.

3.2.1 Aim 1: Synthesis of hydrogel scaffold

This project aimed to design and fabricate biomimetic zonal scaffolds replicating the distinct structural and mechanical properties of native articular cartilage, comprising three specialised layers: superficial, middle, and deep zones, implemented as either discrete multilayered or gradient transition architectures. The scaffold system was developed using a hybrid material approach combining sodium alginate (1-3% w/v) as the natural biodegradable matrix with synthetic polyvinyl alcohol (PVA, 5-10% w/v) for mechanical reinforcement.

To address physiological load-bearing demands where deep zone cartilage experiences greater compressive stresses than superficial layers, the deep articular cartilage or calcified cartilage zones were engineered with enhanced compressive modulus through incorporation of bioceramic reinforcements (hydroxyapatite or bioglass).

While in the superficial zone, the layer requires high elasticity to withstand shear forces during joint articulation and facilitate force distribution. To achieve this, a novel approach incorporating silk fibroin fibres into the hydrogel matrix was introduced. This modification is hypothesised to enhance tensile strength and elasticity for surface-layer functionality and better mimic the collagen-rich structure of native superficial cartilage by providing an oriented and connective fibre sheet.

In brief, this study developed a biomimetic, triphasic cartilage scaffold that replicates the distinct structural and mechanical properties of native articular cartilage zones: the superficial zone (10–20% of thickness), middle zone (40–60%), and deep zone (20–30%).

The base hydrogel matrix consisted of ionically crosslinked alginate (1–3% w/v) reinforced with synthetic polyvinyl alcohol (PVA, 5-10% w/v) to achieve tunable mechanical properties while maintaining chondrocyte compatibility. The materials used for hydrogel fabrication were sourced from *Sigma-Aldrich*, while the empty raw silk cocoons were procured from an Australian supplier, *Everything Silkworms*.

The zonal design of the cartilage scaffold was as follows:

- Superficial zone: Pure PVA-based hydrogel (low stiffness)
- Middle zone: PVA-alginate composite
- Deep zone: PVA-alginate composite reinforced with HAp

For interfacial integration, the zone-specific cartilage scaffold was constructed with a multiphasic structure to enable regeneration within each respective component. The cartilage zonal components must be integrated without risk of delamination, and potential material mismatch issues must be addressed. In this project, bioadhesive interface engineering was employed, using PVA-based adhesive layers to form the overall triphasic scaffold.

3.2.2 Aim 2: To assess the physical and mechanical properties of the scaffolds

The standard physical characterisation procedures for hydrogel scaffolds are outlined below. Subsequent chapters will provide detailed explanations of each experimental methodology, including scientific rationale where applicable.

The morphology and microstructure of the osteochondral hydrogel constructs were assessed using scanning electron microscopy (SEM). Full cross-sectional imaging was performed to evaluate both individual layers and the combined zonal structure. For sample preparation, approximately 1 mm thick dried sections were sputter-coated with 5 nm of iridium (Ir) to render the hydrogel structure electronically conductive, and SEM imaging magnifications were adjusted accordingly to suit the sample characteristics.

To evaluate *in vitro* degradation behaviour, hydrogel samples were immersed in phosphate-buffered saline (PBS) and incubated at 37 °C, 5% CO₂ environment. Samples were prepared using 48-well plates, mould casting to ensure sufficient material volume

and uniform dimensions for testing. The dry weight of the samples was recorded from day 0 as the starting point and measured every 2 or 3 days time interval with a total 30-day period. Percentage weight loss was calculated to quantify degradation over time.

The mechanical properties of the hydrogels were tested under both tensile and compressive loading conditions. The modulus data was generated from the machine, which was calculated from the linear region of the stress–strain curve obtained during testing. All procedures were carried out in accordance with established mechanical testing standards.

3.2.3 Aim 3: Assess biological properties of the zonal scaffold using MSCs

To evaluate the *in vitro* biological properties of the scaffolds, including cell viability and cartilage repair potential, bone marrow-derived mesenchymal stem cells (BMSCs) were seeded onto individual hydrogel layers and integrated multizonal scaffolds. The seeded constructs were cultured in standard growth media, with cell viability and proliferation assessed at designated time points (days 4 and 7) using MTT assays to determine cellular activity and growth trends.

To assess the *in vitro* biological properties of the scaffolds, including cell viability and ability to support cartilage and bone regeneration. Bone marrow-derived mesenchymal stem cells (BMSCs) were cultured on both individual hydrogel zones and the complete multizonal hydrogel scaffold to evaluate cell attachment and proliferation. Constructs were maintained in standard growth media to assess their capacity to sustain and promote cell viability and proliferation over time. Cell growth was monitored using MTT assays.

Histological examination of osteochondral scaffolds was performed after 21 days of culturing with MSCs. Sections were stained with Toluidine blue to reflect cartilage component formation, and Hematoxylin and Eosin (H&E) to evaluate extracellular matrix (ECM) formation and cell distribution.

3.3 Ethical stance

No animal studies will be conducted for this project.

Chapter 4 Degumming of Silk: Silk Fibroin Fibres and Silk Sericin

Secrets of silk spinning and biomedical applications: The long and robust fibres are derived from the Bombyx mori silkworm. Historically, silk fibres have been used mainly for textiles and luxury fabrics. Today, a new revolution in biomedical applications is unfolding ...

4.1 Silk

Silk, a biopolymer fibre from *Bombyx mori* silkworm, has been valued for over 3,000 years, particularly for its use in textiles and luxury fabrics. The origins of sericulture, the cultivation of silkworms, trace back to ancient China, from where it spread globally. The enduring appeal of silk lies in its exceptional properties, including its luxurious texture, remarkable strength, and versatility. Silk fibroin, the primary protein component of the cocoon, forms the core of silk fibres. These long, robust threads are woven into fabrics that have been the cornerstone of the sericulture industry for millennia.

Beyond its historical and industrial significance, silk has emerged as a promising biomaterial for scientific and medical applications. This chapter delves into the structure of silk fibres and explores their potential in biomedical research, highlighting its role in advancing tissue engineering and regenerative medicine.

4.2 Silk Cocoons and Biomimetic Approach in Tissue Engineering

Silk, particularly silk fibroin from *Bombyx mori*, has garnered significant attention as a biomaterial due to its biocompatibility, biodegradability, and excellent mechanical tensile strength.[15] Silkworms are remarkable natural engineers, producing silk cocoons and fibres with exceptional mechanical properties through a simple and eco-friendly process. During cocoon formation, the natural spinning mechanism of the *Bombyx mori* silkworm is facilitated by the rhythmic movement of its head in a figure-eight pattern.[16]

4.2.1 Natural silkworm spinning behaviour and bioinspired approaches

As illustrated in **Figure 4-1**, the silk gland of *Bombyx mori* plays a crucial role in silk production and serves as inspiration for biomimetic electrospinning technology.[17] Scientists have developed electrospinning methods based on the natural silk-spinning process, aiming to mimic the efficiency and structural precision of silkworm silk production. Silkworms possess specialised silk glands responsible for silk protein synthesis. These glands undergo substantial development during the larval stages, ultimately enabling the secretion of silk fibroin and silk sericin proteins.

In previous biomedical research, dialysed liquid silk fibroin has emerged as a prominent biomaterial, particularly as a base material for hydrogel fabrication.[18] Degummed silk fibroin fibre is a natural protein fibre produced by the silkworm and has attracted attention for its excellent tensile strength, biocompatibility and fibrous nature.

Mechanisms of silk spinning, the silk-spinning process begins when the silkworm larva anchors itself to a surface and extrudes silk threads through its narrow spinneret. Over several days, it produces a continuous silk fibre, typically 300 to 900 meters in length, forming a protective cocoon. The transition from a liquid protein solution to a solid silk fibre is driven by flow-induced alignment of fibroin molecules within the silk gland. Shear forces during spinning facilitate this molecular alignment, leading to the formation of a robust and elastic fibre.

Lessons from nature. Inspired by their ingenuity, spinning behaviour, and spinneret, artificial spinning methods such as electrospinning and wet spinning have been developed for biomedical applications.[19] Replicating the controlled fibre production of silkworms, offering a versatile platform for designing scaffolds with tunable properties, including pore size, fibre diameter, and mechanical strength. These bioinspired and biomimetic strategies have significantly optimised the mechanical performance of fibrous structures, paving the way for further functionalisation and broader applications in fibre-based tissue engineering.

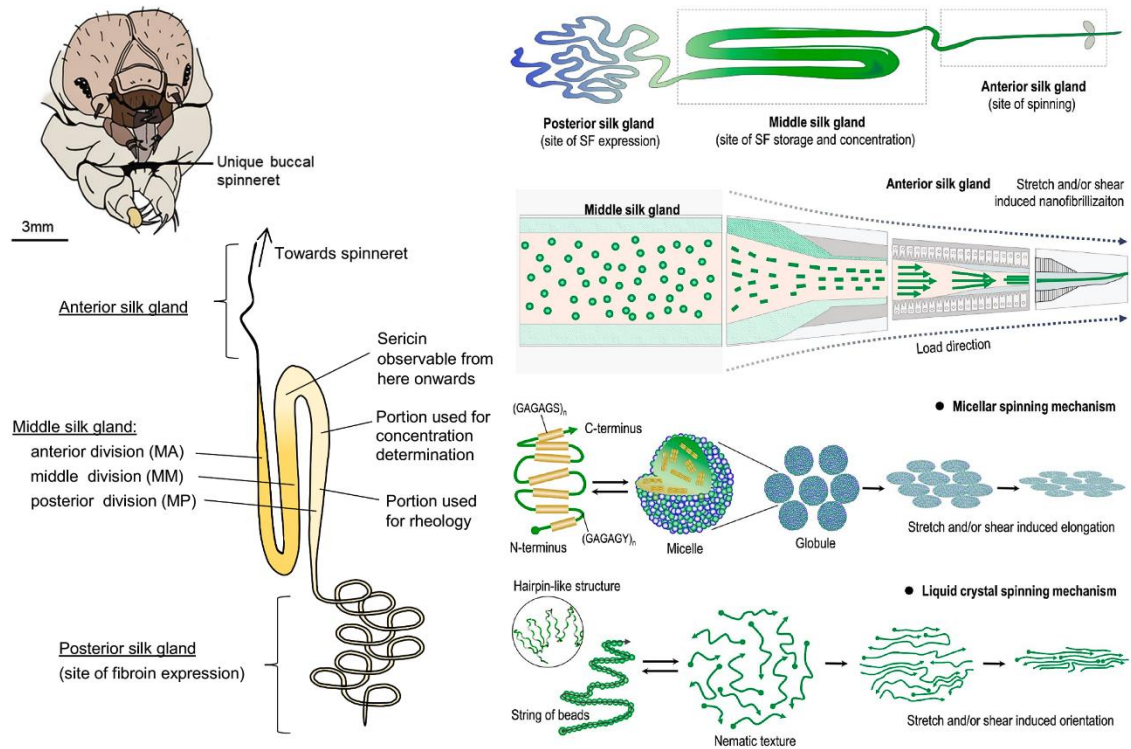


Figure 4-1 A scheme of the buccal spinneret of the silkworm, image adapted from Ref.[19]; the silk gland structure, image adapted from Ref.[17]; and bioinspired process of spinning mechanism, image adapted from Ref.[16]

4.2.2 Silk fibroin fibres and Silk sericin

Commercially available mulberry silk is derived from a single species, *Bombyx mori* silkworms. Their silk cocoons are primarily composed of two self-assembled proteins: silk fibroin (72–81%), which forms the structural core; and silk sericin (19–38%), a gummy coating that binds fibroin fibres together.[20] The cross-section of original silk cocoon fibres (**Figure 4-2**) consists of a structural core of silk fibroin surrounded by a water-soluble silk sericin layer.[21]

During the final developmental stage, the fifth instar, silkworms stop feeding and begin spinning cocoons. The transition from liquid silk fibroin to a solid fibre is induced by the alignment of protein chains under flow conditions. The silk gland of *Bombyx mori* is a tubular epithelium divided into three regions, with the posterior and middle silk glands being responsible for the massive production of silk proteins. Liquid silk proteins are extruded through a pair of spinnerets near the mouth, solidifying upon exposure to air to form silk threads.[17]

To artificially replicate the natural fibre spinning process, in biomimetic artificial fibre spinning, fibres are generated from syringe needles or nozzles, mimicking the natural silk fibre formation from the narrow spinneret of the silkworm.[19; 22] These bioinspired spinning processes have been widely applied in biomedical research to create polymeric fibrous structures.[23] Considering the similarities between natural silk fibres and biomimetic spinning techniques, directly incorporating silk fibres into hydrogel-based tissue engineering scaffolds may offer advantages due to their continuous structural features and tensile strength.

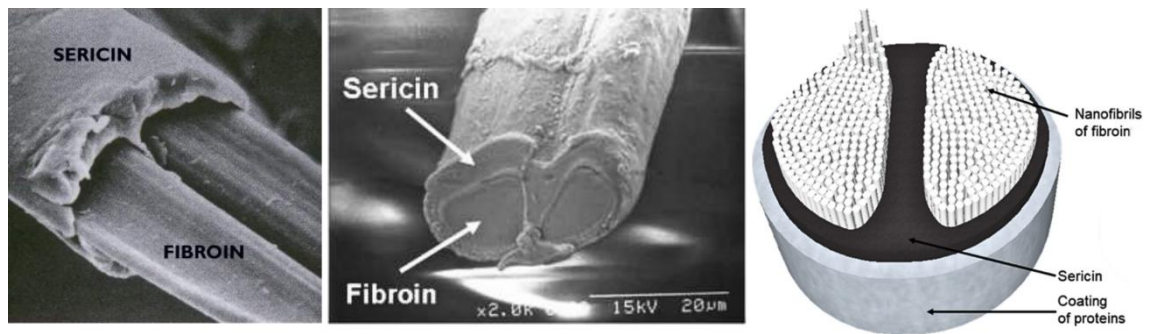


Figure 4-2 Silk structure silk fibroin coating with a layer of sericin, image adapted from Ref.[19]

Silk fibroin is the core structural protein of silk, known for its excellent biocompatibility, mechanical strength, and biodegradability, making it a versatile material for tissue engineering. It consists of heavy and light chains linked by disulfide bonds, providing both strength and flexibility. Silk fibroin's nano- and micro-sized fibres make it ideal for biomedical applications and tissue engineering, particularly in resembling collagen fibre organisations, where it is incorporated into hydrogels to create scaffolds mimicking the mechanical and biological environment of cartilage and bone. These silk-based hydrogels provide a platform for cell attachment, proliferation, and differentiation, and guidance for growing cell orientation.

Silk sericin, a group of polypeptides rich in hydrophilic amino acids, is the second most abundant protein in silk. Traditionally, sericin has been discarded as a byproduct in the textile industry[24] due to concerns and has been misunderstood regarding its role in immune responses.[25; 26] Early studies suggested that sericin might induce inflammation, but recent research indicates that inflammatory responses primarily occur when sericin is associated with fibroin particles, triggering a synergistic immune

response.[27; 28] Despite its historical neglect as a biomaterial, silk sericin has gained attention for its beneficial properties, including antioxidant, anti-inflammatory, antibacterial, and wound-healing effects.[29-31] contributing to wound healing and enhancing cellular functions.[32-34]

Both silk fibroin and silk sericin are composed of 18 amino acids in different ratios, including essential ones such as serine, glycine, aspartic acid, glutamic acid, threonine, and tyrosine, which contribute to their high hydrophilicity.[28; 33; 35] Functional groups such as hydroxyl, carboxyl, and amino groups enable sericin to dissolve in water and interact with other materials. As a naturally derived, non-toxic biomaterial, sericin has been reported to enhance cell viability and promote collagen production in tissue regeneration. [36; 37]

4.2.3 Degumming methods

Silk degumming is the process of removing sericin, the hydrophilic protein that coats silk fibroin fibres, to obtain purified silk fibroin for various applications. Sericin acts as a natural adhesive that binds fibroin fibres together within the silk cocoon, but its presence can affect the mechanical properties, biocompatibility, and processability of silk-based biomaterials. The degumming process involves breaking peptide bonds within sericin, facilitating its detachment while preserving the structural integrity of fibroin.[29]

An ideal degumming method should achieve two key objectives: 1) efficient removal of sericin to enhance silk fibroin purity and functionality, and 2) minimal degradation or damage to the fibroin fibres. Several degumming techniques have been developed, including thermal, chemical, and enzymatic approaches. As summarised in **Table 4-1**, these methods vary in their effectiveness, impact on fibroin structure, and environmental considerations.

Considering the available materials and the ease of handling in this project, an alkaline solution was applied for degumming. Washing soda ($\text{Na}_2\text{CO}_3 \cdot 10\text{H}_2\text{O}$) was chosen as it is expected to cause less damage to the fibroin structure compared to other chemical treatments.

Table 4-1 Summary of main degumming methods for silk cocoons, highlighting their advantages and disadvantages.

Degumming Method	Advantages	Disadvantages	Ref.
High-temperature processing (Autoclaving)	Simple, chemical-free, environmentally friendly	Risk of over-degumming, energy-intensive	[38; 39]
Alkaline solutions (Na₂CO₃, soap)	Effective, preserves fibroin strength	Harm the structural integrity of fibroin, requires pH control	[40; 41]
Acidic solutions (Citric, tartaric acid)	Gentle on fibroin, biodegradable	Can cause partial hydrolysis, needs neutralisation	[42]
Enzymatic processes (Protease, trypsin)	Highly selective for sericin, eco-friendly	Expensive, requires precise conditions	[39; 41]

4.3 Silk Cocoons Degumming Experiment: Methods and Procedures

The separation to extract pure fibroin fibres and sericin is essential for further use in biomedical applications. Degumming silk cocoons generally utilise the alkaline solution and enable the silk to be converted into loose silk fibres, and dissolve sericin protein in the bath solution. The selection of alkaline degumming agents and the sericin extraction method is critical in maintaining the structural integrity of fibroin. In this experiment, sodium carbonate decahydrate (Na₂CO₃·10H₂O), commonly known as washing soda, was chosen as the degumming agent. This method helps to minimise excessive damage to the silk structure by carefully controlling the temperature during the process.

Materials:

- Empty silk cocoons (devoid of silkworms or pupae) purchased from an Australian silkworm supplier, *Everything Silkworms*
- Sodium carbonate decahydrate (Na₂CO₃·10H₂O)

4.3.1 Pre-test: degumming and alignment of fibres

The traditional degumming method was employed to first clean the cocoons and remove the pupa along with any residual debris. The cleaned cocoons were then cut into small pieces to ensure even boiling during the degumming process. A 0.5% w/v solution of sodium carbonate decahydrate ($\text{Na}_2\text{CO}_3 \cdot 10\text{H}_2\text{O}$), also known as crystalline alkali or washing soda, was prepared. The cut cocoon pieces were boiled in 0.5% w/v $\text{Na}_2\text{CO}_3 \cdot 10\text{H}_2\text{O}$ solution at 90-100 °C for approximately 30 minutes until the cocoon fibres loosened, and the bath turned yellow, indicating sericin removal. If necessary, the heating process was repeated with the same concentration and temperature. The dissolved sericin solution was collected and stored for future use, while the degummed silk fibres were rinsed 2-3 times with Milli-Q water until white silk fibres were obtained.

As shown in **Figure 4-3**, the degummed silk fibres were successfully collected after boiling with $\text{Na}_2\text{CO}_3 \cdot 10\text{H}_2\text{O}$ solution. However, these fibres were not suitable for direct scaffold application due to difficulties in maintaining fibre alignment. Cutting the cocoons resulted in discontinuous silk fibres that were randomly dispersed in the bath solution, complicating both collection and alignment.

A review of classical silk fibroin extraction methods[15; 43; 44] suggests that the cutting process is primarily intended to facilitate sericin removal and subsequent dialysis, ultimately yielding an aqueous silk fibroin solution for hydrogel production. However, this method does not support the experimental requirements of this study, which necessitate structured fibre alignment for scaffold fabrication. Thus, alternative approaches must be explored to achieve the desired fibre organisation.

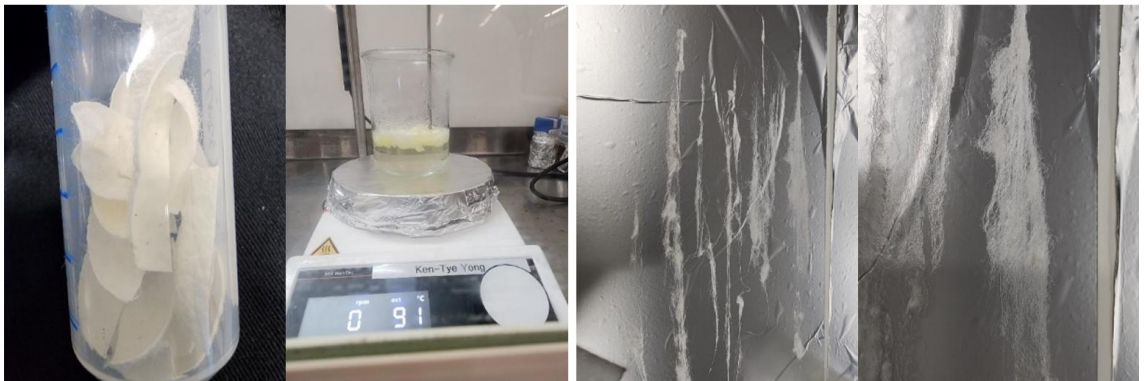


Figure 4-3 Pre-test of silk cocoon pieces showing failure to obtain continuous fibres.

4.3.2 Optimised degumming process of silk cocoons

Traditional silk fibroin extraction methods employed chopped cocoons to produce aqueous solutions that function as hydrogel materials. However, this project required intact silk fibroin fibres to leverage their native mechanical properties and continuous structure for articular cartilage applications. Preliminary trials revealed that conventional cutting procedures yielded discontinuous fibre segments, necessitating the development of an alternative degumming methodology. As illustrated in **Figure 4-4**, whole cocoon processing was adopted to preserve fibre continuity while effectively removing sericin.

Materials:

- *Bombyx mori* silkworm cocoons from the supplier *Everything Silkworms* (empty silkworm cocoon without living organism/pupa inside)
- Sodium carbonate decahydrate ($\text{Na}_2\text{CO}_3 \cdot 10\text{H}_2\text{O}$)
- Absolute ethanol (for residual cleaning)
- Milli-Q water ($18.2 \text{ M}\Omega \cdot \text{cm}$)

Methods:

A 0.5% (w/v) $\text{Na}_2\text{CO}_3 \cdot 10\text{H}_2\text{O}$ degumming solution was prepared in Milli-Q water and preheated to 90-100°C using a hotplate. Intact cocoons were manually inspected to remove residual pupae and debris. Visible particles on the surface were removed with tweezers, and if organic residues persisted, the inside of the cocoons was wiped with ethanol and dried in a fume hood prior to degumming, if necessary.

In the whole-cocoon degumming process, pretreated cocoons were fully immersed in the boiling alkaline solution, maintained 95-100°C for the standard duration of 30-60 minutes, depending on the number of cocoons in the bath beaker. Degumming efficacy was monitored through visual confirmation of yellow sericin dissolved in the bath solution, along with tactile evaluation of fibre separation using tweezers.

The post-degumming process included fibre recovery and sericin byproduct recovery. First, loosened silk fibres were gently separated using tweezers and sequentially washed in Milli-Q water three times until no additional yellow colour or dirt was visible in the wash solution. The fibres were then air-dried in a flow hood. The collected sericin solution was filtered through a 0.2 μm syringe filter to remove impurities for future

experimental use, sterilised by autoclaving, and lyophilised (-80°C , 0.1 mBar, 48 h) to obtain sericin powder for subsequent hydrogel fabrication.

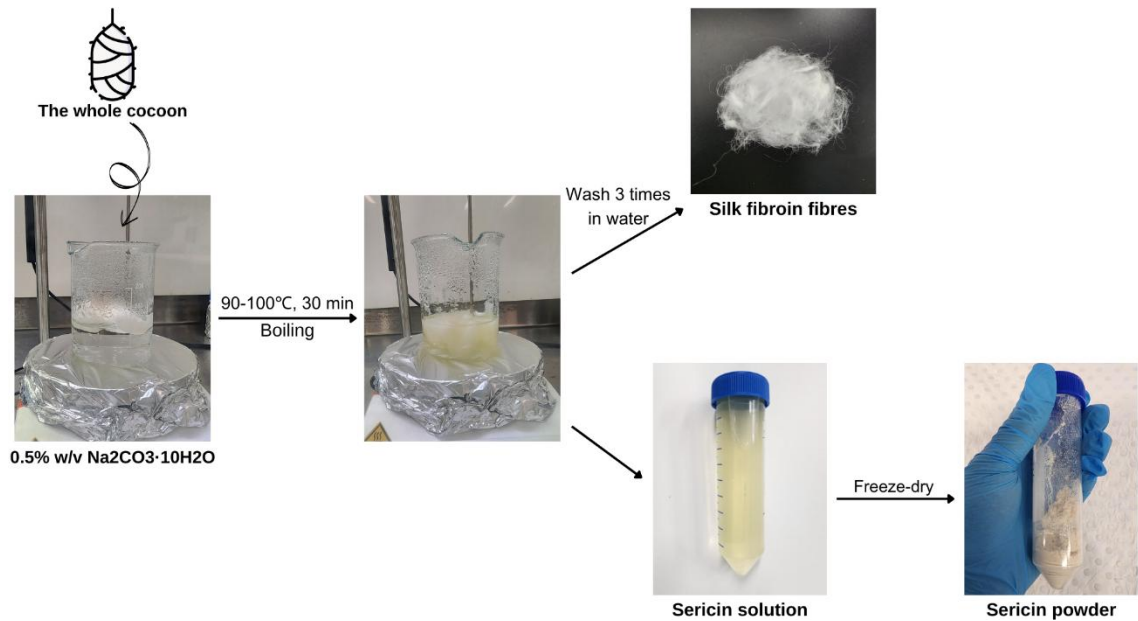


Figure 4-4 Schematic illustration to demonstrate the degumming process of entire silk cocoons.

4.4 Obtain Silk Fibre and Sericin Powder

4.4.1 Expand and collect the silkworm silk fibres

Silkworm silk fibres are initially coated with sericin, a glue-like protein that binds the fibres as they emerge from the silkworm's spinneret. The degumming process removes sericin from the fibres, resulting in separated silk fibroin fibres. Whole silkworm cocoons can be expanded by gently pulling them over a cloth hanger to stretch and align the fibre network. Once expanded, the fibres are left to air dry before further use. **Figure 4-5** demonstrates the process of cocoon fibre network expansion, alignment, and fibre collection.

4.4.2 Sterilisation of silk and sericin before application

Following degumming, two distinct proteins were obtained: silk fibroin fibres and a sericin solution. To prepare the silk fibroin fibres for hydrogel fabrication, contaminants such as dirt and residual particles were removed.

The cleaned fibres were then subjected to six cycles of dry autoclaving to ensure sterilisation before further use. Post-treatment qualitative analysis confirmed that the

autoclaved fibres retained their structural integrity, with no visible degradation. Initial trials using non-autoclaved materials (both silk sericin and silk fibroin fibres) in hydrogel fabrication and cell seeding resulted in significant microbial contamination, invalidating experimental results. Alternative sterilisation methods, such as UV irradiation fail to achieve deep structural sterilisation, while ethanol washing poses the risk of residual endotoxins, were deemed unsuitable. Therefore, silk fibres sterilised by dry autoclaving were stored for use in subsequent experimental stages for hydrogel preparation. Their natural properties, such as strength, shape, and diameter, were utilised to simulate the orientation of natural collagen fibres in scaffold preparation.

The freshly obtained sericin solution often contained sticky impurities, including remnants of silkworm pupae. To purify the solution, syringe filtration was performed 1-3 times using a 0.2 μm syringe filter (smaller pore sizes could be used for potentially improved filtration). After filtration, the solution was sterilised via wet autoclaving to prevent contamination. Following autoclaving, the sericin solution underwent an additional round of syringe filtration before being transferred into smaller containers (e.g., 50 mL centrifuge tubes) and frozen at -80°C for over 12 hours. Once frozen, the solution was freeze-dried to produce sericin in a solid powdered form.

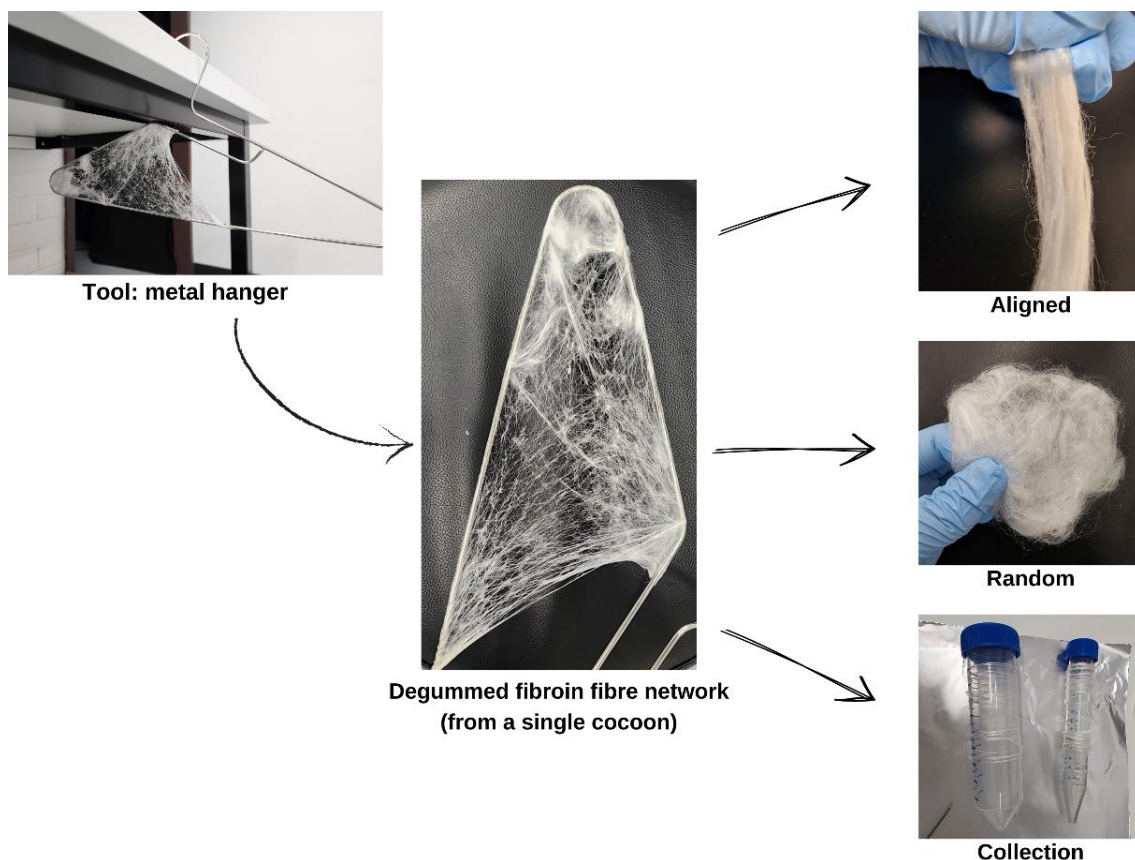


Figure 4-5 Processing steps for degummed silk fibroin fibres: network expansion, air-drying, and subsequent fibre collection.

4.5 Sericin Hydrogel Preparation

Recent studies have highlighted the remarkable utility of silk sericin in hydrogel fabrication, particularly for its roles in skin trauma healing, wound recovery and antifungal properties [32], and bioactive proliferation. These unique characteristics have stimulated a growing interest in the potential of silk sericin for biomedical applications, positioning it as a promising biomaterial for advanced therapeutic strategies. Chapter 5 provides an in-depth exploration of the comprehensive background and step-by-step protocols for sericin hydrogel preparation, offering a detailed guide for researchers and practitioners.

Incorporation of silk sericin into hydrogels is particularly advantageous due to its biocompatible and bioactive properties. Sericin is a natural protein derived from silk, which is not inherently inflammatory [27], making it a safe and effective component for hydrogel formulations. Additionally, sericin-based hydrogels can create a micro-

architecture through lyophilisation, enhancing their mechanical properties and structural integrity.[45]

This project aimed to fill the experimental gap by investigating the potential of silk gel hydrogels in cartilage repair. By optimising the concentration formulations of silk sericin and PVA material and improving the mechanical properties of the hydrogel, the project seeks to expand its application and break through the limitations of wound dressing materials.

4.5.1 Sericin-PVA hydrogel

For bulk PVA hydrogel fabrication, freeze-thawing is a practical and efficient method for achieving physical cross-linking. Past applications of sericin-PVA hydrogels have predominantly focused on antibacterial wound healing.[31; 46; 47] Reviewing related studies, PVA hydrogels prepared through the physical freeze-thaw method typically use concentrations starting from 2% w/v for achieving foldable, expandable, and soft antibacterial films suitable for acute wound applications. Based on these considerations and pre-tests, a 2% w/v sericin concentration was selected for incorporation into the PVA hydrogel design in this project.

This project introduces an innovative concept: adapting sericin-PVA hydrogels for cartilage tissue engineering by modifying material ratios and concentrations to optimise structural and mechanical properties.

In experimental tests, various combinations of sericin and PVA concentrations were explored, detailed observations are documented in **Appendix B1 and B2**. Results demonstrated that PVA concentrations below 5% w/v yielded soft and unstable hydrogels, incapable of forming interconnected structures suitable for weight-bearing cartilage tissue engineering. Conversely, PVA concentrations exceeding 20% w/v formed excessively rigid structures that appeared unsuitable for cell attachment and unfavourable for cellular proliferation. The selection of 2% w/v sericin as the optimal concentration was based on preliminary testing of three concentrations (2%, 5%, and 7.5% w/v) with a fixed 15% w/v PVA base. As detailed in **Appendix B1** (Table B1 and Figure B1), 2% sericin

was chosen because it offered the best balance between biological functionality and material integrity for this study.

After reviewing PVA material properties and conducting optimisations, the tested sericin-PVA hydrogel concentration ratios used in cell pre-tests are summarised in **Table 4-2**:

Table 4-2 Concentration ratios between sericin and PVA (in weight concentration, % w/v).

Sericin (% w/v)	PVA (% w/v)
2	5
2	10
2	15

In the pre-test, pure PVA hydrogels with concentrations ranging from 10-15% w/v exhibited the mechanical strength required for weight-bearing applications. For sericin-PVA hydrogel fabrication, sericin powder was added to heated PVA solutions to form 2% w/v concentration, thoroughly mixed, and dissolved. The final heated solution was cast into well plates for mould-casting.

Through simple freeze-thaw physical crosslinking of PVA components, the hydrogel was formed in the well plate, as shown in **Figure 4-6**. The 1-cycle -20°C freeze-thawed PVA-based hydrogels remained transparent and clear. In comparison, the pure PVA hydrogels were nearly completely transparent (blue circle in the figure). After subjecting the hydrogel to three freeze-thaw cycles at -80 °C, its structural stability and interconnectivity improved due to the repeated formation and growth of ice crystals. The rapid freezing process promoted tighter polymer entanglement, resulting in a semi-transparent hydrogel matrix. Preliminary manual compression tests (finger press) demonstrated enhanced stiffness, while the mechanical strength and shape retention of hydrogels suggested robust structural integrity. These findings indicate that the -80 °C freeze-thaw method, applied over three cycles, yielded PVA-based hydrogels with optimal properties for subsequent applications in this study.

In summary, the physical properties of crosslinked PVA hydrogels can be influenced by two key parameters: freezing temperature (-20 °C or -80 °C), and number of freeze-thaw cycles.[48; 49] The experimental observations in this project (**Appendix B3**) indicate that the relatively lower temperature (-80 °C) strengthens physical crosslinking within the

PVA network, while additional cycles improve matrix interconnectivity. These qualitative findings confirm that both reduced temperatures and increased cycling enhance the structural stability of hydrogels.

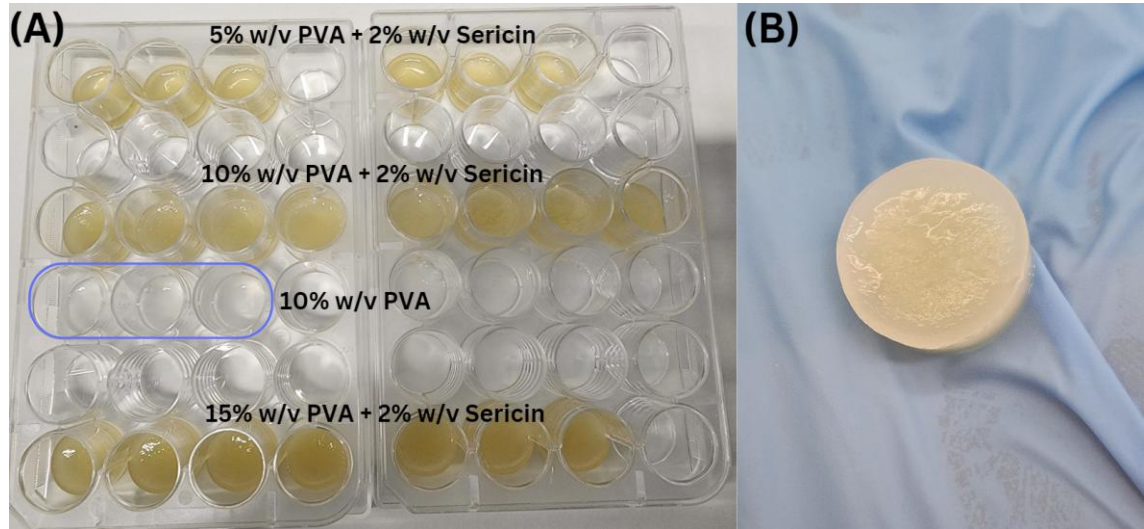


Figure 4-6 PVA-based hydrogel with the addition of 2% w/v sericin powder: (A) Hydrogel samples after one freeze-thaw cycle, frozen at -20°C and thawed at room temperature; (B) Photograph of hydrogel samples after three freeze-thaw cycles, with the last two cycles frozen at -80°C and thawed at room temperature.

4.5.2 Preliminary sericin/PVA hydrogel cell seeding

The pre-test of the hydrogel demonstrated the trend for the PVA material concentration in relation to cell growth. In a preliminary biocompatibility test, 1×10^5 cells/well of BEAS-2B cancer cells were seeded on 24-well plate-based hydrogel samples to assess toxicity and determine whether sericin could be applied in biomaterials for tissue engineering. This cancer cell line was chosen due to its high proliferative capacity and frequent use in cytotoxicity assessments.[50]

A BEAS-2B cell suspension was prepared and seeded at 1×10^5 cells/well on hydrogel samples. Two blank wells (without hydrogels) served as controls. After allowing 1 hour for cell attachment, DMEM supplemented with 10% fetal bovine serum (FBS) was added, and the plates were incubated at 37°C and 5% CO_2 . Cell viability was evaluated via MTT assay.

At the day 3 time point, the medium was replaced with 20 μL of 5 mg/mL 3-(4,5-Dimethylthiazol-2-yl)-2,5-diphenyltetrazolium bromide (MTT solution) and 200 μL

fresh DMEM, followed by incubation for 3-4 hours. Viable cells metabolised MTT into purple formazan crystals, with colour intensity varying across hydrogel samples. The MTT solution was then carefully aspirated, and 200 µL DMSO was added to dissolve the formazan crystals. The plate was gently shaken for 10 minutes to ensure complete dissolution.

Prior to absorbance measurement, hydrogels were removed with tweezers to minimise bubbles, and any debris was cleared. Absorbance readings were measured at 570 nm using a spectrophotometer. Data were analysed to assess cell viability, material-dependent proliferation effects, and growth trends between time points.

Cell viability was quantified using the formula:

$$\text{Level of cell proliferation} = \frac{ab_{\text{sample}}}{ab_{\text{blank}}} \times 100$$

The results are presented in **Figure 4-7**. The inert pure PVA material (10% w/v PVA hydrogel in this preliminary test), which exhibited very low cell proliferation promotion, yielded a light-yellow colour in the MTT assay, indicating minimal viable cell density.

The MTT assay revealed distinct colour variations across the formulations, with the intensity of purple colour varying across the three formulation samples in the photo. The 5% PVA-2% sericin composite shows light orange colouration with minimal purple particles and the lowest absorbance, indicating limited cell proliferation. The 10% PVA-2% sericin samples exhibited a deeper orange background with visible purple segments, demonstrating moderate cellular activity, while the 15% PVA-2% sericin sample displayed the most intense purple colouration. For the absorbance reading numerical results, as estimated and considered the significant error bar exhibited in 10% PVA sample, the 15% PVA-2% sericin formulation demonstrated the highest and consistent promotion of cell growth, as reflected by the colour intensity of the MTT solution and the error margins considered for cell growth in each group. These colourimetric results, supported by absorbance measurements, confirmed that the 15% PVA-2% sericin formulation promoted the highest level of cell viability among the tested composites.

Quantitative analysis of the data presented in **Figure 4-7**, data presented as mean ± SD (n = 3), reveals significant differences in cellular responses between PVA-only hydrogels

and sericin-containing PVA hydrogels. The most notable finding demonstrates that 10% w/v PVA hydrogel incorporating 2% w/v sericin supported approximately 5-fold greater cell proliferation compared to pure 10% w/v PVA hydrogel. Key observations include dose-dependent enhancement, evidenced by the fact that all tested PVA concentrations (when combined with fixed 2% w/v sericin) consistently showed significantly higher proliferation rates than the pure PVA hydrogels. And the non-toxicity confirmation, supported by the sustained enhancement across multiple concentrations, confirms that 2% sericin is not only non-cytotoxic but actively promotes cell proliferation.

In summary, the preliminary tests provided insight for the concentration standardisation as: 1) The addition of sericin to the PVA hydrogel promotes cell growth, as the comparative evaluation between the 10% PVA base samples with and without sericin addition, pure PVA demonstrated minimal cell growth and retained the light-yellow colour of the original MTT solution. 2) Within the tested concentration range $< 15\%$ w/v, the increase of PVA material concentration resulted in enhanced cell growth on the hydrogel samples. 3) The materials can be considered non-toxic, as they did not kill the BEAS-2B cancer cells, and results suggested the possibility for using PVA and sericin in hydrogel for cell growth applications.

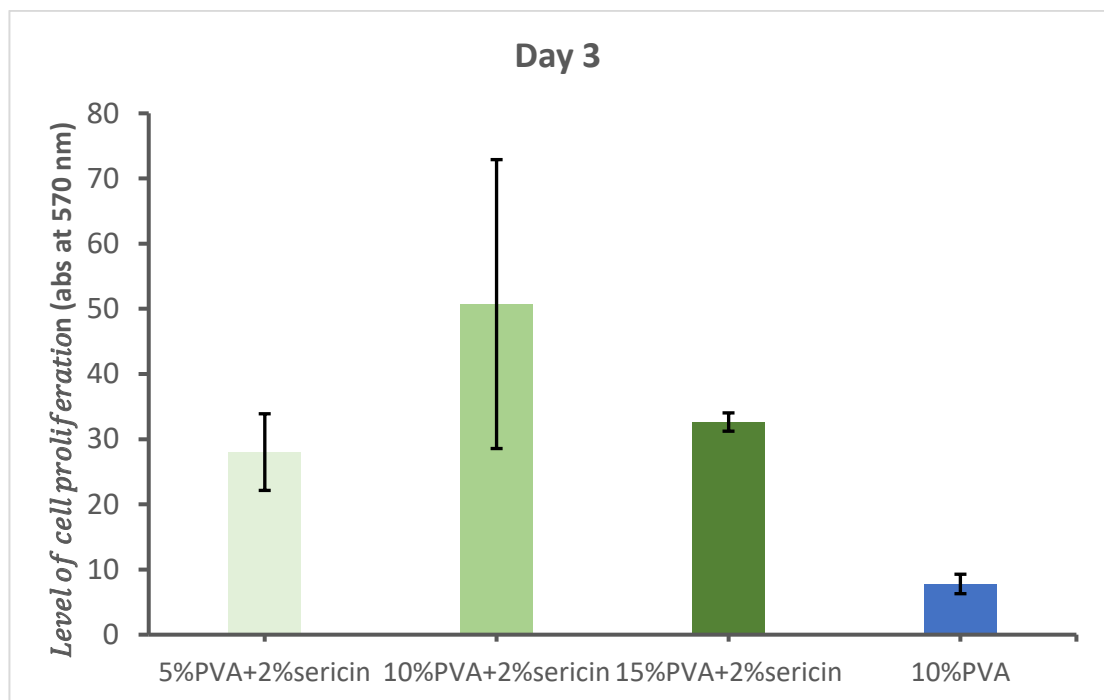
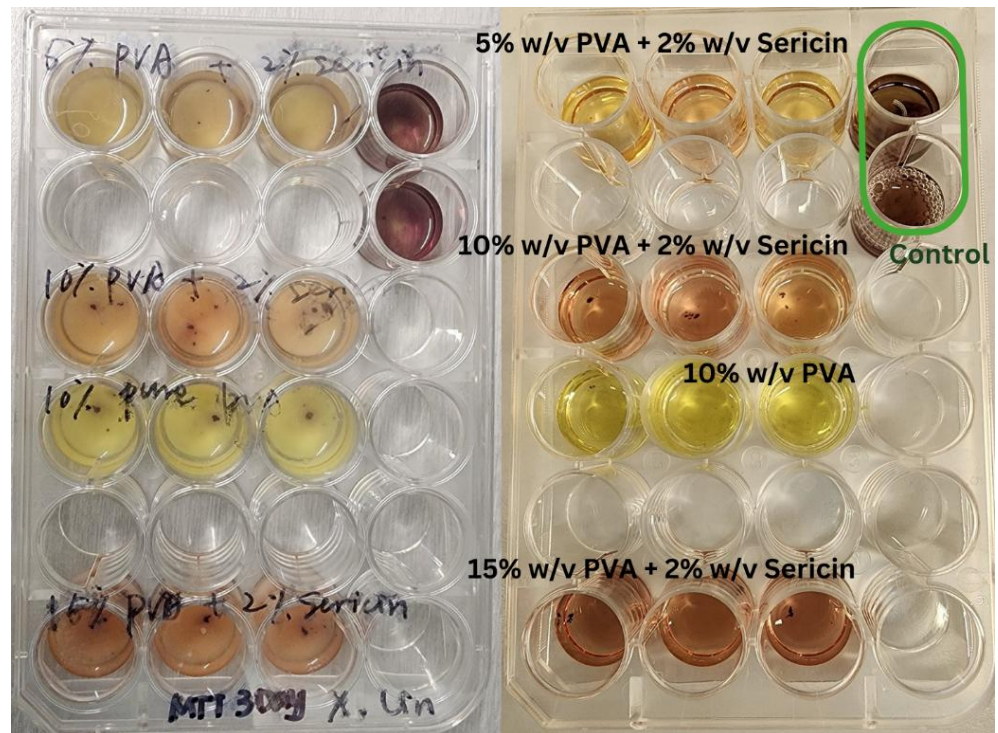


Figure 4-7 Above: Representative image of cell viability in pre-test PVA-sericin hydrogel groups ; below: Quantitative cell viability analysis of cells cultured on PVA hydrogels with varying concentrations. Data presented as mean \pm SD (n = 3) (below).

4.6 Summary, Optimisation & Outline of Scaffold Designs and Fabrication Procedures

Compared to polymeric fibres produced by other spinning methods, degummed natural silk fibroin fibres demonstrate promising potential, exhibiting excellent tensile strength for biomedical applications, particularly in musculoskeletal tissue engineering, where complex structural reconstruction and functional restoration are required.

The degummed silk fibres were dried at room temperature or in a 60°C dryer before being autoclaved to prepare them for direct incorporation into the hydrogel matrix, as detailed in Chapter 5.

In summary, the experimental results in this chapter indicate that the addition of 2% w/v sericin and a PVA concentration below 15% w/v provides appropriate mechanical stiffness. Pre-test results showed that cell growth increases with higher PVA concentrations. The selection of 15% PVA with 2% sericin as the optimal formulation was based on balancing mechanical properties and cell viability. Experimental data showed that 15% PVA provided superior mechanical stiffness under compression compared to lower concentrations. Additionally, the addition of 2% sericin enhanced cell viability without compromising these mechanical properties. Therefore, the optimal concentration for the superficial zone was determined to be 15% w/v PVA with 2% w/v sericin. This concentration has been used in subsequent experiments and scaffold designs.

Chapter 5 Multilayered Hydrogel Scaffolds: Design and Optimisation

Alginate and PVA hydrogels were used to create composite hydrogel scaffolds through sequential layering methods, forming biomimetic zonal scaffolds designed to replicate the hierarchical structure of cartilage tissue.

5.1 Hydrogels in Tissue Engineering

Hydrogels are three-dimensional, highly hydrated, polymeric, interconnected networks capable of retaining a large amount of water, resembling the physicochemical characteristics of the natural extracellular matrix (ECM).[51] Their inherent versatility, biocompatibility, and tunable properties have established hydrogels as essential materials in tissue engineering, particularly for scaffold fabrication.[52] By replicating the native microenvironment, hydrogels provide a supportive framework for cellular processes, making them indispensable in developing advanced biomaterials for regenerative medicine.[5; 53]

Hydrogels are formed via crosslinking mechanisms that create a stable network structure, either physically reversible crosslinking or permanent chemical network structures. The high-water content intrinsic to hydrogels creates a biomimetic environment that facilitates key biological functions such as cell adhesion, proliferation, and differentiation.[54] Additionally, their adaptability and multifunctionality drive advancements in next-generation materials for therapeutic and regenerative applications.

Mechanical properties and strength of hydrogels are critical factors in determining their suitability for biomedical applications, particularly in musculoskeletal tissue engineering. Key properties such as compressive modulus, tensile strength, and elasticity are essential for supporting load-bearing tissues and maintaining structural integrity under mechanical stress. Traditional studies have shown that hydrogels often face the challenge of poor mechanical strength.[55; 56] To address this limitation, this project focuses on investigating materials, composite formulations, and reinforced hydrogels to enhance the mechanical performance of chondral hydrogel scaffolds. These improvements aim to better mimic the mechanical environment of native tissues, supporting their application

in tissue engineering and tissue regeneration. These mechanical enhancements ensure that the hydrogels can mimic the mechanical environment of native tissue, supporting their application in tissue engineering and regeneration.

5.1.1 Alginate hydrogels

In the experimental section of this project, the material used for the fabrication of hydrogels is alginate. Alginate is a naturally occurring polysaccharide derived from brown algae and is widely utilised in hydrogel synthesis due to its biocompatibility and ease of gelation. Alginate hydrogels are three-dimensional (3D), highly hydrated polymeric networks that closely resemble the natural extracellular matrix (ECM), making them ideal for biomedical applications such as bone tissue engineering.[57]

In the review of the synthesis of alginate hydrogel, it is known that the presence of divalent or trivalent cations facilitates the gelation of alginate [58; 59], which promotes crosslinking by replacing sodium ions (Na^+) in the carboxylic groups of the alginate chains. In clinical applications, calcium ions (Ca^{2+}) are commonly used due to their non-toxic nature compared to other cations. The most conventional ionic crosslinking method involves the use of soluble calcium salts[60-62], such as the calcium chloride (CaCl_2) solution bath. This process enables the diffusion of calcium ions to bind with the glucuronic segments of alginate, forming a fast gelation of the hydrogel network. However, the rapid gelation induced by CaCl_2 can result in uneven crosslinking, leading to droplet-like hydrogels that lack structural integrity and fail to maintain the expected shape as the mould.

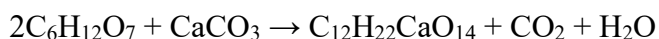
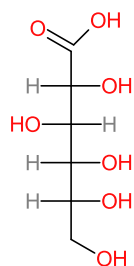
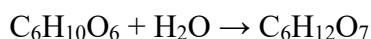
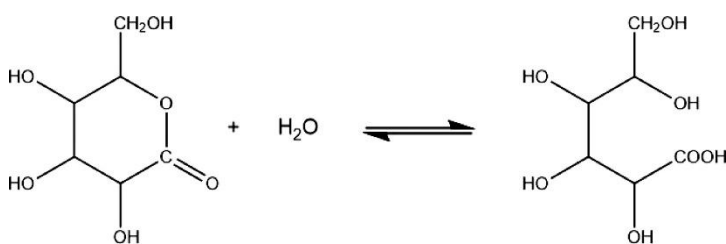
Unlike the conventional gelation method using CaCl_2 , the introduction of ‘internal ionotropic gelation’,[63] an advanced technique enabling cryogelation offers a novel approach to hydrogel preparation. The gelation procedure utilises the insoluble or chelated form of metal carbonate or hydrocarbon suspension mixed with aqueous sodium alginate for hydrogel preparation.

In this project, CaCO_3 powder was dispersed in sodium alginate and subsequently subjected to mild acidification through the release of H^+ from the slow hydrolysis of glucono- δ -lactone (GDL). The dissolution of CaCO_3 gradually released Ca^{2+} ions,

facilitating internal crosslinking of the alginate matrix. Crosslinking density, a key factor influencing pore size and mechanical compliance, subsequently impacts cell growth. The concentration of Ca^{2+} primarily determines the degree of crosslinking, with CaCO_3 acting as the divalent ion source. Meanwhile, the internally generated CO_2 gas contributes to the formation of macroporosity and the overall pore architecture within the hydrogel matrix.

Glucono- δ -lactone (GDL) (chemical formula $\text{C}_6\text{H}_{10}\text{O}_6$), due to its slow hydrolysis properties, GDL powder was used to hydrolyse in the aqueous phase of the sodium alginate solution, producing gluconic acid ($\text{C}_6\text{H}_{12}\text{O}_7$). The resulting gluconic acid solution dissolved the CaCO_3 powder suspension, eventually releasing calcium gluconate ($\text{C}_{12}\text{H}_{22}\text{CaO}_{14}$) as a calcium ion source along with carbon dioxide gas. The free Ca^{2+} ions subsequently interacted with the carboxyl groups of alginates, promoting further crosslinking and hydrogel formation.

The reaction between the proton donor (GDL) and CaCO_3 proceeds as follows:



A related study [64] demonstrated that using the insoluble metal salt CaCO_3 as an ionic crosslinker source, along with glucose δ -lactone (GDL) as the acid source, facilitates the formation of a homogeneous alginate network. **Figure 5-1** compares the slow-gelling alginate hydrogel produced via the CaCO_3 -GDL method with the conventional CaCl_2 fast

diffusion gelation. Another study [65] investigating alginate hydrogels generated using a similar CaCO_3 -GDL system confirmed their potential as a cell carrier for cartilage repair. Additionally, this method provides a significant advantage for porosity design, as the amount of CaCO_3 not only influences the crosslinking density and resulting mechanical stiffness but also affects the CO_2 released during gelation. The generation of CO_2 gas contributes to the formation and stabilisation of the internal porous architecture, a process known as carbon dioxide-induced gelation.

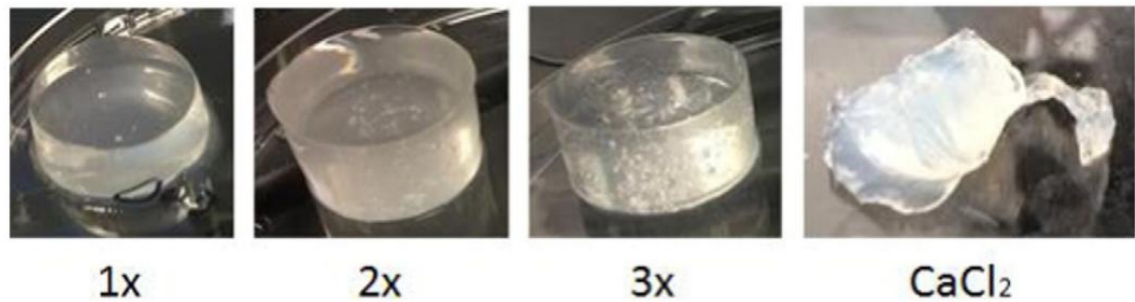


Figure 5-1 Comparison of slow-gelling alginate hydrogels (first three from the left) produced using the CaCO_3 -GDL method at different concentrations versus the instantaneously crosslinked macroblock formed by CaCl_2 -alginate (right). Image adapted from Ref.[64]

5.1.2 PVA hydrogels

Polyvinyl alcohol (PVA) is a synthetic macromolecular polymer widely employed in hydrogel fabrication due to its excellent biocompatibility, non-toxicity, and mechanical versatility.[66] PVA hydrogels form three-dimensional, water-retentive networks through either physical or chemical crosslinking processes. The chosen crosslinking method significantly affects the biological and mechanical properties of PVA hydrogels by modulating the interactions between PVA chains during synthesis.[66]

Among various fabrication techniques, the freeze-thaw method is a widely adopted physical approach due to its simplicity, efficiency, and the avoidance of chemical crosslinking agents that could introduce cytotoxicity.[67] The freeze-thaw process involves repeated cycles of freezing and thawing a PVA solution, inducing the formation of crystalline domains in the polymer matrix. These crystalline regions serve as physical crosslinks, stabilising the hydrogel structure.[66] During freezing, water molecules separate from the polymer chains and form ice crystals, concentrating the PVA chains in the unfrozen phase. Upon thawing, the PVA chains rearrange and establish stable

hydrogen bonds, leading to hydrogel crosslinking.[68] The number of freeze-thaw cycles, along with freezing temperature and PVA concentration, significantly influences the mechanical properties, pore size, and water retention capacity of the hydrogel.

Numerous studies have reported significant improvements in the mechanical properties of physically crosslinked PVA hydrogels, making them promising candidates for cartilage repair applications.[69] Whereas, layered scaffold designs based on PVA materials for osteochondral tissue engineering have demonstrated strong interfacial bonding and integration between bone and cartilage compartments, achieved by a simple layering mould-casting technique.[70] Overall, PVA hydrogels fabricated via freeze-thaw cycling exhibit remarkable mechanical strength, elasticity, and viscoelastic behaviour, closely resembling the properties of articular cartilage and meniscus. These attributes make them highly attractive biomaterials for tissue engineering applications.[68] Furthermore, their non-toxic and chemically inert nature enhances their suitability for various biomedical applications, including tissue engineering, drug delivery, and wound healing. The tunable properties of PVA hydrogels allow for customisation based on specific application requirements, such as optimising stiffness and elasticity by adjusting the number of freeze-thaw cycles.

5.2 Materials and Hydrogel Samples Preparation

5.2.1 Materials

Alginate crosslinked via the CaCO_3 -GDL crosslinking method:

- Sodium alginate powders ($\text{C}_6\text{H}_9\text{NaO}_7$, *Sigma-Aldrich*, CAS-No.: 9005-38-3)
- Calcium carbonate powder (CaCO_3 , *Sigma-Aldrich*, CAS-No.: 471-34-1)
- Gluconolactone/glucono- δ -lactone ($\text{C}_6\text{H}_{10}\text{O}_6$, *Sigma-Aldrich*, CAS-No.: 90-80-2)

PVA freeze-thaw:

- Poly (vinyl alcohol) powder ($[\text{CH}_2\text{CH}(\text{OH})]_n$, *Sigma-Aldrich*, CAS-No.: 9002-89-5)

5.2.2 Alginate-based hydrogel preparations and pre-test

Sodium alginate (SA) hydrogels are crosslinked through an internal ionotropic gelation process utilising calcium carbonate (CaCO_3) and glucono- δ -lactone (GDL) system as crosslinking agents. This approach benefits from the slow hydrolysis of GDL, which gradually acidifies the system, facilitating controlled calcium ions (Ca^{2+}) release from CaCO_3 . The gradual gelation process ensures uniform hydrogel formation, yielding hydrogels with a fine shape and consistent cylindrical structure, as shown in **Figure 5-2**.

During gelation, internally generated carbon dioxide (CO_2) gases create spaces or pores within the hydrogel. This novel and controllable process provides a biomimetic microarchitecture that resembles natural tissue layers. The extent of CO_2 release and subsequent pore formation can be controlled by the amount and ratio of CaCO_3 relative to GDL added into the gelation system, ensuring the complete reaction and uniform distribution of pores within the hydrogel body. These characteristics make alginate hydrogels suitable for applications requiring tunable porosity and tissue-mimicking properties.

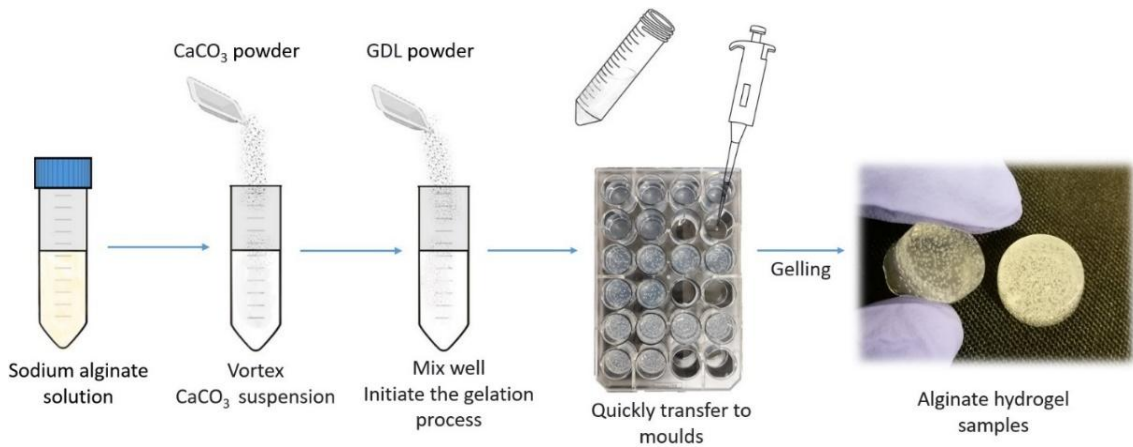


Figure 5-2 Flowchart illustrating the preparation process of alginate hydrogel via CaCO_3 -GDL internal ionotropic gelation.

Through pre-testing, it was concluded that a sodium alginate to CaCO_3 mass ratio of 4:1 (SA: CaCO_3 = 4:1) is optimal for forming a hydrogel with a fit and well-defined shape. Based on the molar mass calculation ' $2\text{C}_6\text{H}_{12}\text{O}_7 + \text{CaCO}_3 \rightarrow \text{C}_{12}\text{H}_{22}\text{CaO}_{14} + \text{CO}_2 + \text{H}_2\text{O}$ ', the molar ratio of GDL is supposed to be double that of CaCO_3 .

The concentration groups for the three components, based on this ratio, are presented in **Table 5-1**. In the ratio calculation, the molar weights of sodium alginate ($C_6H_9NaO_7$), calcium carbonate ($CaCO_3$), and GDL ($C_6H_{10}O_6$) are 216.12 g/mol, 100.089 g/mol, and 178.14 g/mol, respectively. To maintain a neutral pH in the hydrogel environment, the molar ratio of GDL to $CaCO_3$ was consistently maintained at 2:1. This ratio ensured that the produced gluconic acid just completely dissolved the $CaCO_3$ powder, resulting in a transparent, gelled hydrogel. Hence, the overall molar ratio is SA: $CaCO_3$: GDL = 4: 1: ~3.6

As presented in **Figure 5-3**, three alginate hydrogel concentration groups were fabricated for comparison, marked as 1% w/v, 2% w/v, and 3% w/v. Scanning electron microscopy (SEM) imaging demonstrated that the 3% w/v formulation (incorporating the highest concentration of $CaCO_3$) of alginate hydrogel exhibited the most uniform microstructure, characterised by a dense distribution of fine gas pores formed during gelation. Qualitative observations under hydrated conditions further confirmed the presence of these pores, which are attributed to in situ CO_2 generation via the acid-induced decomposition of $CaCO_3$ by glucono- δ -lactone (GDL) within the hydrogel network. The resulting CO_2 -induced microporosity facilitated enhanced interfacial interactions with the surrounding medium through the formation of interconnected void spaces, ultimately contributing to the superior mechanical stiffness observed in this formulation compared to lower-concentration hydrogels.

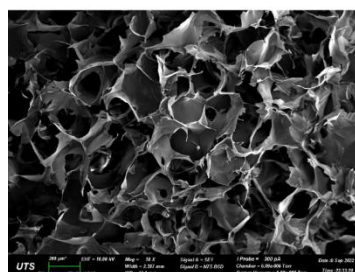
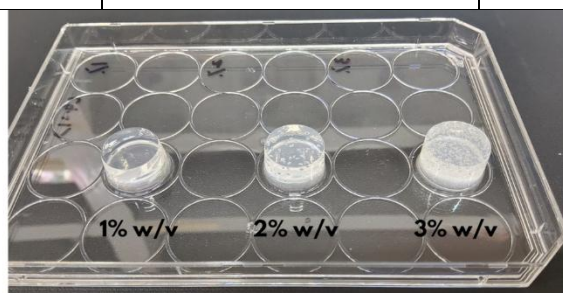
Preliminary experimental observations indicated that pore formation in alginate hydrogels was primarily governed by two interrelated factors. First, the acid-base reaction between $CaCO_3$ and glucono- δ -lactone (GDL) played a fundamental role in bubble generation. The gradual hydrolysis of GDL generated protons that reacted with $CaCO_3$ to produce CO_2 gas in situ, creating a dispersed gaseous phase within the polymer matrix. This reaction kinetics was particularly significant as the slow acid release from GDL hydrolysis allowed for controlled and uniform bubble formation throughout the gelation process.

Second, alginate concentration significantly influenced the final pore morphology. Higher polymer concentrations (3% w/v alginate) formed a denser cross-linked network, physically restricting bubble growth and coalescence. The increased viscosity and

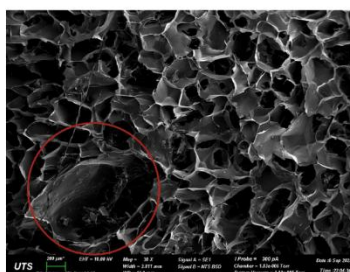
reduced pore size of concentrated alginate solutions limit CO₂ diffusion, resulting in smaller pore volumes but a greater number of pores. This microstructural modification directly contributed to the enhanced stiffness observed in these formulations, as the uniformly distributed pores acted as stress concentrators while the dense polymer network maintained structural integrity.

Table 5-1 Mass concentrations of the three components (sodium alginate, calcium carbonate, and glucono- δ -lactone) used in the fabrication of alginate hydrogels.

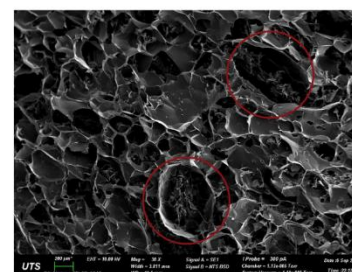
Sodium Alginate	CaCO ₃ powder	GDL
1% w/v	0.25% w/v	0.90% w/v
2% w/v	0.50% w/v	1.80% w/v
3% w/v	0.75% w/v	2.70% w/v



1% w/v group



2% w/v group



3% w/v group

Figure 5-3 SEM imaging of pure alginate hydrogel samples fabricated via CaCO₃-GDL ionotropic gelation. Cross-sectional morphology of three concentration groups, highlighting CO₂-induced porous features (red circles).

Despite these advantageous properties, pure alginate hydrogels are unsuitable for direct application at weight-bearing sites due to their low mechanical stretchability, thus easy to collapse under compressive load. The freeze-thawing technique is an alternative promising approach to modify the internal structure of alginate hydrogels post-gelation. During freezing, ice crystal formation introduces micropores into the hydrogel matrix. Upon thawing, these micropores promote interconnectivity, resulting in a more porous

and stretchable hydrogel structure, better suited for applications requiring flexibility and interconnective integration.

As illustrated in **Figure 5-4** the comparison between the original pure alginate hydrogel and the freeze-thawed samples highlights significant differences in mechanical properties and structural behaviour. The original hydrogel, characterised by a jelly-like body with high stiffness, eventually fractured under compressive force loading. In contrast, the freeze-thawed hydrogel samples exhibited a stretchable, spongy-like structure due to their interconnected polymer network, which retained water within the voids. The stress-strain curve for the two types of hydrogels displays a significant difference. The curve for the original hydrogel exhibited a sharp decline at its endpoint, corresponding to its fracture under compression. Whereas the freeze-thawed sample showed a consistent and gradually increasing trend, indicating its ability to withstand compressive forces without structural destruction.

Briefly, the compressive modulus of the original hydrogel was nearly 10 times higher than that of the freeze-thawed samples; this modification significantly reduced mechanical stiffness, rendering the freeze-thawed hydrogels unsuitable for standalone applications at weight-bearing sites. Therefore, even if alginate is a natural and biocompatible material with a crosslinking process, it alone is insufficient for fabricating scaffolds capable of withstanding weight loads in chondral tissue engineering. To address this, further development of double-network crosslinked composites incorporating other materials, such as synthetic polymers with superior mechanical strength, is necessary for designing scaffolds with enhanced functionality and durability.

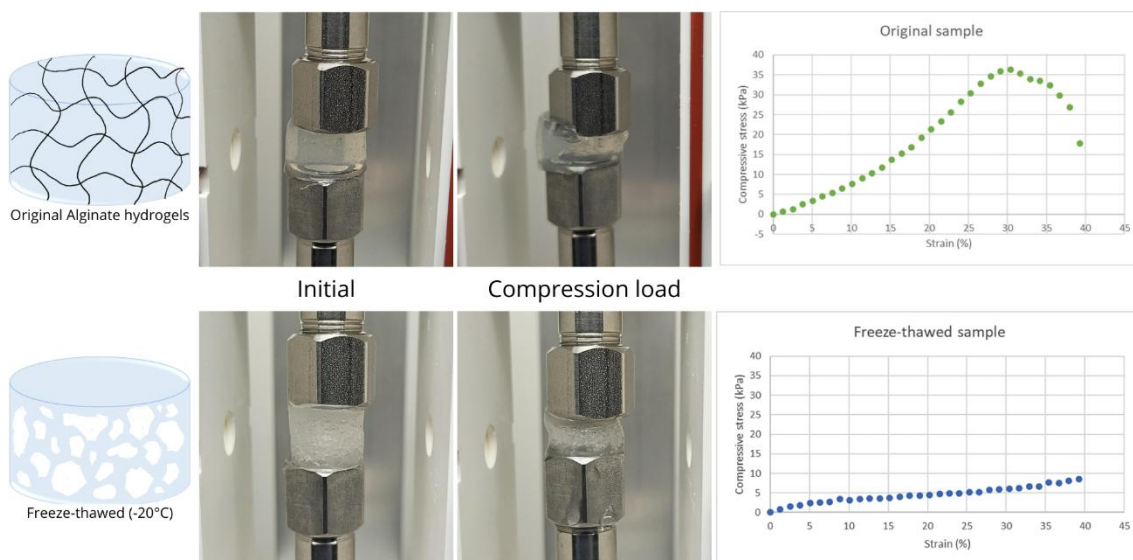


Figure 5-4 The photos and graphs illustrate the differences between the original pure alginate hydrogel and the freeze-thawed alginate hydrogel, with the same concentration and composition. Significant differences in stiffness and stretchability are revealed.

5.2.3 PVA hydrogel preparation and concentration range determination

Polyvinyl alcohol (PVA) was evaluated for hydrogel preparation, with pre-test results shown in **Figure 5-5** showing the status of fabricated PVA hydrogels with different thicknesses. For the experimental procedure, PVA powder was dissolved in Milli-Q water at 90–100°C to obtain a clear aqueous PVA solution, indicating the fully dissolved state of the material. The solution was then transferred to moulds (e.g., a 24-well plate) to produce the designed thickness of the hydrogel.

The freeze-thaw physical crosslinking method was employed for hydrogel fabrication. After being transferred to the moulds, the PVA solution was placed in a freezer at -20°C or -80°C. The influence of freezing temperature on hydrogel properties was initially assessed through qualitative manual compression tests (finger press). As detailed in **Appendix B3**, comparative analysis revealed stiffness and structural variations attributable to freezing temperature differentials. The -80°C freezing condition demonstrated superior hydrogel stability and interconnectivity, as evidenced by preliminary compression testing, and was therefore selected for subsequent experimental phases. Additionally, increasing the number of freeze-thaw cycles in PVA hydrogels promoted hydrogen bond formation, resulting in enhanced structural stability and rigidity, along with reduced swelling ratios.[31; 71]

The overall pre-test findings suggested that a PVA concentration of approximately 15% w/v was optimal for pure PVA hydrogel preparation. Hydrogels fabricated via the freeze-thaw method demonstrated unique stretchable and elastic properties characteristic of PVA material, making them suitable for mimicking the superficial zone of articular cartilage. Additionally, PVA is compatible with forming double-network crosslinking composite hydrogels, such as PVA-alginate based composite materials..[72; 73] This combination leverages the biocompatibility of alginate and the stretchability of PVA, creating advanced materials for diverse biomedical applications.



Figure 5-5 Pure PVA hydrogel in a thin layer (left) and a mould-casting thick hydrogel (right).

5.2.4 PVA-sericin hydrogel fabrication

PVA-sericin hydrogels were fabricated using the freeze-thaw method and tested for toxicity via a preliminary MTT assay. The determined concentration formulation was planned to be used in the superficial layer of a zonal hydrogel to function as the surface of articular cartilage, providing primary shock absorption.

Following Chapter 4, Section 4.5, the extraction and collection of silk sericin solution and freeze-dried sericin powder from degummed silk cocoons were utilised as additives in the PVA-based hydrogel, synthesised via the freeze-thaw physical crosslinking method at freezing temperatures of -20°C and -80°C . The procedures and differences in hydrogels produced at these freezing temperatures are demonstrated in **Figure 5-6**.

Building on the fabrication of pure PVA hydrogels, the sericin addition involved pre-filtration of the sericin solution obtained from the degumming process using a 0.2 μm syringe filter to remove visible debris, resulting in a clear, pale-yellow solution. After 6 or 8 cycles of liquid autoclaving, the sterilised sericin solution was frozen and then subjected to a freeze-drying process to collect sericin powder. Contamination control was essential throughout the procedure. Following the outlined PVA hydrogel fabrication method, the freeze-dried sericin powder was added to the PVA solution after the complete dissolution of PVA powder in Milli-Q water, with the heating temperature maintained at 90-100 °C. The mixture was then thoroughly combined and transferred to a well plate for further processing.

Notably, freezing temperature significantly affected the pore structure and mechanical stiffness of the hydrogels. As documented in **Appendix B3**, poly(vinyl alcohol) (PVA) hydrogels prepared via freeze-thaw crosslinking demonstrated temperature-dependent stiffness variations attributable to differential ice crystal formation kinetics and subsequent polymer chain entanglements. Preliminary characterisation, including visual analysis (**Figure 5-6**), revealed distinct morphological differences between samples processed at -20°C and -80°C. The -80°C frozen hydrogels exhibited a sponge-like macroporous structure, while -20°C samples displayed smoother surfaces and reduced mechanical integrity, suggesting inferior crosslinking density, posing a risk of collapse during manual compression. Comparative visual analysis indicated that the hydrogel prepared via the -80°C freezing process achieved enhanced structural stability through an interconnected pore network and increased surface roughness. These characteristics render the -80°C-treated hydrogel more suitable for load-bearing applications in this study and subsequent multi-layer scaffold preparation. These observations align with established literature, confirming that increasing freeze-thaw cycles enhance mechanical properties and elasticity[48], and freezing at -80°C in a low-temperature freezer produces hydrogels with consistent structural integrity[49]. However, this study found that freezing PVA hydrogels in liquid nitrogen to -196°C produces brittle PVA hydrogels with significantly reduced transparency.[49] Collectively, the experimental observations and representative studies indicate that the number of freeze-thaw cycles, freezing temperature, and freezing method have a critical impact on material performance, warranting further systematic investigation to optimise fabrication protocols.

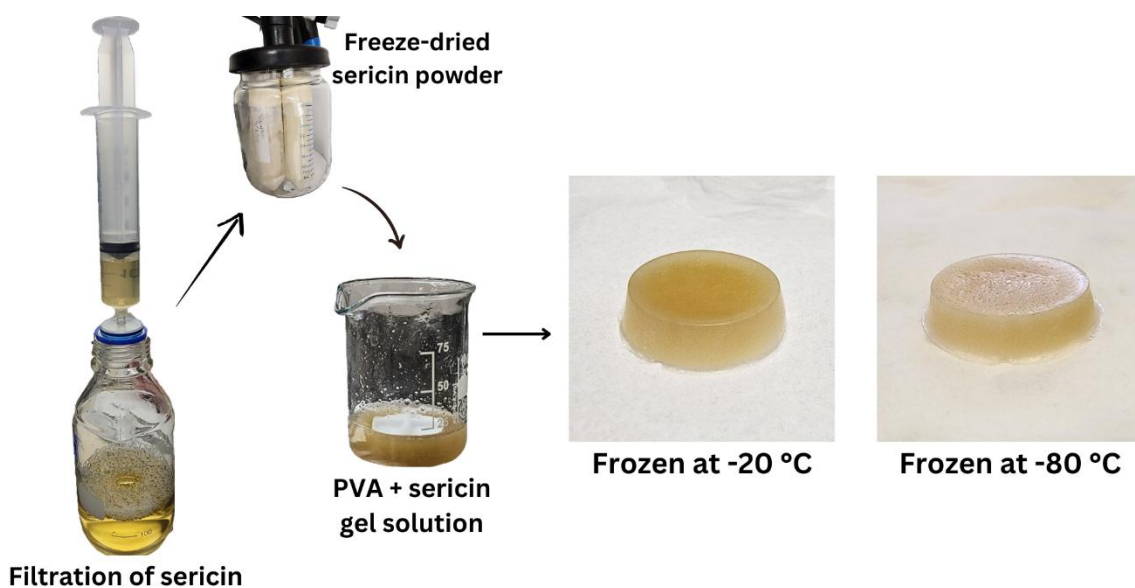


Figure 5-6 Flowchart illustrating the preparation process of PVA-sericin hydrogel synthesized using the freeze-thaw physical crosslinking method, along with photographs comparing freeze-thawed samples frozen at different temperatures.

Compared to previous studies, PVA-sericin hydrogels have been widely used in burn wound dressings, demonstrating antimicrobial activity and promoting accelerated burn wound healing while preventing scarring.[32; 33; 46; 74] While numerous studies have explored sericin-PVA hydrogels for wound dressing and antibacterial applications, their use in cartilage tissue engineering remains an experimental gap. A recent study [75] developed ciprofloxacin-loaded sericin/PVA hydrogels aimed at promoting bone cell proliferation and ultimately treating osteomyelitis. Together with this, the porous microstructure of the sericin hydrogel is expected to offer space for cells to proliferate and survive, as well as a microenvironment for the retention and release of bioactive molecules.[76]

Hence, this experiment aims to develop a PVA-sericin hydrogel as a partial chondral construct, utilising the antibacterial properties of sericin along with the tunable concentration of PVA and its excellent tensile strength to provide shock absorption at the cartilage site. The outcome of the PVA-sericin hydrogel is expected to not only exhibit antibacterial properties but also support and enhance cell growth in cartilage tissue engineering.

5.3 Step-by-Step Standardisation of Sequential Layering Procedures

5.3.1 Time intervals test sequential layering: Biphasic alginate-based hydrogel

To understand and establish a functional sequential layering protocol for composite scaffold fabrication, systematic time interval optimisation was performed as the foundational step. This project employed a double-network system comprising poly(vinyl alcohol) (PVA) and alginate components, where the gelation sequence follows two distinct mechanisms: first, internal ionotropic crosslinking of the alginate part via Ca^{2+} release from controlled CaCO_3 hydrolysis, followed by physical crosslinking of PVA through freeze-thaw cycles. The success of this layered architecture lies in determining the temporal intervals that can achieve complete stabilisation of the alginate matrix while maintaining interfacial bonding capability.

The use of pure alginate hydrogels in preliminary testing was intended to evaluate optimal time intervals for layer-by-layer mould casting. Since alginate gelation is the initial crosslinking step in the Alginate-PVA double network system, understanding the gelation behavior of pure alginate provides critical insights into timing and layer formation. This approach allowed optimization of the time window—found to be approximately 30 to 60 minutes—for achieving well-defined, stable layered structures. Although pure alginate hydrogels are known to fracture under compression, their study here was not for mechanical performance but to inform processing parameters critical for subsequent fabrication of composite hydrogels with enhanced mechanical properties.

As demonstrated in the preliminary test (**Figure 5-7**), the fabricated bilayered alginate hydrogels exhibited clearly defined two-layer architectures formed through internal ionotropic gelation via the CaCO_3 -GDL system. The porous microstructure within the hydrogel layer resulted from CO_2 bubble formation during the gelation process, where glucono- δ -lactone (GDL) underwent gradual hydrolysis to produce gluconic acid. This acidic environment subsequently reacted with CaCO_3 , generating CO_2 microbubbles that became entrapped within the crosslinked alginate matrix. These bubbles enhanced cell adhesion and ingrowth and could be tailored by adjusting the induced/suspended CaCO_3 amount. Alternatively, bubble formation could be minimised or reduced in size by placing the hydrogel sample in a 4°C refrigerator for approximately 24 h.

In addition, characterising hydrogel pore size and porosity was identified as a key objective for future research. Preliminary observations indicated that reduced CaCO_3 content yielded smaller and fewer internally induced pores, producing structures more closely resembling natural cartilage. The quantity and concentration of generated CO_2 could be precisely controlled to create interconnected pore networks that facilitate cell migration and scaffold integration. During internal gelation, CaCO_3 dissolution enabled porous structure development. Future studies should systematically investigate optimal CaCO_3 concentrations for generating irregular pore morphologies and designing interconnected architectures that maximise tissue integration potential.

Based on the alginate hydrogel fabrication method, simple bilayered hydrogels were prepared by incorporating ~5% w/v hydroxyapatite (HAp) into the bottom layer to mimic the mineralised deep zone or calcified cartilage layer. The results indicated that a 15-30 min time interval (which might vary due to different concentrations) for alginate hydrogel gelation and crosslinking could be applicable for making the double-layered scaffold.

Building on the simple biphasic architecture developed at this stage, the next experimental design focused on composite double-network crosslinking and gradient composition formation. This approach involved manipulating time intervals to adjust the proportions and concentrations of hydrogel materials, along with varying the fraction of added bioceramics. These modifications aimed to enhance the integration of the gradient transition between cartilage zonal layers, providing a more biomimetic and effective scaffold design.



Figure 5-7 Alginate-based bilayered scaffold. The pure alginate hydrogel forms the cartilage layer, while the bottom mineralised layer was prepared using hydrogel material mixed with hydroxyapatite (HAp) (left) or bioactive glass (right).

5.3.2 Alginate-PVA composite double-network crosslinking hydrogels

Building upon prior findings, alginate was chosen as a base material due to its intrinsic biocompatibility and easily controlled crosslinking process in the presence of Ca^{2+} ions. To enhance its mechanical properties, polyvinyl alcohol (PVA) was incorporated to form a composite hydrogel with a double-network crosslinking structure. Conventional pure PVA hydrogels typically utilise concentrations ranging from 10-15% w/v to achieve well-shaped and stable structures that remain intact under compression, as demonstrated in Chapter 4 preliminary tests. However, for this composite system, reduced PVA concentrations (5% and 10% w/v) were selected for combination with alginate, creating a synergistic material that integrates the elastic properties of PVA with the tunable porous structure generated through alginate CO_2 -induced crosslinking. This approach maintains the advantageous characteristics of each component while enabling layered structure fabrication. The concentration gradient across layers was strategically designed to create gradual transitions, with PVA content decreasing systematically (10% w/v and 5% w/v were selected) while alginate concentration increased correspondingly (1% w/v and 2% w/v were selected).

For the fabrication process, firstly, PVA powder was dissolved in Milli-Q water at the desired concentration (5% or 10% w/v). The solution was heated to 90-100° and stirred continuously with a magnetic stirrer until the PVA was completely dissolved.

Sodium alginate and CaCO_3 powders were weighed to prepare 1% w/v and 2% w/v alginate solutions. For example, 0.1 g of sodium alginate powder was dissolved in 10 mL of the prepared PVA solution to create a 1% w/v alginate concentration. The alginate solutions were then mixed with PVA solutions to form composite solutions (e.g., 5% w/v or 10% PVA w/v composited with 1% w/v or 2% w/v alginate) for testing.

The concentration groups for the Alginate-PVA composite hydrogels are presented in **Table 5-2**:

Table 5-2 Concentration designs of Alginate/PVA composite scaffold test.

PVA (% w/v)	Alginate (% w/v)
5	1
5	2
10	1
10	2

In order to form the chemical crosslinking of the alginate material part, the PVA-alginate- CaCO_3 mixture was stirred at high speed to ensure even CaCO_3 distribution. A 24-well plate was prepared as the mould for hydrogel casting. Once ready, GDL powder was added in the required ratio, and the mixture was stirred vigorously (higher speed, approximately 5 seconds) to dissolve the GDL, reaching a ‘just-dissolved-and-beginning-to-crosslink’ state.

The PVA-alginate- CaCO_3 -GDL mixture was quickly transferred into each well, ensuring consistent volume and thickness. The mould was placed on a flat surface (e.g., bench) and left overnight (>8 hours) at room temperature to allow GDL hydrolysis into gluconic acid. This acid then reacted with the insoluble CaCO_3 , releasing Ca^{2+} ions to form a crosslinked alginate network.

Following the chemical crosslinking of alginate, the hydrogels underwent freeze-thaw cycles to physically crosslink the PVA part. Three cycles were performed to stabilise the dual-network structure of the alginate-PVA hydrogel.

The fabricated hydrogels with varying composition ratios are shown in **Figure 5-8**. The composite hydrogels combining PVA and alginate exhibited significantly enhanced

stiffness and stretchability due to their double-network crosslinking, outperforming single-network PVA hydrogels and pure alginate hydrogels in mechanical performance.

Based on qualitative visual assessment and manual compression testing (finger press), the '5% PVA-2% alginate' and '10% PVA-1% alginate' hydrogels maintained their intended cylindrical morphology with uniform diameter and minimal deformation, exhibiting optimal structural integrity within these four groups.

In comparison, '5% PVA-1% Alginate' formulation was excessively soft, making it unsuitable for weight-bearing applications. The hydrogel exhibited significant gravitational deformation (wider base than top) and collapsed under manual compression, displaying a jelly-like consistency. In contrast, '10% PVA-2% Alginate' group was overly rigid, leading to reduced flexibility and compromised functional performance. Given these observations, the intermediate formulations ('5% PVA-2% alginate' and '10% PVA-1% alginate') were selected for further experimentation due to their balanced mechanical properties.

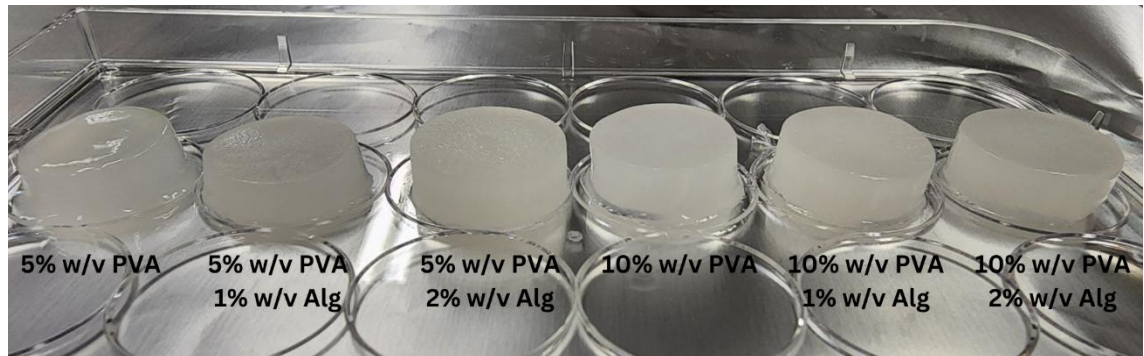


Figure 5-8 Alginate-PVA double-network crosslinking hydrogel fabricated with three freeze-thawing cycles.

5.3.3 Composite Alginate-PVA bi-layered scaffold

Building upon previous works with double-network crosslinking and sequential layering, the composite alginate-PVA bi-layered scaffold was developed with distinct layers for functional zones resembling natural architecture. The bottom layer, composed of a crosslinked alginate hydrogel, was allowed to undergo partial gelation for approximately 15 minutes, achieving a semi-gel state. Following this, the top layer, made of pure PVA,

was added to finalise the structure. The entire scaffold was then frozen at either -20°C or -80°C to facilitate PVA crosslinking and enhance mechanical stability.

As shown in **Figure 5-9**, the bilayered PVA-based hydrogel revealed a smooth gradient transition between the soft upper hydrogel layer and the mechanically reinforced bottom layer, which was enhanced with hydroxyapatite (HAp) for improved strength.

- Top layer: PVA hydrogel with an additional of 2% sericin
- Bottom layer: PVA-alginate composite with additional hydroxyapatite (HAp)

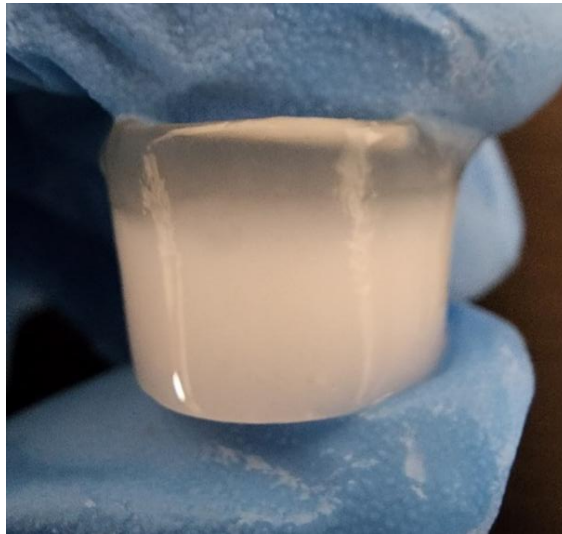


Figure 5-9 Combined scaffold showing the pure PVA hydrogel layer at the top (simulating cartilage) and the PVA-alginate-HAp double-network crosslinking hydrogel at the bottom (simulating subchondral bone).

5.3.4 Tri-layered hydrogel mimicking zonal articular cartilage

After several tests to optimise material concentration, interaction, and integration between adjacent layers, a tri-layered hydrogel scaffold was fabricated to mimic zonal articular cartilage, reflecting the superficial, middle, and deep zones. The ideal design incorporated a gradient concentration profile, where the alginate content increased from the superficial layer to the deep layer, creating gradually finer and more uniform porous layers. Conversely, the PVA concentration decreased from the superficial to the deep zones, as the superficial layer used PVA as the primary hydrogel material. This composition reflects the mechanical requirements of the superficial zone, which must remain highly elastic and functional for force distribution as the contact surface layer in chondral or osteochondral systems during knee movement.

Figure 5-10, shows the fabricated tri-layered chondral hydrogel scaffold photos. The scaffold exhibited strong interlayer integrity with smooth transitions and no abrupt changes in outline. The three layers were distinctly separate but well-integrated, as seen in the images of the wet-state scaffold. Under manual compression (finger pressing on the entire scaffold), the middle layer swelled slightly but remained structurally intact without deformation, even after repeated compression. Additionally, the dry-state scaffold confirmed that the layers did not separate, further demonstrating the integration and stability of the construct.

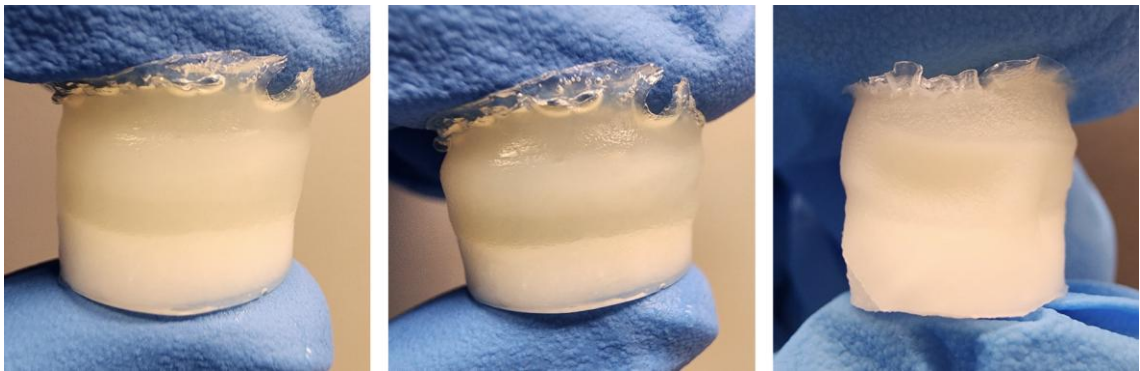


Figure 5-10 Tri-layered hydrogel examples and composition confirmation. From left to right: a freshly fabricated tri-layered scaffold, the scaffold under compressive force, and the scaffold in a swollen state after the swelling test.

Based on preliminary testing, the formulation and layer design of the tri-layered scaffold were finalised, and fabrication procedures were established. As illustrated in **Figure 5-11**, the scaffold layers and their compositions were optimised to closely mimic native articular cartilage in terms of thickness and zonal ratios.

Following confirmation of material compositions, degummed silk fibroin fibres (Chapter 4) were selected for the superficial zone. Prior to use, these silk fibroin fibres underwent sterilisation (autoclaving and UV exposure) to ensure biocompatibility and prevent hydrogel contamination. The horizontally aligned collagen fibres in the superficial zone of native cartilage were replicated using silk fibres, which not only reinforced the hydrogel but also provided directional guidance for cell attachment. The rationale for silk fibre incorporation included their biocompatibility, elastic strength, and structural alignment, which enhanced the mechanical stability of this thin hydrogel layer.

5.3.4.1 Hydrogel preparations and fabrication procedures

Prepare degummed silk fibroin fibres and sterilised sericin powder (autoclaved and UV light sterilised). Material extraction details are provided in Chapter 4.

PVA powder and alginate powder were dissolved in Milli-Q water in designated concentration sets and ratios to create the composite and pure materials hydrogels, as detailed procedures in the section 5.3.2.

5.3.4.2 Sequential layering for tri-layered zonal architecture

For the sequential layering of hydrogel layers, the layer-by-layer mould-casting process began with the bottom deep layer, followed by the middle and superficial layers. A 20-30 min interval was maintained between each layer to allow for partial crosslinking, ensuring architectural stability and consistent thickness. The thickness of each layer was designed to reflect the proportions of natural articular cartilage zones, approximately in the ratio of 10%: 60%: 30% for the superficial, middle, and deep layers, respectively.

- Deep layer: Approximately 300 μ L of the ‘5% PVA + 2% Alg + 5% HAp’ solution was transferred into a 24-well plate, ensuring the solution fully covered the mould bottom. The hydrogel layer was left with the lid cover on the plate to stand, allowing the alginate component to crosslink.
- Middle layer: After 20–30 min, the deep layer gel solution exhibited a film-like surface. Then, 600 μ L of the ‘10% PVA + 1% Alg’ solution was carefully poured on the deep layer. Light shaking ensured that the middle layer made full contact and was spread evenly over the deep layer.
- Incorporating silk fibroin fibres: Silk fibroin fibres were aligned using ethanol to maintain sterility on a flat plate, and a large piece of aligned directional silk fibre sheet was obtained. The fibre sheet was then cut into small squares matching the mould size, keeping the alignment intact. When the middle layer gelation was achieved, a cut silk fibre sheet was gently placed on its surface using tweezers, ensuring it adhered closely without disrupting the gel layer.
- Superficial layer: Finally, 100-200 μ L of the ‘15% PVA + 2% Sericin’ solution was gently transferred over the middle layer to fully cover the silk fibre sheet, maintaining fibre alignment while incorporating this sheet to form a thin layer of superficial zone.

5.3.4.3 Freeze-thaw stabilisation and layer integration

To stabilise the stratified structure, the assembled scaffold was frozen at -20°C (or -80°C for faster processing). Post-thawing at room temperature, PVA gelation occurred.

Optionally, in case of the difference in time interval might result in weak integration, after freezing and then thawing at room temperature, the PVA became a gel-like layer. To enhance the integration between layers, microwave heating could be applied (a pre-test is required to ensure safe use and time control). In this experiment, 5 seconds of microwaves was appropriate to melt the PVA part across the entire tri-layered scaffold, the partially melted PVA became liquidised, and due to the gravity, the PVA liquid was gradually deposited, then frozen at -80°C freezer ensured placed on a flat surface, the freeze-thawed sample could form a smooth transition between layer and would not result in mechanical delamination under compressive force loading. Repeated three times of freeze-thaw cycles to stabilise the entire joined tri-layered scaffold.

5.3.4.4 Discussion and possibility in this project

The fabricated tri-layered scaffold, as shown in **Figure 5-11** (right), demonstrates the implementation of the final optimised design parameters. The scaffold features aligned silk fibres incorporated into a thin superficial layer, with the overall layer thickness adjusted to approximately 20% superficial, 50% middle, and 30% deep zones to better accommodate practical fabrication constraints while maintaining the essential functional gradient resembling native cartilage tissue.

The material composition was designed to replicate the biomechanical properties of articular cartilage. In the superficial layer, the combination of 15% w/v PVA with 2% w/v sericin provides the necessary elasticity to withstand shear forces during joint movement. The addition of aligned silk fibres serves a dual purpose, reinforcing the thin hydrogel structure and mimicking the oriented collagen network of native superficial cartilage, which is crucial for both mechanical strength and cellular guidance. The middle layer, composed of 10% w/v PVA and 1% w/v alginate, creates a transitional zone that balances flexibility with compressive resilience, similar to the proteoglycan-rich middle region of natural cartilage. The deep layer incorporates 5% w/v PVA, 2% w/v alginate, and 5% w/v hydroxyapatite (HAp) to achieve greater stiffness, reflecting the mechanical requirements

of the deep zone and calcified cartilage zone while potentially enhancing integration with subchondral bone.

This graduated material design effectively addresses the functional demands of cartilage during movement. The high elasticity of the superficial layer ensures durability under repetitive loading, while the progressively stiffer middle and deep layers provide the necessary support and load distribution. The inclusion of HAp in the deep layer not only increases mechanical stability but may also promote osteochondral integration, which could be particularly beneficial for potential clinical applications where scaffold-bone interaction is critical.

The fabrication of this tri-layered structure demonstrates the feasibility of creating complex, biomimetic tissue engineering scaffolds using relatively simple materials and techniques. The combination of natural (silk fibres, alginate) and synthetic (PVA) polymers, along with ceramic components (HAp), offers a balanced approach to achieving both biological compatibility and mechanical functionality. This design strategy could serve as a foundation for developing more advanced cartilage repair solutions, with the potential for further optimisation through cell seeding and mechanical conditioning in future studies.

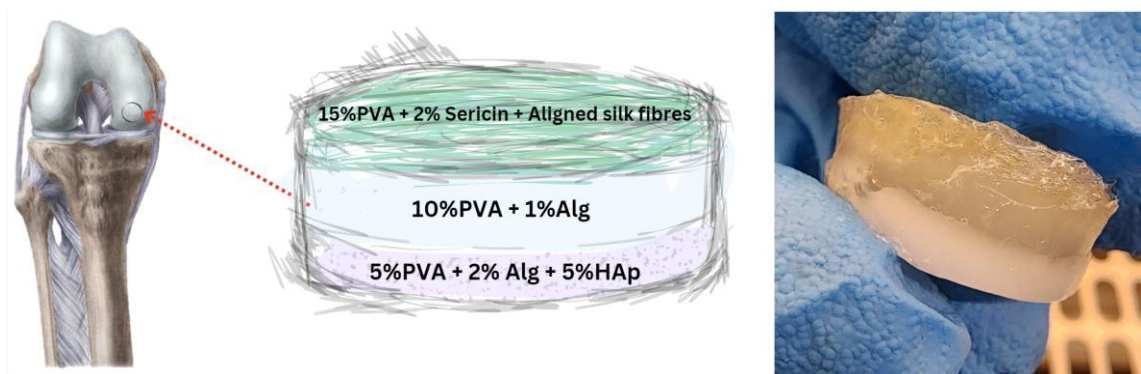


Figure 5-11 Final design of the tri-layered chondral scaffold, including compositions and materials used for each layer.

5.4 Summary

In summary, by utilising Ca^{2+} -induced internal ionotropic gelation of alginate and physically crosslinked PVA hydrogel, the double-network alginate-PVA hydrogel serves as the foundation for the tri-layered chondral scaffold. And PVA-sericin was employed

as a coating material for direct silk fibre incorporation, forming the superficial layer of articular cartilage, which plays a crucial role in force distribution at weight-bearing sites.

Regarding the parameters of hydrogel fabrication methods, the ratio and concentration of chemical crosslinkers significantly influence the primary pore architecture and porosity of the construct, while the subsequent freeze-thaw process affects its mechanical tensile behaviour.[73] Detailed examination and definitions merit further study and investigation.

What's more, PVA hydrogel can be combined with other materials to enhance its functionality. For example, incorporating chitosan can generate an antiseptic and swelling-resistant porous structure.[77; 78] Additionally, the integration of microspheres can create macroporous structures, promoting cell adhesion and proliferation guidance.[79] Another innovative application involves incorporating carbon dots to enhance visualisation in biomedical engineering.[71]

Chapter 6 Physical Characterisations

Comprehensive physical characterisation of hydrogels is essential for understanding the correlation between their architecture and functional properties, which directly influence their performance in tissue engineering applications.

6.1 Overview

The physical properties of hydrogels encompass key parameters such as morphology, porosity, swelling behaviour, degradation rate, mechanical properties and mechanical integration of the zonal scaffold. These properties play a vital role in determining the functionality of hydrogels in tissue engineering, particularly for chondral and osteochondral repair. Among these tests, assessing the tri-layered chondral scaffold is crucial for optimising its performance under load-bearing conditions. This Chapter presents a comprehensive analysis of the morphological characteristics, water absorption capacity, degradation behaviour, and mechanical properties, providing key insights for scaffold design and application.

6.2 Hydrogel Characterisation Procedures

In the characterisation and biological assessment of the multizonal hydrogel scaffold in this project, the samples were prepared to evaluate the properties of each layer for a more specific understanding. Physical characterisation tests, such as an overview of the tri-layered cross-section and overall compression loading, were conducted and presented to assess the properties and integration of the joined multizonal scaffold. For swelling and degradation tests, each hydrogel formulation corresponding to the superficial, middle, and deep layers was individually fabricated to ensure consistency between samples and to obtain accurate measurements.

Based on the preliminary tests and discussion in Chapter 5, to fulfil the gradient concentration of materials corresponding to the elasticity, along with the silk fibroin fibres incorporated to form a fibre sheet mimicking the aligned native collagen fibre

orientation in the superficial zone. The hydrogel confirmed formulations, and their corresponding designed positions are listed below in **Table 6-1**:

Table 6-1 Hydrogel concentration sets and the corresponding layers in the multizonal chondral scaffold design.

Formulations	Designed position
15% w/v PVA + 2% w/v sericin	Superficial layer (+ silk fibres)
10% w/v PVA + 1% w/v alginate	Middle layer
5% w/v PVA + 2% w/v alginate + 5% w/v HAp	Deep layer

6.2.1 Sample freeze drying & Morphology analysis

The fabricated hydrogel samples for individual layer and integrated tri-layered hydrogels were kept in moulds and frozen at -80°C for at least 12 hours before undergoing freeze-drying to ensure that the overall structure would not collapse during drying under a vacuum environment. Then the frozen samples were retained in well plates, with the entire well plate covered by a piece of aluminium foil pierced with several small holes created using a tweezer tip. These prepared well plates were then placed into a freeze-dryer for the main drying process.

The freeze-dryer conditions (as set in the lab) were set at -85°C and with 0.1 bar pressure. The main drying process was maintained for at least 24 hours, with 48 hours recommended for 24-well plate-sized samples according to the thickness and size of the hydrogel, until completely dried and exposed the status as interconnective porous scaffold samples.

The fully dried porous samples were then removed from the wells and sliced into approximately 1 mm thickness thin layer to expose the porous cross-section. Each sliced cross-section sample was mounted on SEM stubs using carbon tape and sputter-coated with a 5 nm iridium (Ir) layer to achieve electrical conductivity. Finally, the morphologies of the sample cross-sections were imaged and analysed under a 10 kV accelerating voltage.

6.2.2 Hydrogel swelling test and liquid uptake

A swelling test was performed to evaluate the liquid/water absorption capacity of the fabricated hydrogel samples, which is critical for nutrient diffusion and mechanical properties. The samples were fabricated using a 24-well plate mould to facilitate testing and observation of sample properties. In this experiment, each prepared sample had 4 replicates ($n = 4$), with one sample placed in each well, as presented in **Figure 6-1**, enabling more precise tracking of weight changes for individual samples.

First, the fabricated hydrogel samples were dried at room temperature on a bench (preferably on aluminium foil). Once fully dried and shrunken, each hydrogel sample was weighed, and the numerical results were recorded as W_0 (or W_{dry}).

To test water uptake capacity, each sample was immersed in $1 \times$ PBS solution using a 12-well plate as the container. Each well contained more than 5 mL of PBS solution, with one sample placed in per well to facilitate easy tracking of the weight change for each sample. The entire plate was placed into an incubator and incubated at 37°C in a $5\% \text{ CO}_2$ for a designated period.

The time intervals for the test were set as 0, 1 h, 3 h, 5 h, 6 h, 8 h, 12 h, 24 h, 36 h, and 60 h. At each time point, the hydrogel samples were removed from the PBS bath solution, gently wiped to remove excess surface water, and then weighed on a balance, and the results recorded as W_t at each time point.

The results were recorded, and the solution uptake ratio was calculated using the formula:

$$\text{Solution uptake} = \frac{W_{wet} - W_{dry}}{W_{dry}} \times 100$$

In this experiment, each time point was recorded, and the swelling ratio was calculated using the formula:

$$SR(\%) = \frac{W_t - W_0}{W_0} \times 100$$



Figure 6-1 Photograph of the swelling test setup, showing 3 groups of hydrogel samples (superficial, middle, and deep layers), each with 4 replicates ($n = 4$).

6.2.3 Degradation test

To assess the degradation behaviour of hydrogels, three separate concentration sets of samples were prepared, reflecting the superficial, middle and deep zones. The degradation tests were conducted over a period of 30 days, during which the change in dry weight was monitored to quantify the degradation.

Hydrogels were fabricated following the standardised protocol outlined in Chapter 5. Each sample was cast using 600 μL of solution in a 48-well plate as the mould. To ensure sufficient replicates for the 30-day testing period, at least 27 hydrogel samples were prepared per group, divided across 9 time points. After gelation, the samples were removed from the moulds, rinsed with Milli-Q water, and carefully wiped with Kimwipes to remove any excess surface liquid.

To ensure uniform immersion, three samples ($n = 3$) from each group were submerged in 5 mL of 1 \times PBS solution within a 15 mL centrifuge tube. Each group was divided into 9 tubes, corresponding to the designated time points, with each tube containing three replicates. All tubes were clearly labelled and vertically positioned in the incubator using a tube holder rack (**Figure 6-2**). The samples were incubated at 37°C with 5% CO_2 to simulate physiological conditions. Day 0 samples, which were not immersed in 1 \times PBS, were used as the baseline to record the initial dry weight (W_0) for each group.

At the designated time points (2, 5, 8, 12, 16, 20, 25, and 30 days), one tube from each group was retrieved from the incubator. The samples were removed from the PBS solution using sterilised tweezers, gently rinsed with Milli-Q water to remove the residual medium and patted dry with Kimwipes to eliminate excess moisture.

Each sample was placed on aluminium foil and allowed to air-dry at room temperature for 2 days (or longer, depending on the sample thickness) to ensure complete drying. The dry weight of each sample at each time point was recorded as W_t .

The weight loss rate (%) was calculated as follows:

$$\text{Weight loss \%} = \frac{W_0 - W_t}{W_0} \times 100$$

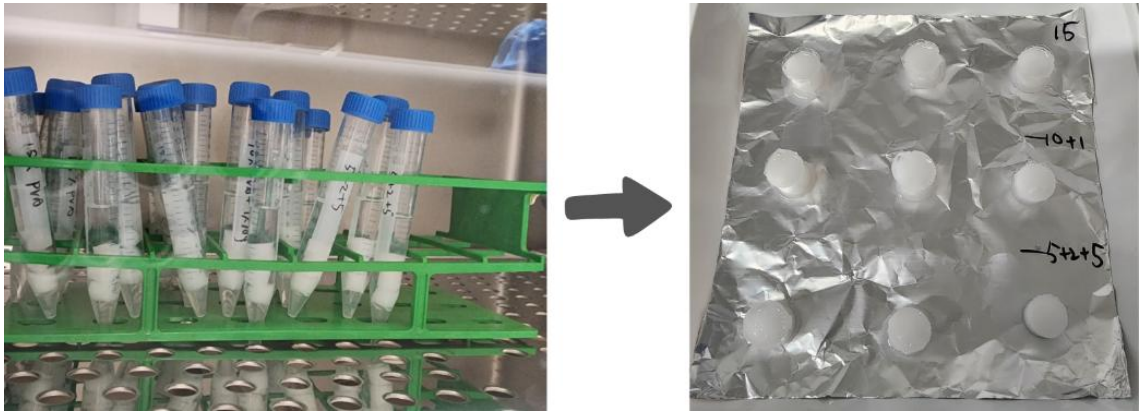


Figure 6-2 Photograph of the degradation test, 3 groups of hydrogel samples with 3 replicates (n=3) in each.

6.2.4 Mechanical properties

The mechanical properties of the hydrogel scaffolds were assessed with the assistance of USYD technical staff using a TA Instruments Discovery DMA 850 mechanical testing system. Results were directly generated by the mechanical testing instrument, and the concluded results were provided by the technical staff. For both compression and tensile tests, the ramp rate was set to 1.0 N/min, with a maximum force of 17.0 N. Three hydrogel groups, including superficial, middle, and deep zone samples were tested individually. Additionally, the overall compression test was conducted on the entire tri-layered chondral scaffold.

Hydrogel layers were adjusted in shape, length, and thickness according to the test requirements, as detailed below.

6.2.4.1 Compression test

The hydrogel solutions were prepared and poured into 24-well plates to ensure consistency in concentration and thickness among replicates. Specifically, 1 mL of the prepared gel solution was poured into each well of a 24-well plate during the crosslinking process. For each group, three replicates (n=3) were prepared with the following compositions:

- Superficial hydrogel: Aligned silk fibroin fibres coated with 15% w/v PVA + 2% w/v sericin
- Middle hydrogel: 10% w/v PVA + 1% w/v alginate
- Middle hydrogel: 5% w/v PVA + 2% w/v alginate + 5% w/v HAp

For the tri-layered chondral scaffold compression test, the thickness of each layer was adjusted to resemble the theoretical ratios between the superficial, middle, and deep zones. The middle zone accounted for the majority of the scaffold thickness. Details of the tri-layered scaffold fabrication are provided in Chapter 5. For the compression test, cylindrical hydrogel samples with an approximate diameter of 18 mm and a height of 5 mm were prepared.

6.2.4.2 Tensile test

Tensile tests were conducted on single-layer hydrogel samples. Three groups of hydrogel compositions were prepared ‘15% w/v PVA + 2% w/v sericin’, ‘10% w/v PVA + 1% w/v Alginate’, and ‘5% w/v PVA + 2% w/v Alginate + 5% w/v HAp’. To prepare the samples, the gel mixtures were poured into flat plates (e.g., well plate lids) to form hydrogels with a thickness of 1-2 mm. For silk fibre-incorporated samples, aligned silk fibroin fibres were placed in one direction within the gel, followed by filling the plate with 15% w/v PVA + 2% w/v sericin hydrogel. Once crosslinked, the hydrogels were cut into small rectangular shapes, ensuring the silk fibre orientation was aligned with the direction of the tensile force.

6.3 Results and Discussion

6.3.1 Morphology of hydrogel cross-section

6.3.1.1 Pre-test: Sequential layering of hydrogel

As scanning electron microscopy (SEM) images present in **Figure 6-3**, the scaffold cross-sections revealed distinct morphological features for the hydrogel cartilage layer and the polymer material incorporating hydroxyapatite (HAp) to simulate subchondral bone. The pure hydrogel layer, representing cartilage, exhibited a smooth surface and pore outlines. In contrast, the addition of HAp particles to the subchondral bone layer resulted in a rough hole/pore surface, reflecting the influence of ceramic particle dispersion on the morphology of the scaffold. These findings highlight the structural differences between the two compositions and mineral content modification, emphasising the need for further investigation into the correlation between material concentration and pore size to optimise scaffold design for specific applications.

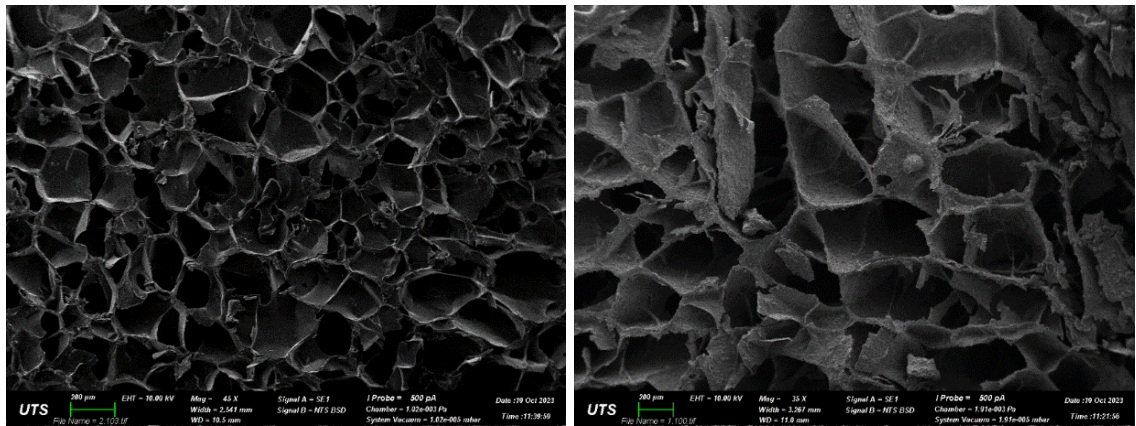


Figure 6-3 The cross-section SEM images (pre-test). Pure alginate-based hydrogel resembling the cartilage layer (left), and hydrogel with the addition of the hydroxyapatite for the subchondral bone layer (right).

6.3.1.2 PVA-sericin Hydrogels

The pure PVA-sericin hydrogel exhibits a highly interconnective structure. At a designed concentration of 15% w/v PVA, the freeze-dried hydrogel scaffold appears in a shrunken state rather than the expected porous structure. The high concentration PVA base results in increased rigidity, making it difficult to slice, with the cross-section revealing a flat surface and minimal porosity. These findings suggest that high-concentration PVA-based hydrogels may be more suitable as coating materials, acting as adhesive layers between

scaffold zones. Overall, the non-porous nature of this PVA-sericin formulation may limit cellular infiltration and ingrowth.

6.3.1.3 PVA-Alginate composite hydrogels

The concentration of PVA-alginate composite hydrogels was tested, and a preliminary assessment using manual compression (finger press) indicated that both 5% PVA-2% alginate and 10% PVA-1% alginate formulations, after undergoing three freeze-thaw cycles, exhibited the expected stiffness while maintaining a well-interconnected structure.

Figure 6-4 presents the cross-section of the PVA-alginate composite hydrogels. The alginate component was crosslinked via Ca^{2+} induced chemical crosslinking, while the PVA component underwent physical crosslinking through freeze-thaw cycles, resulting in a double-network hydrogel structure. Compared to pure alginate hydrogels synthesised via internal ionotropic gelation (section 6.3.1.1), the pore morphology of the composite hydrogels appeared less defined, with less distinct pore outlines, possibly due to the influence of the physically crosslinked PVA component.

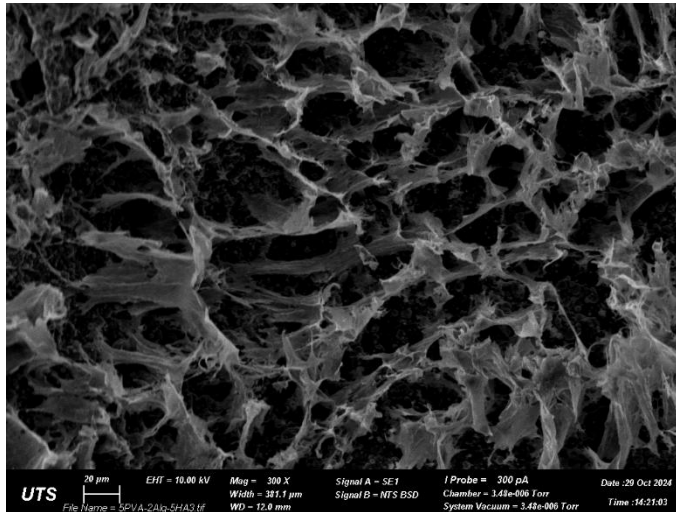
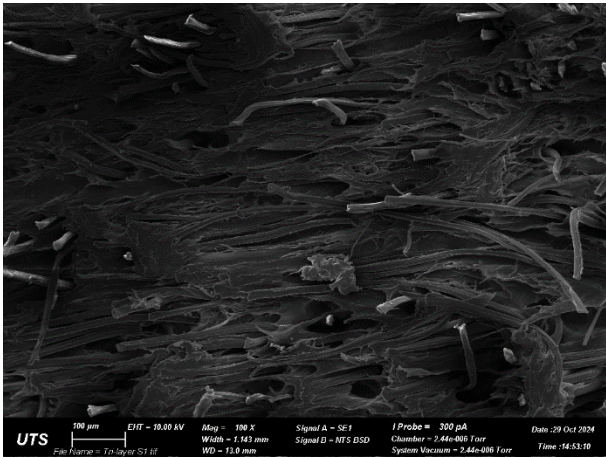
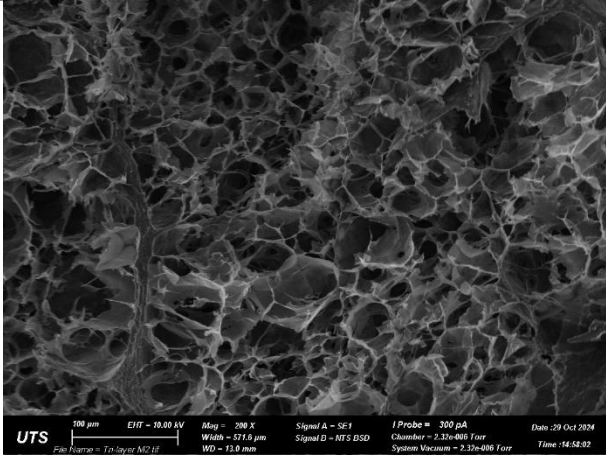
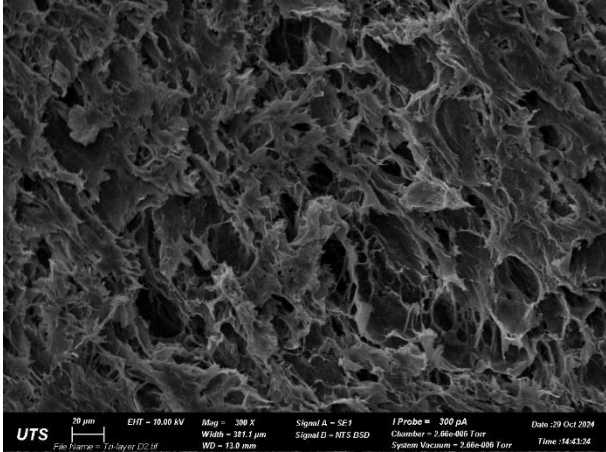


Figure 6-4 The PVA-alginate hydrogel forms a double-crosslinked network through a combination of freeze-thaw-induced physical crosslinking and internal ionotropic chemical crosslinking.

6.3.1.4 Multizonal chondral hydrogel scaffold

As shown in **Table 6-2**, SEM images were obtained to characterise the morphology of the layers. The fibrous superficial layer exhibited a horizontal and aligned fibre orientation, which is essential for facilitating load distribution across the articular cartilage surface.

Table 6-2 SEM images of the three layers: superficial, middle, and deep zones, along with their descriptions.

<p>Superficial zone</p> <ul style="list-style-type: none"> • Layer: Aligned silk fibroin fibres (sheet) coated with 15% w/v PVA + 2% w/v Sericin. • Aligned Fibrous Structure: The silk fibroin fibres were aligned to form a sheet (Chapter 4), mimicking the natural orientation of collagen fibres in the superficial cartilage zone. • Integration: To adhere the superficial layer to the underlying scaffold, the silk fibres were immersed and coated with PVA-based materials. • Function: Provides lubrication and distributes compressive forces. Offers resistance against shear forces, reducing the risk of joint damage during movement. 	
<p>Middle zone</p> <ul style="list-style-type: none"> • Layer: 10% w/v PVA + 1% w/v Alginate • Porous hydrogel: PVA and alginate composite hydrogel layer. • Function: Serves as a transition layer between the superficial and deep zones. Provides resistance to compressive forces. 	
<p>Deep zone</p> <ul style="list-style-type: none"> • Layer: 5% w/v PVA + 2% w/v Alginate + 5% w/v HAp • Mineral Porous Hydrogel: A composite scaffold combining PVA, alginate, and HAp to create mineral content distribution and a smoother transition to calcified and subchondral bone. • Function: Supports the overlying load and provides the highest resistance to compressive forces. 	

The overall SEM image is shown in **Figure 6-5**, indicating the distinct layer morphologies while connected together by seamless transitions. **Figure 6-6** shows the superficial-to-middle interface and the middle-to-deep gradient transition, respectively. The transitional layers exhibit seamless integration, ensuring a smooth transition from the fibrous superficial layer to the porous middle layer. Notably, the fibrous structure visible in the SEM cross-section highlights the incorporation of silk fibroin fibres. Since the hydrogel naturally forms a porous structure only after freeze-drying, the silk fibres directly applied to the superficial layer exhibit aligned orientation. This represents a key novelty of the project, as the silk fibre sheet mimics the native collagen fibre orientation in this region while maintaining connectivity.

Based on qualitative visual analysis of the SEM images, the superficial zone incorporates aligned silk fibroin fibres, which directly adhere to the underlying porous middle zone. This integration is achieved through a gradual concentration change of PVA materials across the zones. The gradient porous transition progresses from larger pores in the middle zone to smaller, denser pores in the deeper zone. The cross-section reveals a smooth layer transition with no abrupt changes observed in the SEM images.

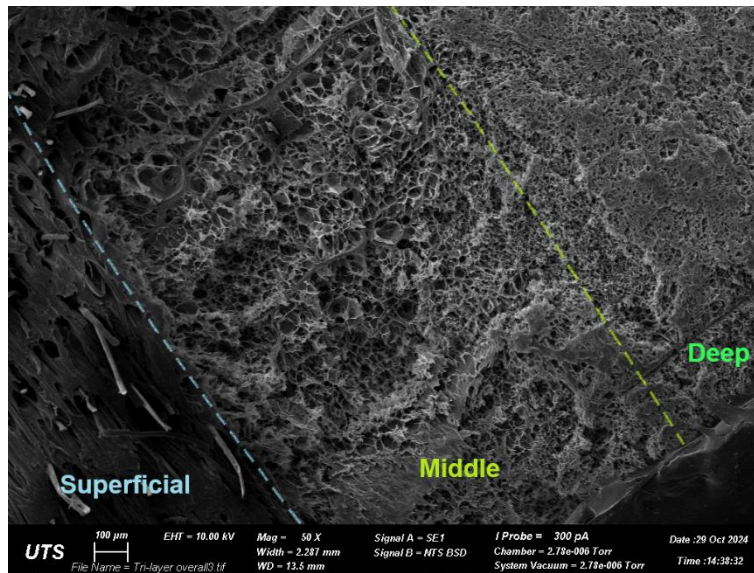


Figure 6-5 SEM image of the cross-section morphology of the tri-layered scaffold exhibiting three distinct zones.

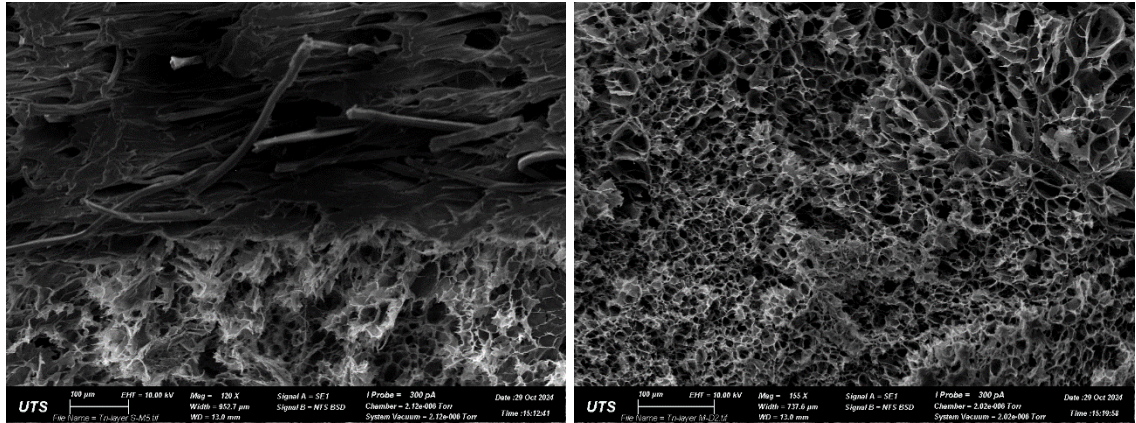


Figure 6-6 SEM images of the superficial-to-middle layer transition (left) and middle-to-deep layer transition (right).

In this study, SEM imaging was employed to examine the inter-polymeric network and overall hydrogel cross-section morphology. Admittedly, since vacuum freeze-drying had to be performed prior to the SEM analysis, the observed pore structure was greatly affected by the pores created during the freezing process and the drying conditions of the freeze-dryer, and did not fully reflect the structure of the native hydrogel. Consequently, these images provide limited representations of the hydrogel properties in its hydrated state and its actual behaviour upon implantation for cartilage tissue engineering.

From a structural perspective, the porous architecture plays a dual role: first, pore channels facilitate cell migration from surrounding tissues and facilitate the permeation of interstitial fluids through capillary action. Second, the interconnected porous network provides a three-dimensional framework with a high surface area, promoting cell adhesion and proliferation within the scaffold.

Reviewing studies on scaffold-based cartilage tissue engineering, native cartilage exhibits depth-dependent variations in pore size, ranging from 2 to 6 nm, with a gradual increase from the superficial to the deep zone.[80] In articular cartilage scaffolds, pore size is a critical parameter that influences cell migration, as well as the diffusion of nutrients and metabolic waste. The pore size design is supposed to be appropriate to allow cell infiltration while preventing excessive pore enlargement relative to cell size, as oversized pores may hinder cell adhesion. For hydrogels designed to promote chondrocyte adhesion and cell ingrowth in cartilage repair, the optimal pore size ranges from 150–500 µm.[69]

Compared with the SEM images of the tri-layered chondral scaffold design, the superficial aligned silk-incorporated layer features gaps between silk fibres, providing structural spaces to allow cell ingrowth. In the porous layers, the middle layer exhibits pore sizes smaller than 100 μm , while the deep zone contains smaller and denser pores around 20 μm . This trend contrasts with the native cartilage structure, where pore sizes gradually increase from the superficial to deep zones. In this project, it is necessary to achieve a balance between pore size, stiffness, and material composition. While the mould-casting method cannot independently adjust pore size, the pore size and porosity parameters are inherently linked to stiffness, and stiffness is listed as a priority consideration in this study. For future optimisation, advanced manufacturing techniques such as 3D printing are of interest, as these techniques would enable precise control over pore patterning and sizing through tailored structural designs.

Furthermore, SEM imaging reveals that the overall porous architecture of the hydrogel can vary depending on the freezing temperature prior to lyophilisation, which helps preserve a controlled pore size. The size of ice particles formed during freezing within the hydrogel is highly dependent on the growth rate of ice crystals. For example, a study presents that freezing at -80°C or -196°C before lyophilisation can result in smaller, elongated and collapsed pores.[27] Considering the different tissue engineering applications, along with material selection and crosslinking methods, freezing temperature is also a key factor in fabricating controllable and modifiable hydrogel scaffolds for musculoskeletal tissue engineering.

In the parameters of hydrogel components and compositions, fabrication methods of composite hydrogels significantly influence their structural properties. In this study, polyvinyl alcohol (PVA) and alginate were used as base materials, with their fabrication steps playing a crucial role in defining the final hydrogel characteristics. During the composite hydrogel fabrication step, the alginate polymer was first crosslinked via ionic exchange, where Ca^{2+} replaced sodium ions while binding two alginate polymer chains, forming irreversible chemical crosslinked alginate hydrogels. This was followed by a freeze-thaw process for PVA, which resulted in a milky-white, non-uniform structure [81], primarily enhancing the stretchability and mechanical strength of the entire hydrogel. Consequently, the alginate network serves as the fundamental framework determining the overall pore architecture.

For further optimisation and controlled modification (refer to **Appendix A, Figure A 1** to **Figure A 8**), the alginate network can be tailored to enhance porosity and increase pore size by adjusting the dissolution volume of CaCO_3 . Theoretically, the initial distribution and dissolution of CaCO_3 powders play a crucial role in the formation of macro-sized pores.[82]

A representative study[82] demonstrates an anatomical view of the internal structure, highlighting the differences between conventional non-porous alginate hydrogels fabricated via CaCl_2 diffusion and the expected porous hydrogels. The porous architecture was achieved through the incorporation of insoluble vaterite CaCO_3 crystals, which functioned as sacrificial templates while simultaneously serving as a Ca^{2+} source. The internal generation of CO_2 gas within the crosslinked polymer network further contributed to pore formation.

In conclusion, optimising the balance between pore morphology and material composition remains a critical field for future research and is worth more specific and in-depth investigation.

6.3.2 Hydrogel swelling and water uptake

To test the swelling of the hydrogel samples for the application in biomedical use, the dry state samples were immersed in PBS solution at 37°C , resembling the environment of the hydrogel implanted into the human body for tissue engineering. Theoretically, the swelling test primarily reflects the crosslinking density of the hydrogel matrix, where a lower crosslinking density facilitates rapid water absorption, whereas a higher crosslinking density limits swelling due to tighter polymer entanglement, resulting in reduced free space for water uptake. The porosity of hydrogel can also play a role; more porous hydrogels exhibit greater water absorption but often at the cost of reduced mechanical strength.

At predetermined time intervals, the weight of the hydrogel samples was recorded to track swelling kinetics. As illustrated in **Figure 6-7**, all three hydrogel layers exhibited rapid water uptake within the first 8 hours, indicating an initial phase of rapid hydration. By the 12-hour time point, swelling equilibrium was reached, indicating complete swelling as

evidenced by a plateau in the swelling curve. Comparative analyses of the three distinct layers revealed varying swelling capacities; the superficial layer (PVA-sericin hydrogel) exhibited a relatively lower swelling ratio, which could be attributed to its dense polymer network. The middle layer demonstrated the highest water uptake capacity among the three groups, suggesting a more open network structure. The deep layer (PVA-Alg-HAp hydrogel) showed restricted swelling, which may be attributed to higher polymer entanglement and the presence of hydroxyapatite (HAp).

Regarding compositional impact, the swelling ratio of PVA-based hydrogels is inherently high due to the hydrophilic nature of PVA. However, the incorporation of HAp plays a crucial role in regulating the swelling behaviour. HAp enhances mechanical stability and biocompatibility; its rigid structure can reduce overall swelling capacity. The presence of alginate in the hydrogel composition further influences swelling dynamics, where lower alginate concentrations contribute to better water retention.

In comparison with the existing studies, the swelling behaviour of hydrogels is a key parameter affecting their biomedical performance. Swelling capacity is predominantly governed by hydrogel network structure, crosslinking density, and hydrophilic functional groups. Additionally, environmental factors such as pH and ionic strength significantly influence swelling, with pH-responsive hydrogels exhibiting different behaviours in acidic and basic conditions. These findings emphasise the importance of optimising hydrogel composition to tailor swelling properties for specific applications, including tissue engineering and potential drug delivery.

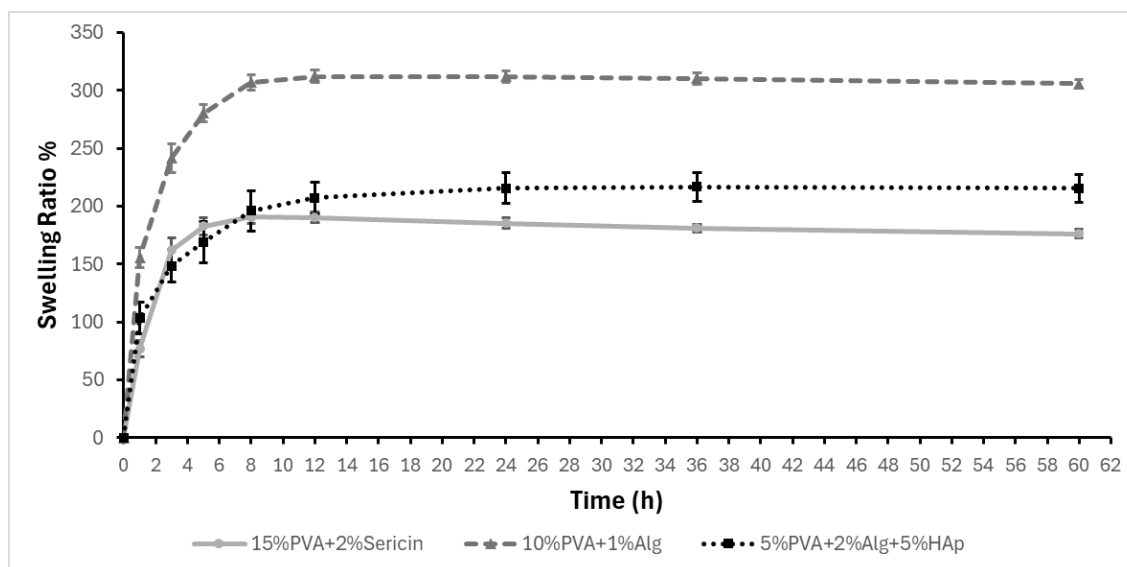


Figure 6-7 Swelling behaviour of three hydrogel concentration sets, showing water uptake capacity reflected by the swelling ratio over time (hours) within a total duration of 60 h.

An additional swelling test was conducted to assess the behaviour of the joined tri-layered hydrogel scaffold and confirm the integration between layers. **Figure 6-8** presents photos showing the state changes from the as-prepared tri-layered hydrogel to the fully dried, shrunken state after air drying at room temperature, and finally to the swollen state after immersion in PBS solution. The results demonstrated that the tri-layered scaffold maintained its structural integrity, with no significant delamination or mismatch between layers during the swelling process. It is hypothesised that the middle layer, being sandwiched between the superficial and deep layers, had reduced contact area and direct exposure to the surrounding liquid, which may have limited its water uptake capacity. Consequently, the swelling behaviour of the joined tri-layered hydrogel differed slightly from that of individual layers. The relatively higher liquid absorption capacity observed in the single middle layer may be beneficial for its role within the scaffold, facilitating a smooth transition between layers while maintaining overall structural integration.

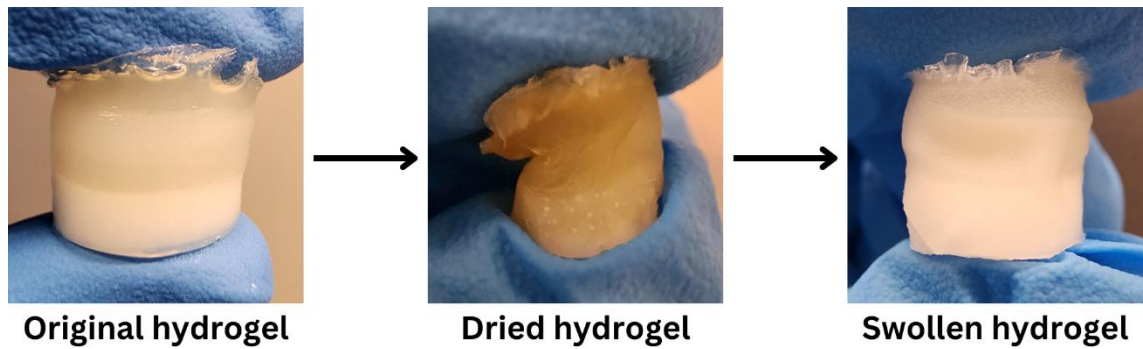


Figure 6-8 Comparison of the hydrogel in different states during the swelling test. From left to right: as-prepared hydrogel, fully dried state, and swollen state after PBS immersion.

In the discussion, hydrogels with high swelling ratios are well-suited for applications requiring significant water absorption, such as wound dressings. However, in this project, the hydrogel is designed to support structure and function at the weight-bearing site and therefore requires a lower swelling ratio to maintain mechanical integrity.

The crosslinking density of alginate in this study relies on Ca^{2+} ions within the calcium alginate hydrogel system, which aligns with previous findings regarding alginate hydrogel swelling behaviour.[83] Besides, factors such as uniform pore distribution, porosity, and pore diameter contribute to enhanced liquid uptake capacity.[84] The choice of swelling medium, such as distilled water or PBS, can also influence the swelling ration [85], which is supposed to be considered in future research.

Regarding the goal of achieving a biomimetic structure in this project, even if the middle layer exhibits a higher swelling ratio than the other two layers, its position sandwiched between them and its contact area with the surrounding medium limit excessive expansion. The similar swelling behaviour of the layers, along with tests on the integrated tri-layered construct, confirms that no deformation or layer separation occurs during liquid uptake.

6.3.3 Degradation

Degradation refers to the breakdown of the hydrogel polymer network, which can occur through various mechanisms, including hydrolysis, enzymatic action, and physical

processes. The rate of degradation is influenced by factors such as the hydrogel composition, crosslink density, porosity, and environmental conditions.

The graph in **Figure 6-9** presents varying weight loss percentages over 30 days, depending on the hydrogel compositions. Initially, all formulations exhibited a noticeable increase in weight loss by day 2. The '10% PVA + 1% Alg' hydrogel had the highest degradation rate, reaching approximately 30–40% weight loss, whereas the '5% PVA + 2% Alg + 5% HAp' and '15% PVA + 2% sericin' formulations exhibited lower degradation, around 10–20%.

During the mid-term period (5-16 days), the '10% PVA + 1% alginate' hydrogel continued to degrade at a significantly higher rate, reaching nearly 40% weight loss. In contrast, the other two formulations remained more stable, with weight loss ranging between 10-20%. By the final phase (20–30 days), the '10% PVA + 1% Alg' hydrogel continued to exhibit the highest degradation rate, exceeding 40% weight loss, whereas the '5% PVA + 2% Alg + 5% HAp' (deep layer) and '15% PVA + 2% sericin' (superficial coating) hydrogels degraded more gradually, stabilising at 15–20% weight loss. The degradation behaviour aligns with the observed swelling ratios, as both properties depend on the hydrogel crosslinking density and the water resistance of the crosslinked polymer network. Notably, the incorporation of hydroxyapatite (HAp) contributed to enhanced structural stability, thereby slowing the degradation rate.

These findings indicated that although the '10% PVA + 1% Alg' hydrogel was the most degradable, it was intentionally positioned in the middle layer to integrate with the other two layers, reducing direct contact with the biophysiological environment. Meanwhile, the '5% PVA + 2% Alg + 5% HAp' hydrogel exhibited a moderate degradation rate, balancing stability and resorption, while the '15% PVA + 2% sericin' hydrogel remained the most stable, making it suitable for applications requiring prolonged structural integrity. It is presumed that when the three scaffolds are combined, the balanced degradation rates between the three layers are expected to promote good integration, minimise significant differences in interlayer degradation, and ensure structural cohesion throughout the degradation process.

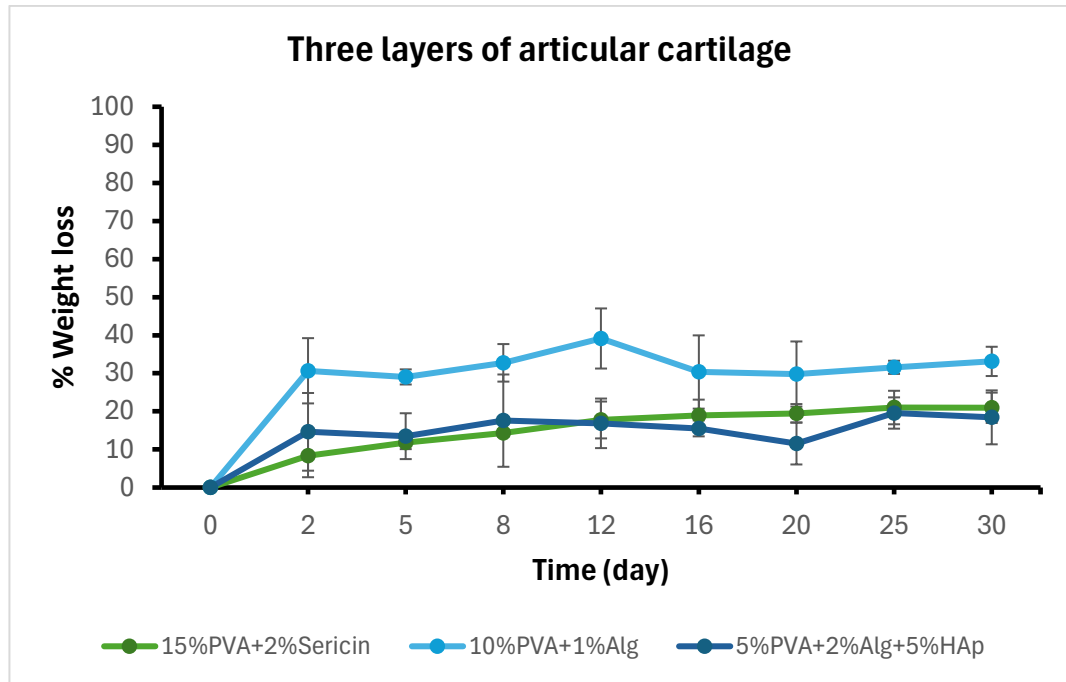


Figure 6-9 Degradation rates of three hydrogel formulations (three separated layers) over 30 days.

Theoretically, hydrogels degrade through various mechanisms, including hydrolysis, enzymatic action, and the dissolution of crosslinked polymer networks. In this project, degradation primarily involves the hydrolysis of freeze-thawed synthetic polyvinyl alcohol (PVA), where hydrogen bonding strengthens the gel structure, with the degradation rate largely dependent on the degree of crosslinking and water absorption capacity.[31; 48] Alginate-based hydrogels degrade primarily through ion-exchange reactions, in which the dissolution of Ca^{2+} -crosslinked alginate occurs due to ion diffusion and environmental factors such as pH, temperature, and mechanical stress.[86; 87]

The degradation behaviour of hydrogels is critical for maintaining structural integrity and interconnectivity at the defect site. For animal testing and potential clinical translation, the hydrogel is expected to maintain its structure for at least 14 days, providing sufficient support for early-stage tissue regeneration. Since chondral tissues require a longer timeframe for complete restoration, a controlled degradation profile is essential to ensure scaffold functionality throughout the healing process.

Ideally, the degradation rate should match the regrowth rate of the target zone, allowing gradual replacement by newly formed tissue. Furthermore, as this scaffold features a

stratified zonal design, it must maintain structural cohesion without layer mismatch to function effectively as an integrated unit.

Regarding the factors that might influence the degradation rate, as confirmed in this study, material type, concentration, and crosslinking chemistry significantly impact degradation behaviour. Higher PVA content increases stability, whereas higher alginate concentrations promote faster degradation. In future designs, particularly for 3D-printed constructs, additional structural factors such as pore size, architecture, and interconnectivity will also play a crucial role in determining degradation behaviour and tissue integration.

6.3.4 Mechanical properties.

The mechanical properties were evaluated using compression and tensile tests, which are critical for assessing the scaffold's performance. The tri-layered scaffold was tested to examine layer integration and overall resistance to compressive loads. Individual layers were also tested separately to determine their compression and tensile properties. For original plots, refer to **Appendix C**.

6.3.4.1 Superficial layer: 15% PVA + 2% sericin + aligned silk incorporated

Figure 6-10 displays photos from the compression and tensile mechanical tests, pre-test and post-test, the superficial layer of the articular cartilage scaffold, resembling the native superficial cartilage, was subjected to compression and tensile tests to assess its mechanical characteristics.

In the compression test, the layer maintained its shape without collapsing and retained sufficient interconnective architecture during the compression test. The comparison graphs are presented in **Figure 6-11**. In the tensile test, the incorporation of aligned silk fibroin fibres in the PVA-based hydrogel, aligned with the tensile force direction, allowed the samples to maintain their linking part without breaking and preserving their integrity. The related graphs are displayed in **Figure 6-12**.

The natural superficial cartilage zone is expected to exhibit adequate elasticity to resist force and facilitate force distribution to the underlying zones. This layer, being the surface

of weight-bearing cartilage, requires high resistance to shear forces and the ability to maintain integrity, reducing the risk of damage during joint movement.

To achieve this, the hydrogel must withstand compressive pressure and remain connected under tensile forces, mimicking the structure and function of the superficial zone. Based on the mechanical tests designed to replicate the superficial hydrogel layer, it can be concluded that the silk fibre sheet can preserve the scaffold and support the regrowth of cartilage tissue to withstand compressive forces at the surface contact area during movement. Additionally, the PVA-based hydrogel enhances stretchability and lubrication, making it suitable for superficial layer applications.

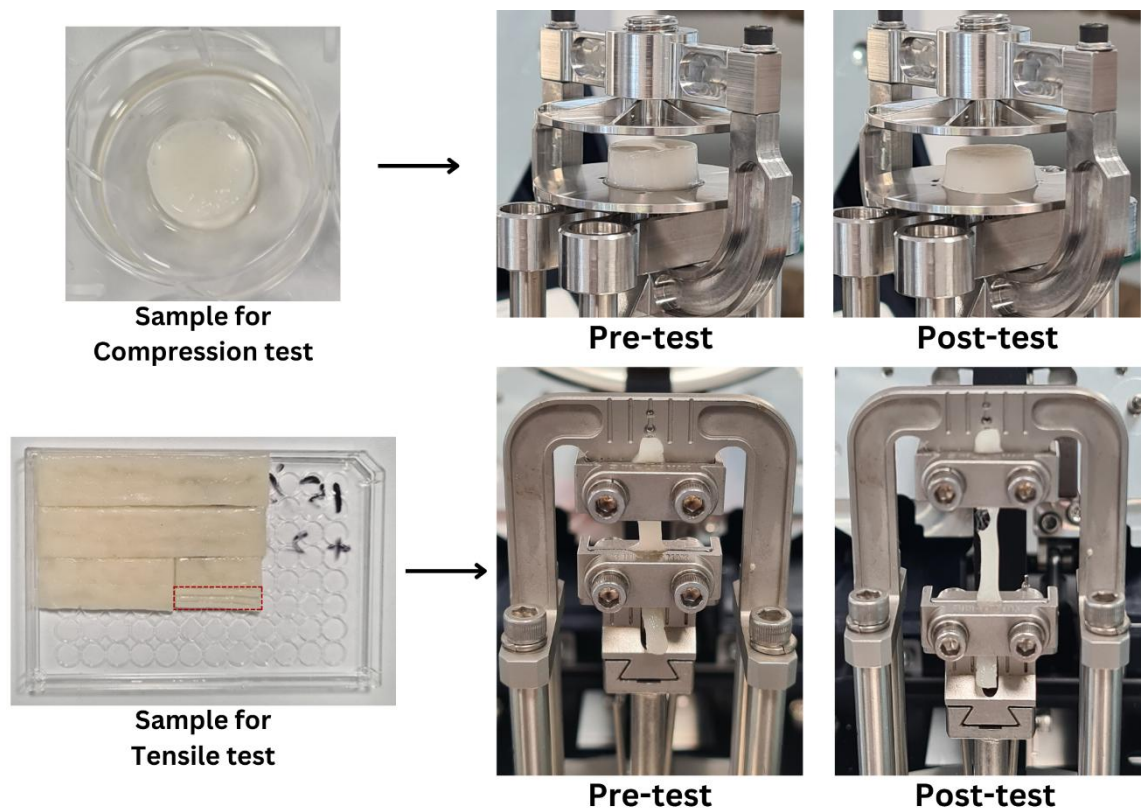


Figure 6-10 Photos during the compression and tensile mechanical test, pre-test and post-test of the '15%PVA + 2%sericin + aligned silk fibres' superficial hydrogel.

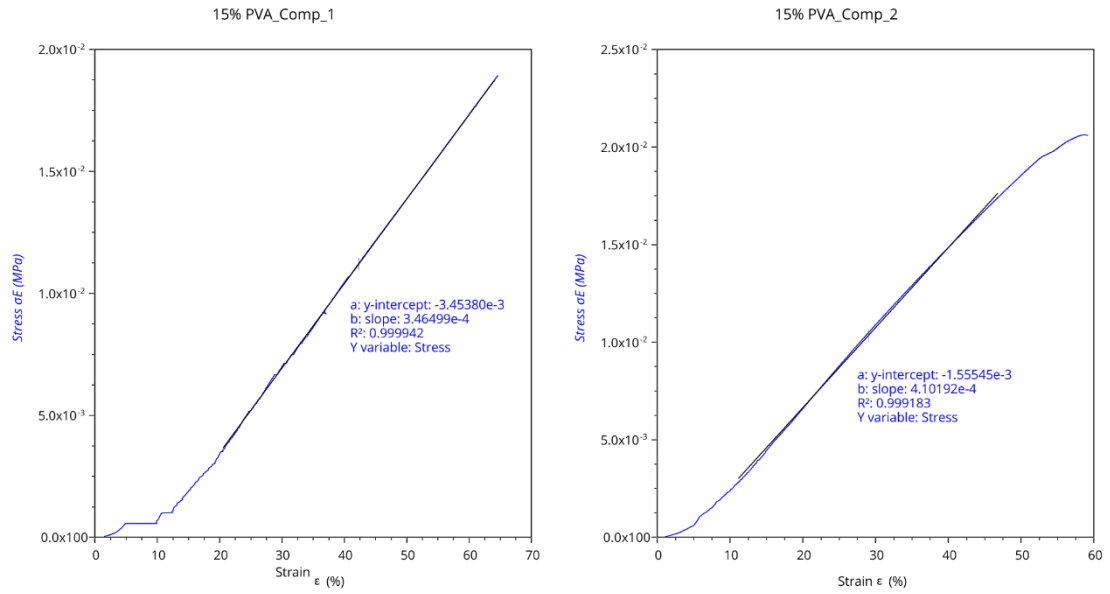


Figure 6-11 Compression test results and graphs generated by the instrument of the superficial hydrogel layer.

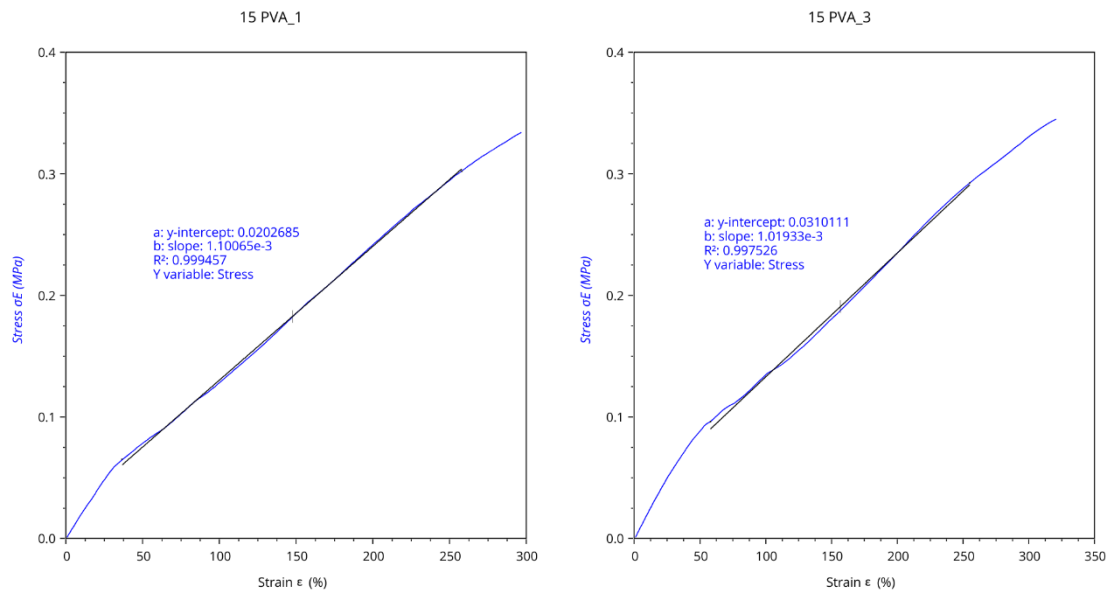


Figure 6-12 Tensile test results and graphs generated by the instrument for the superficial hydrogel layer.

6.3.4.2 Middle layer: 10% PVA + 1% alginate

Figure 6-13 exhibits photos from the compression and tensile mechanical tests pre-test and post-test. The hydrogel, resembling the middle zone of the articular cartilage, underwent mechanical compression and tensile tests. In the compression test, the layer maintained its shape without collapsing and retained sufficient interconnective architecture. The comparison graphs are presented in **Figure 6-14**. In the tensile test, the

hydrogel sample broke apart at the end of the tensile force, the related graphs are displayed in **Figure 6-15**. The natural middle cartilage zone is expected to exhibit adequate resistance against compressive force loads, function as the main transitional zone combining the superficial and deep zones, and maintain integration while absorbing shock.

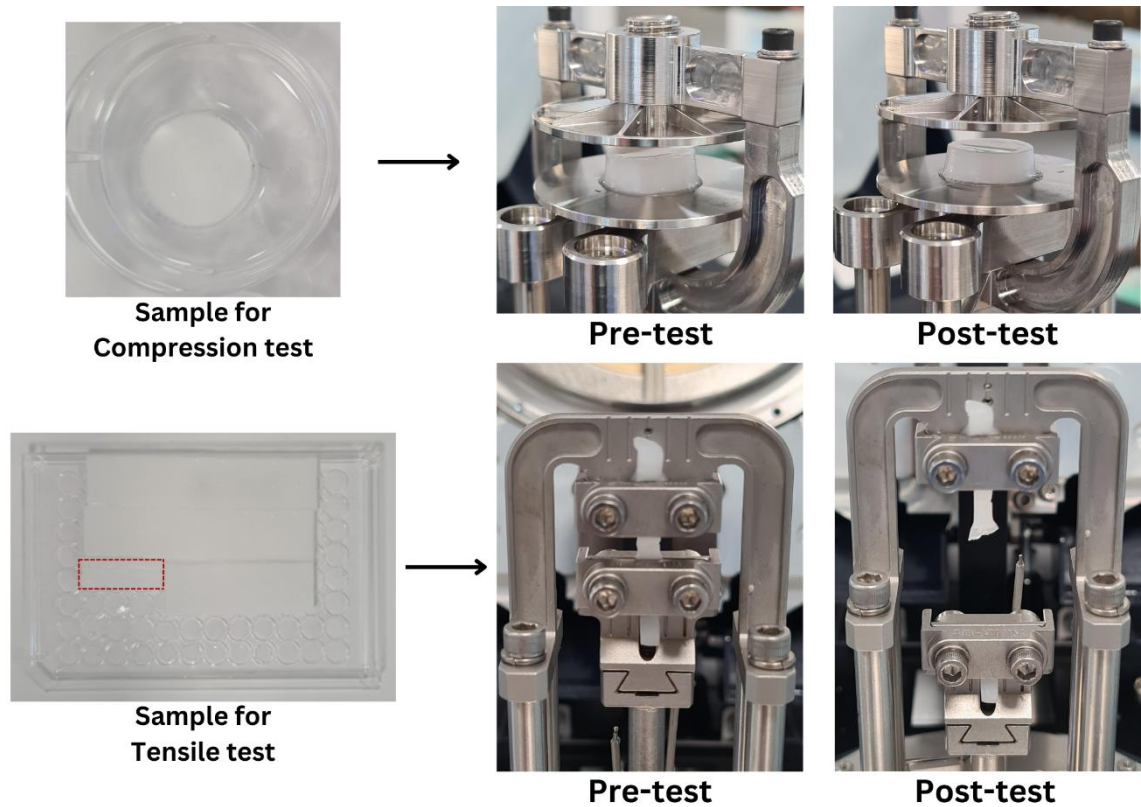


Figure 6-13 Photos during the compression and tensile mechanical test, pre-test and post-test of the '10% PVA + 1% Alginate' middle hydrogel.

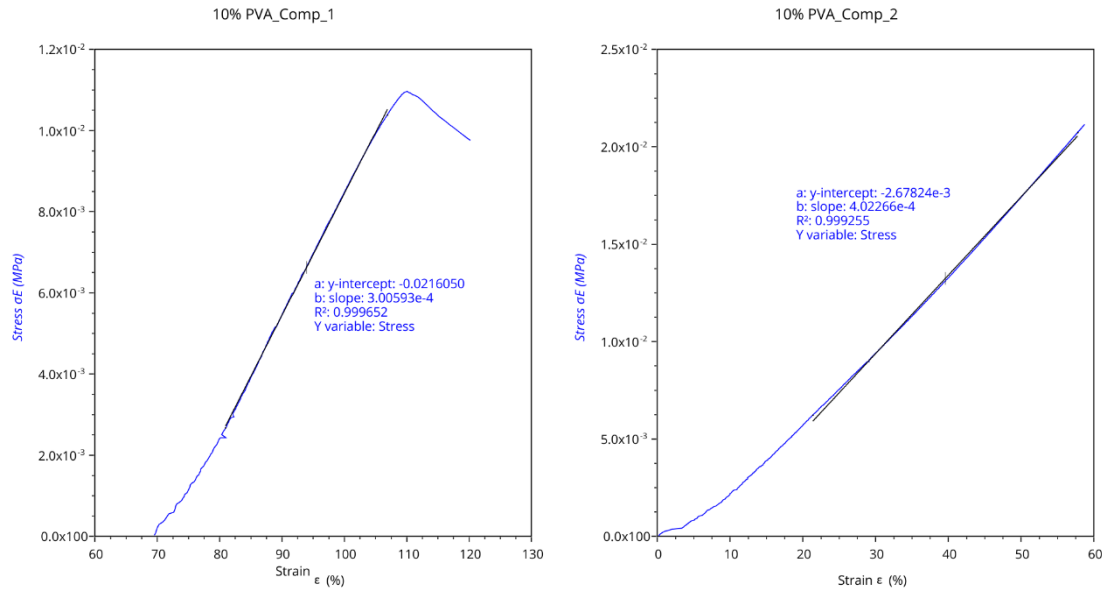


Figure 6-14 Compression test results and graphs generated by the instrument of the middle hydrogel layer.

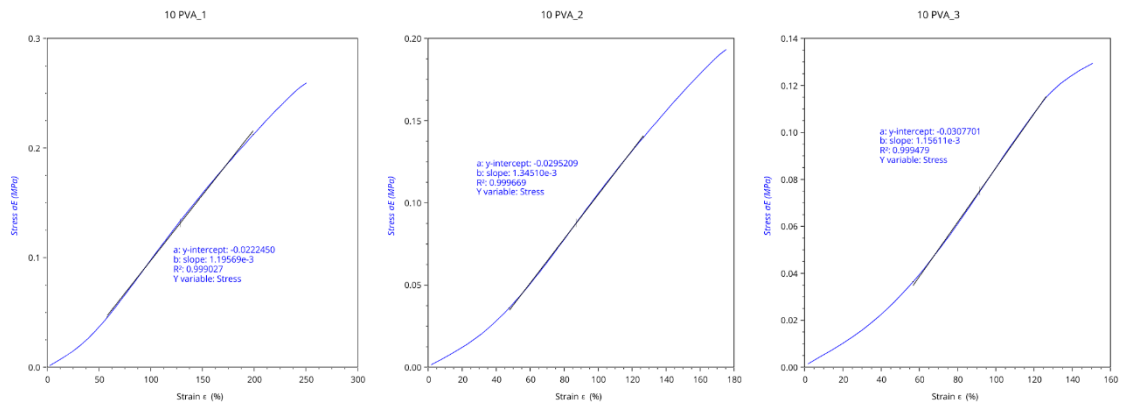


Figure 6-15 Tensile test results and graphs generated by the instrument for the middle hydrogel layer.

6.3.4.3 Deep zone: 5% PVA + 2% alginate + 5% HAp

The photos from the compression and tensile mechanical tests, both pre-test and post-test, are shown in **Figure 6-16**. The deep layer of the articular cartilage scaffold, designed to resemble native deep cartilage, was subjected to compression and tensile tests to evaluate its stiffness.

In the compression test, the deep layer maintained its shape without collapsing and retained sufficient interconnected architecture, demonstrating its structural integrity. The comparison graphs are presented in **Figure 6-17**. Conversely, in the tensile test, the

hydrogel samples fractured under tensile force, as shown in the related graphs in **Figure 6-18**.

The deep cartilage zone is expected to function as the foundational layer of the entire cartilage scaffold and further transition seamlessly to the underlying calcified cartilage and resilient subchondral bone. In this project, mineral content was incorporated into the deep layer to facilitate this transition and support the multizonal chondral scaffold.

Mineralised polymeric materials ensure this functionality, as PVA-based materials enable easy and robust integration between layers, resulting in a more interconnected architecture. This design approach differs from brittle ceramic scaffolds, offering enhanced durability and compatibility for multizonal tissue engineering.

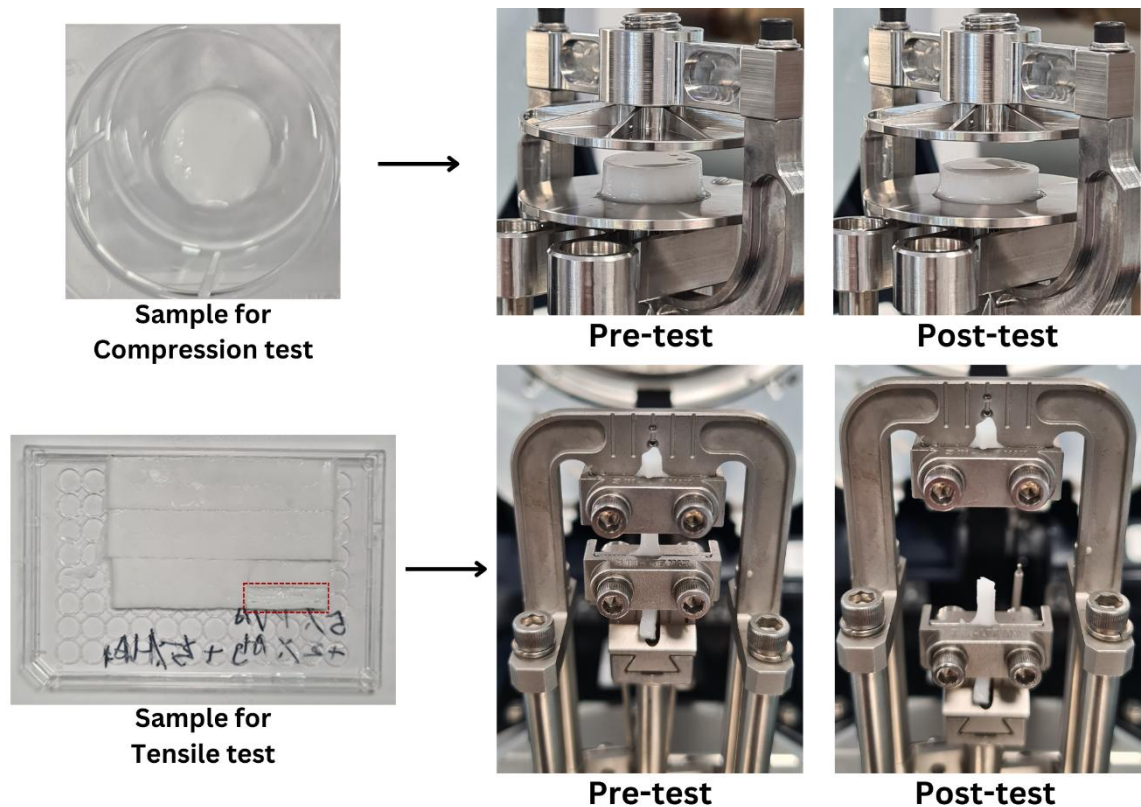


Figure 6-16 Photos during the compression and tensile mechanical test, pre-test and post-test of the '5% PVA + 2%Alginate + 5%HAp' deep hydrogel.

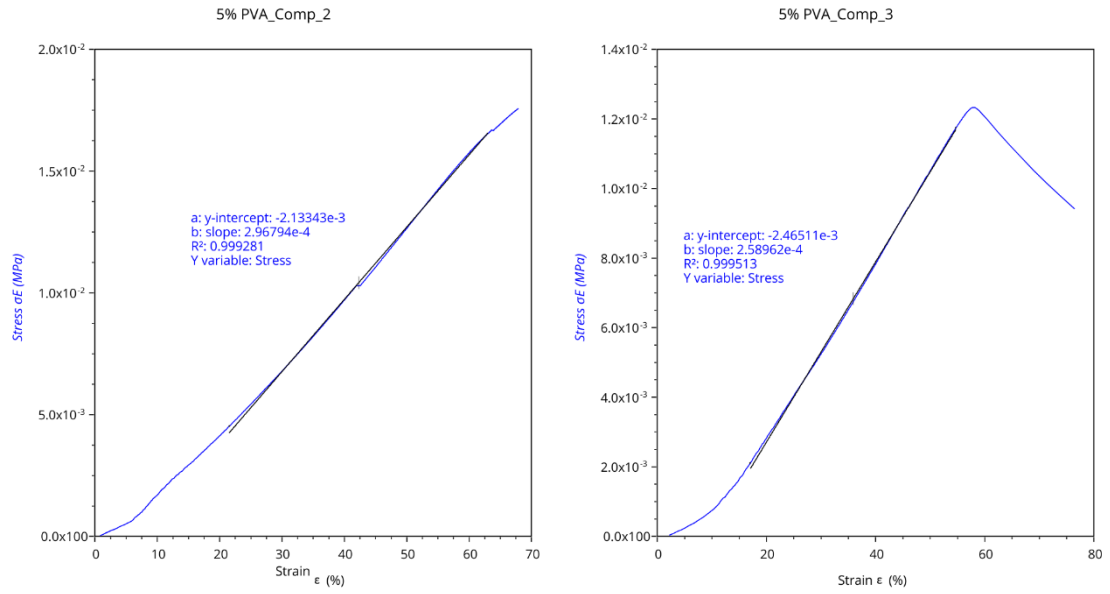


Figure 6-17 Compression test results and graphs generated by the instrument of the deep hydrogel layer.

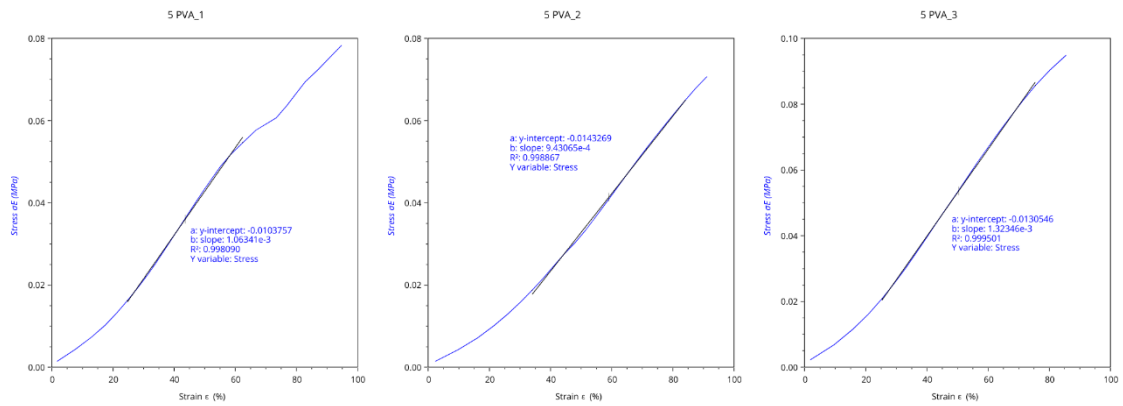


Figure 6-18 Tensile test results and graphs generated by the instrument for the deep hydrogel layer.

6.3.4.4 Compression of the overall tri-layered zonal chondral scaffold

The mechanical compression test of the tri-layered chondral scaffold, including both pre-test and post-test results, is presented in **Figure 6-19**. The multizonal scaffold is expected to maintain excellent integration between layers. In this design, the joined tri-layered chondral scaffold remained interconnected under compressive force, with no collapse observed in the post-test state. Therefore, the results successfully fulfilled the aims and research objectives of this project, demonstrating that the multizonal scaffold can function as a cohesive unit at weight-bearing cartilage defect sites.

The overall design of this project mimicked the joined superficial, middle, and deep layers, which were subjected to compression tests to assess their function at weight-bearing sites. This approach aims to contribute to the application of cartilage tissue engineering. The comparison graphs are presented in **Figure 6-20**.

The gradient change of decreasing PVA and alginate polymeric concentrations, coupled with increasing mineral content from the superficial to deep zone, achieved a functional gradient with minimal differences between the layers. All layers maintained their structural integrity without collapsing. The integration method using PVA-based composite hydrogel and glue also proved effective for multizonal scaffold fabrication.

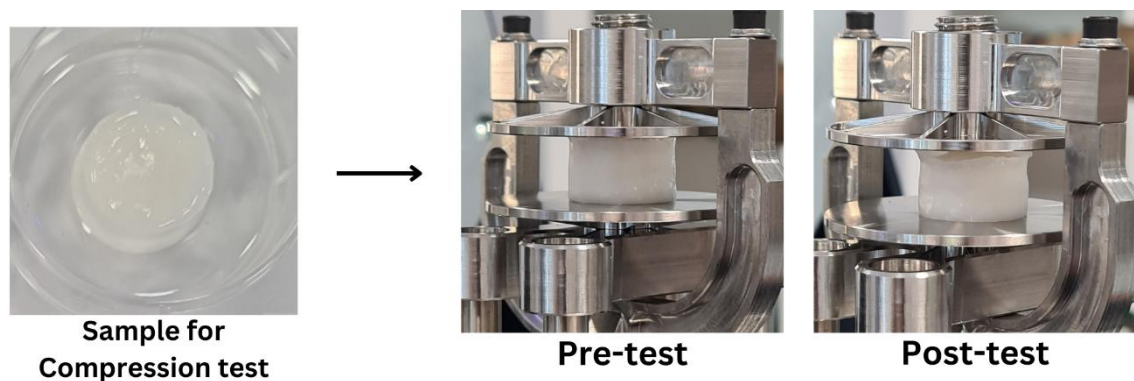


Figure 6-19 Photos during the compression mechanical test, pre-test and post-test of the tri-layered chondral hydrogel scaffold.

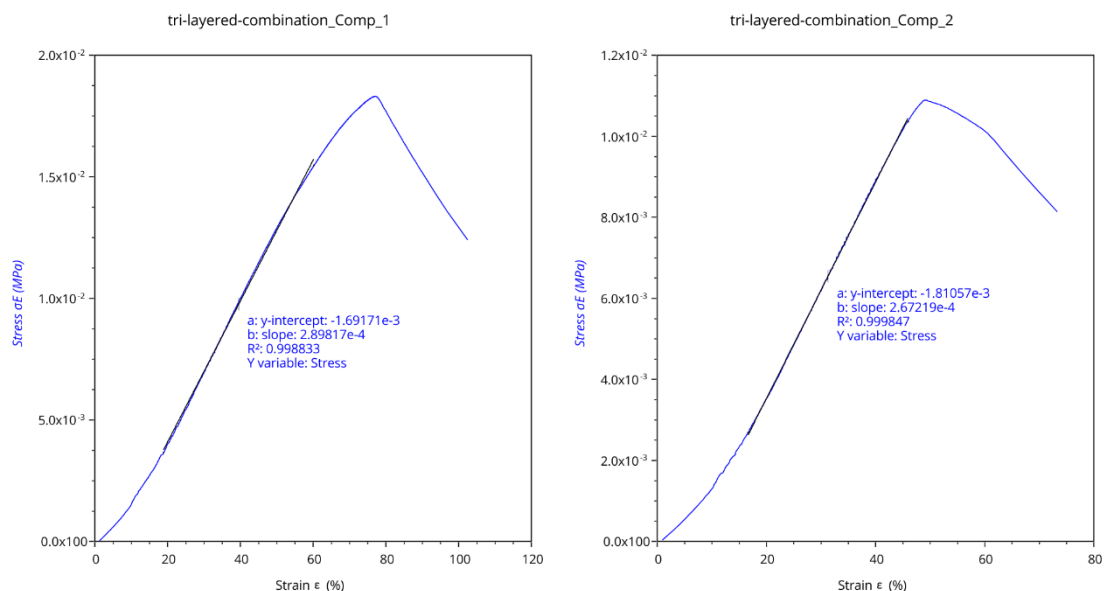


Figure 6-20 Compression test results and graphs generated by the instrument of the tri-layered chondral scaffold.

As summarised from the graph generated by the test instrument, the numerical results for Young's modulus in both tensile and compression tests are presented in **Table 6-3**. Force ramp rate was set to 1.0 N/min, and the maximum force was set to 17.0 N.

The tri-layered combination exhibited an intermediate Young's modulus (~ 0.027 MPa), suggesting a compromise between the individual layers, which may provide gradual stress distribution and better structural integration. The minimal differences in numerical values from the compression test across the layers suggest a relatively smooth transition, helping to avoid delamination under compressive force loading.

Table 6-3 Summary of numerical mechanical test results.

Sample	Young's Modulus (MPa)						
	Compression		Avg	SD	Tensile		SD
15%PVA + 2%Sericin + Silk	0.0346	0.0410	0.0378	0.00453	0.1101	0.1019	0.1060
10%PVA + 1%Alg	0.0301	0.0402	0.03515	0.00714	0.1196	0.1156	0.1176
5%PVA + 2%Alg + 5%HAp	0.0297	0.0259	0.0278	0.00269	0.1063	0.0943	0.1003
Tri-layered combination	0.029	0.0267	0.02785	0.00163			

The plot graph for the compression test results of the three separated layers and the joined tri-layered scaffold is shown in **Figure 6-21**. Among the three layers, with the same thickness for separated tests, the superficial zone exhibited the highest compressive Young's modulus, averaging 0.0378 MPa, suggesting superior resistance to deformation under compressive load, consistent with its functional role in resisting shear forces in native articular cartilage. In contrast, the middle and deep layers demonstrated slightly lower compressive moduli, which can be attributed to their distinct compositions. Specifically, these layers contained a lower proportion of PVA and a higher content of alginate and hydroxyapatite (HAp), materials selected to replicate zone-specific biomechanical characteristics of native cartilage.

Overall, the results form a smooth gradient of decreasing compressive strength from the superficial to the deep layers. This is attributed to the consistent and same thickness of all three separated layers during fabrication, which also influences the compression values. In a more biomimetic design, however, the tri-layered chondral scaffold should ideally incorporate the superficial, middle, and deep layers in a thickness ratio of approximately

10%:60%:30%, respectively. This variation in layer thickness is expected to affect the overall mechanical performance; for instance, a thinner superficial layer may retain higher tensile strength and ensure structural integrity under compressive loads. In the joined tri-layered construct, the mineralised deep layer, positioned at the bottom, is intended to provide the primary resistance to compressive forces, mimicking the supportive role of the subchondral region in native osteochondral tissue.

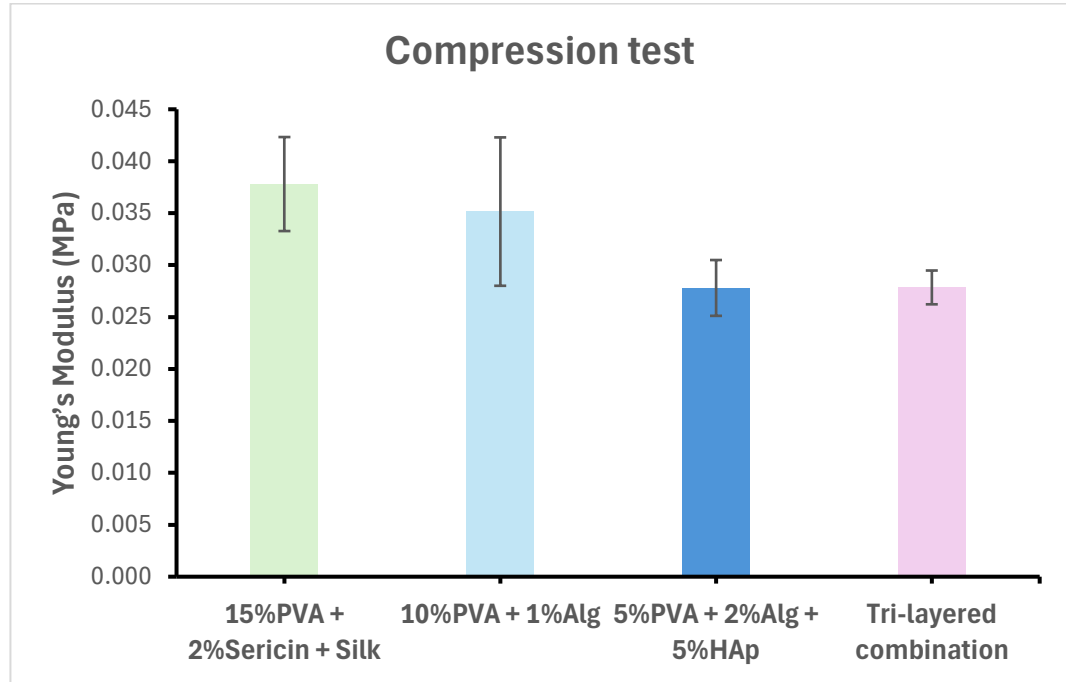


Figure 6-21 Graph illustrating the compression test results for three individual layers of similar thickness and the combined tri-layered scaffold fabricated through sequential layering.

As presented in **Figure 6-22**, the tensile strength was enhanced by the addition and composite of PVA and alginate materials. The freeze-thawed method created a more interconnected structure, resulting in the PVA-alginate composite middle layer hydrogel exhibiting the highest tensile strength. Although there was no significant difference between the three layers, this ensures the integration of the entire structure at the weight-bearing site. The scaffold is expected to maintain its structural integrity even under twisting forces, such as those experienced during knee movement.

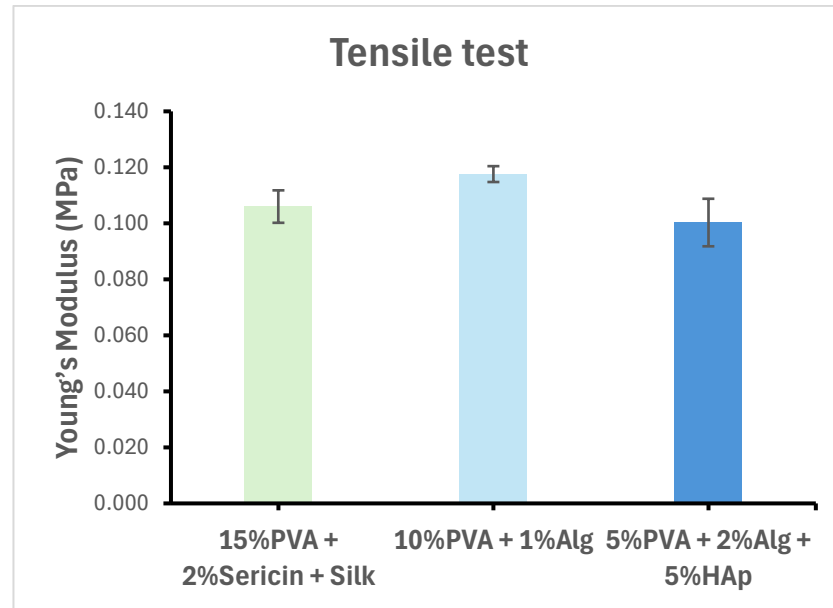


Figure 6-22 Graph depicting the tensile test results for three separated layers of similar thickness.

Native human articular cartilage exhibits a compressive Young's modulus ranging from 0.2 to 9.8 MPa (from the superficial to deep zones) and an overall tensile Young's modulus of 5–10 MPa, depending on the specific zone and testing conditions.[10] Compared to these values, the tri-layered hydrogel scaffold demonstrates a lower compressive modulus (~ 0.027 MPa) and tensile modulus (~ 0.1 MPa). While these values are lower than those of native cartilage, the scaffold's gradient structure and intermediate mechanical properties provide a biomimetic approach to stress distribution and tissue integration.

Admittedly, it is challenging for polymeric materials to achieve high stiffness without compromising their ability to support cell growth. However, further optimisation of material composition, such as crosslinking density, reinforcing agents, and pore architecture, including pore size and interconnectivity, warrants deeper investigation. These strategies could help develop scaffolds with mechanical properties that more closely resemble those of native cartilage while maintaining a favourable environment for cell attachment and proliferation.

Moreover, the scaffold's ability to retain structural integrity under torsional forces suggests promising potential for functional integration in dynamic environments, such as the knee joint. To comprehensively evaluate its suitability for such applications,

additional mechanical characterisation is necessary. This should include shear and rheological testing to assess parameters such as shear modulus, viscoelastic behaviour, and resistance to dynamic loading.[88]

6.4 Summary

The physical characterisation results, including SEM morphology, swelling tests, and degradation studies, provide valuable insights into the structure and performance of the three separated layers and the combined tri-layered chondral scaffold designed in this thesis. The SEM images reveal the overall structure of the tri-layered scaffold, showcasing its biomimetic design. The superficial zone exhibits a fibrous morphology, while the middle and deep layers demonstrate a gradient porous structure. This design closely mimics the zonal organisation of native cartilage.

The swelling and degradation tests assess the correlation between crosslinking densities and hydrogel properties, while mechanical tests confirm the potential of the tri-layered scaffold to maintain structural integration as a functional unit at the defect site without delamination.

In summary, the physical characterisations highlighted the critical features of the tri-layered construct cross-section. They confirmed the feasibility of incorporating aligned fibrous layers through the direct integration of silk fibres, while maintaining overall structural integrity and achieving smooth interfacial transitions between layers. Prospectively, to further optimise fabrication and meet more precise biomimetic requirements, the application of advanced manufacturing techniques is recommended. Additionally, further investigation is warranted into the effects of crosslinking density on tissue regrowth and long-term functional performance, which remains a key gap in the current field.

Chapter 7 *In vitro* Chondral Tissue Regeneration using Human Mesenchymal Stem Cells

Biological assessment was conducted to evaluate the attachment and proliferation of BMSCs on the scaffold, as well as to assess cartilage formation through histological staining.

7.1 Overview

This chapter presents the biological assessments of the fabricated hydrogel samples described in Chapter 5, utilising MTT assay and biological staining to assess their properties. The tri-layered scaffold is highlighted for its ability to promote cell proliferation by MTT assay and chondrogenesis histological analysis. These findings underscore the scaffold's suitability for tissue engineering applications, particularly in cartilage regeneration.

7.2 Biological Assessments and Methods

Cells: human Bone Marrow Mesenchymal Stem Cell (BMSCs)

7.2.1 Sterilisation of hydrogels

For clinical applications, complete removal of contaminants is essential to prevent bacterial growth on hydrogels, which is crucial for successful cell regeneration. In cell-based biological assessments, hydrogel samples used in this chapter must meet sterilisation standards and remain free from contamination. The sterilisation protocol was adapted from the literature [89-91], is outlined below and illustrated in **Figure 7-1**. The entire procedure is ideally conducted in a biosafety cabinet to minimise the risk of contamination.

1. Pre-sterilisation treatment (optional UV irradiation): UV irradiation may be applied as a pre-treatment for powder-form materials used in hydrogel fabrication. However, it is important to verify whether UV irradiation affects the properties of the material and triggers the material. In this project, the selected material powders were not affected or triggered by UV exposure. Therefore, as a pre-treatment, all powder

materials were placed in a fume hood and exposed to UV light for 30 min before being used in hydrogel fabrication.

2. After fabrication, hydrogel samples remained in the well plate, maintaining a thickness of no more than 3 mm for the subsequent cell seeding and biological testing.
3. Ethanol immersion steps: The primary terminal sterilisation step involved ethanol disinfection to eliminate bacterial contamination. This step is designed to eliminate bacterial contamination and is applicable to most hydrogel types.
 - The well plates containing hydrogel samples were placed in the fume hood.
 - 70–80% ethanol was sprayed directly onto each well to effectively kill microbes.
 - Ensure each hydrogel sample was fully immersed in ethanol and left to stand for 30 minutes.
4. Post-sterilisation washing: Since the hydrogel/scaffold is designed for cell culture applications, removing residual ethanol is crucial.
 - Ethanol removal: Following ethanol disinfection, autoclaved 1×PBS was added to each well, ensuring that the hydrogel samples were fully covered. The samples were left for 5 minutes to allow ethanol diffusion.
 - PBS washing: The ethanol-containing PBS was aspirated, and the samples were washed three times with fresh PBS, with gentle shaking to aid ethanol removal.
 - Afterward, a final wash was performed using autoclaved Milli-Q water. All handling steps were performed under sterile conditions such as inside a fume hood using sterile pipettes.
5. Post-washing handling: After ethanol disinfection, UV irradiation was used as an additional sterilisation step. However, its effectiveness was limited by hydrogel thickness, as reduced transmission decreased sterilisation efficiency. UV irradiation alone was not sufficient for terminal sterilisation and was used as a supplementary step rather than a replacement for ethanol washing.
6. Finally, the sterilised hydrogel samples were stored with a small amount of autoclaved Milli-Q water at 4°C or kept in the sterilised well plate within the fume hood. Samples were maintained under sterile conditions until they were used for biological studies and cell seeding.

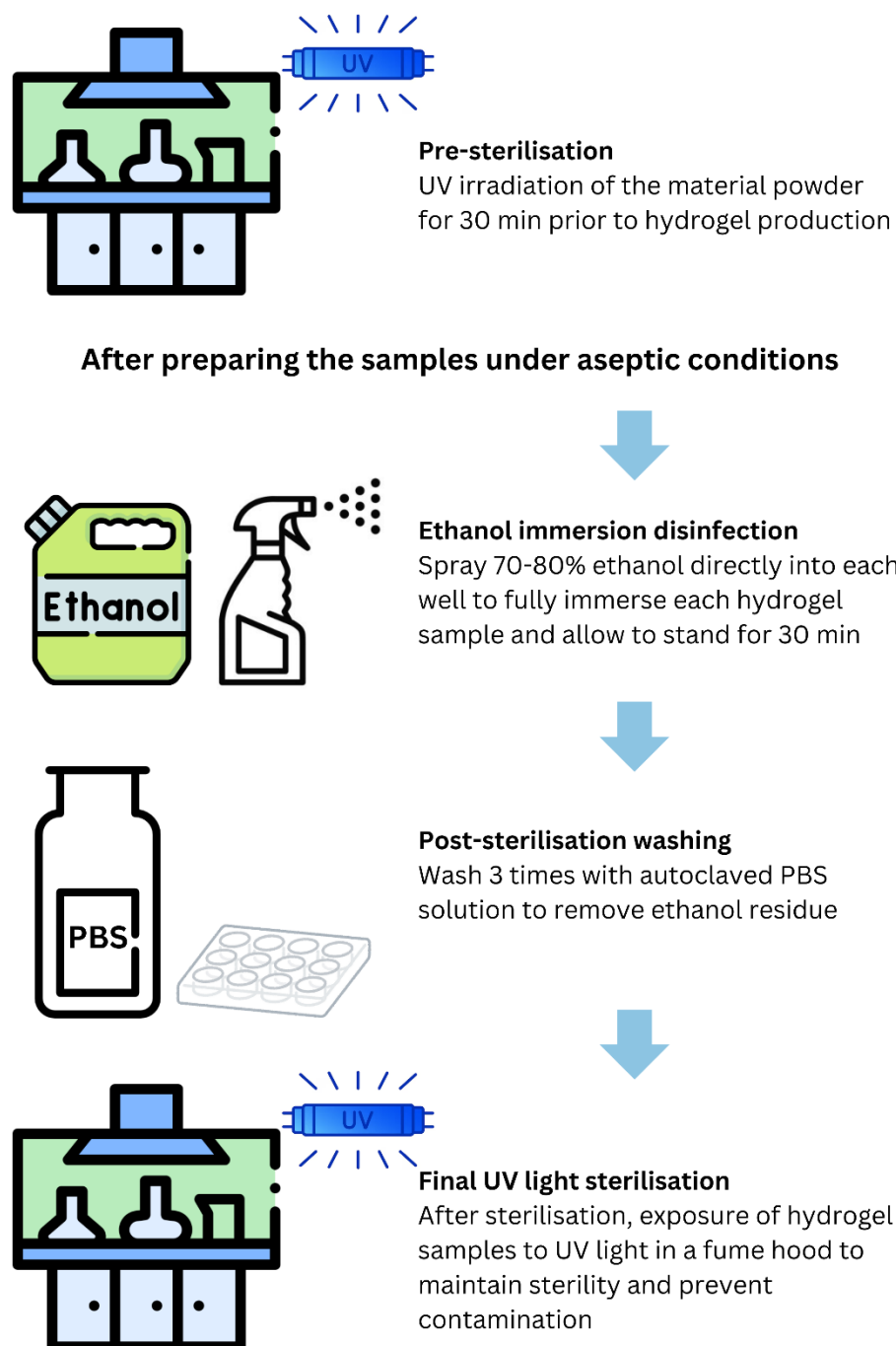


Figure 7-1 Flowchart of the sterilisation protocol for hydrogel samples before biological assessment.

Sterilisation procedures are essential to prevent contamination during scaffold fabrication and subsequent biological evaluation. Based on qualitative visual analysis, no significant morphological changes were observed in the silk fibroin fibres after undergoing sterilisation processes, including degumming, dry autoclaving, and ethanol treatment. This indicates that these methods are compatible with preserving the structural integrity

of the silk fibres, which were incorporated into this project primarily to form an aligned fibrous architecture.

Additionally, ethanol treatment was necessary for disinfecting the fabricated hydrogel scaffolds prior to *in vitro* cell culture testing. No visible structural damage to the hydrogel was observed following ethanol exposure, suggesting the process is suitable for hydrogel sterilisation. Proper removal of residual ethanol remains critical to prevent cytotoxic effects and to ensure accurate biological assessment. Overall, these sterilisation and preparation steps are fundamental for preserving scaffold quality and functionality in tissue engineering applications.

7.2.2 Cell seeding and MTT assay

- Objective: The MTT assay was conducted to evaluate the metabolic activity of bone marrow stromal cells (BMSCs) to assess cell viability and proliferation on the scaffold from day 4 to day 7.
- Cell density: 15,000 cells per sample/well
- Samples: Five sample groups with 4 replicates in each group (n=4) were prepared via the 48-well plate as the mould, with consistent thickness among a group and with approximately 2 mm thickness of the hydrogel samples.

A cell suspension was prepared, and 15,000 cells were seeded onto the surface of each hydrogel well. Two wells without samples were set as controls. Two wells without added samples served as the control group. After seeding, the cells were allowed to adhere for 1 hour, followed by the addition of additional medium. Subsequently, DMEM medium containing 10% foetal bovine serum (FBS) was added to the seeded cell samples, and the culture plates were incubated at 37°C and 5% CO₂. MTT assays were performed at designated time points, day 4 and day 7.

At each time point (day 4 and day 7), the culture medium was removed from all wells and replaced with 20 µL of 5mg/mL 3-(4,5-Dimethylthiazol-2-yl)-2,5-diphenyltetrazolium bromide (MTT) solution and 200 µL fresh DMEM culture medium, incubate at 37°C, 5% CO₂ for 3-4 hours. After incubation, the hydrogel scaffolds exhibited varying extents of purple colour, indicating the formation of formazan crystals inside viable cells, as shown

in **Figure 7-2**. Afterwards, the MTT solution was carefully removed without disturbing the hydrogel samples. 200 μ L of DMSO was added to each well to dissolve the formazan crystals, and the whole plate was gently shaken for 10 min to allow the complete dissolution.

For absorbance measurement, the hydrogel samples were carefully removed using tweezers to avoid bubble formation, and any visible debris in the wells was removed. Finally, the absorbance of the coloured solution was measured at 570 nm using a spectrophotometer.

Absorbance values at day 4 and day 7 were collected and analysed according to the procedures described above to compare the differences between groups in assessing cell viability, properties of materials that promote cell proliferation, and trends in cell growth from day 4 to day 7.

Cell viability (level of cell proliferation) was quantified using the formula:

$$\text{Level of cell proliferation} = \frac{ab_{\text{sample}}}{ab_{\text{blank}}} \times 100$$

Where ab_{sample} and ab_{blank} represent absorbance values of hydrogel-cultured cells and blank medium, respectively.

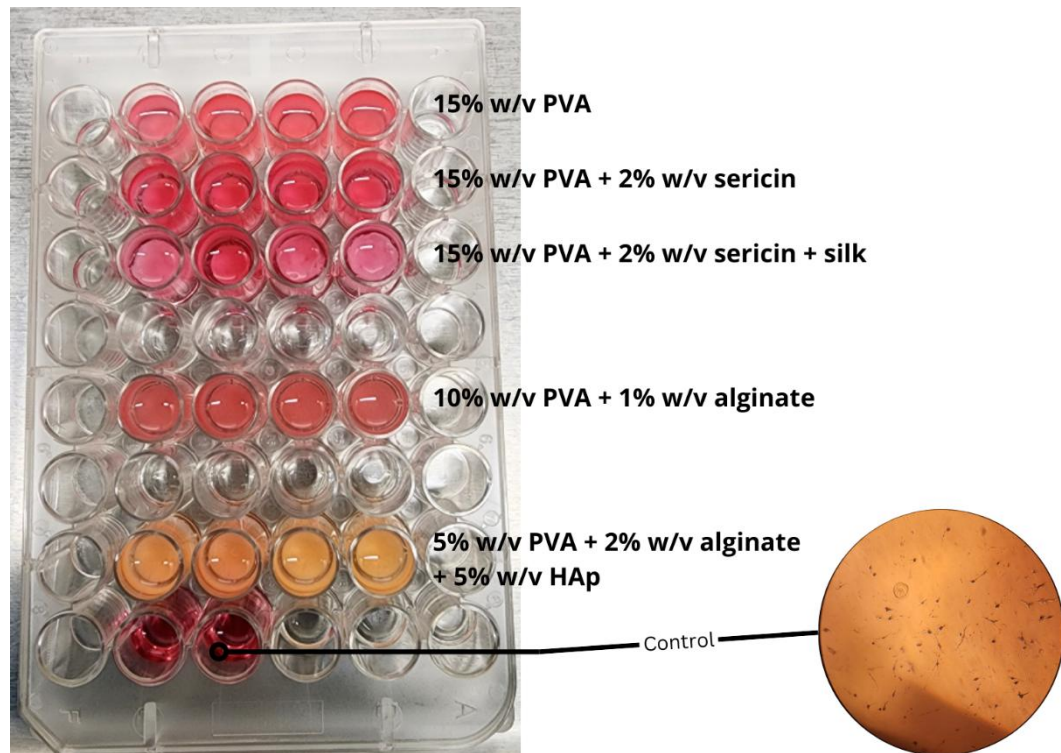


Figure 7-2 MTT assay photo shows hydrogel samples in each tested well, with a visible purple colouration after incubation, indicating cell viability.

7.2.3 Chondrogenesis Histology

- Objective: To assess cell attachment, proliferation, and extracellular matrix (ECM) deposition on the scaffold through histological staining.
- Cell density: 75,000 cells per sample/well
- Samples: Four sample groups with 4 replicates in each group ($n=4$), including three separated individual layer groups and one joined tri-layered hydrogel, were prepared via the 24-well plate as the mould.
- Media used: StemMACS™ ChondroDiff Medium, a differentiation medium for generating chondrocytes from human mesenchymal stromal cells (MSCs), with medium replacement every three days.

After cell seeding, the samples were incubated for 14 days. The culture medium was removed, and samples were gently rinsed with PBS. The cell-seeded hydrogels were then fixed with 10% formalin at room temperature for 6 hours. After fixation, samples were rinsed with PBS 3 times to remove excess fixative.

Then, samples were dehydrated using a graded ethanol series: 70%, 80%, 95% and 100%. For embedding and sectioning, the dehydrated samples were first embedded in paraffin wax. Thin sections (~5 µm thick) were then obtained using a microtome to expose the cross-section of the hydrogel samples. The sections were mounted onto glass slides and air-dried before staining.

In this project, histological staining, two staining techniques, Hematoxylin and Eosin (H&E) and Toluidine Blue Staining, were applied to assess the composition of cell-seeded hydrogel samples. Specifically, H&E Staining was used to evaluate the general tissue morphology, cellularity, and distribution of the scaffold components. And toluidine blue staining is particularly effective in identifying cartilage matrix and cell morphology, especially for detecting proteoglycans and sulphated GAGs.

7.3 Results and Discussion

7.3.1 Cell seeding and MTT

The MTT assay was performed to evaluate cell viability and metabolic activity on hydrogel samples. The overall results, summarised in **Figure 7-3**, illustrate cell proliferation levels after 4 and 7 days of incubation with different hydrogel formulations. The data indicate that BMSCs seeded on hydrogel samples exhibited higher viability compared to the control group (without hydrogel). The absorbance values, which reflect the metabolic reduction of MTT to formazan by viable cells, along with the observed increase in cell proliferation from day 4 to day 7, suggest that the hydrogels developed in this study effectively supported cell attachment and growth over time.

The absorbance values obtained from the MTT assay were used to assess cell viability. To account for background interference, the average absorbance reading of the no-cell control wells, which consisted only of the clear plastic at the bottom of the well plate without cells, was subtracted from each sample reading. This correction ensures that the final absorbance values more accurately reflect the metabolic activity of viable cells rather than background absorbance from the plate material itself.

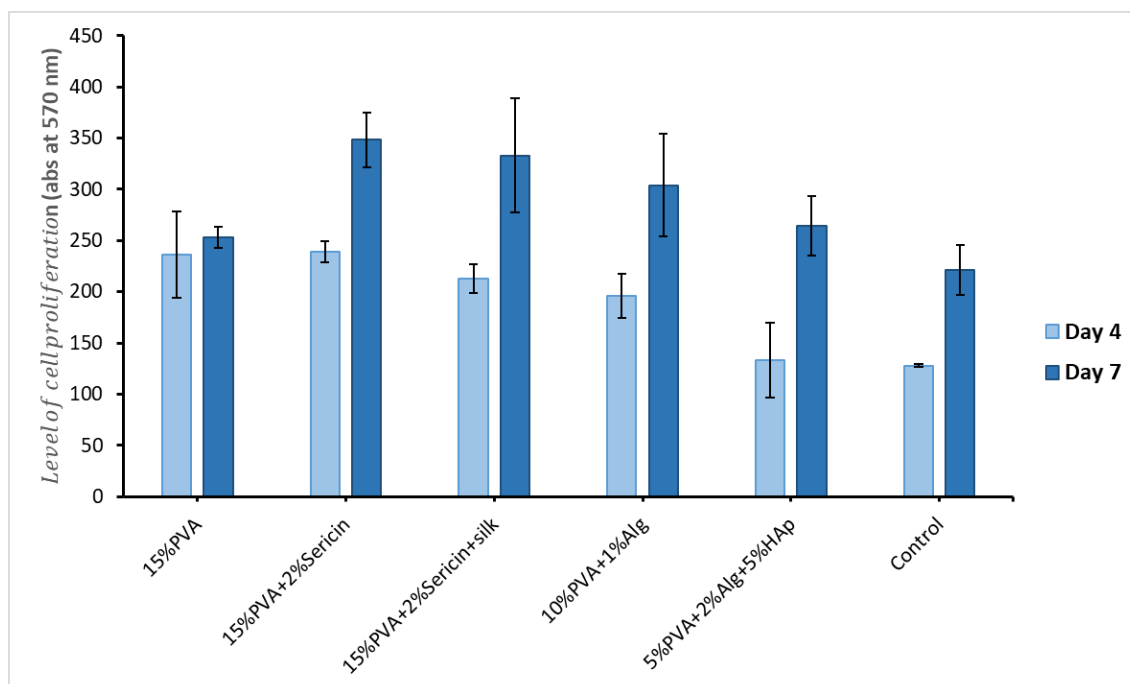


Figure 7-3 Overview: Comparison of cell proliferation levels among different hydrogel formulations, including 15% PVA, 15% PVA + 2% sericin with and without silk incorporation, 10% PVA + 1% alginate composite hydrogel, and 5% PVA + 2% alginate + 5% HAp mineralised hydrogel, on day 4 and day 7.

A key finding from these results is the positive effect of silk sericin, a glue-like protein derived from silk cocoons, on BMSC proliferation. As shown in **Figure 7-4**, PVA hydrogels supplemented with 2% w/v sericin exhibited significantly higher cell viability compared to pure PVA hydrogels. This is particularly evident in the comparison between the 15% PVA and 15% PVA + 2% sericin groups, where the concentration of PVA was fixed to isolate the effect of sericin addition. Furthermore, no significant difference in cell viability was observed between PVA-sericin hydrogels with and without the incorporation of silk fibres within the hydrogel matrix. This suggests that the addition of sericin plays a critical role in enhancing cell viability.

A comparative analysis confirmed that the addition of sericin led to a noticeable increase in cell proliferation from day 4 to day 7. In contrast, pure PVA control exhibited only minimal cell growth over the same period, indicating limited bioactivity and a reduced capacity to promote cell proliferation. And this confirmed the role of sericin addition as an independent bioactive factor promoting BMSC proliferation.

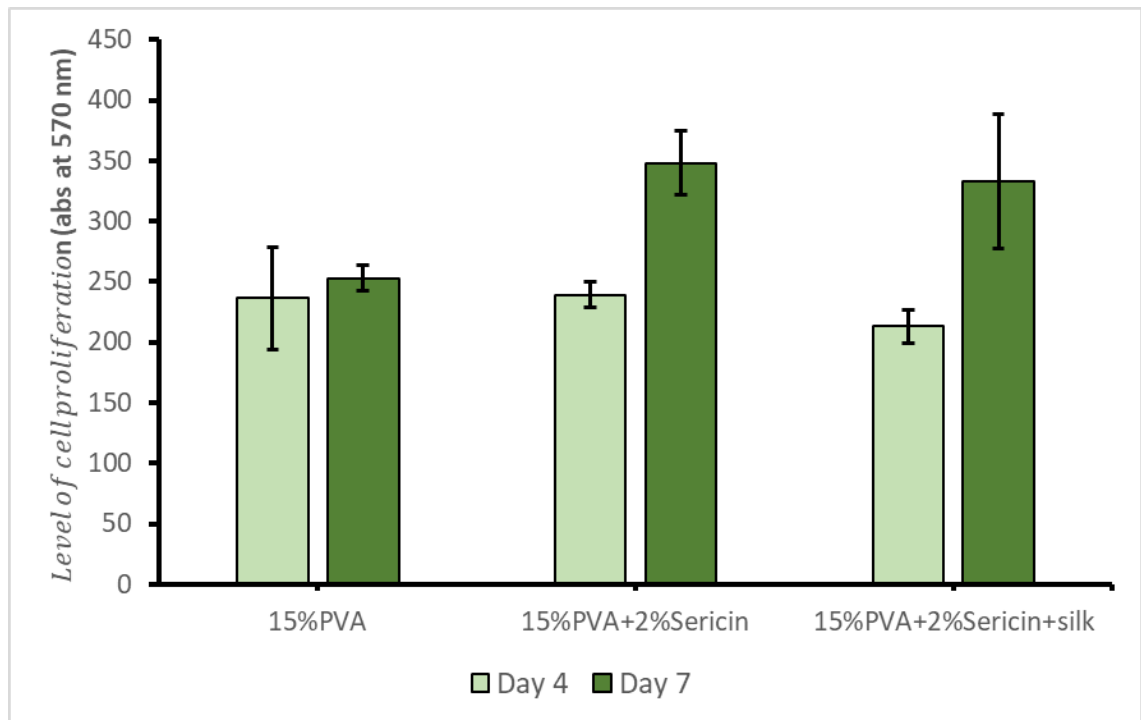


Figure 7-4 Comparison: The impact of sericin incorporation on cell proliferation in 15% w/v PVA-based hydrogels, highlighting increased cell growth from day 4 to day 7.

The MTT results further demonstrate the proliferation trends across the three distinct hydrogel layers designed in this study (**Figure 7-5**). The middle-layer hydrogel exhibited lower cell proliferation than the superficial sericin-PVA hydrogel, while the deep-layer hydrogel showed the least proliferation. This resulted in a gradient-like proliferation pattern, resembling the native cell density distribution across the zones of articular cartilage. The increasing cell viability from the deep to the superficial zone suggests that the material composition and concentration of these hydrogel layers create a favourable microenvironment for cartilage tissue engineering applications.

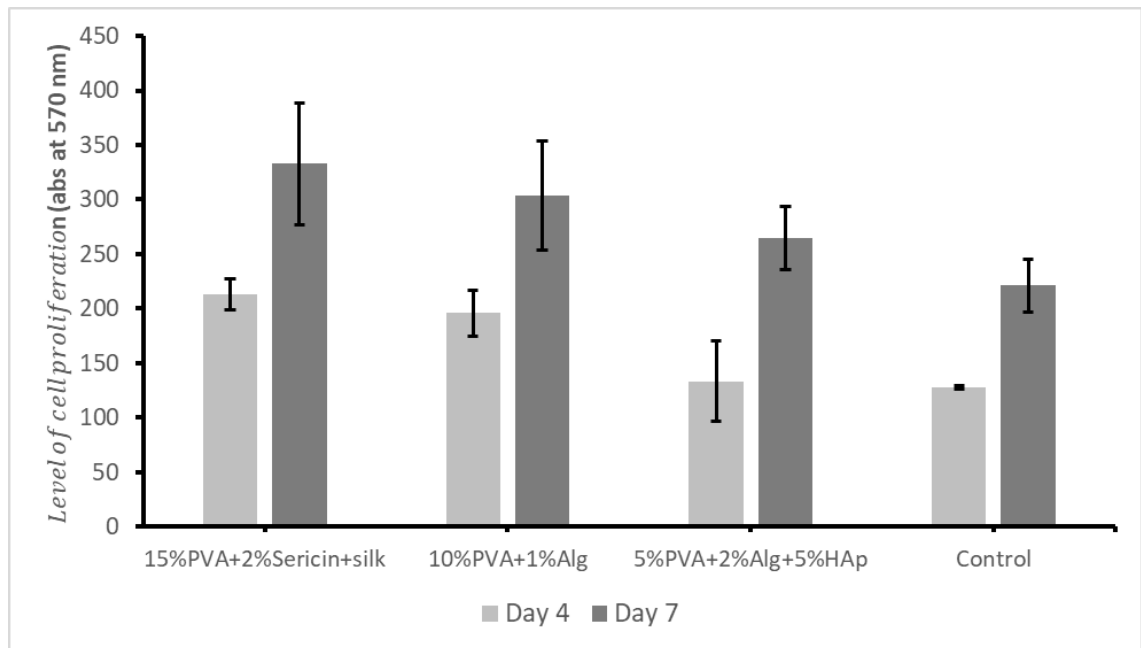


Figure 7-5 Designed Hydrogel Layers: Comparison of cell viability across the three hydrogel layers, indicating a zonal proliferation trend consistent with native cartilage structure.

In summary, the comparison of various hydrogel formulations highlights the beneficial role of silk sericin in promoting BMSC proliferation, with significant improvements observed in sericin-incorporated hydrogels with or without silk fibres. The data and graphical results indicate that when alginate and sericin are separately composited with inert polyvinyl alcohol (PVA) material, they can both promote the proliferation of bone marrow mesenchymal stem cells (BMSCs), although this may be achieved through different mechanisms. Notably, the hydrogel layers exhibited a zonal pattern of cell proliferation, mimicking the natural cartilage structure, where cell density decreases from the superficial to the deep zone.[92] These findings suggest that the designed hydrogels provide a favourable microenvironment for cell adhesion and growth, making them promising candidates for cartilage tissue engineering. The MTT results further confirm that the hydrogel composition supports zone-specific cell proliferation, aligning with the native characteristics of articular cartilage.

A limitation of the current experimental design was the absence of no-cell controls. While preliminary validation tests confirmed that individual components (PVA, sericin, and alginate) exhibited negligible absorbance at 570 nm (the measurement wavelength for the MTT assay), suggesting minimal background signal contribution from the hydrogel

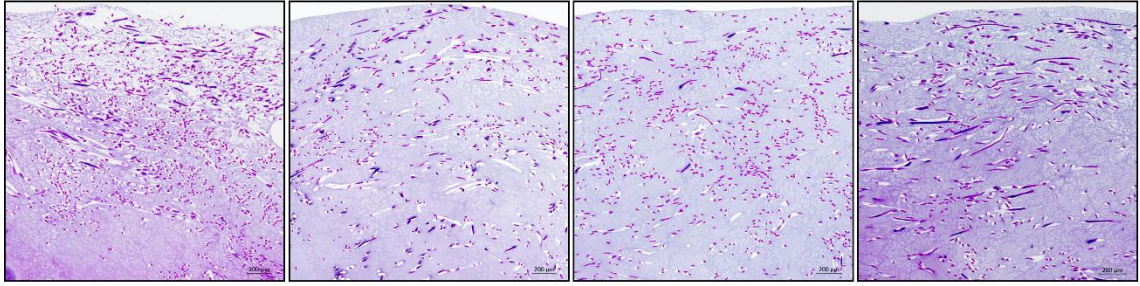
materials, future studies should incorporate no-cell controls to ensure comprehensive experimental validation.

7.3.2 Chondrogenesis Histology

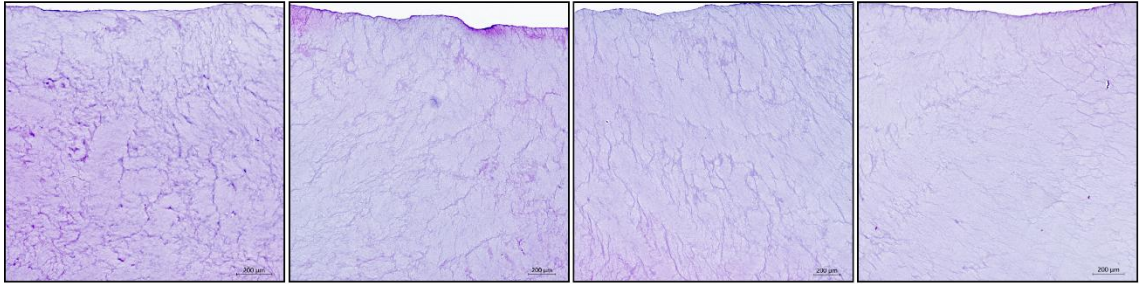
H&E staining was performed to assess the morphology, cell distribution, and integration of the cell-seeded scaffold. The results of the three distinct hydrogel layers, seeded with BMSCs for 14 days, are shown in **Figure 7-6**. Histological images revealed that cells were well distributed within the superficial silk-incorporated PVA layer. As hypothesised, the aligned silk fibres appeared to create micro-spaces within this layer, facilitating cell attachment, as evidenced by the dense clusters of purple-stained nuclei. In contrast, both the middle and deep hydrogel layers exhibited only a thin layer of cells on their surfaces, revealing that the porous architecture did not effectively support cell migration and ingrowth, possibly due to the limited pore sizes in these two hydrogel designs. However, the presence of adhered cells confirmed the ability of these layers to promote initial cell attachment.

In terms of cellular organisation, histological cross-sections of silk fibres incorporated into hydrogels showed a tendency for cells to align along horizontal directions. This observation supports the hypothesis that the fibrous structure can influence cellular alignment by guiding the cells along the fibre direction. In addition, stained sections showed that the tri-layered scaffolds maintained their structural integration throughout sectioning, staining, and preparation, indicating strong interfacial bonding between the layers.

Superficial layer (H&E)



Middle layer (H&E)



Deep layer (H&E)

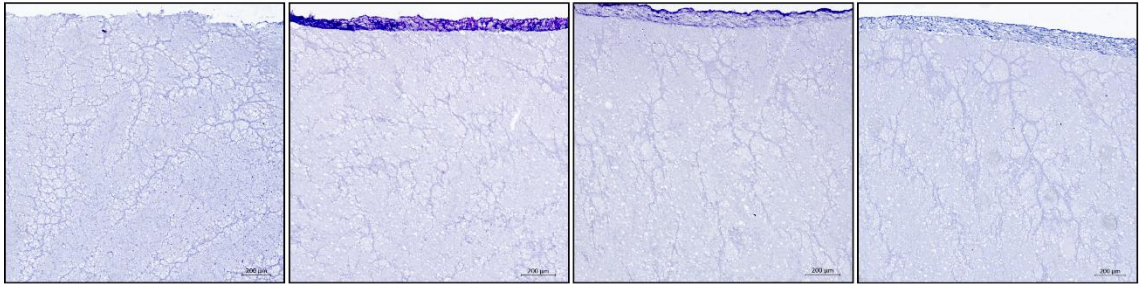
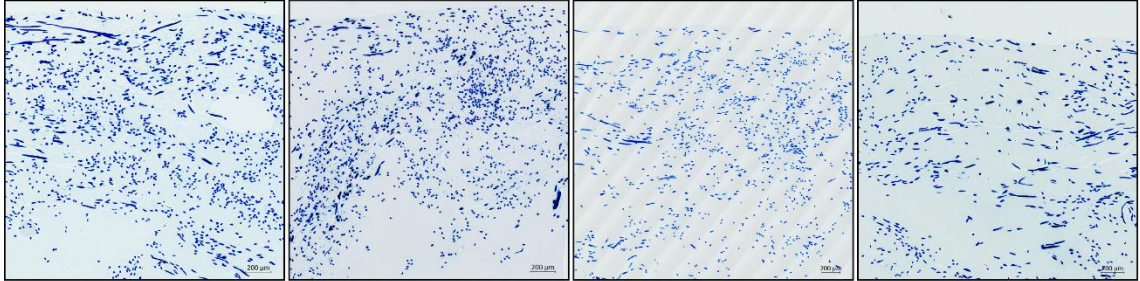


Figure 7-6 H&E-stained sections of the three separated hydrogel layers, indicating cell attachment, distribution, and ingrowth capacity across different layer concentration formulations.

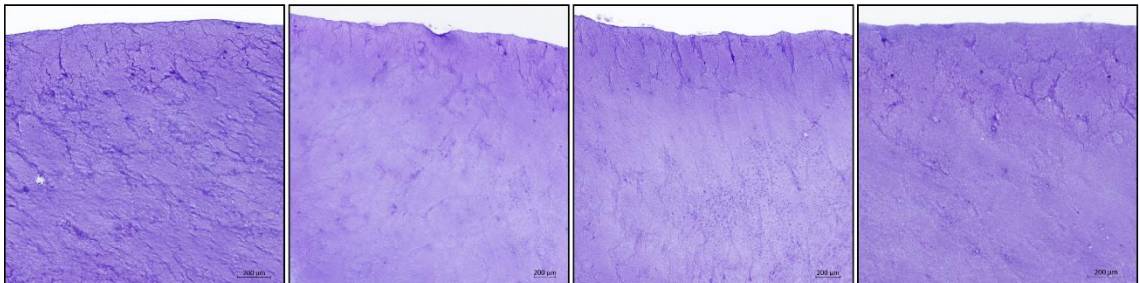
Toluidine blue staining was applied to evaluate the deposition of cartilage-specific extracellular matrix (ECM), particularly sulphated glycosaminoglycans (sGAGs), which are critical for cartilage regeneration. **Figure 7-7** illustrates the zonal variations observed with toluidine blue staining. The superficial PVA-based hydrogel containing sericin and aligned silk fibres displayed a pale background with less purple colour staining; however, like the H&E-stained images, the superficial layer exhibited a dense blue dot pattern. The middle and deep layers showed more intense toluidine blue staining, reflecting the material composition. Both the middle and deep layers contained calcium alginate as the hydrogel base, and toluidine blue staining revealed a strong purple colouration throughout these layers, possibly due to the affinity of alginate for the dye. As the zone depth

increased, the deep layer exhibited stronger staining intensity than both the middle and superficial layers, correlating with the mineral content in this region.

Superficial layer (Toluidine Blue)



Middle layer (Toluidine Blue)



Deep layer (Toluidine Blue)

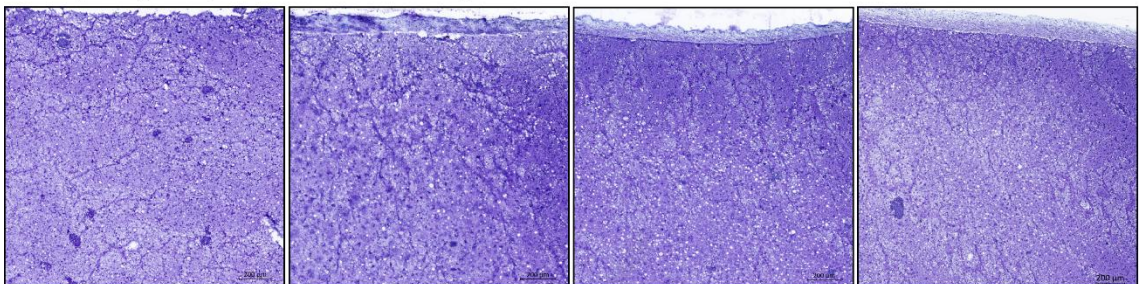
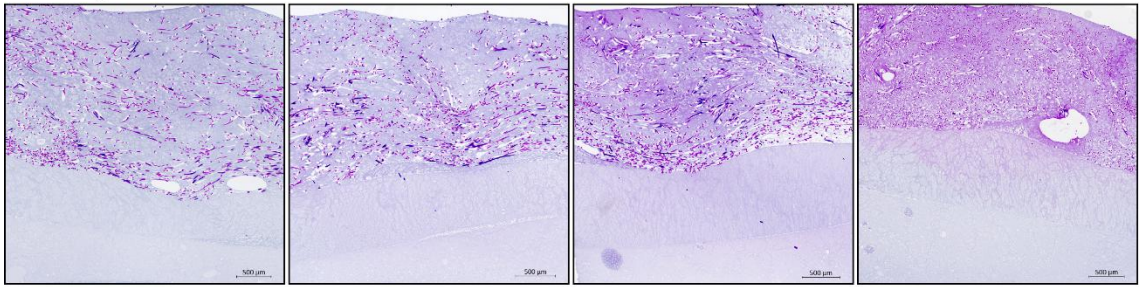


Figure 7-7 Toluidine blue-stained sections of the three separate hydrogel layers, indicating the cell growth and ingrowth capacity of each concentration group.

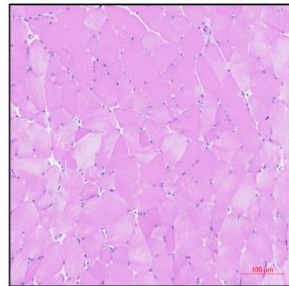
Figure 7-8 demonstrates histological staining of the cell-seeded tri-layered scaffold using H&E and toluidine blue staining, a comparison was made with mouse joint cartilage and a blank tri-layered scaffold (without cells). The results indicate that the superficial zone, where aligned silk fibres were applied and coated with 15% w/v PVA-sericin, provided some space for cell ingrowth. However, in the underlying middle and deep layers, cells were unable to penetrate deeper, which restricted the scaffold's function in tissue engineering. This limitation was primarily due to the small pore size and low porosity of the hydrogel in its hydrated state.

When compared with existing studies on the zonal structure of native cartilage and its corresponding cellular organisation,[93] the designed tri-layered scaffold demonstrated a comparable layer composition. Histological staining results confirmed that the hydrogel scaffold supported cell adhesion, proliferation, and the formation of cartilage-like layers, as evidenced by the characteristic staining patterns of H&E and toluidine blue. The incorporation of silk sericin and alginate appeared to enhance these properties, reinforcing the potential of hydrogel body for cartilage regeneration.

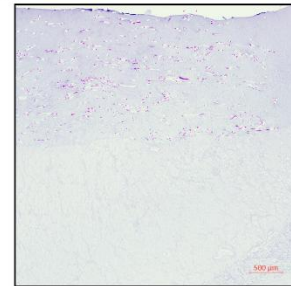
Tri-layered scaffold (H&E)



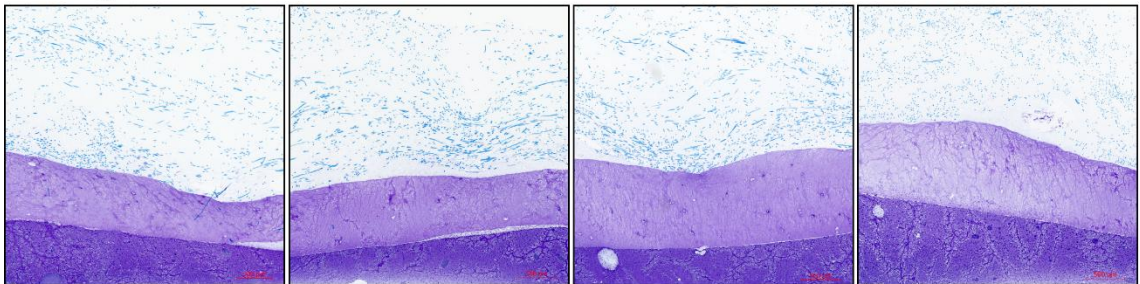
H&E stained joint model, surface (control):



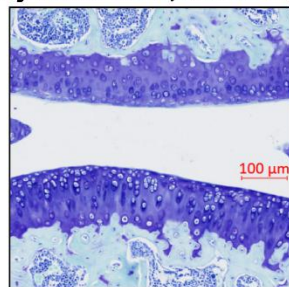
Blank:



Tri-layered scaffold (Toluidine Blue)



TB stained joint model, surface (control):



Blank:

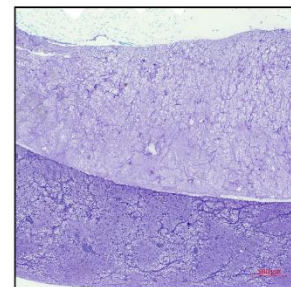


Figure 7-8 H&E and toluidine blue-stained images of the cell-seeded tri-layered scaffold, compared with mouse joint cartilage and a blank tri-layered scaffold (without cells).

In terms of scaffold integration and the tri-layered structure, beyond cell ingrowth and spreading in the superficial zone, a comparison was made between histological staining and SEM morphology. Notably, the SEM results presented in Chapter 6 have inherent

limitations due to the freeze-drying process required before imaging. The freeze-dried porous architecture formed by ice crystals may not accurately reflect the hydrated state of the scaffold or its tri-layered integration during actual use.

By comparing H&E and toluidine blue staining with SEM images, the transition between layers and distinct compositions were identified. **Figure 7-9** illustrates the comparison between the stained tri-layered scaffold and its corresponding fibrous and porous morphology observed in SEM. As hypothesised, the aligned fibrous superficial layer may provide more space for cell infiltration and migration.

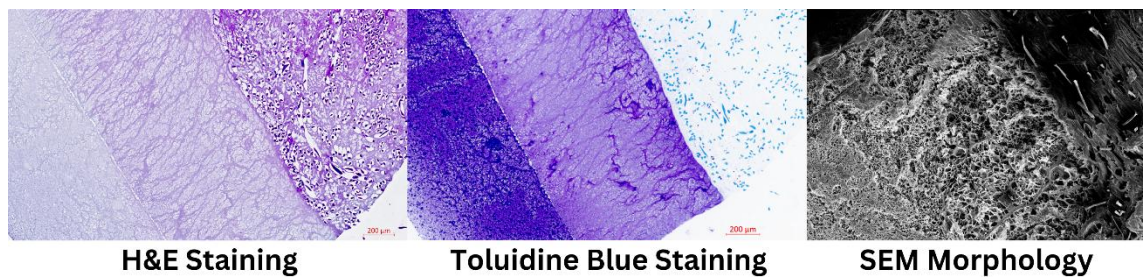


Figure 7-9 Staining and SEM image comparison reflecting tri-layered scaffold integration and structure.

The experimental results suggest that further optimisation of pore size is necessary to facilitate BMSCs migration and proliferation within the hydrogel. Insufficient pore size restricts nutrient transport and limits the scaffold's applicability in cartilage tissue engineering. Future studies should focus on optimising porosity while preserving mechanical stability to enhance functionality in cartilage repair.

To evaluate chondrogenic potential, toluidine blue staining was employed to detect glycosaminoglycans (GAGs), a major component of the cartilage extracellular matrix. However, a key limitation of this method is its lack of specificity, as toluidine blue can bind non-specifically to other acidic tissue components rather than exclusively to GAGs.[94] Consequently, its reliability as a definitive marker of chondrogenesis in this study is reduced.

For future optimisation, additional investigations should improve histological specificity. One critical improvement would be incorporating control groups of cells cultured without chondrogenic induction media to differentiate between spontaneous and induced GAG production. Furthermore, more specific staining techniques such as Alcian blue or

immunohistochemical staining for cartilage-specific markers (e.g., aggrecan or collagen type II) could provide more accurate assessments of chondrogenic differentiation.[95]

A key limitation of this experimental design was the absence of a non-chondrogenic media control group, which would have allowed for more comprehensive comparisons. Since this study primarily focused on scaffold optimisation rather than detailed chondrogenic characterisation, such controls were not included. Future work is expected to incorporate control groups for comparative analysis, including cells cultured in standard growth media (baseline control), cells in chondrogenic induction media (positive control), and cells in mixed differentiation media (to assess specificity). This approach will enable more definitive evaluation of GAGs production and staining specificity, strengthening the validity of chondrogenic assessments.

7.4 Summary

The biological assessment, including the MTT assay and histological staining, was conducted to evaluate the potential of the hydrogel material in promoting cell adhesion and proliferation.

The MTT assay demonstrated that cells successfully grew on the hydrogel surface, maintaining viability and proliferation over time. These findings suggest that the materials used in the tri-layered scaffold are biocompatible and non-toxic.

Histological staining further revealed that the incorporation of silk fibres facilitated cell attachment and distribution by creating micro-spaces between the aligned fibre structures. However, the pore size in the porous middle and deep layers appeared to restrict cell migration and ingrowth. To enhance cell infiltration, future optimisation strategies are supposed to focus on developing larger porous structures with sufficient porosities to support cell migration and promote effective cartilage tissue repair. Therefore, advanced technologies, such as additive manufacturing, are recommended for controlled hydrogel patterning and precise architectural design.

Chapter 8 Conclusion and Outlook

Conclusion, Optimisation, and Future Directions.

'For a theory to be considered scientific, it must be falsifiable.' ----- Popper's falsifiability principle

8.1 Conclusion of this project

This thesis demonstrates the potential of biomimetic scaffolds in addressing critical challenges in chondral and osteochondral tissue engineering by replicating the zonal properties of articular cartilage. The research systematically explored the design, fabrication, and evaluation of stratified cartilage scaffolds, integrating silk fibres and natural-synthetic composite polymers to repair cartilage defects and support functional cartilage zonal regeneration.

Key findings of this project include, first, the potential application of silk cocoon-extracted degummed silk fibroin fibres and silk sericin in tissue engineering. The alignment of silk fibres successfully mimicked the organised collagen fibre orientation in the superficial zone of cartilage. SEM imaging revealed that the integrated scaffold exhibits a distinct fibrous superficial layer, which then transitions into a porous hydrogel middle layer with a gradient distribution of pores extending into the deep layer. The deep regions contained mineralised components and denser pores, suitable for further applications in the construction of more complex osteochondral scaffolds. Physical characterisations, including swelling, degradation, and mechanical compression and tensile tests, demonstrated that the tri-layered chondral scaffold design exhibited closely matched swelling and degradation rates across all layers. Furthermore, the compression strength of the three layers was well-balanced, allowing the tri-layered scaffold to resist load-bearing applications without delamination.

The biological evaluations further supported the feasibility of this scaffold design. MTT assays confirmed that sericin-containing composite hydrogels were non-toxic and supported cell viability and proliferation. These findings validate the feasibility of stratified scaffold designs for cartilage tissue engineering. Preliminary histological staining evaluations confirmed that both individual layers and the tri-layered scaffold

promoted cell adhesion to the hydrogel while maintaining structural integrity under physiological conditions. The stratified scaffold effectively facilitated seamless integration between zonal cartilage layers, reducing the risk of mechanical mismatch and enhancing biological performance.

Despite these promising outcomes, several limitations remain. The mould-casting method constrained the hydrogel scaffold design, allowing only sequential layering without precise control over pore size and spatial distribution, which are crucial for modifying scaffold properties for targeted tissue applications. Additionally, the limited pore structure restricted cell migration and ingrowth within the hydrogel, ultimately reducing its effectiveness in supporting cartilage repair. Another challenge was the difference between the freeze-dried and hydrated states of the scaffold. The porous architecture observed under SEM imaging appeared larger than what is likely present in the wet-state hydrogel, potentially affecting the actual cell infiltration and nutrient diffusion.

Regardless, MTT assay confirmed the non-toxic nature of the scaffold materials associated with concentration formulations, and critical limitations in experimental design warrant discussion. The absence of no-cell controls in MTT analysis, despite preliminary validation showing negligible background absorbance at 570 nm, suggests the need for more rigorous validation in future studies. Histological evaluation using toluidine blue staining revealed successful cell attachment to scaffold surfaces but poor penetration into the hydrogel matrix, particularly in the tri-layered structure. This limited cellular migration likely contributed to the reduced proliferation observed in PCR analysis, potentially confounding gene expression results.

The current findings highlight two key optimisation requirements: 1) architectural modification to improve pore size for enhanced cell infiltration, and 2) methodological improvements for more reliable characterisation. Specifically, regarding histological assessment, the non-specific nature of toluidine blue staining and lack of non-chondrogenic controls limit definitive conclusions about chondrogenic differentiation. For future research, three critical improvements should be implemented, including scaffold redesign to optimise pore architecture while maintaining mechanical stability, and comprehensive controls for comparative analysis: no-cell controls for MTT assays,

non-induced cell controls for histological analysis, standard growth media controls for PCR studies.

Despite these challenges, this study lays the foundation for future improvements in scaffold fabrication, particularly in refining pore architecture and enhancing cellular integration for more effective cartilage regeneration. In addition, further studies will explore clinical applications in small and large animal models with the ultimate goal of human trials. In conclusion, the outcomes of this study highlight the potential of biomimetic scaffolds in restoring musculoskeletal function, offering promising implications for treating chondral and osteochondral defects and degenerative conditions such as osteoarthritis.

8.2 Future perspectives

This thesis introduces the zonal functions of articular cartilage and provides an overview of multizonal scaffold designs from conceptualization to fabrication. By understanding the natural mechanisms of tissue development and formation, researchers can further advance the fabrication of multilayered structures. While the multizonal scaffolding strategy shows great potential, additional studies are necessary to refine scaffold properties and ensure successful clinical translation.

A critical area for further exploration in this study is the biomechanical properties of cartilage zones, particularly the transition between soft cartilage tissue and the tough bone layer. Ensuring biomechanical compatibility and seamless integration across interfaces and regions remains a key challenge. Given that cartilage defects primarily occur in weight-bearing joints like the knee, future research suggests designing scaffolds that can both support body weight after implantation and promote regeneration of surrounding tissues. This could involve the development of scaffolds with large or irregular pores in the bony regions to enhance mechanical stability and facilitate cell infiltration.[96; 97]

Advanced materials and innovative pore designs will play a crucial role in achieving these objectives. The fabrication of biomimetic structures resembling the cartilage layer could be significantly enhanced by precise control techniques such as bioprinting or direct writing electrospinning.[98-101] Subchondral spongy bone, in particular, could be

fabricated using computer-aided design (CAD) and scanning software, guided by anatomical and biomedical principles. This approach presents a promising direction for improving our understanding of native tissue structures and developing more effective treatment strategies. These advancements could lead to significant improvements in the structural and functional repair of engineered cartilage and tissue interfaces.

Additionally, simulating microfibrils in different regions represents an emerging approach in cartilage tissue engineering. Techniques such as electrospinning or wet-spinning can be employed to guide the alignment of printed fibres, mimicking the natural orientation of collagen fibres within each cartilage zone.[102; 103] Drawing inspiration from the textile industry, where fibres are woven into varying patterns, the tendon-bone interface (**Figure 8-1**) could be an ideal site for exploring fibre manipulation to enhance mechanical strength and tensile properties. In particular, fibrocartilage soft-hard interface may be well-suited for direct silk fibre incorporation strategies, as the arrangement of silk fibres can more closely resemble the native thick collagen fibres.[104; 105]

Building on the direct incorporation of silkworm silk fibres, silk fibroin fibres could also be adapted for additional tissue engineering applications, such as replicating the structure and function of the intervertebral disc.[21] As shown in **Figure 8-2**, preliminary experiments have already demonstrated the feasibility of using silk fibres to function as the annulus fibrosus in intervertebral disc tissue engineering, highlighting their potential for further development in this field.

Moreover, future studies could also investigate the potential of silk derived from other species, such as spiders. Spider silk, renowned for its exceptional tensile strength and toughness compared to silkworm silk,[22; 106] could offer significant advantages for applications requiring enhanced durability and mechanical performance. This innovation could pave the way for fibre-based tissue engineering strategies, with potential applications in both implantable and wearable scaffolds.

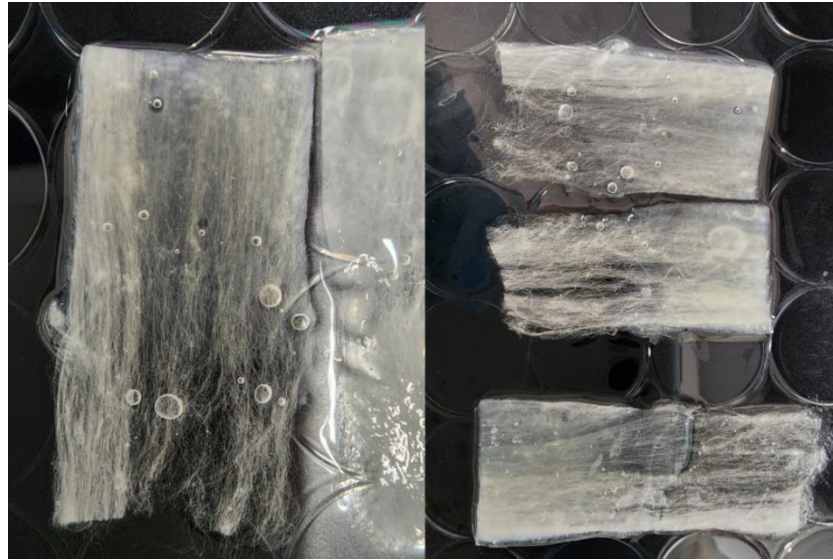


Figure 8-1 Tendon-bone model which can further apply textile technique to modify the transitional fibrocartilage zones.

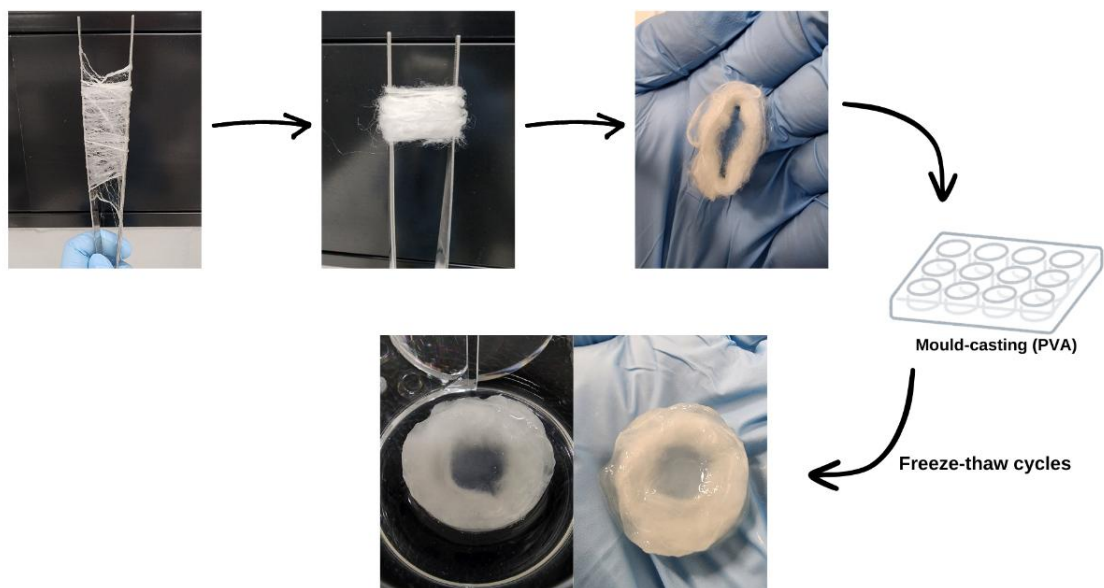


Figure 8-2 Future application of silk fibres in tissue engineering for musculoskeletal disease (intervertebral disc)

Bibliography

- [1] Zhou, L., Gijm, V. O., Malda, J., Stoddart, M. J., Lai, Y., Richards, R. G., Ki-Wai Ho, K., & Qin, L. (2020). Innovative Tissue-Engineered Strategies for Osteochondral Defect Repair and Regeneration: Current Progress and Challenges. *Advanced Healthcare Materials*, 9(23), 2001008. <https://www.ncbi.nlm.nih.gov/pubmed/33103381>
- [2] Frassica, M. T., & Grunlan, M. A. (2020). Perspectives on Synthetic Materials to Guide Tissue Regeneration for Osteochondral Defect Repair. *ACS Biomaterials Science & Engineering*, 6(8), 4324-4336. <https://doi.org/10.1021/acsbiomaterials.0c00753>
- [3] Yan, L. P., Oliveira, J. M., Oliveira, A. L., & Reis, R. L. (2015). Current Concepts and Challenges in Osteochondral Tissue Engineering and Regenerative Medicine. *ACS Biomaterials Science & Engineering*, 1(4), 183-200. <https://doi.org/10.1021/ab500038y>
- [4] Tamaddon, M., Wang, L., Liu, Z., & Liu, C. (2018). Osteochondral tissue repair in osteoarthritic joints: clinical challenges and opportunities in tissue engineering. *Bio-Design and Manufacturing*, 1(2), 101-114. <https://doi.org/10.1007/s42242-018-0015-0>
- [5] Wei, W., & Dai, H. (2021). Articular cartilage and osteochondral tissue engineering techniques: Recent advances and challenges. *Bioactive Materials*, 6(12), 4830-4855. <https://doi.org/10.1016/j.bioactmat.2021.05.011>
- [6] Urbanek, O., Kołbuk, D., & Wróbel, M. (2018). Articular cartilage: New directions and barriers of scaffolds development – review. *International Journal of Polymeric Materials and Polymeric Biomaterials*, 68(7), 396-410. <https://doi.org/10.1080/00914037.2018.1452224>
- [7] Paatela, T., Vasara, A., Nurmi, H., Kautiainen, H., & Kiviranta, I. (2020). Assessment of Cartilage Repair Quality With the International Cartilage Repair Society Score and the Oswestry Arthroscopy Score. *Journal of Orthopaedic Research*, 38(3), 555-562. <https://doi.org/10.1002/jor.24490>
- [8] Wasyleczko, M., Sikorska, W., & Chwojnowski, A. (2020). Review of Synthetic and Hybrid Scaffolds in Cartilage Tissue Engineering. *Membranes*, 10(11), 348. <https://doi.org/10.3390/membranes10110348>
- [9] Wang, Z., Le, H., Wang, Y., Liu, H., Li, Z., Yang, X., Wang, C., Ding, J., & Chen, X. (2022). Instructive cartilage regeneration modalities with advanced therapeutic implantations under abnormal conditions. *Bioactive Materials*, 11, 317-338. <https://doi.org/10.1016/j.bioactmat.2021.10.002>
- [10] Lin, X., Zhang, Y., Li, J., Oliver, B. G., Wang, B., Li, H., Yong, K.-T., & Li, J. J. (2025). Biomimetic multizonal scaffolds for the reconstruction of zonal articular cartilage in chondral and osteochondral defects. *Bioactive Materials*, 43, 510-549. <https://doi.org/10.1016/j.bioactmat.2024.10.001>
- [11] ICRS Clinical Cartilage Injury Evaluation System. <https://cartilage.org/society/publications/icrs-score/>
- [12] Ai, C., Lee, Y. H. D., Tan, X. H., Tan, S. H. S., Hui, J. H. P., & Goh, J. C. (2021). Osteochondral tissue engineering: Perspectives for clinical application and preclinical development. *Journal of Orthopaedic Translation*, 30, 93-102. <https://doi.org/10.1016/j.jot.2021.07.008>

- [13] Jang, S., Lee, K., & Ju, J. H. (2021). Recent Updates of Diagnosis, Pathophysiology, and Treatment on Osteoarthritis of the Knee. *International journal of molecular sciences*, 22(5), 2619. <https://doi.org/10.3390/ijms22052619>
- [14] Zhang, B., Huang, J., & Narayan, R. J. (2020). Gradient scaffolds for osteochondral tissue engineering and regeneration. *Journal of Materials Chemistry B*, 8(36), 8149-8170. <https://doi.org/10.1039/d0tb00688b>
- [15] Yonesi, M., Garcia-Nieto, M., Guinea, G. V., Panetsos, F., Perez-Rigueiro, J., & Gonzalez-Nieto, D. (2021). Silk Fibroin: An Ancient Material for Repairing the Injured Nervous System. *Pharmaceutics*, 13(3), 429. <https://doi.org/10.3390/pharmaceutics13030429>
- [16] Yang, S., Zhao, C., Yang, Y., Ren, J., & Ling, S. (2023). The Fractal Network Structure of Silk Fibroin Molecules and Its Effect on Spinning of Silkworm Silk. *ACS Nano*, 17(8), 7662-7673. <https://doi.org/10.1021/acsnano.3c00105>
- [17] Laity, P. R., Gilks, S. E., & Holland, C. (2015). Rheological behaviour of native silk feedstocks. *Polymer*, 67, 28-39. <https://doi.org/10.1016/j.polymer.2015.04.049>
- [18] Khosropanah, M. H., Vaghasloo, M. A., Shakibaei, M., Mueller, A. L., Kajbafzadeh, A. M., Amani, L., Haririan, I., Azimzadeh, A., Hassannejad, Z., & Zolbin, M. M. (2022). Biomedical applications of silkworm (*Bombyx Mori*) proteins in regenerative medicine (a narrative review). *J Tissue Eng Regen Med*, 16(2), 91-109. <https://doi.org/10.1002/term.3267>
- [19] Belbéoch, C., Lejeune, J., Vroman, P., & Salaün, F. (2021). Silkworm and spider silk electrospinning: a review. *Environmental Chemistry Letters*, 19(2), 1737-1763. <https://doi.org/10.1007/s10311-020-01147-x>
- [20] Kwon, K.-J., & Seok, H. (2018). Silk Protein-Based Membrane for Guided Bone Regeneration. *Applied Sciences*, 8(8). <https://doi.org/10.3390/app8081214>
- [21] Croft, A. S., Spessot, E., Bhattacharjee, P., Yang, Y., Motta, A., Woltje, M., & Gantenbein, B. (2022). Biomedical applications of silk and its role for intervertebral disc repair. *JOR Spine*, 5(4), e1225. <https://doi.org/10.1002/jsp2.1225>
- [22] Liu, Y., Ren, J., & Ling, S. (2019). Bioinspired and biomimetic silk spinning. *Composites Communications*, 13, 85-96. <https://doi.org/10.1016/j.coco.2019.03.004>
- [23] Ling, S., Qin, Z., Li, C., Huang, W., Kaplan, D. L., & Buehler, M. J. (2017). Polymorphic regenerated silk fibers assembled through bioinspired spinning. *Nature Communications*, 8(1), 1387. <https://doi.org/10.1038/s41467-017-00613-5>
- [24] Jiao, Z., Song, Y., Jin, Y., Zhang, C., Peng, D., Chen, Z., Chang, P., Kundu, S. C., Wang, G., Wang, Z., & Wang, L. (2017). In Vivo Characterizations of the Immune Properties of Sericin: An Ancient Material with Emerging Value in Biomedical Applications. *Macromol Biosci*, 17(12). <https://doi.org/10.1002/mabi.201700229>
- [25] Li, Y., Wei, Y., Zhang, G., & Zhang, Y. (2023). Sericin from Fibroin-Deficient Silkworms Served as a Promising Resource for Biomedicine. *Polymers*, 15(13), 2941. <https://doi.org/10.3390/polym15132941>
- [26] Liu, J., Shi, L., Deng, Y., Zou, M., Cai, B., Song, Y., Wang, Z., & Wang, L. (2022). Silk sericin-based materials for biomedical applications. *Biomaterials*, 287, 121638. <https://doi.org/10.1016/j.biomaterials.2022.121638>

- [27] Zhang, Y., Zhao, Y., He, X., Fang, A., Jiang, R., Wu, T., Chen, H., Cao, X., Liang, P., Xia, D., & Zhang, G. (2019). A sterile self-assembled sericin hydrogel via a simple two-step process. *Polymer Testing*, 80. <https://doi.org/10.1016/j.polymertesting.2019.106016>
- [28] Wang, J., Liu, H., Shi, X., Qin, S., Liu, J., Lv, Q., Liu, J., Li, Q., Wang, Z., & Wang, L. (2024). Development and Application of an Advanced Biomedical Material-Silk Sericin. *Advanced Materials*, 2311593. <https://doi.org/10.1002/adma.202311593>
- [29] Silva, A. S., Costa, E. C., Reis, S., Spencer, C., Calhelha, R. C., Miguel, S. P., Ribeiro, M. P., Barros, L., Vaz, J. A., & Coutinho, P. (2022). Silk Sericin: A Promising Sustainable Biomaterial for Biomedical and Pharmaceutical Applications. *Polymers*, 14(22). <https://doi.org/10.3390/polym14224931>
- [30] Kunz, R. I., Brancalhão, R. M., Ribeiro, L. F., & Natali, M. R. (2016). Silkworm Sericin: Properties and Biomedical Applications. *Biomed Res Int*, 2016, 8175701. <https://doi.org/10.1155/2016/8175701>
- [31] Ekasurya, W., Sebastian, J., Puspitasari, D., Asri, P. P. P., & Asri, L. (2023). Synthesis and Degradation Properties of Sericin/PVA Hydrogels. *Gels*, 9(2). <https://doi.org/10.3390/gels9020076>
- [32] Bakadia, B. M., Lamboni, L., Qaed Ahmed, A. A., Zheng, R., Ode Boni, B. O., Shi, Z., Song, S., Souho, T., Mukole, B. M., Qi, F., & Yang, G. (2023). Antibacterial silk sericin/poly (vinyl alcohol) hydrogel with antifungal property for potential infected large burn wound healing: Systemic evaluation. *Smart Materials in Medicine*, 4, 37-58. <https://doi.org/10.1016/j.smain.2022.07.002>
- [33] Munir, F., Tahir, H. M., Ali, S., Ali, A., Tehreem, A., Zaidi, S., Adnan, M., & Ijaz, F. (2023). Characterization and Evaluation of Silk Sericin-Based Hydrogel: A Promising Biomaterial for Efficient Healing of Acute Wounds. *ACS Omega*, 8(35), 32090-32098. <https://doi.org/10.1021/acsomega.3c04178>
- [34] Baptista-Silva, S., Bernardes, B. G., Borges, S., Rodrigues, I., Fernandes, R., Gomes-Guerreiro, S., Pinto, M. T., Pintado, M., Soares, R., Costa, R., & Oliveira, A. L. (2022). Exploring Silk Sericin for Diabetic Wounds: An In Situ-Forming Hydrogel to Protect against Oxidative Stress and Improve Tissue Healing and Regeneration. *Biomolecules*, 12(6). <https://doi.org/10.3390/biom12060801>
- [35] Manesa, K. C., Kebede, T. G., Dube, S., & Nindi, M. M. (2022). Fabrication and Characterization of Sericin-PVA Composite Films from *Gonometa postica*, *Gonometa rufobrunnea*, and *Argema mimosae*: Potentially Applicable in Biomaterials. *ACS Omega*, 7(23), 19328-19336. <https://doi.org/10.1021/acsomega.2c00897>
- [36] Tuancharoensri, N., Sonjan, S., Promkrainit, S., Daengmankhong, J., Phimmuan, P., Mahasaranon, S., Jongjitwimol, J., Charoensit, P., Ross, G. M., Viennet, C., Viyoch, J., & Ross, S. (2023). Porous Poly(2-hydroxyethyl methacrylate) Hydrogel Scaffolds for Tissue Engineering: Influence of Crosslinking Systems and Silk Sericin Concentration on Scaffold Properties. *Polymers*, 15(20). <https://doi.org/10.3390/polym15204052>
- [37] Aramwit, P., Kanokpanont, S., Nakpheng, T., & Srichana, T. (2010). The effect of sericin from various extraction methods on cell viability and collagen production. *International journal of molecular sciences*, 11(5), 2200-2211. <https://doi.org/10.3390/ijms11052200>

- [38] Gaviria, A., Jaramillo-Quiceno, N., Motta, A., & Restrepo-Osorio, A. (2023). Silk wastes and autoclaved degumming as an alternative for a sustainable silk process. *Sci Rep*, 13(1), 15296. <https://doi.org/10.1038/s41598-023-41762-6>
- [39] Wang, R., Zhu, Y., Shi, Z., Jiang, W., Liu, X., & Ni, Q.-Q. (2018). Degumming of raw silk via steam treatment. *Journal of Cleaner Production*, 203, 492-497. <https://doi.org/10.1016/j.jclepro.2018.08.286>
- [40] Rastogi, S., & Kandasubramanian, B. (2020). Processing trends of silk fibers: Silk degumming, regeneration and physical functionalization. *The Journal of The Textile Institute*, 111(12), 1794-1810. <https://doi.org/10.1080/00405000.2020.1727269>
- [41] Seo, S. J., Das, G., Shin, H. S., & Patra, J. K. (2023). Silk Sericin Protein Materials: Characteristics and Applications in Food-Sector Industries. *Int J Mol Sci*, 24(5). <https://doi.org/10.3390/ijms24054951>
- [42] Khan, M. R., Tsukada, M., Gotoh, Y., Morikawa, H., Freddi, G., & Shiozaki, H. (2010). Physical properties and dyeability of silk fibers degummed with citric acid. *Bioresour Technol*, 101(21), 8439-8445. <https://doi.org/10.1016/j.biortech.2010.05.100>
- [43] Hossain, S., Ali, R., & Hasan, T. (2023). Extraction and Characterization of Sericin from Cocoon of Four Different Silkworm Races Bombyx Mori L. *European Journal of Advanced Chemistry Research*, 4(3), 45-52. <https://doi.org/10.24018/ejchem.2023.4.3.134>
- [44] Kaewchuchuen, J., Roamcharern, N., Phuagkhaopong, S., Bimbo, L. M., & Seib, F. P. (2023). Microfibre-Functionalised Silk Hydrogels. *Cells*, 13(1). <https://doi.org/10.3390/cells13010010>
- [45] Zhang, Y., Wang, S., Li, Y., Li, X., Du, Z., Liu, S., Song, Y., Li, Y., & Zhang, G. (2023). A Sterile, Injectable, and Robust Sericin Hydrogel Prepared by Degraded Sericin. *Gels*, 9(12). <https://doi.org/10.3390/gels9120948>
- [46] Tao, G., Wang, Y., Cai, R., Chang, H., Song, K., Zuo, H., Zhao, P., Xia, Q., & He, H. (2019). Design and performance of sericin/poly(vinyl alcohol) hydrogel as a drug delivery carrier for potential wound dressing application. *Materials Science & Engineering C*, 101, 341-351. <https://doi.org/10.1016/j.msec.2019.03.111>
- [47] He, H., Cai, R., Wang, Y., Tao, G., Guo, P., Zuo, H., Chen, L., Liu, X., Zhao, P., & Xia, Q. (2017). Preparation and characterization of silk sericin/PVA blend film with silver nanoparticles for potential antimicrobial application. *Int J Biol Macromol*, 104(Pt A), 457-464. <https://doi.org/10.1016/j.ijbiomac.2017.06.009>
- [48] Adelnia, H., Ensandoost, R., Shebbrin Moonshi, S., Gavgani, J. N., Vasafi, E. I., & Ta, H. T. (2022). Freeze/thawed polyvinyl alcohol hydrogels: Present, past and future. *European Polymer Journal*, 164. <https://doi.org/10.1016/j.eurpolymj.2021.110974>
- [49] Górska, A., Baran, E., Knapik-Kowalczyk, J., Szafraniec-Szczyński, J., Paluch, M., Kulinowski, P., & Mendyk, A. (2024). Physically Cross-Linked PVA Hydrogels as Potential Wound Dressings: How Freezing Conditions and Formulation Composition Define Cryogel Structure and Performance. *Pharmaceutics*, 16(11). <https://doi.org/10.3390/pharmaceutics16111388>
- [50] Garcia-Canton, C., Minet, E., Anadon, A., & Meredith, C. (2013). Metabolic characterization of cell systems used in in vitro toxicology testing: lung cell system BEAS-2B as a working example. *Toxicol In Vitro*, 27(6), 1719-1727. <https://doi.org/10.1016/j.tiv.2013.05.001>

- [51] El-Sherbiny, I. M., & Yacoub, M. H. (2013). Hydrogel scaffolds for tissue engineering: Progress and challenges. *Glob Cardiol Sci Pract*, 2013(3), 316-342. <https://doi.org/10.5339/gcsp.2013.38>
- [52] Radulescu, D. M., Neacsu, I. A., Grumezescu, A. M., & Andronescu, E. (2022). New Insights of Scaffolds Based on Hydrogels in Tissue Engineering. *Polymers (Basel)*, 14(4). <https://doi.org/10.3390/polym14040799>
- [53] Hafezi, M., Nouri Khorasani, S., Zare, M., Esmaeely Neisiany, R., & Davoodi, P. (2021). Advanced Hydrogels for Cartilage Tissue Engineering: Recent Progress and Future Directions. *Polymers*, 13(23). <https://doi.org/10.3390/polym13234199>
- [54] Bashir, S., Hina, M., Iqbal, J., Rajpar, A. H., Mujtaba, M. A., Alghamdi, N. A., Wageh, S., Ramesh, K., & Ramesh, S. (2020). Fundamental Concepts of Hydrogels: Synthesis, Properties, and Their Applications. *Polymers (Basel)*, 12(11). <https://doi.org/10.3390/polym12112702>
- [55] Yan, X., Huang, H., Bakry, A. M., Wu, W., Liu, X., & Liu, F. (2024). Advances in enhancing the mechanical properties of biopolymer hydrogels via multi-strategic approaches. *Int J Biol Macromol*, 272(Pt 2), 132583. <https://doi.org/10.1016/j.ijbiomac.2024.132583>
- [56] Parvin, N., Kumar, V., Joo, S. W., & Mandal, T. K. (2024). Cutting-Edge Hydrogel Technologies in Tissue Engineering and Biosensing: An Updated Review. *Materials (Basel)*, 17(19). <https://doi.org/10.3390/ma17194792>
- [57] Liu, W., Madry, H., & Cucchiaroni, M. (2022). Application of Alginate Hydrogels for Next-Generation Articular Cartilage Regeneration. *International journal of molecular sciences*, 23(3), 1147. <https://doi.org/10.3390/ijms23031147>
- [58] Malektaj, H., Drozdov, A. D., & deClaville Christiansen, J. (2023). Mechanical Properties of Alginate Hydrogels Cross-Linked with Multivalent Cations. *Polymers*, 15(14), 3012. <https://doi.org/10.3390/polym15143012>
- [59] Mikula, K., Skrzypczak, D., Ligas, B., & Witek-Krowiak, A. (2019). Preparation of hydrogel composites using Ca²⁺ and Cu²⁺ ions as crosslinking agents. *SN Applied Sciences*, 1(6). <https://doi.org/10.1007/s42452-019-0657-3>
- [60] Zhang, Y., Li, H., Xu, H., Wang, L., Zhang, M., Liu, J., & Tan, F. (2021). Alginate hydrogels crosslinked with different strontium-calcium ratios as injectable scaffolds for bone tissue engineering. *Journal of Materials Science*, 56(30), 17221-17234. <https://doi.org/10.1007/s10853-021-06382-3>
- [61] Jing, Z., Dai, X., Xian, X., Du, X., Liao, M., Hong, P., & Li, Y. (2020). Tough, stretchable and compressive alginate-based hydrogels achieved by non-covalent interactions. *RSC Adv*, 10(40), 23592-23606. <https://doi.org/10.1039/d0ra03733h>
- [62] Sarker, M., Izadifar, M., Schreyer, D., & Chen, X. (2018). Influence of ionic crosslinkers (Ca²⁺/Ba²⁺/Zn²⁺) on the mechanical and biological properties of 3D Bioplotted Hydrogel Scaffolds. *Journal of Biomaterials Science, Polymer Edition*, 29(10), 1126-1154. <https://doi.org/10.1080/09205063.2018.1433420>
- [63] Gurikov, P., & Smirnova, I. (2018). Non-Conventional Methods for Gelation of Alginate. *Gels*, 4(1). <https://doi.org/10.3390/gels4010014>
- [64] Growney Kalaf, E. A., Flores, R., Bledsoe, J. G., & Sell, S. A. (2016). Characterization of slow-gelling alginate hydrogels for intervertebral disc tissue-engineering applications. *Materials Science and Engineering*, 63, 198-210. <https://doi.org/10.1016/j.msec.2016.02.067>
- [65] Gao, X., Gao, L., Groth, T., Liu, T., He, D., Wang, M., Gong, F., Chu, J., & Zhao, M. (2019). Fabrication and properties of an injectable sodium alginate/PRP

- composite hydrogel as a potential cell carrier for cartilage repair. *J Biomed Mater Res A*, 107(9), 2076-2087. <https://doi.org/10.1002/jbm.a.36720>
- [66] Zhong, Y., Lin, Q., Yu, H., Shao, L., Cui, X., Pang, Q., Zhu, Y., & Hou, R. (2024). Construction methods and biomedical applications of PVA-based hydrogels. *Front Chem*, 12, 1376799. <https://doi.org/10.3389/fchem.2024.1376799>
- [67] Liu, Y., Wang, W., Gu, K., Yao, J., Shao, Z., & Chen, X. (2021). Poly(vinyl alcohol) Hydrogels with Integrated Toughness, Conductivity, and Freezing Tolerance Based on Ionic Liquid/Water Binary Solvent Systems. *ACS applied materials & interfaces*, 13(24), 29008-29020. <https://doi.org/10.1021/acsami.1c09006>
- [68] Holloway, J. L., Lowman, A. M., & Palmese, G. R. (2013). The role of crystallization and phase separation in the formation of physically cross-linked PVA hydrogels. *Soft Matter*, 9(3), 826-833. <https://doi.org/10.1039/c2sm26763b>
- [69] Li, H., Wu, C., Yu, X., & Zhang, W. (2023). Recent advances of PVA-based hydrogels in cartilage repair application. *Journal of Materials Research and Technology*, 24, 2279-2298. <https://doi.org/10.1016/j.jmrt.2023.03.130>
- [70] Lan, W., Xu, M., Qin, M., Cheng, Y., Zhao, Y., Huang, D., Wei, X., Guo, Y., & Chen, W. (2021). Physicochemical properties and biocompatibility of the bi-layer polyvinyl alcohol-based hydrogel for osteochondral tissue engineering. *Materials & Design*, 204, 109652. <https://doi.org/10.1016/j.matdes.2021.109652>
- [71] Wang, Y., Xue, Y., Wang, J., Zhu, Y., Zhu, Y., Zhang, X., Liao, J., Li, X., Wu, X., Qin, Y. X., & Chen, W. (2019). A Composite Hydrogel with High Mechanical Strength, Fluorescence, and Degradable Behavior for Bone Tissue Engineering. *Polymers*, 11(7), 1112. <https://doi.org/10.3390/polym11071112>
- [72] Muangsri, R., Chuysinuan, P., Thanyacharoen, T., Techasakul, S., Sukhavattanakul, P., & Ummartyotin, S. (2022). Utilization of freeze thaw process for polyvinyl alcohol/sodium alginate (PVA/SA) hydrogel composite. *Journal of Metals, Materials and Minerals*, 32(2), 34-41. <https://doi.org/10.55713/jmmm.v32i2.1257>
- [73] Shams Es-haghi, S., Mayfield, M. B., & Weiss, R. A. (2018). Effect of Freeze/Thaw Process on Mechanical Behavior of Double-Network Hydrogels in Finite Tensile Deformation. *Macromolecules*, 51(3), 1052-1057. <https://doi.org/10.1021/acs.macromol.7b02418>
- [74] Bakadia, B. M., Zhong, A., Li, X., Boni, B. O. O., Ahmed, A. A. Q., Souho, T., Zheng, R., Shi, Z., Shi, D., Lamboni, L., & Yang, G. (2022). Biodegradable and injectable poly(vinyl alcohol) microspheres in silk sericin-based hydrogel for the controlled release of antimicrobials: application to deep full-thickness burn wound healing. *Advanced Composites and Hybrid Materials*, 5(4), 2847-2872. <https://doi.org/10.1007/s42114-022-00467-6>
- [75] Noosak, C., Iamthanaporn, K., Meesane, J., Voravuthikunchai, S. P., & Sotthibandhu, D. S. (2023). Bioactive functional sericin/polyvinyl alcohol hydrogel: biomaterials for supporting orthopedic surgery in osteomyelitis. *Journal of Materials Science*, 58(12), 5477-5488. <https://doi.org/10.1007/s10853-023-08356-z>
- [76] Wang, Z., Zhang, Y., Zhang, J., Huang, L., Liu, J., Li, Y., Zhang, G., Kundu, S. C., & Wang, L. (2014). Exploring natural silk protein sericin for regenerative medicine: an injectable, photoluminescent, cell-adhesive 3D hydrogel. *Scientific reports*, 4, 7064. <https://doi.org/10.1038/srep07064>

- [77] Peng, L., Zhou, Y., Lu, W., Zhu, W., Li, Y., Chen, K., Zhang, G., Xu, J., Deng, Z., & Wang, D. (2019). Characterization of a novel polyvinyl alcohol/chitosan porous hydrogel combined with bone marrow mesenchymal stem cells and its application in articular cartilage repair. *BMC Musculoskelet Disord*, 20(1), 257. <https://doi.org/10.1186/s12891-019-2644-7>
- [78] Luo, C., Zhao, Y., Sun, X., & Hu, B. (2020). Developing high strength, antiseptic and swelling-resistant polyvinyl alcohol/chitosan hydrogels for tissue engineering material. *Materials Letters*, 280. <https://doi.org/10.1016/j.matlet.2020.128499>
- [79] Liu, S., Zhou, X., Nie, L., Wang, Y., Hu, Z., Okoro, O. V., Shavandi, A., & Fan, L. (2021). Anisotropic PLGA microsphere/PVA hydrogel composite with aligned macroporous structures for directed cell adhesion and proliferation. *International Journal of Polymeric Materials and Polymeric Biomaterials*, 72(5), 397-406. <https://doi.org/10.1080/00914037.2021.2018317>
- [80] Majda, D., Bhattarai, A., Riikonen, J., Napruszewska, B. D., Zimowska, M., Michalik-Zym, A., Töyräs, J., & Lehto, V. P. (2017). New approach for determining cartilage pore size distribution: NaCl-thermoporometry. *Microporous and Mesoporous Materials*, 241, 238-245. <https://doi.org/10.1016/j.micromeso.2017.01.005>
- [81] Cui, L., Tong, W., Zhou, H., Yan, C., Chen, J., & Xiong, D. (2020). PVA-BA/PEG hydrogel with bilayer structure for biomimetic articular cartilage and investigation of its biotribological and mechanical properties. *Journal of Materials Science*, 56(5), 3935-3946. <https://doi.org/10.1007/s10853-020-05467-9>
- [82] Sergeeva, A., Vikulina, A. S., & Volodkin, D. (2019). Porous Alginate Scaffolds Assembled Using Vaterite CaCO₃ Crystals. *Micromachines*, 10(6), 357. <https://doi.org/10.3390/mi10060357>
- [83] Serrano-Aroca, A., Ruiz-Pividal, J. F., & Llorens-Gamez, M. (2017). Enhancement of water diffusion and compression performance of crosslinked alginate films with a minuscule amount of graphene oxide. *Scientific reports*, 7(1), 11684. <https://doi.org/10.1038/s41598-017-10260-x>
- [84] Zhang, L. (2022). Strong and Tough PAM/SA Hydrogel with Highly Strain Sensitivity. *Journal of Renewable Materials*, 10(2), 415-430. <https://doi.org/10.32604/jrm.2022.016650>
- [85] Khaleghi, M., Ahmadi, E., Khodabandeh Shahraki, M., Aliakbari, F., & Morshedi, D. (2020). Temperature-dependent formulation of a hydrogel based on Hyaluronic acid-polydimethylsiloxane for biomedical applications. *Heliyon*, 6(3), e03494. <https://doi.org/10.1016/j.heliyon.2020.e03494>
- [86] Zhang, X., Wang, K., Hu, J., Zhang, Y., Dai, Y., & Xia, F. (2020). Role of a high calcium ion content in extending the properties of alginate dual-crosslinked hydrogels. *Journal of Materials Chemistry A*, 8(47), 25390-25401. <https://doi.org/10.1039/d0ta09315g>
- [87] Hu, C., Lu, W., Mata, A., Nishinari, K., & Fang, Y. (2021). Ions-induced gelation of alginate: Mechanisms and applications. *Int J Biol Macromol*, 177, 578-588. <https://doi.org/10.1016/j.ijbiomac.2021.02.086>
- [88] Li, J., Liu, H., Wang, C., & Huang, G. (2017). A facile method to fabricate hybrid hydrogels with mechanical toughness using a novel multifunctional cross-linker. *RSC Advances*, 7(56), 35311-35319. <https://doi.org/10.1039/c7ra05645a>

- [89] Stoppel, W. L., White, J. C., Horava, S. D., Henry, A. C., Roberts, S. C., & Bhatia, S. R. (2014). Terminal sterilization of alginate hydrogels: efficacy and impact on mechanical properties. *Journal of Biomedical Materials Research Part B: Applied Biomaterials*, 102(4), 877-884. <https://doi.org/10.1002/jbm.b.33070>
- [90] Galante, R., Pinto, T. J. A., Colaco, R., & Serro, A. P. (2018). Sterilization of hydrogels for biomedical applications: A review. *Journal of Biomedical Materials Research Part B: Applied Biomaterials*, 106(6), 2472-2492. <https://doi.org/10.1002/jbm.b.34048>
- [91] Bento, C. S. A., Gaspar, M. C., Coimbra, P., de Sousa, H. C., & Braga, M. E. M. (2023). A review of conventional and emerging technologies for hydrogels sterilization. *International Journal of Pharmaceutics*, 634, 122671. <https://doi.org/10.1016/j.ijpharm.2023.122671>
- [92] Dimaraki, A., Díaz-Payno, P. J., Minneboo, M., Nouri-Goushki, M., Hosseini, M., Kops, N., Narcisi, R., Mirzaali, M. J., van Osch, G. J. V. M., Fratila-Apachitei, L. E., & Zadpoor, A. A. (2021). Bioprinting of a Zonal-Specific Cell Density Scaffold: A Biomimetic Approach for Cartilage Tissue Engineering. *Applied Sciences*, 11(17), 7821. <https://doi.org/10.3390/app11177821>
- [93] Guo, Y., Zhou, Y., Yan, S., Qu, C., Wang, L., Guo, X., & Han, J. (2019). Decreased Expression of CHST-12, CHST-13, and UST in the Proximal Interphalangeal Joint Cartilage of School-Age Children with Kashin-Beck Disease: an Endemic Osteoarthritis in China Caused by Selenium Deficiency. *Biol Trace Elem Res*, 191(2), 276-285. <https://doi.org/10.1007/s12011-019-1642-9>
- [94] Sridharan, G., & Shankar, A. A. (2012). Toluidine blue: A review of its chemistry and clinical utility. *J Oral Maxillofac Pathol*, 16(2), 251-255. <https://doi.org/10.4103/0973-029X.99081>
- [95] Zheng, K., Ma, Y., Chiu, C., Xue, M., Zhang, C., & Du, D. (2024). Enhanced articular cartilage regeneration using costal chondrocyte-derived scaffold-free tissue engineered constructs with ascorbic acid treatment. *J Orthop Translat*, 45, 140-154. <https://doi.org/10.1016/j.jot.2024.02.005>
- [96] Jiao, C., Xie, D., He, Z., Liang, H., Shen, L., Yang, Y., Tian, Z., Wu, G., & Wang, C. (2022). Additive manufacturing of Bio-inspired ceramic bone Scaffolds: Structural Design, mechanical properties and biocompatibility. *Materials & Design*, 217, 110610. <https://doi.org/10.1016/j.matdes.2022.110610>
- [97] Koushik, T. M., Miller, C. M., & Antunes, E. (2023). Bone Tissue Engineering Scaffolds: Function of Multi-Material Hierarchically Structured Scaffolds. *Adv Healthc Mater*, 12(9), e2202766. <https://doi.org/10.1002/adhm.202202766>
- [98] Abueidda, D. W., Bakir, M., Abu Al-Rub, R. K., Bergström, J. S., Sobh, N. A., & Jasiuk, I. (2017). Mechanical properties of 3D printed polymeric cellular materials with triply periodic minimal surface architectures. *Materials & Design*, 122, 255-267. <https://doi.org/10.1016/j.matdes.2017.03.018>
- [99] Agarwal, S., Saha, S., Balla, V. K., Pal, A., Barui, A., & Bodhak, S. (2020). Current Developments in 3D Bioprinting for Tissue and Organ Regeneration—A Review. *Frontiers in Mechanical Engineering*, 6, 589171. <https://doi.org/10.3389/fmech.2020.589171>
- [100] Antich, C., de Vicente, J., Jimenez, G., Chocarro, C., Carrillo, E., Montanez, E., Galvez-Martin, P., & Marchal, J. A. (2020). Bio-inspired hydrogel composed of hyaluronic acid and alginate as a potential bioink for 3D bioprinting of articular

- cartilage engineering constructs. *Acta Biomaterialia*, 106, 114-123. <https://doi.org/10.1016/j.actbio.2020.01.046>
- [101] Chen, H., Malheiro, A., van Blitterswijk, C., Mota, C., Wieringa, P. A., & Moroni, L. (2017). Direct Writing Electrospinning of Scaffolds with Multidimensional Fiber Architecture for Hierarchical Tissue Engineering. *ACS applied materials & interfaces*, 9(44), 38187-38200. <https://doi.org/10.1021/acsami.7b07151>
- [102] Zhang, P., Han, F., Chen, T., Wu, Z., & Chen, S. (2020). "Swiss roll"-like bioactive hybrid scaffolds for promoting bone tissue ingrowth and tendon-bone healing after anterior cruciate ligament reconstruction. *Biomater Sci*, 8(3), 871-883. <https://doi.org/10.1039/c9bm01703h>
- [103] Xu, X., Si, Y., Zhao, Y., Ke, Q., & Hu, J. (2022). Electrospun Textile Strategies in Tendon to Bone Junction Reconstruction. *Advanced Fiber Materials*, 5(3), 764-790. <https://doi.org/10.1007/s42765-022-00233-9>
- [104] Teuschl, A., Heimel, P., Nurnberger, S., van Griensven, M., Redl, H., & Nau, T. (2016). A Novel Silk Fiber-Based Scaffold for Regeneration of the Anterior Cruciate Ligament: Histological Results From a Study in Sheep. *Am J Sports Med*, 44(6), 1547-1557. <https://doi.org/10.1177/0363546516631954>
- [105] Cai, J., Xie, X., Li, D., Wang, L., Jiang, J., Mo, X., & Zhao, J. (2020). A novel knitted scaffold made of microfiber/nanofiber core-sheath yarns for tendon tissue engineering. *Biomaterials Science*, 8(16), 4413-4425. <https://doi.org/10.1039/d0bm00816h>
- [106] Andersson, M., Johansson, J., & Rising, A. (2016). Silk Spinning in Silkworms and Spiders. *International journal of molecular sciences*, 17(8), 1290. <https://doi.org/10.3390/ijms17081290>

List of Appendices

- **Appendix A: Original SEM images in physical characterisations**
- **Appendix B: Summary tables of hydrogel visual observations and documentation**
- **Appendix C: Original mechanical plots: files provided by USYD who did the mechanical testing**

Appendix A: Original SEM images in physical characterisations

The all-SEM images involved in this master thesis generate during the experiments.

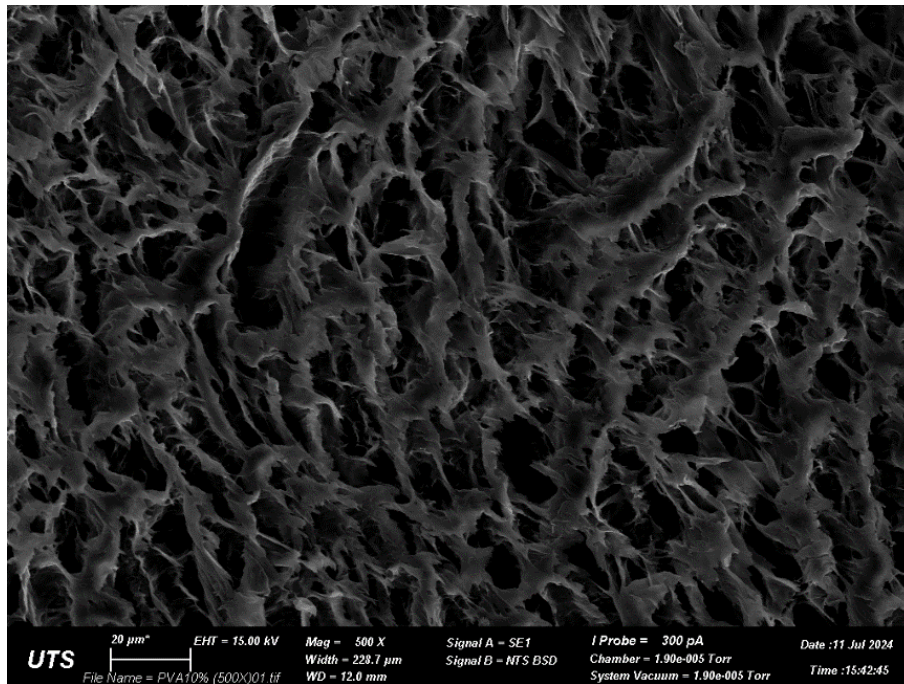


Figure A 1: Cross-section of a 10% PVA hydrogel, revealing a porous structure with a non-uniform tear outline (500× magnification).

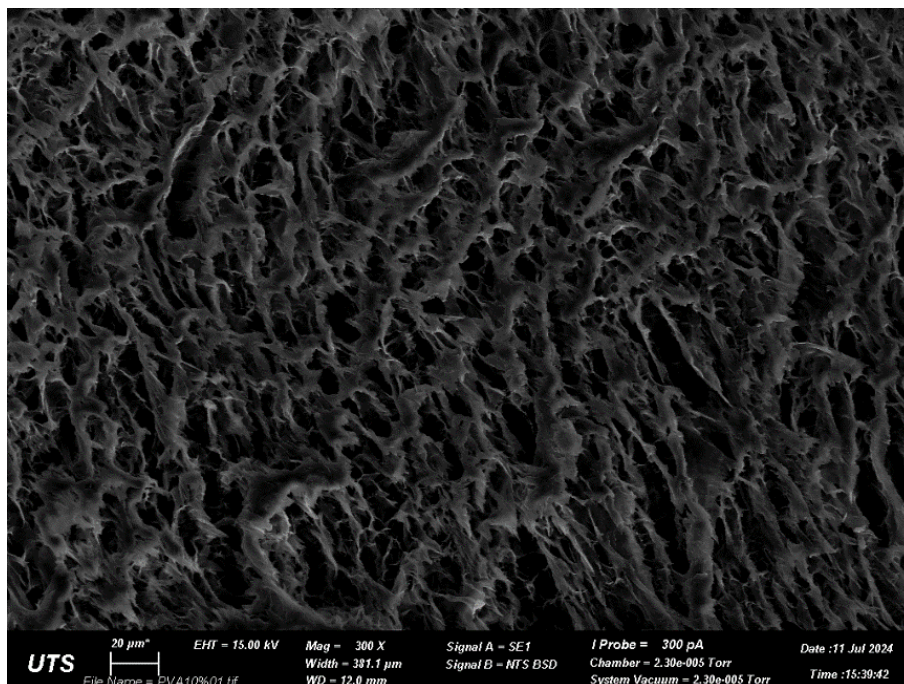


Figure A 2: Overview cross-section of a 10% PVA hydrogel, revealing a porous structure with a non-uniform tear outline (300× magnification).

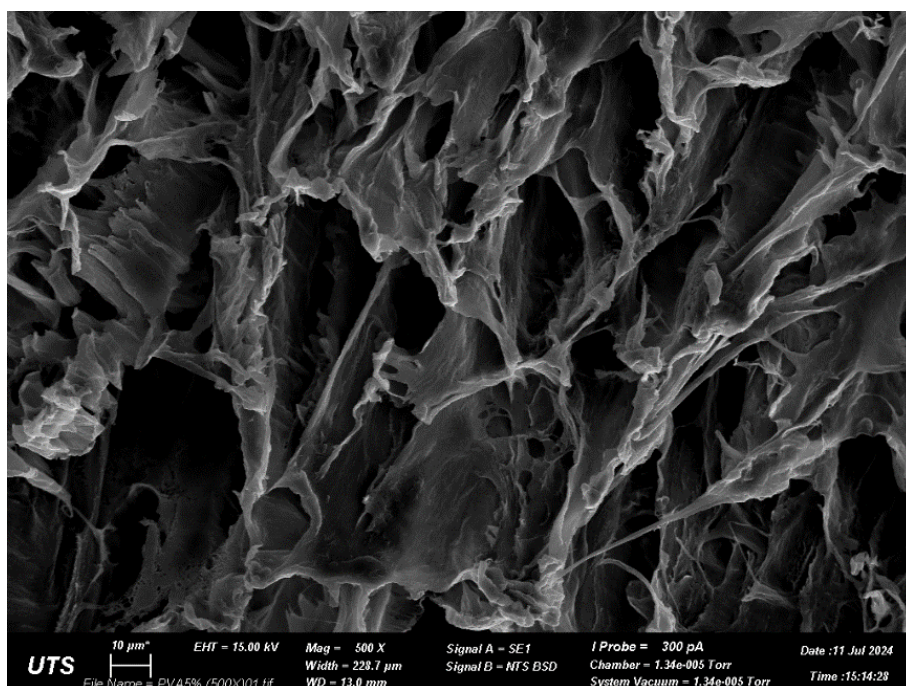


Figure A 3: Cross-section of a 5% PVA hydrogel, revealing a porous structure with a non-uniform outline (500 \times magnification).

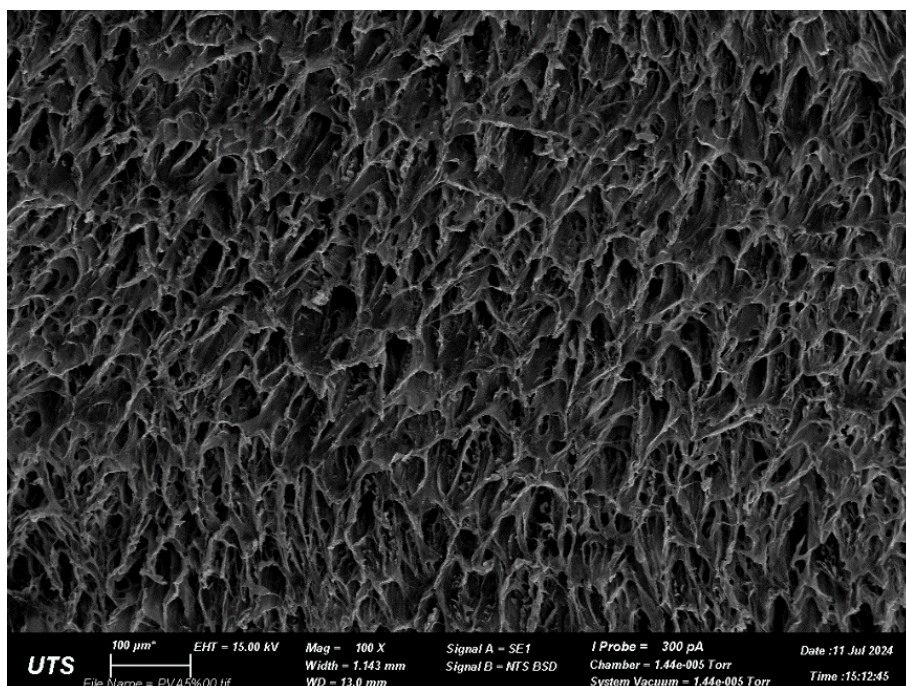


Figure A 4: Overview cross-section of a 5% PVA hydrogel, a porous structure with a non-uniform outline (100 \times magnification).

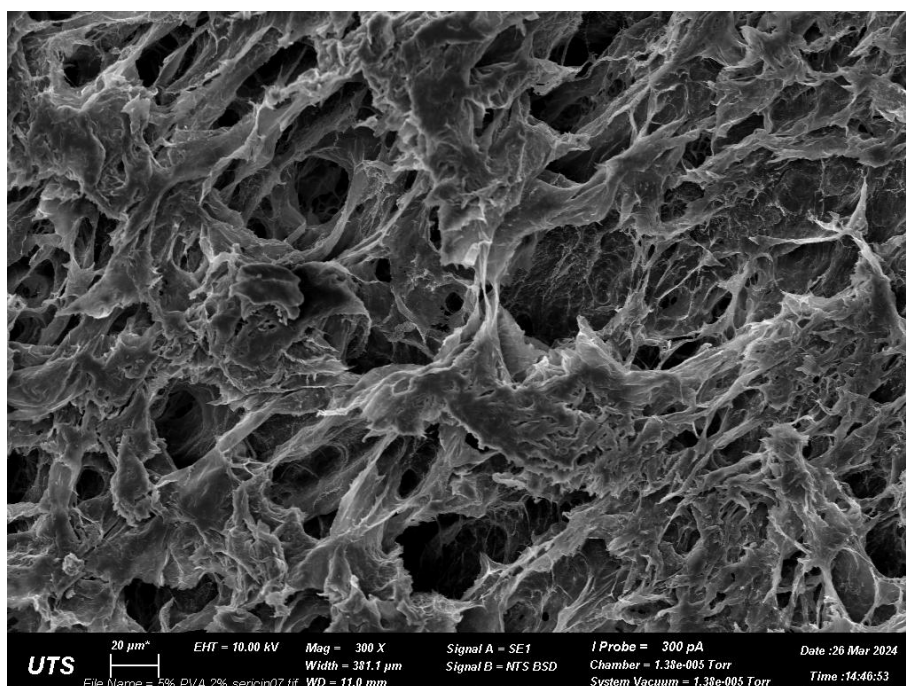


Figure A 5: Cross-section of a 5% PVA-2% sericin hydrogel, revealing a porous structure with a non-uniform outline (300× magnification).

Alternative test 10% PVA + 3% alginate cross-sections, the porous architecture mainly contributed by the internal ionotropic gelation of alginate hydrogel part.

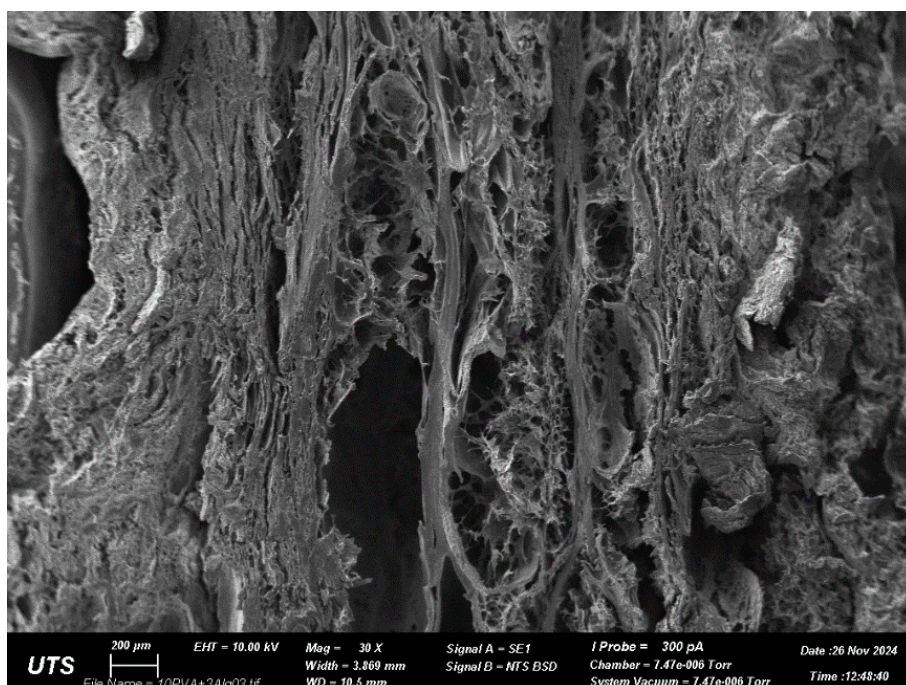


Figure A 6: Overview cross-section of a 10% PVA-3% alginate dual-network crosslinked hydrogel, revealing a porous structure with a collapsed network and a more foldable structure (30× magnification).

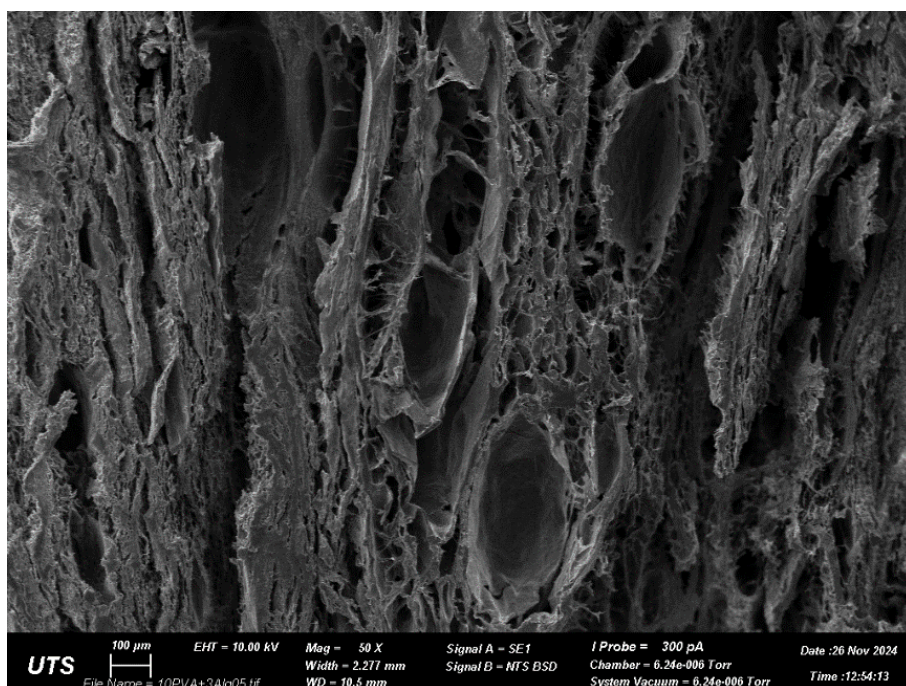


Figure A 7: Overview cross-section of a 10% PVA-3% alginate dual-network crosslinked hydrogel, revealing a porous structure with a collapsed network and a more foldable structure (50 \times magnification).

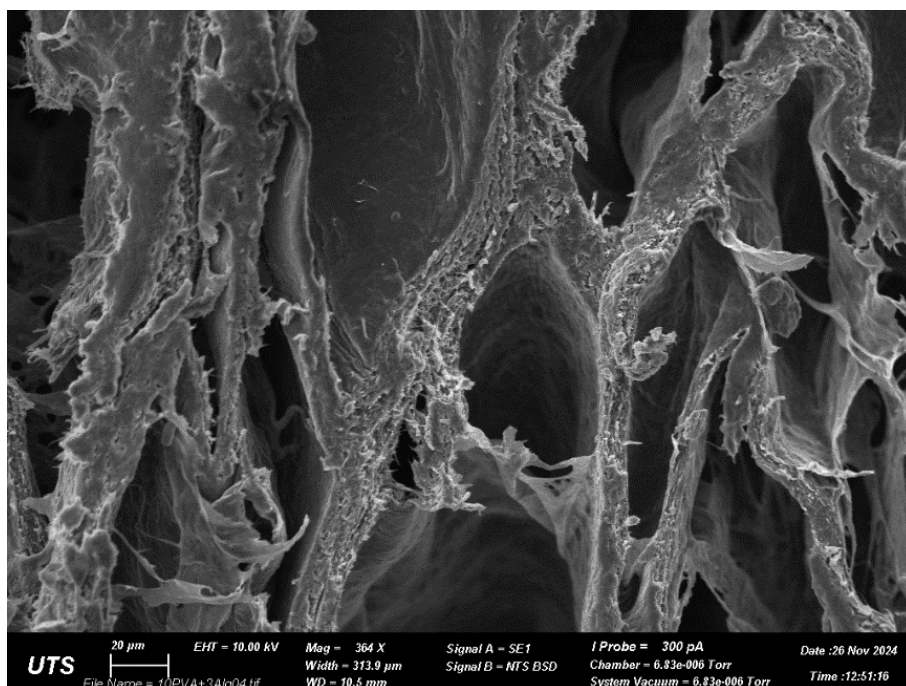


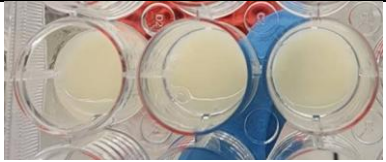
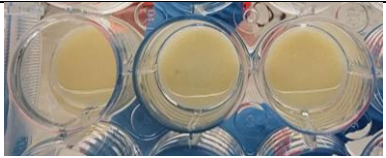
Figure A 8: Cross-section of a 10% PVA-3% alginate dual-network crosslinked hydrogel, revealing a porous structure (364 \times magnification).


Appendix B: Summary tables of hydrogel visual observations and documentation

B1: Experiment notes on sericin-PVA hydrogel ratio and concentration series (preliminary tests)

This section documents the preliminary tests of the 15% w/v PVA base with varying sericin additions. A summary of the detailed findings is provided in **Table B 1**, and an overall photo of the samples is shown in **Figure B 1**. Comparative evaluation of the tested concentrations (2%, 5%, and 7.5% w/v) revealed that only the 2% formulation maintained optimal mechanical integrity and handling properties.

Table B 1. Summary of observations from preliminary testing of PVA-sericin composite hydrogels (15% w/v PVA base with varying sericin concentrations).

Concentration ratio	Observations	Photo
15% w/v PVA + 2% w/v sericin	The PVA hydrogel with 2% w/v sericin, fabricated using standard project protocols, exhibited a smooth surface and maintained structural elasticity both before and after ethanol sterilisation. In contrast to higher sericin concentrations, this formulation demonstrated favourable mechanical integrity, suggesting better suitability for the intended application. Thus, the 2% w/v sericin was selected to concentration was selected as the optimal formulation for subsequent hydrogel development in this project.	
15% w/v PVA + 5% w/v sericin	The PVA hydrogel incorporating 5% w/v sericin displayed a rough surface and elevated stiffness post-fabrication. After ethanol sterilisation, the material retained toughness but lost elasticity, resulting in unfavourable mechanical properties. Given these properties, this formulation may not be suitable for the intended application, as it could hinder cell compatibility and scaffold performance.	

15% w/v PVA + 7.5% w/v sericin	<p>The addition of 7.5% w/v sericin to the 15% w/v PVA-based gel solution resulted in an uneven mixture, with partial clumping and incomplete dissolution during fabrication. After mould-casting and freeze-thawing, the resulting hydrogel exhibited an extremely hard and uneven surface. Post-sterilization, the material became brittle and tough, thus these properties unsuitable for this project. Given these characteristics, cell infiltration and migration into the scaffold are unlikely to occur as intended.</p>	
--------------------------------	----------------------------------------------------------------------------------------------------------------------------------------------------------------------------------------------------------------------------------------------------------------------------------------------------------------------------------------------------------------------------------------------------------------------------------------------------------------------------------------------------------------------------------	-------------------------------------------------------------------------------------

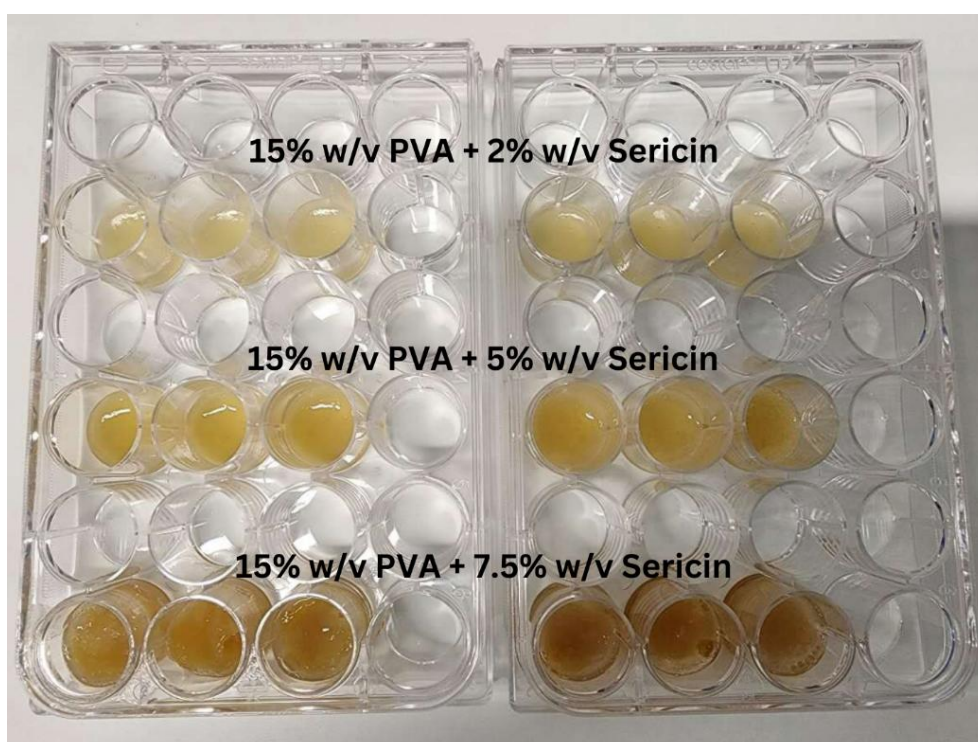


Figure B 1. Preliminary test of 15% w/v PVA-based hydrogels incorporated with varying concentration series of sericin.

B2: Preliminary evaluation of sericin-PVA hydrogel compositions (Fixed 2% w/v sericin with varying PVA concentrations)

Preliminary testing revealed that PVA concentrations of 10% w/v and 15% w/v demonstrated favourable material properties. Manual compression testing (finger press) indicated these formulations achieved the desired elastic hydrogel characteristics while maintaining excellent workability, including precise concentration control during preparation and mould-casting. In

contrast, higher PVA concentrations (20-25% w/v PVA) presented progressive processing challenges, including increased solution viscosity and difficulties in both concentration preparation and achieving consistent thickness during mould-casting, and the hydrogel stiffness might be too hard for cell attachment. A summary of the detailed findings is provided in **Table B 2**, and a photo of the samples is shown in **Figure B 2**.

Table B 2. Summary of observations from preliminary characterization of PVA-sericin composite hydrogels (Fixed 2% w/v sericin concentration with varying PVA concentrations: 10-25% w/v).

Concentration ratio	Observations
10% w/v PVA + 2% w/v sericin	Soft hydrogel and flexible structure with fully dissolved sericin addition
15% w/v PVA + 2% w/v sericin	Soft hydrogel and flexible structure with fully dissolved sericin addition
20% w/v PVA + 2% w/v sericin	Relatively hard hydrogel body, sticky gel solution during fabrication prepare for mould-casting.
25% w/v PVA + 2% w/v sericin	Hard crosslinked hydrogel, and extremely sticky gel solution might cause the difficulty in controlling the thickness in mould-casting.

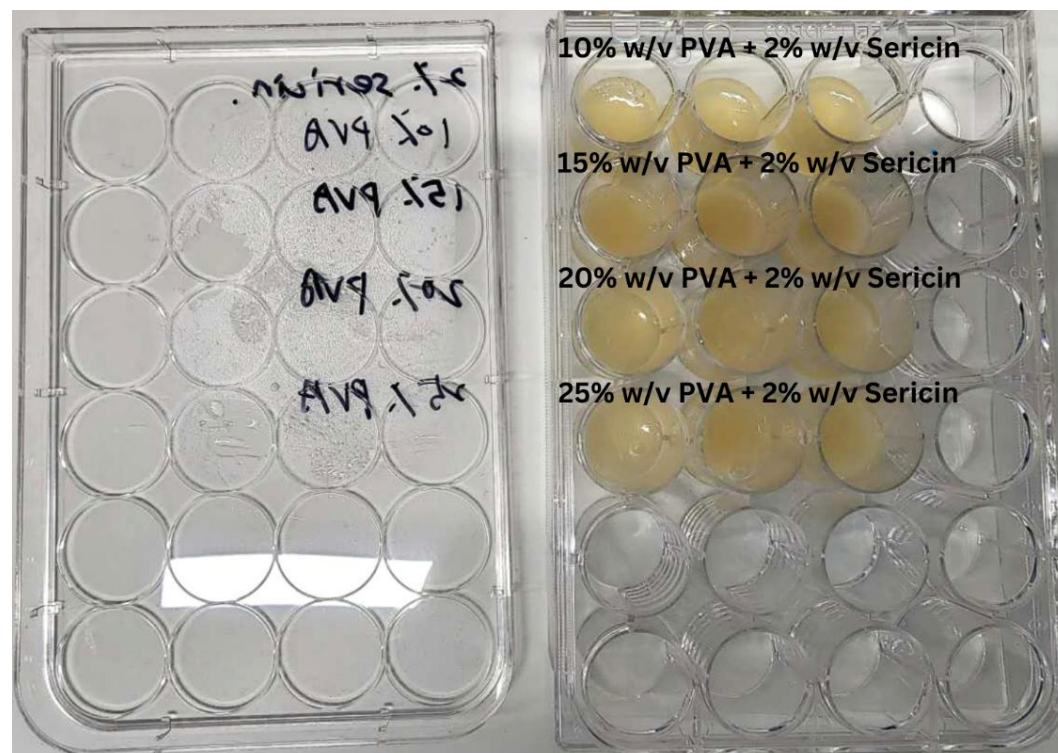




Figure B 2. Photo of PVA-based hydrogels with fixed 2% w/v sericin and varying PVA concentrations (10-25% w/v).

B3: Freeze-Thaw cycle optimization for PVA-based hydrogels

This section analyses the effects of freezing temperature (-20°C and -80°C) and cycle repetition (1-3 cycles) on the physical crosslinking properties of fabricated PVA hydrogels. Qualitative assessment through manual compression testing revealed temperature-dependent effects on crosslinking density, structural stability, and elastic recovery.

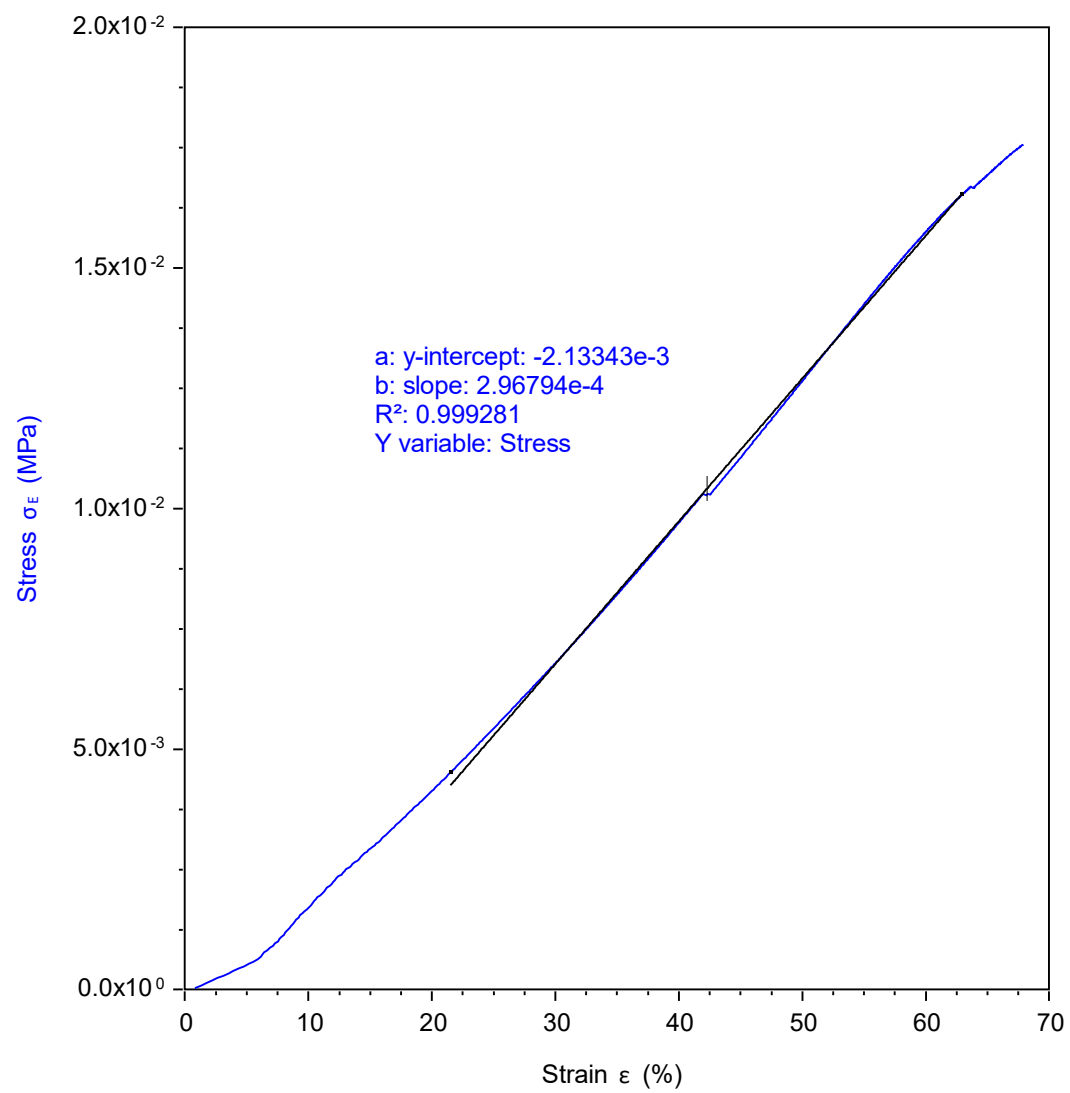
Key findings are documented in **Table B 3**. Evaluation of freeze-thaw parameters on PVA hydrogel properties., demonstrating how freeze-thaw parameters influence hydrogel mechanical performance.

Table B 3. Evaluation of freeze-thaw parameters on PVA hydrogel properties.

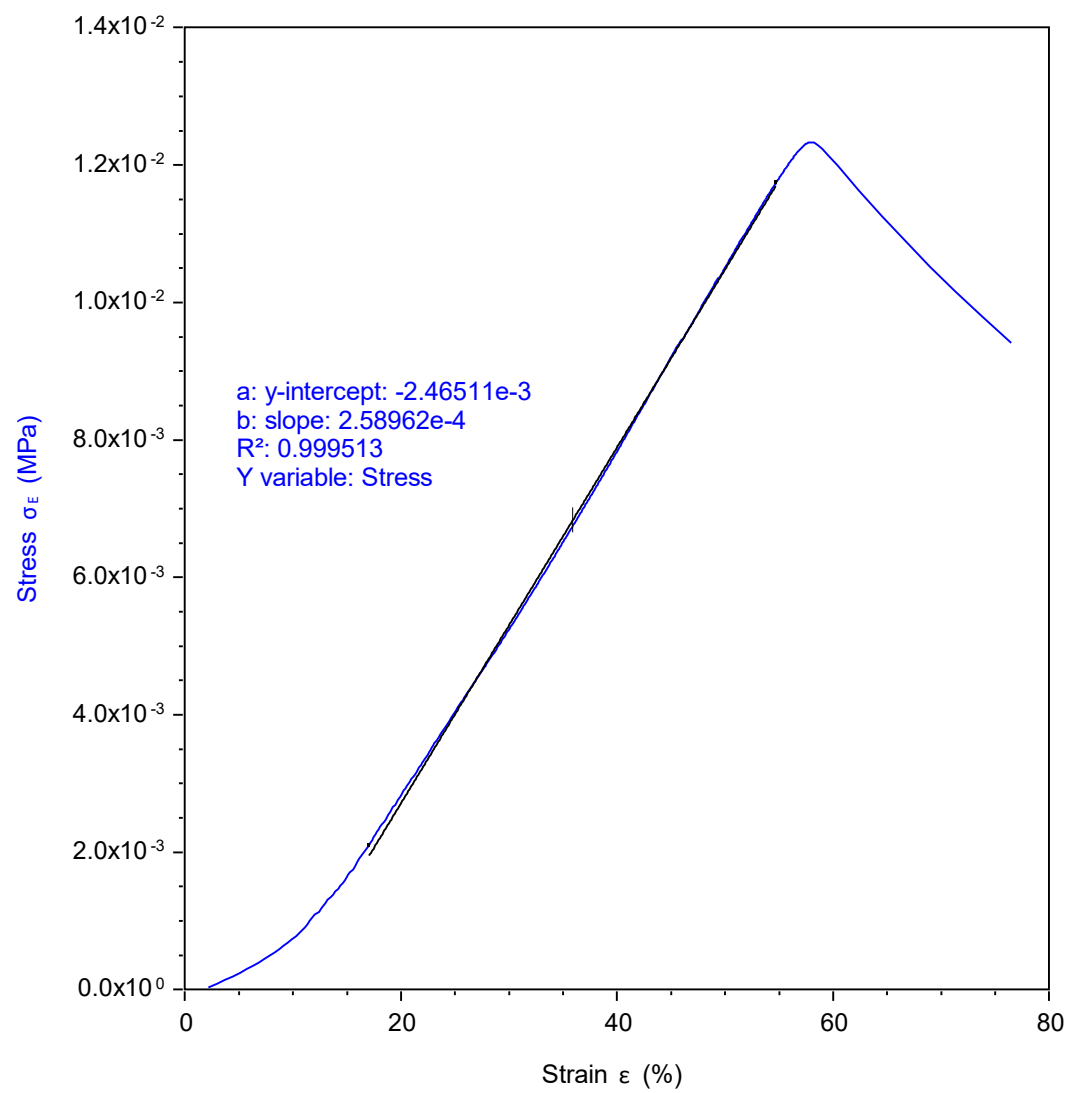
Freezing temperature	Observations	Photos
-20°C	The prepared PVA-based hydrogel exhibited a jelly-like structure with a smooth and hydrated surface. It demonstrated moderate crosslinking density and balanced elasticity, but may undergo structural deformation under high compressive stress.	
-80°C	The same PVA-based hydrogel subjected to -80°C freeze-thaw cycles exhibited a sponge-like surface and significantly increased stiffness, as confirmed by preliminary manual compression testing. This enhanced performance resulted from high crosslinking density due to rapid ice crystal formation during freezing, which further enhanced structural stability through multiple freeze-thaw cycles.	

Appendix C: Original mechanical plots: Original mechanical plots: files provided by USYD who did the mechanical testing

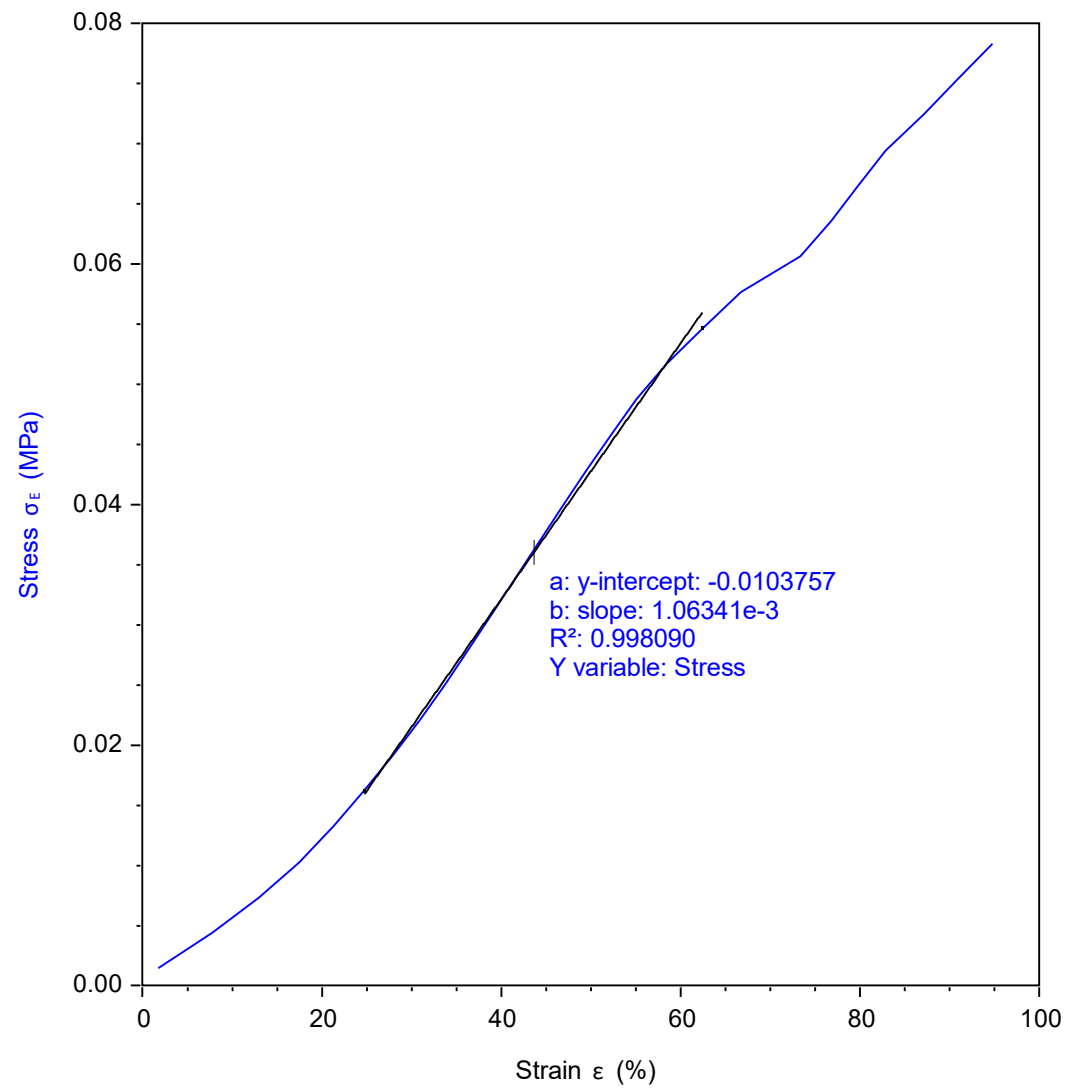
5% PVA_Comp_2



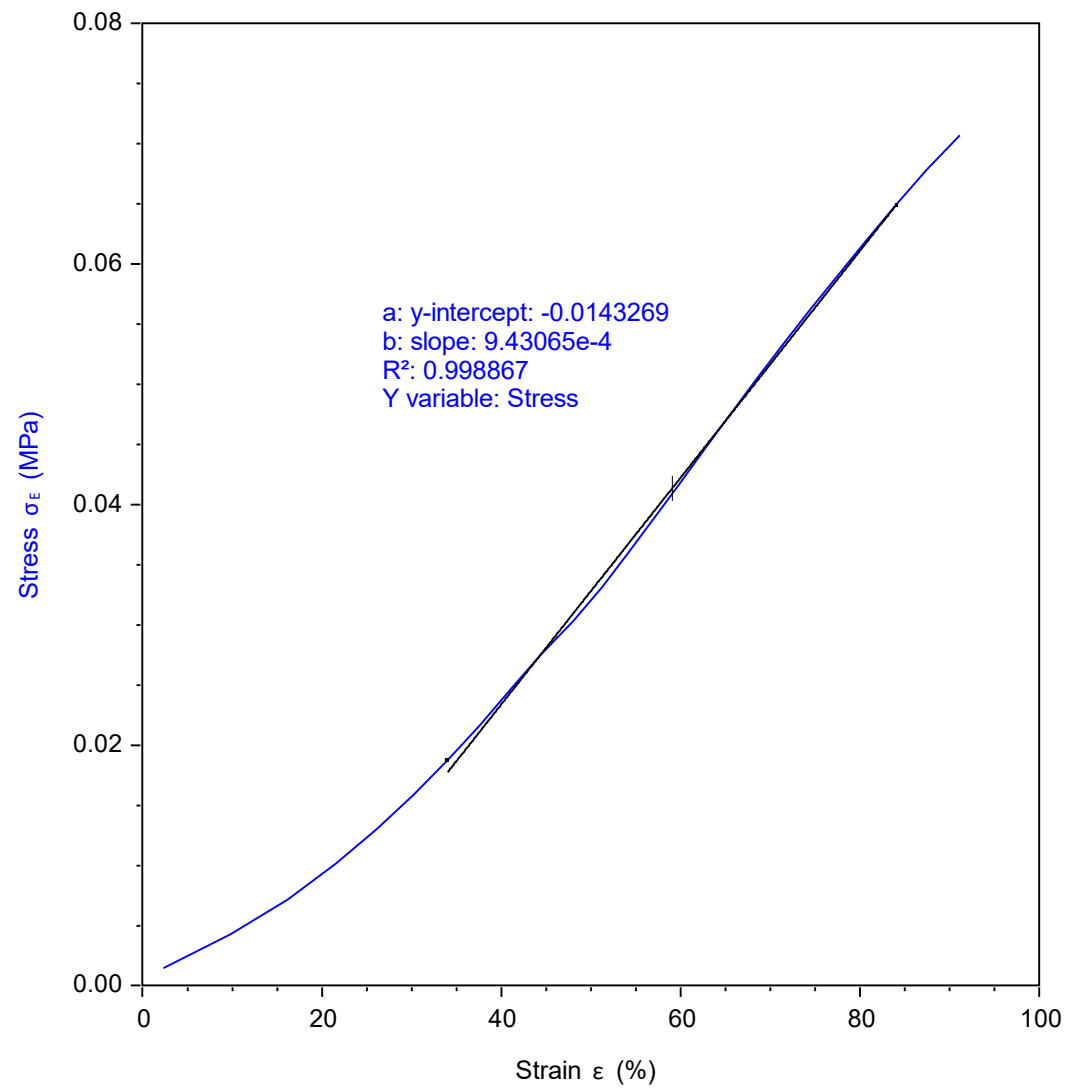
5% PVA_Comp_3



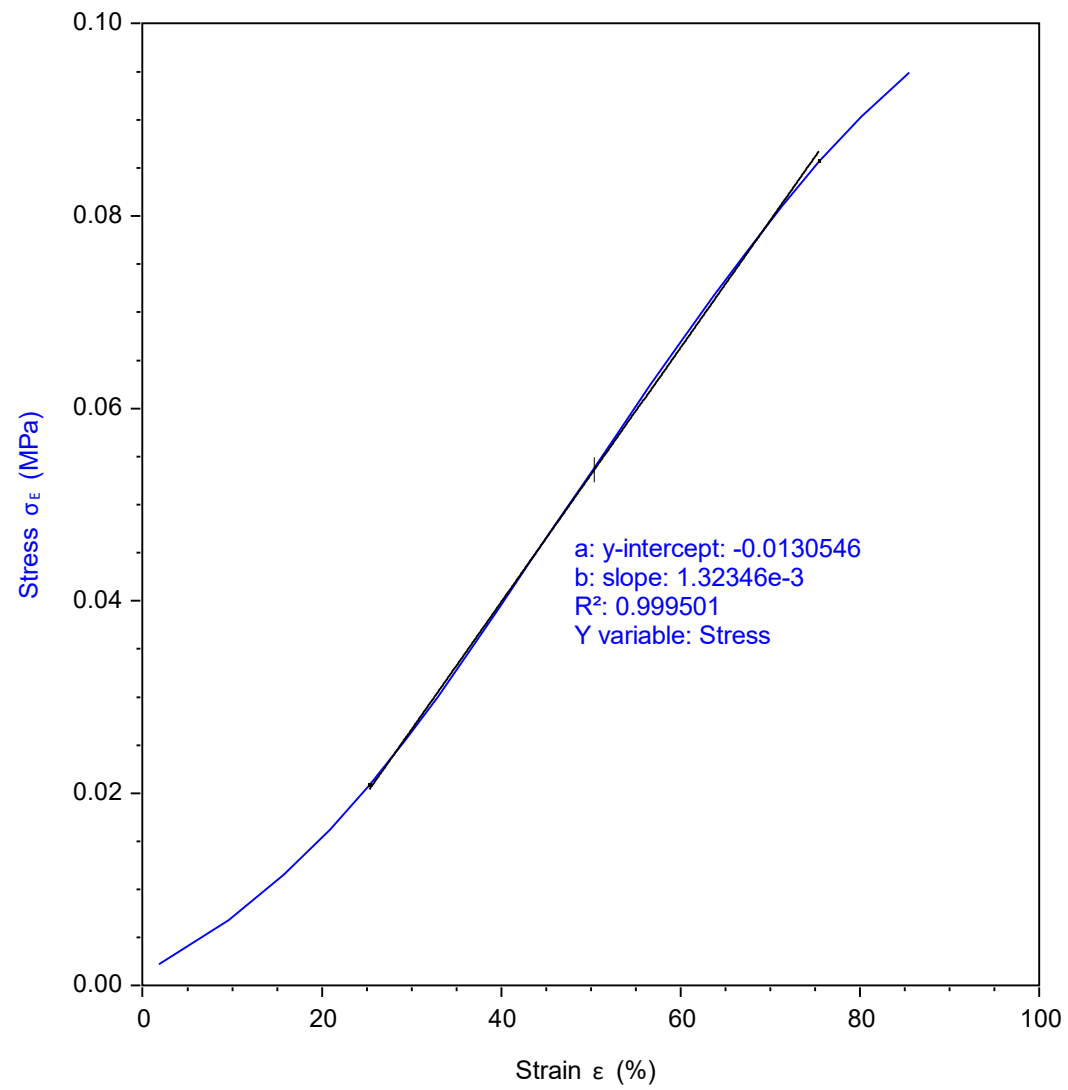
5 PVA_1



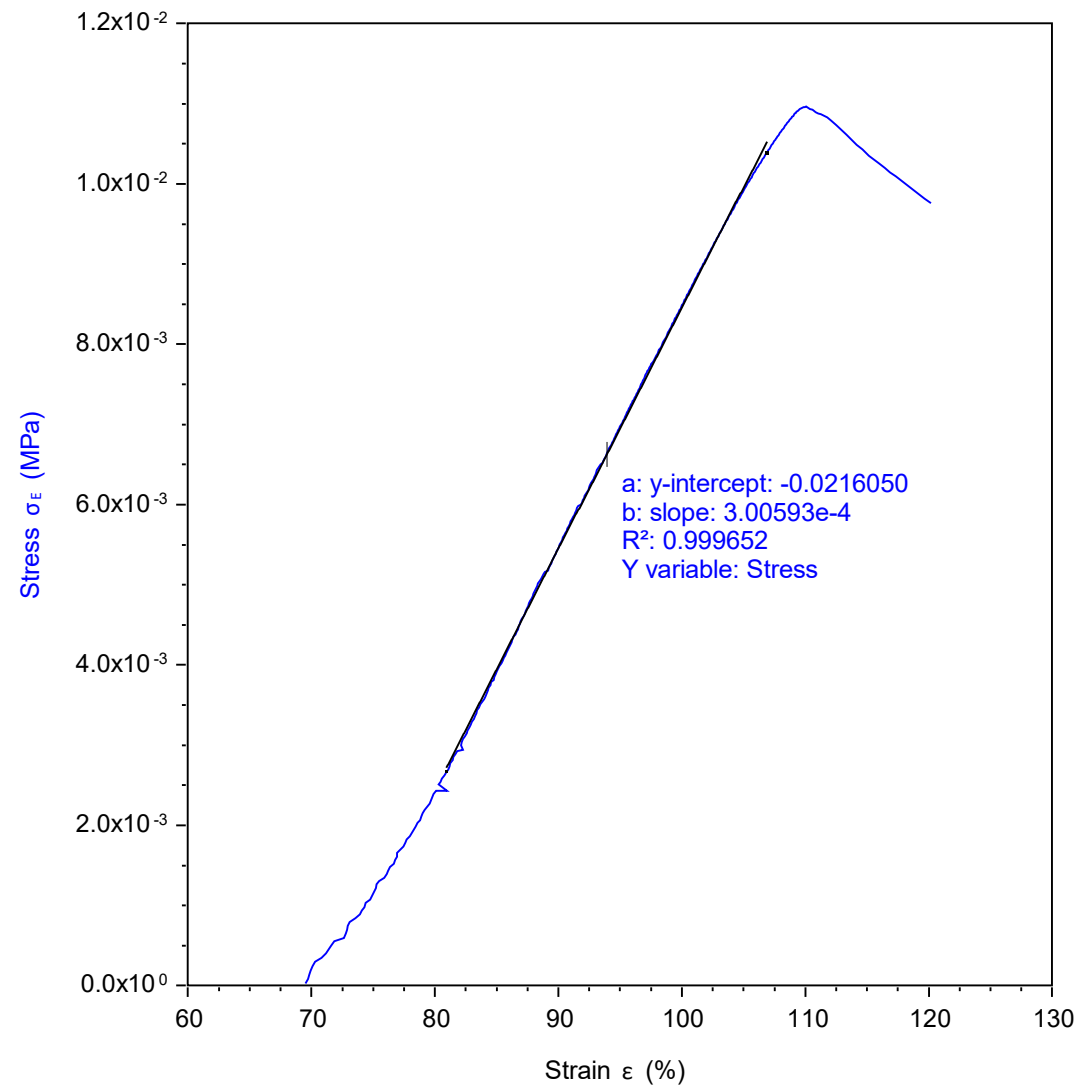
5 PVA_2



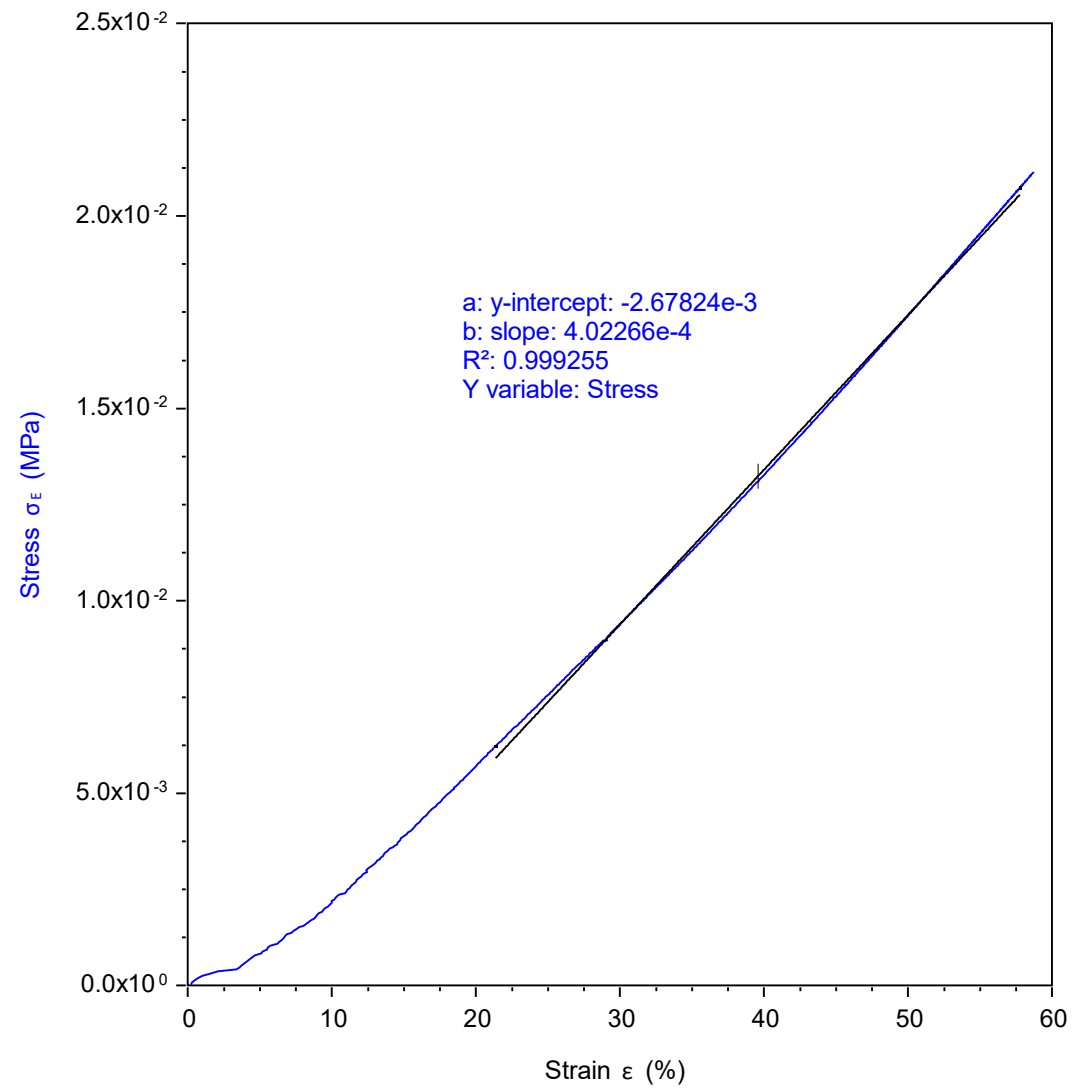
5 PVA_3



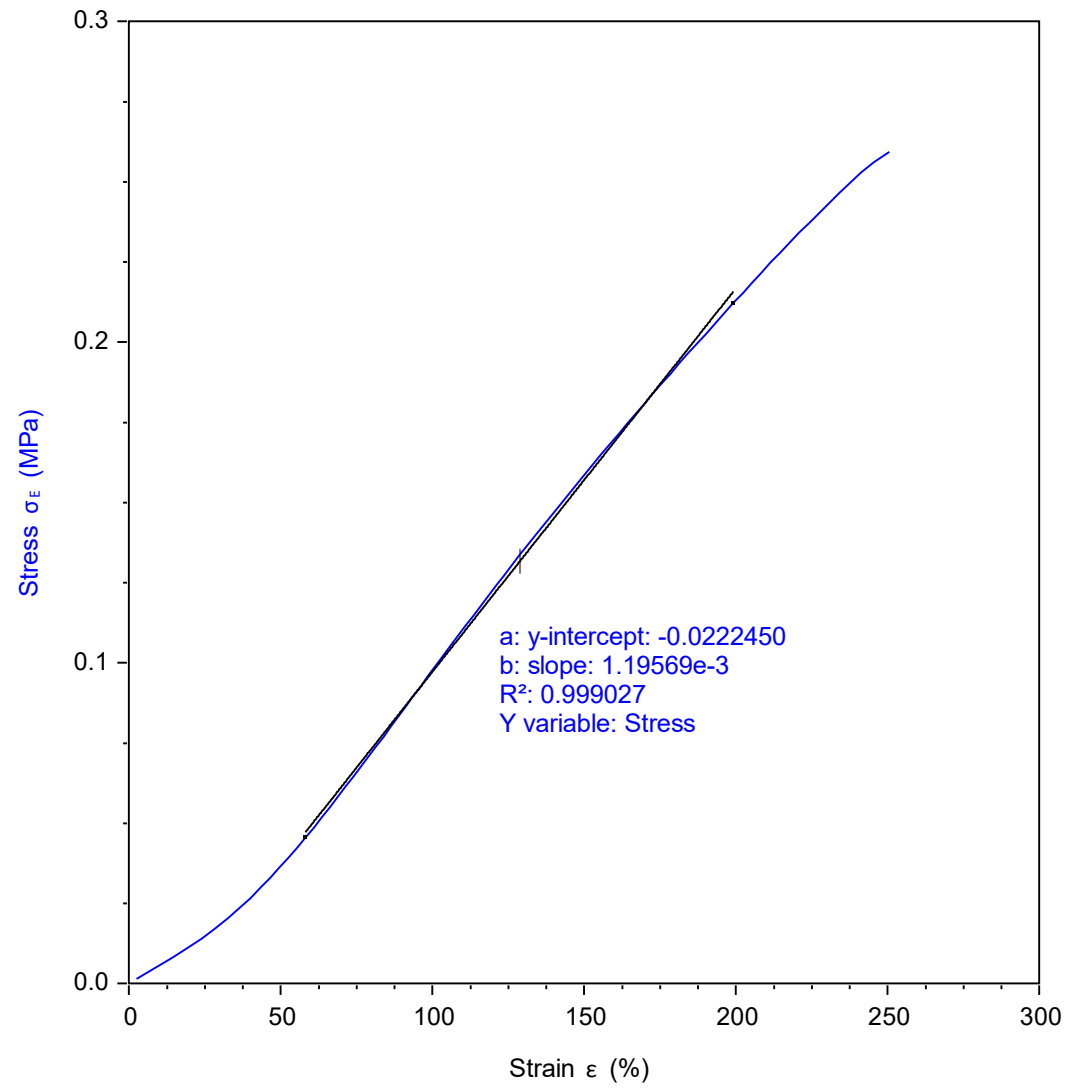
10% PVA_Comp_1



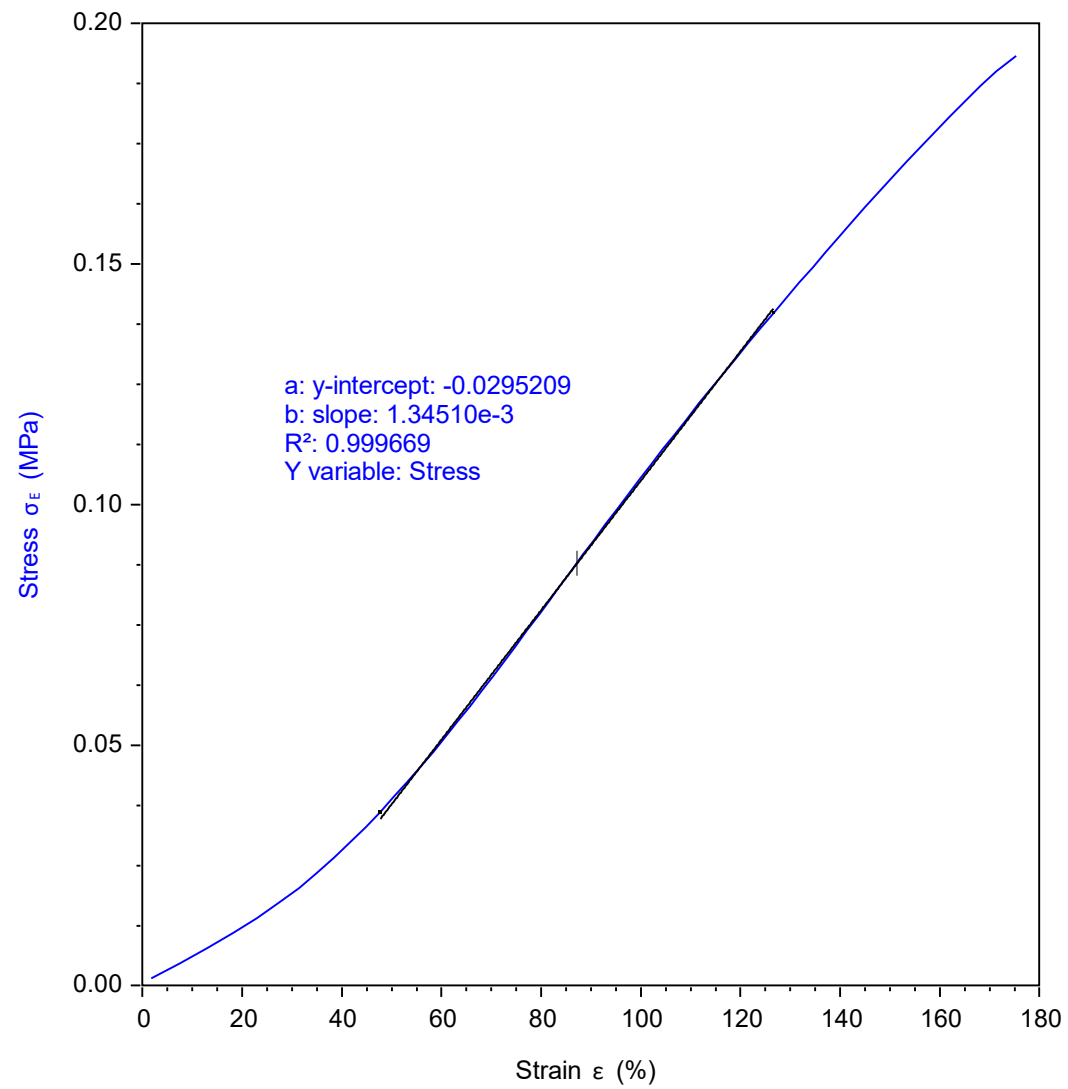
10% PVA_Comp_2



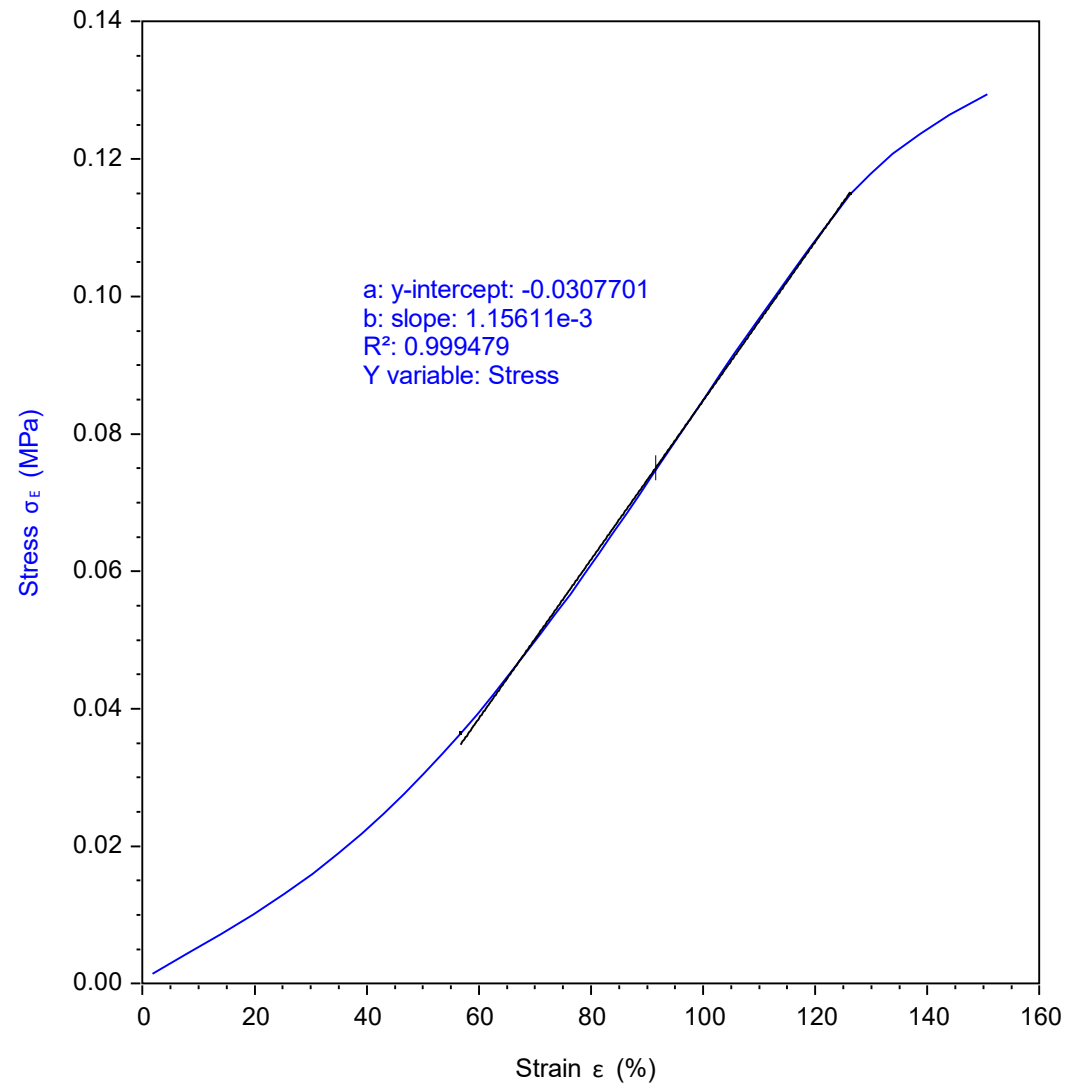
10 PVA_1



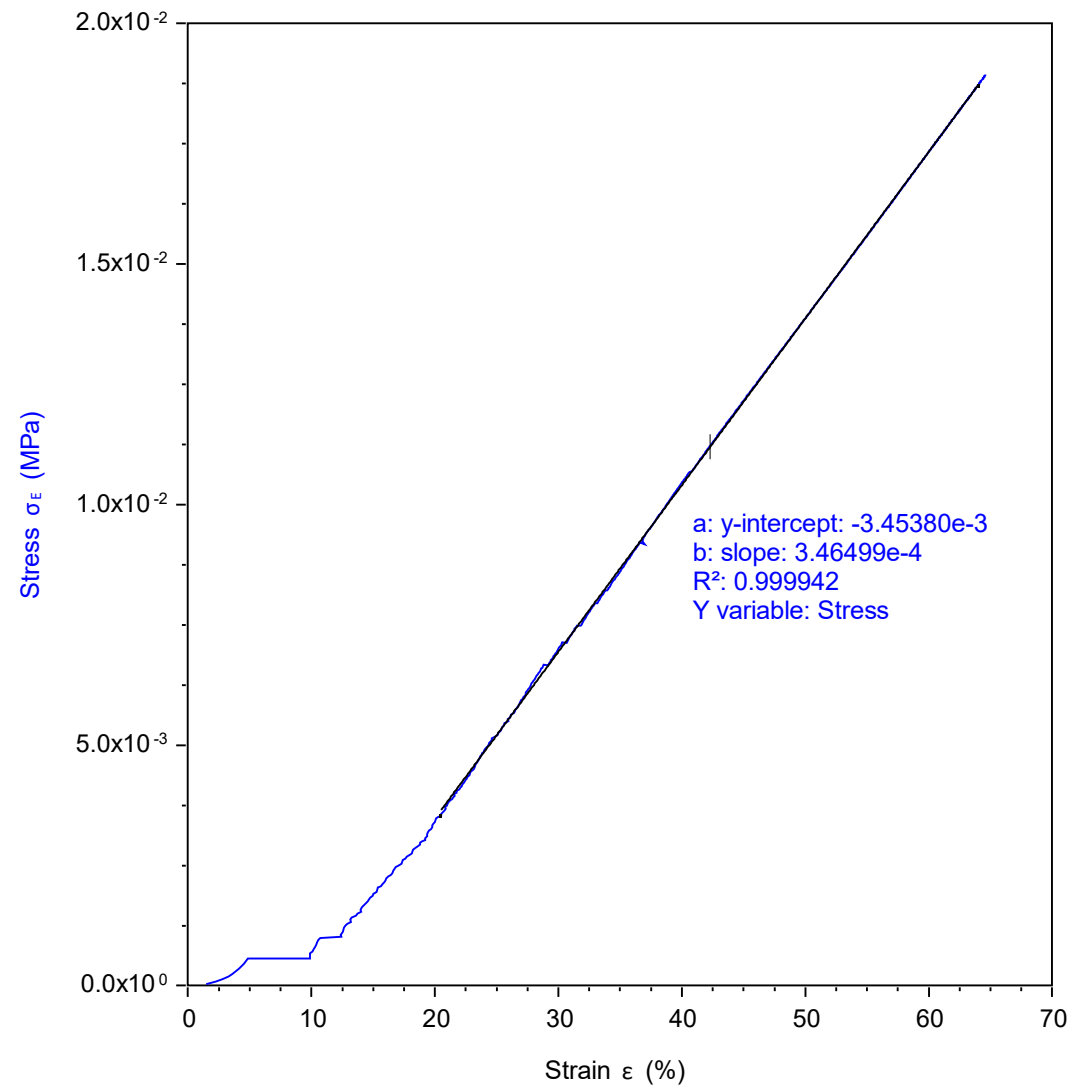
10 PVA_2



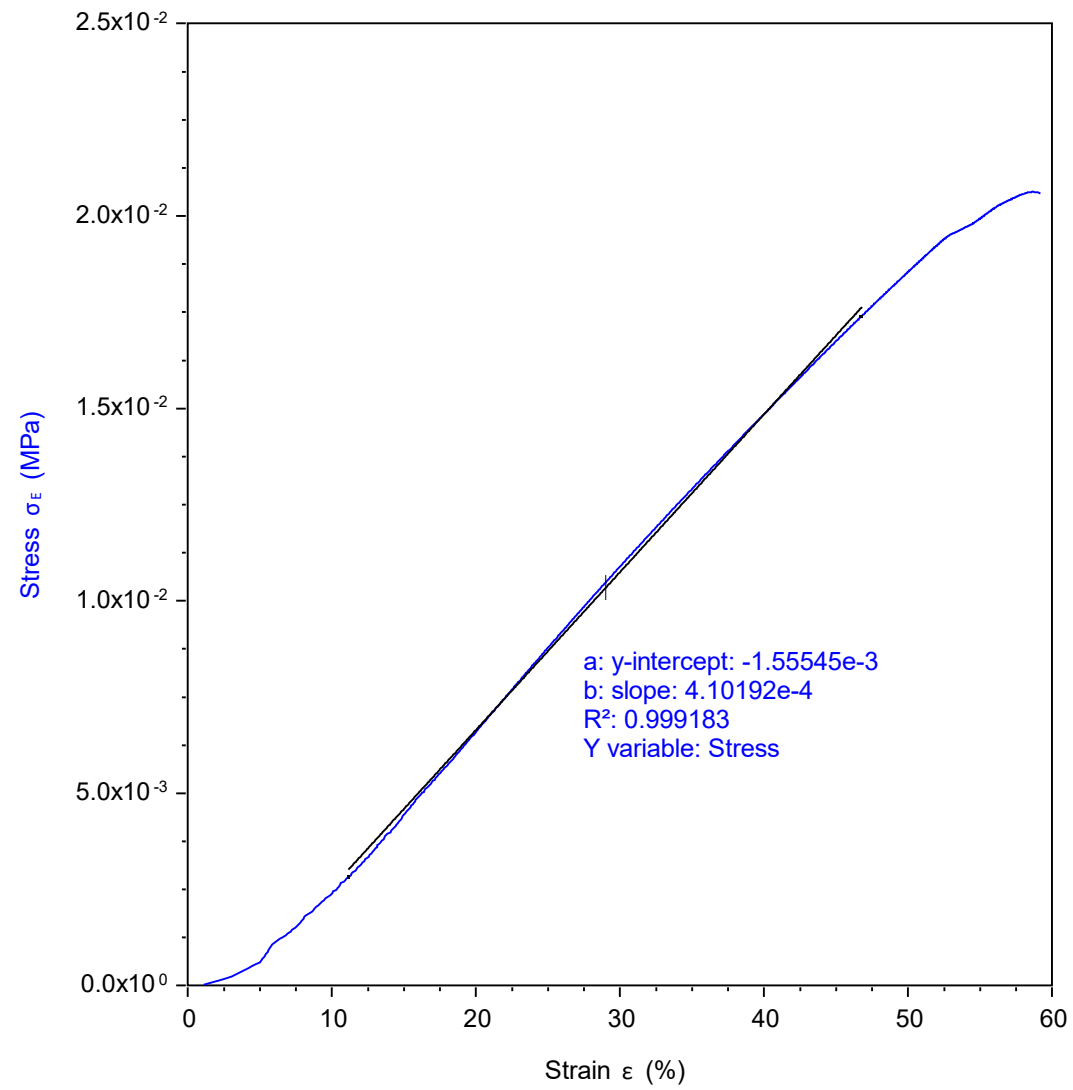
10 PVA_3



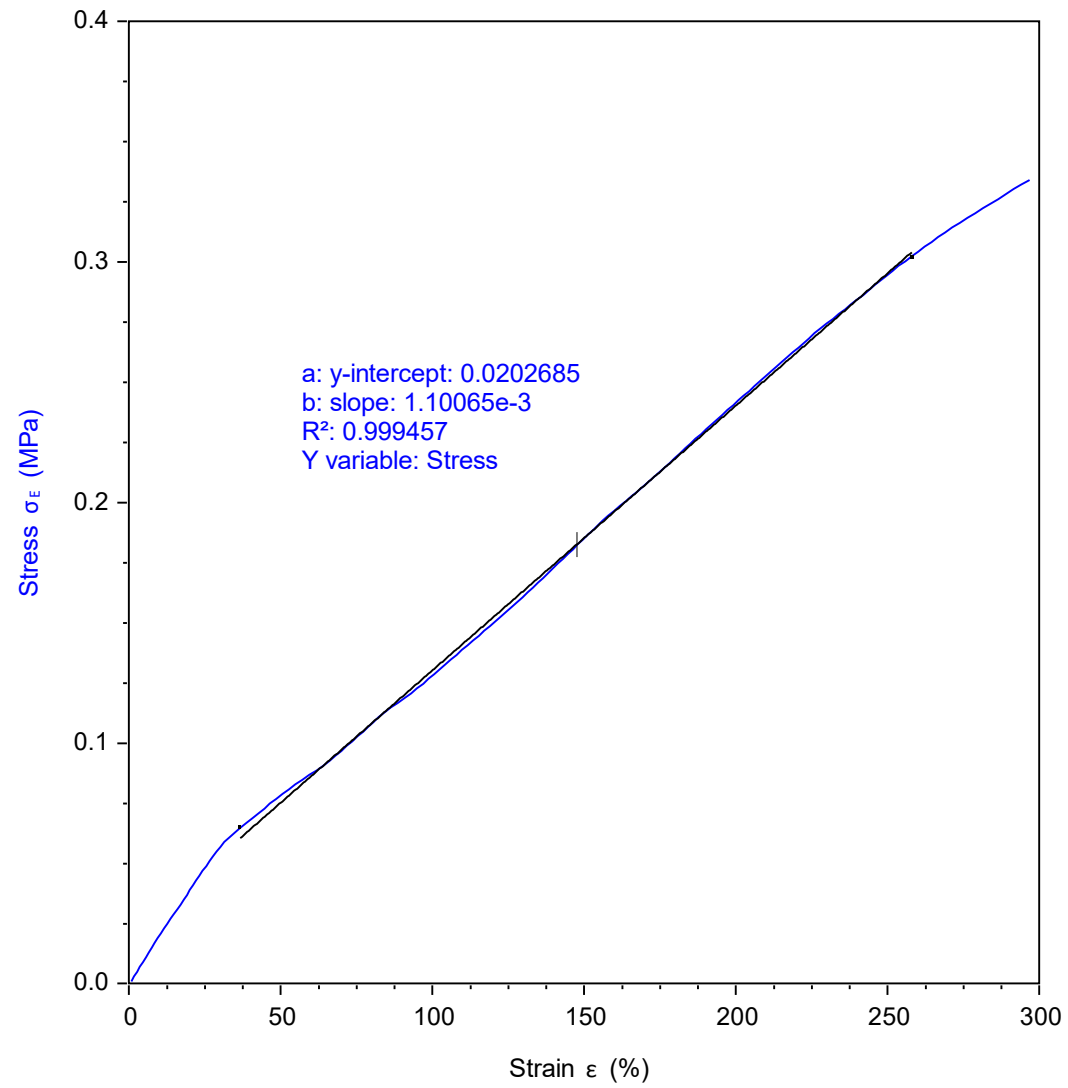
15% PVA_Comp_1



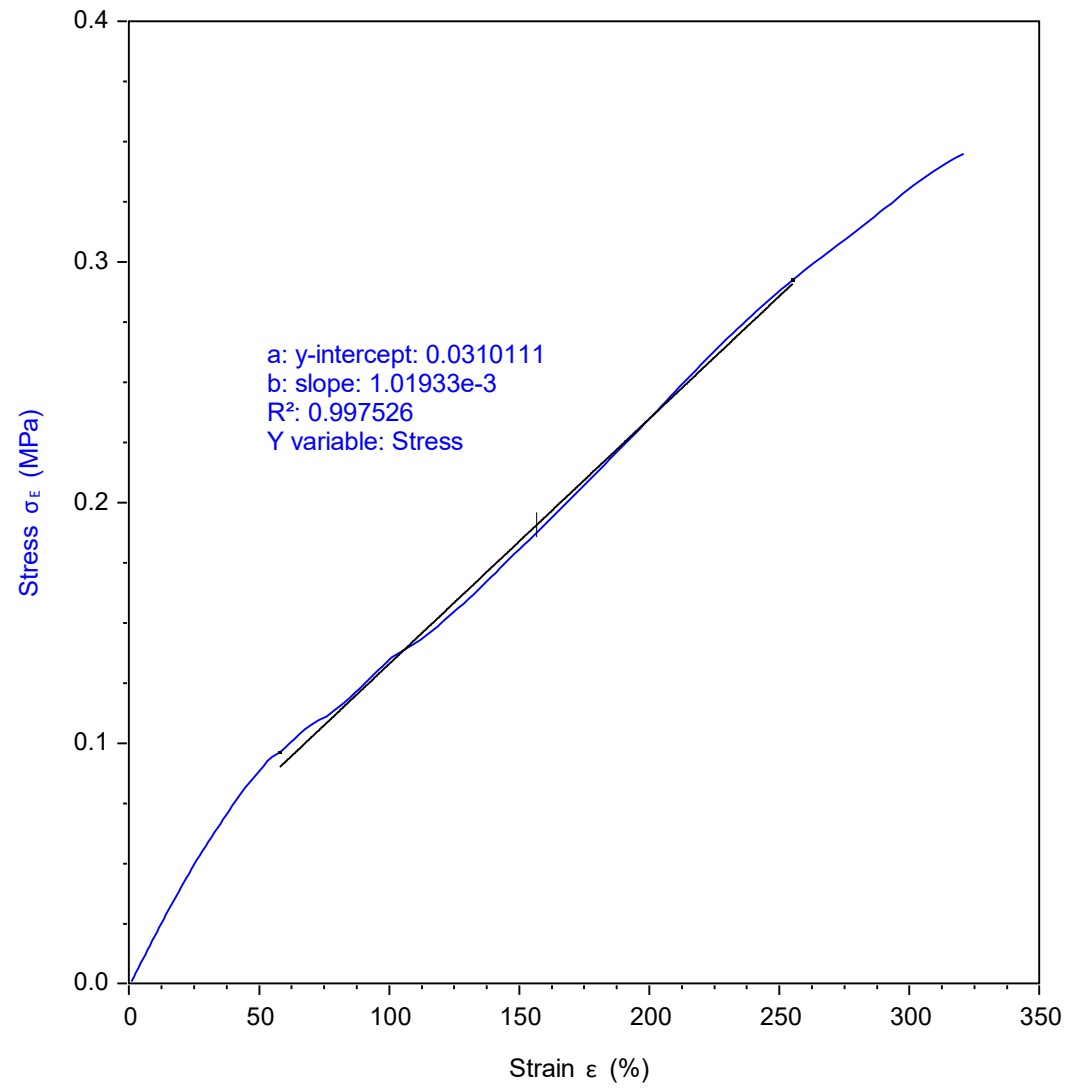
15% PVA_Comp_2



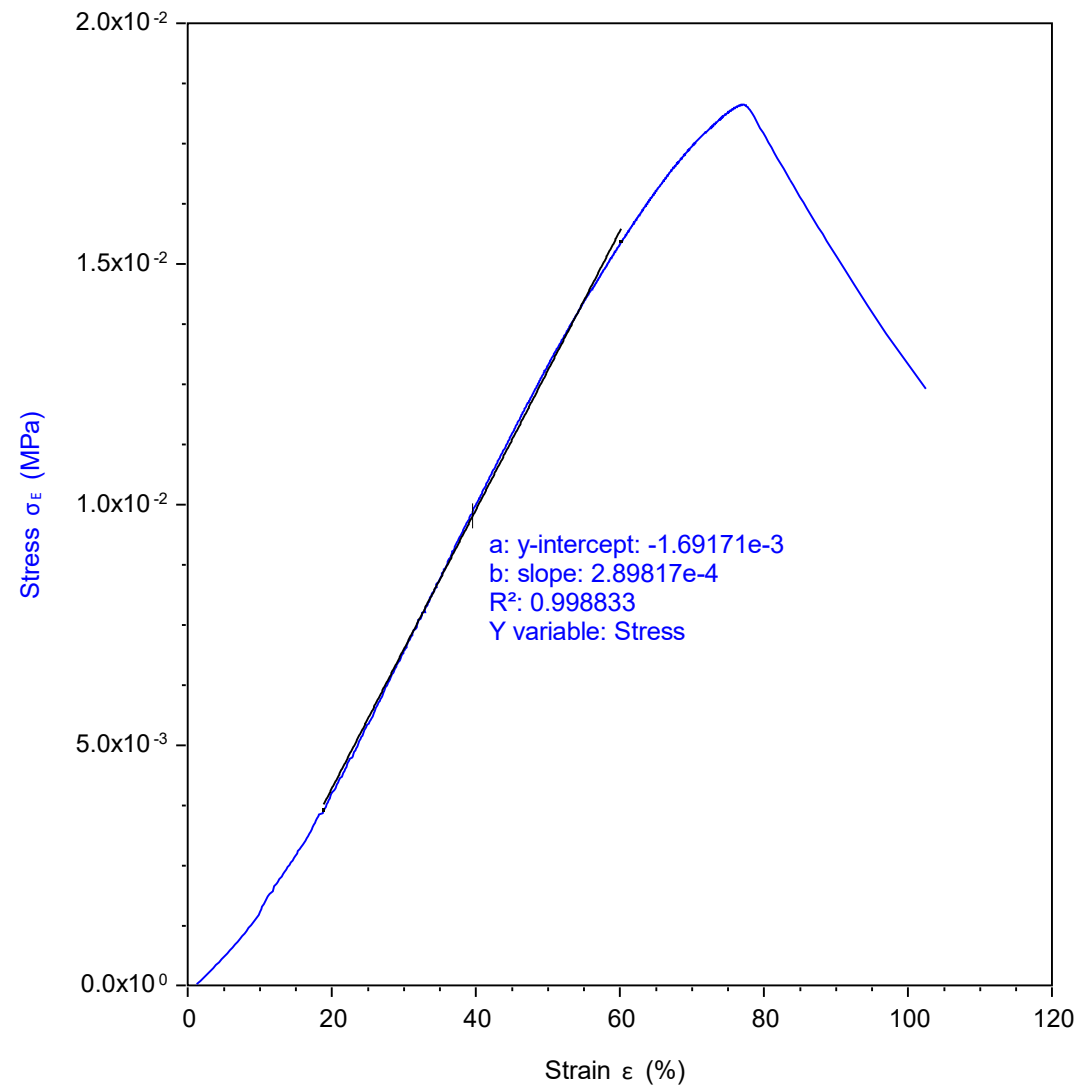
15 PVA_1



15 PVA_3



tri-layered-combination_Comp_1



tri-layered-combination_Comp_2

